Modeling Groundwater Flow and Transport of Contaminants at a Former Manufactured Gas Plant in the Midwestern USA

by

Obai Mohammed

Submitted to:

Dr. Bruce H. Kjartanson

Dr. Eltayeb Mohamedelhassan

This thesis is submitted in partial fulfillment of the requirements for the degree of

MASTER OF SCIENCE IN ENGINEERING

in

Environmental Engineering

Faculty of Engineering
Lakehead University

Thunder Bay, Ontario

2012

ABSTRACT

The processes used to produce manufactured gas for heating, cooking and lighting purposes in North America from the early 1800s to the mid-1900s have generated by-products such as coal tar containing Monocyclic Aromatic Hydrocarbons (MAHs) and Polycyclic Aromatic Hydrocarbons (PAHs), coke, light oil derivatives, and ammonia. Improper disposal of these wastes has resulted in contaminated soils, groundwater and sediments at these sites, potentially affecting human health and the environment. There is an increasing reliance on using numerical groundwater modeling to predict fate and transport of contaminants as well as employing predictive simulations to anticipate concentrations of contaminants in groundwater in order to evaluate a remedial action. To this end, developing a Visual MODFLOW-based model to simulate groundwater flow and transport of selected MAH and PAH compounds at a former MGP site located in the Midwestern U.S. is the main goal of this study. Available site data were compiled to develop the conceptual site model to assess contaminant fluxes and field-scale attenuation rates and to calibrate the groundwater flow model using WINPEST as a finishing step.

The groundwater flow analyses indicate that a decreased thickness and a decreased hydraulic conductivity of the granular alluvium layer at the site have a major influence on the groundwater potentiometric surface and groundwater flow pattern. The hydraulic gradient is relatively high through this “pinch zone” and relatively low elsewhere on the site. The calibrated groundwater flow model was used to simulate the fate and transport of benzene, naphthalene and benzo(a)pyrene and to carry out parameter sensitivity analyses to assess the effects of systematically varying transport parameters on contaminant plume evolution. The contaminant fate and transport model (MT3DMS) was

calibrated against the observed benzene, naphthalene and benzo(a)pyrene plumes. The modeling results illustrate the effect that the natural attenuation processes of sorption and biodegradation have on reducing the extent of the contaminant plumes. The benzene plume was highly affected by the biodegradation process which caused the plume to shrink closer to the former MGP source area. The benzo(a)pyrene plume was highly affected by the sorption process and did not expand significantly downgradient from the source area. The naphthalene plume has a downgradient extent between the benzene and benzo(a)pyrene plumes and was significantly affected by both the sorption and biodegradation processes.

ACKNOWLEDGMENTS

Writing this thesis was a major undertaking, and I would not have been able to complete it without the assistance and encouragement from my friends, family, and professors. I would like to acknowledge and sincerely thank my thesis supervisor, Dr. Bruce Kjartanson, for his creative ideas and guidance throughout the thesis development, presentation and writing. His scientific, technical and editorial advice helped me improve my thesis immensely. I would also like to acknowledge Dr. Eltayeb MohamedElhassan, my thesis co-supervisor, for his great support and valuable comments which increased the quality of this work.

My sincere thanks to the program coordinator, Dr. Baoqiang Liao, for his guidance during the Master's program.

I also appreciate the invaluable comments and support provided by Schlumberger Water Service technical team.

I am indebted to my student colleagues for providing a stimulating and fun environment in which to learn and grow. I am especially grateful to Ahmed, Basil, Shazli, Emad, Marissa, Jeremy, and Ram.

Finally, I wish to thank my entire family for providing a loving environment for me. My wife, Nawal, is the backbone of my achievements. I greatly appreciate her efforts that made my thesis a success. My father Yousif, my step-mother Basamat, my brothers and sisters were particularly supportive.

TABLE OF CONTENTS

LIST OF TABLES

LIST OF FIGURES

Chapter 1 Introduction

1.1 Background

Manufactured gas plants (MGPs) were widely used for the production of gas from coal, coke, and oil for lighting, cooking and heating in North America from the early 1800s to mid-1900s (Lee et al. 1998). The three predominant types of manufactured gas were coal gas, carbureted water gas and oil gas. When an alternative less expensive and higher energy source, natural gas, was introduced in the 1950s, MGPs closed down because they were unable to compete with the new energy source and regulatory bodies were raising concerns regarding the discharge of toxic tars to the environment (Hatheway 1997).

The manufactured gas processes typically produced by-products such as tar, coke, light oil derivatives, and ammonia. These by-products were sold or utilized as much as possible. For example, tars were refined into useful chemicals and products such as creosote, road tars, fuel and various pitches. In the decades during which many of these MGPs operated, however, substantial amounts of wastes and by-products including tar were disposed on-site in pits, leaked from storage and processing facilities or were discharged into nearby water bodies. Impacted soils, groundwater and sediments which came into contact with the tar became heavily contaminated, and in many cases remain contaminated (Lee et al. 1998).

Birak and Miller (2009) indicate that several thousand MGPs operated in the U.S. between the early 1800s to the 1950s. Hatheway (2012) estimates the number of sites in

the U.S. in a range between 32,860 to as high as 50,108 sites. Birak and Miller (2009) also note that today, many of these sites are located in urban areas and are therefore attractive for redevelopment. In many cases, the utility companies responsible for the sites converted them to commercial or industrial uses (Neuhauser et al. 2009). Continuing contamination from tar impedes redevelopment and reuse of these sites and creates risks for the surrounding environment and communities.

As described, one of the primary wastes from manufactured gas production is tar. Birak and Miller (2009) indicate that tars are a complex mixture of predominantly organic aromatic compounds. Most tars are composed primarily of polycyclic aromatic hydrocarbons (PAHs). In addition, tars likely contain monocyclic aromatic hydrocarbons (MAHs) and may also contain heterocyclic compounds and inorganic compounds such as arsenic and cyanide. The composition of tar depends on the gas manufacturing process, including the process temperature and feedstock, and weathering (e.g. dissolution and/or volatilization of lower molecular weight compounds over time will change the composition of tars). Birak and Miller (2009) also note that the total number of compounds in tars has been estimated as high as 10,000, with the presence of compounds with as many as 210 rings. Many compounds in tars remain unidentified. In terms of physicochemical properties, tars are dense non-aqueous phase liquids (DNAPLs), and, within a granular aquifer, can sink below the water table until a fine grained confining unit is encountered.

It is widely accepted that sites contaminated with DNAPLs are the most difficult to characterize and remediate. Much work has been done on single component DNAPLs such as trichloroethylene and terachloroethylene (e.g. Pankow and Cherry 1996). Of the DNAPL contaminants, tars in the subsurface at former MGP sites pose one of the most difficult environmental challenges because of their complex chemical composition. Moreover, a major complication in defining the tar source and studying long term contaminant plume evolution at a given site is that dissolution of individual tar compounds varies both temporally and spatially. Because of their variability and complexity, tars are difficult to study even in a laboratory bench-scale setting. Chlorinated solvents, on the other hand, such as trichloroethylene and terachloroethylene, are a well-defined, single component source in the subsurface and can be obtained commercially for both bench scale and pilot field scale testing. Neuhauser et al. (2009) note that the cost to address contamination at former MGP sites can range from $1 million to well over $10 million per site and as of 2007, more than 1000 former MGP sites were being investigated and remediated within the U.S.

Experience has shown that remedial approaches such as pump-and-treat have been ineffective and inefficient for remediating former MGP sites (Birak and Miller 2009; Neuhauser et al. 2009). Analyses by D'Affonseca et al. (2008) show that mass fluxes from a tar source can continue for more than 1000 years. Current approaches to remediate MGP sites focus first on source zone removal (e.g. contaminated soil excavation and treatment), source zone containment (e.g. sheet pile wall, in situ stabilization) and/or source zone destructive treatment (in situ chemical oxidation, in situ

thermal treatment) to the extent practicable followed by monitored natural attenuation (MNA). Lingle and Brehm (2003) describe this approach as applied to former MGP sites in Wisconsin. This approach has been termed monitored enhanced natural attenuation (Golchin et al. 1998) or enhanced natural attenuation (Herold et al. 2011; Martin et al. 2002). In most cases a substantial amount of residual tar is left in the subsurface after source treatments, particularly below the water table. Further treatments may be applied to control or reduce the extent of dissolved contaminant plumes, including injection of oxygen (O_2) and hydrogen peroxide (H_2O_2) into contaminated groundwater (e.g. Herold et al. 2011) and the use of a funnel-and-treatment gate system (e.g. Martin et al. 2002).

A very important aspect of the remediation is a well-designed and effective groundwater monitoring program in which monitoring well concentration data can be used to assess plume evolution, mass fluxes across monitoring well transects and attenuation and degradation coefficients of contaminants. Another very important aspect of remediation is the calibration and application of a site specific contaminant fate and transport model. The calibrated model can be used to explore the feasibility and effectiveness of different remedial scenarios and to simulate natural attenuation processes and estimate time frames for site cleanup (D'Affonseca et al. 2008; Birak and Miller 2009; Herold et al. 2011). In fact, Birak and Miller (2009) note "Field-scale modeling assessments, like the one described above (referring to the D'Affonseca et al. 2008 paper), are important tools in understanding the time scales involved for natural attenuation to occur, along with the impacts further source reduction would have on that time scale."

It must be emphasized that for modeling tar contaminated sites, simplifying assumptions are typically required due to the complexity of the tar source, both spatially and temporally. For example, D'Affonseca et al. (2008) modeled the release from a coal tar source zone using several selected individual and representative chemicals from the tar and Herold et al. (2011) note that "considerable uncertainty remained" in the results of their simulations due to substantial spatial and temporal variability in hydrogeochemical parameters and uncertainty in geochemical reactions. This issue is further highlighted by the reported results of an extensively monitored and studied emplaced coal tar creosote source experiment conducted within the Borden research aquifer (Fraser et al. 2008; Thomson et al. 2008; Sudicky and Illman 2011). Sudicky and Illman (2011) summarize a key outcome of this work; "The complex evolution of these plumes has been well documented, but understanding the controlling biotransformation processes is still elusive. This study has shown that anticipating bioattenuation patterns should only be considered at the broadest scale." These reported studies indicate that analysis and modeling of the fate and transport of contaminants released from tar into the groundwater at these sites will likely need to be treated using a phenomenological approach rather than a micro-mechanistic approach and that analysis of well characterized and monitored field studies are especially important to make progress in remediation of tar contaminated sites.

In this regard, a former MGP site in the Midwestern U.S. has been extensively characterized, monitored and analyzed through several research studies (e.g. Kjartanson et al. 2002; Biyani 2003; Stenback and Ong 2003; Golchin et al. 2004; Rogers et al.

2007a). In particular, Biyani (2003) modeled the fate and transport of several contaminants at the site using available site data up to August 2001. The primary goal of this thesis research is to develop a groundwater flow and contaminant transport model for this site that is calibrated using the most recently available site conditions. The calibrated model can then be used as a tool to assess the effectiveness of future coal tar source remediation activities and the impact of these source remediation activities on the long-term evolution of dissolved contaminant plumes.

1.2 Research Objectives

The specific objectives for this thesis research are listed below:

1. Compile available site geology, hydrology, and soil and groundwater contamination data for the former MGP site in the Midwestern U.S. to develop a geologic, hydrogeologic and contaminant conceptual site model. This includes geologic cross-sections, hydrogeologic properties and groundwater flow patterns, the nature and extent of the coal tar source(s) and the nature and extent of dissolved contaminant plumes. Select several MAH and PAH compounds with concentrations in groundwater that are consistently above regulatory standards for fate and transport analysis.

2. Use groundwater monitoring results to assess contaminant fluxes across monitoring well control planes and assess field scale attenuation rates for selected MAH and PAH compounds. Compare attenuation rates to field and laboratory scale rates for these compounds reported in the literature.

3. Develop a visual MODFLOW with MT3DMS based model to simulate groundwater flow and transport of selected MAH and PAH compounds at the former MGP site.

Define hydrogeologic and contaminant transport parameters from available site information, and use literature derived information as required. Define source terms for the contaminant transport model and compare these with source terms used for similar modeling studies as reported in the literature.

4. Calibrate the groundwater flow model using observed water levels in the site monitoring wells. Using the calibrated groundwater flow model, simulate contaminant transport and compare simulated selected MAH and PAH plumes with measurements from monitoring wells. Carry out parameter sensitivity analysis to assess the effects of varying transport parameters on selected MAH and PAH plume evolution.

1.3 Thesis Organization

This thesis begins with an Introduction chapter including a brief background section and a description of the thesis project objectives, followed by Chapter 2, literature review and background information associated with former MGP sites and related environmental concerns. Information on MGP sites, processes, contaminants and chemicals of concern and their related properties, monitoring and remediation methods for former MGP sites, including groundwater monitoring and strategies, source zone remediation and plume remediation are provided. Fate and transport of MGP site contaminants as well as flux based site management principles are also discussed in detail in Chapter 2, followed by a description of Visual MODFLOW and MT3DMS as groundwater flow modeling and contaminant transport modeling tools. Additionally, model calibration is discussed and the chapter closes with an examination of relevant case studies from the literature.

Chapter 3 describes the specific characteristics of the site under investigation, starting with a site description and summary, followed by site geology, hydrogeology and recharge, and site contamination details. Chapter 4 describes the groundwater flow modeling methodology, the groundwater flow properties, boundary conditions, simulation results, model calibration with WINPEST, and the results of initial as well as the calibrated model runs. Chapter 5 provides details and discusses the contaminant transport modeling simulations and results. Assumptions and limitations of the model are also included in Chapter 5. Chapter 6 summarizes and concludes the thesis and provides recommendations for further research activities on modeling and remediation.

Chapter 2 Literature Review and Background Information

2.1 MGP Processes

Manufactured gas was produced by means of three processes (Lee et al. 1998): coal carbonization process, carburetted water gas process, and oil gas process. Each process produced different quantities and types of by-products and pollutants based on the temperature of the gas production process, feedstock, period of distillation and other operating factors. Table 2.1 highlights the manufactured gas processes, time periods and the operating conditions with general properties of tars and compositions produced (Lee et al. 1998; Birak and Miller 2009).

Following are details on each process and its related contaminant releases.

Coal Carbonization / Coal Gas Process

This was the primary and simplest commercial mode of manufacturing gas from 1816 to 1875. After 1875, newer processes and technologies gradually replaced coal carbonization. Coal gas was produced through the distillation of coal in heated, anaerobic vessels called retorts. In this process, coal was broken down into its volatile components through the action of heat (Lee et al. 1998). During the retorting phase, approximately two-fifths of the coal's weight was converted into volatile non-solids or gases. Most of the remaining amount of the coal was converted into solids, primarily coke. From the retort, the gases were drawn off into a device known as the hydraulic main where some of the vapors were condensed to liquids and the rest remained in a gaseous state. The resulting liquids consisted of contaminated water and coal tar (Heritage Research Center

2007). The remaining vaporous material was coal gas comprising mainly hydrogen, methane and carbon monoxide with a typical heating value of 18.63 to 21.24 MJ/m^3 (Lee et al. 1998). The gas ran through a condenser where the gas cooled and additional coal tar and other impurities were removed. The coal gas, however, still contained impurities, primarily gaseous ammonia and sulfur compounds. These were removed by "washing" the gas in water and by running the gas through beds of moist lime or moist iron oxides. After this final purification process, the coal gas passed through the station meter, where it was measured, and passed to the storage holder where it was then distributed to the consumer. The primary by-products resulting from carbonization were coke, tar, and ammonia (Lee et al. 1998; Heritage Research Center 2007).

Carburetted Water Gas Process

Invented by Professor L. Lowe of Pennsylvania in 1873, this process was a technological advance in the U.S. manufactured gas industry. At its core, the process consisted of enriching a form of gas, known as water gas (sometimes called blue gas) and thus increasing its energy value. A coke bed was exposed to blasts of air and steam during which it was burned to incandescence, and steam then passed through the hot coke bed to form the water gas. By injecting oil into a vessel containing heated water gas, the oil and vapor combined, forming a gaseous fuel known as carburetted water gas with a thermal content of approximately 20.12 MJ/m^3. This gas was composed mainly of carbon monoxide, hydrogen, and carbon dioxide. In a few years, the process came to dominate the manufactured gas industry in the U.S. as residential and industrial consumers demanded the more efficient fuel source. The carburetted water gas process produced less

coke, tar, and ammonia compared to the coal carbonization process (Lee et al. 1998; Heritage Research Center 2007).

Oil Gas Process

The oil gas process is the only one of the three manufactured gas processes discussed here that did not use coal as a raw material, and the gas produced from oil was less commonly used because of the high cost associated with oil gas production. The process as a whole was very similar to the carburetted water gas process in the essence of enriching the gas through oil injection. Specifically, the oil gas process consisted of thermo-cracking oil in a steam environment to produce the raw gas rather than distilling coal. The oil was heated and cracked in a vessel similar to the generator used in the carburetted water gas process. From there the gas passed to a vaporizer, where it was enriched with additional injections of oil. Then, the gas was scrubbed and processed for distribution in much the same way as the carburetted water gas. Beside oil derivatives, lampblack, and naphthalene, many of the same waste products related to the production of coal gases, notably tars containing PAHs, were also generated during the oil gas manufacturing (Heritage Research Center 2007; Lee et al. 1998).

2.2 MGP Process Residuals

Residuals and wastes produced varied at each former MGP site depending on the process configuration and raw source used. As indicated in Table 2.2, various forms of tar were produced by all three processes. In general, coke residuals were reused as a raw material for the carburetted water gas production process. Ash and clinker were the final residuals

from the coal carbonization and water gas processes. They are relatively stable and the only concern is the gradual leaching of trace metals (Lee et al. 1998).

Another by-product was ammonia liquors produced in significant amounts from the processes, most of which evaporated or otherwise escaped from the disposal sites.

Table 2.2 summarizes different wastes and by-products produced from different gas manufacturing processes. Among the residuals and wastes produced, tar is receiving increasing attention because it is chemically complex, difficult to remediate, and also it was produced in large volumes usually disposed of in pits or landfilled on-site (Birak and Miller 2009). The following section details coal tar characteristics, compositions, and concerns.

2.3 Coal Tar Source Characteristics

Obtained by the destructive distillation of bituminous coal, coal tar is a dense non-aqueous phase liquid (DNAPL) that contains a complex mixture of free carbon and over a thousand organic compounds, most of which are polycyclic aromatic hydrocarbons (PAHs). The relative distribution of the monocyclic aromatic hydrocarbons, MAHs, (such as benzene and toluene) and PAHs (such as benzo(a)pyrene and naphthalene) are similar for all coal tars with naphthalene being the single-most common compound (Brown et al. 2006).

Physical characteristics of coal tar can be summarized as follows: black, viscous liquid (or semi-solid), naphthalene-like odor, combustible, soluble in ether, benzene, carbon

disulfide, and chloroform; partially soluble in alcohol, acetone, methanol, and benzene; and only slightly soluble in water (Agency for Toxic Substances and Disease Registry 2011).

Two key physicochemical properties of tars, specific gravity and viscosity, are summarized by Birak and Miller (2009). Table 2.3 lists the specific gravity and viscosity data for several tar samples from each major category of gas manufacturing in the U.S (Birak and Miller 2009). The data in Table 2.3 further illustrate variations in tar properties with changes in the gas manufacturing process. Viscosity, which is a measure of a liquid's internal resistance to flow, is highly dependent on the temperature of the manufacturing gas process. Due to the complexity of different tars, no methods are available to convert tar viscosities to values corresponding to typical subsurface temperatures (e.g., 10 °C) (Birak and Miller 2009). In general, the specific gravity varies from 1.061 to 1.334. There is considerable overlap among each major category of tar; nevertheless, the specific gravity is generally lowest in the water-gas tars and highest in the oil-gas tars. For coal tars, increases in the specific gravity are positively correlated to the temperature of the specific process. Additionally, there is a significant increase in the specific gravity for water-gas tars produced using heavy oils. On the other hand, for oil–gas tars, the data illustrate changes in specific gravity due to both temperature and feedstock changes. In general, the tars with the lowest amount of quantified PAHs have the highest specific gravity and viscosity values because the fraction that cannot be quantified is high molecular weight compounds (Birak and Miller 2009).

Coal tar properties have a strong influence on the fate and transport of coal tar within the subsurface. For instance, viscosity and density influence free coal tar product movement in the subsurface. On the other hand, tars containing less free carbon have a lower specific gravity and are richer in benzene and other light hydrocarbons than those containing more free carbon. In addition, tars containing more free carbon have higher viscosity and more pitch (Lee et al. 1998). With a low degree of solubility in water, coal tar tends to bond together, and when released into a body of water or aquifer it migrates downward until a low-permeability layer is reached where it slowly releases toxic compounds and chemicals of concern into the groundwater that have the ability to travel long distances. Because of the large number of compounds with large variation in properties, it is important to understand how the composition of coal tar changes over time and distance when selecting and developing remediation plans from available remediation alternatives. Consequently, environmental remediation of coal tars poses many challenges due to the wide range of physical, chemical, and toxicological properties of the individual constituents that make up coal tar (Brown et al. 2006).

2.4 Chemicals of Concern at Former MGP Sites

Gas manufacturing plants have produced a broad array of chemical compounds today considered as hazardous to the environment and to people in general. For example, most of aromatic hydrocarbons that are prevalent in coal tars MAHs and PAHs are classified as carcinogens. Table 2.4 lists MAH and PAH chemical compositions and Figure 2.1 shows the relative distribution of some MAH and PAH compound concentrations found in coal tar with enhanced concentrations of naphthalenes & phenanthrene (Brown et al. 2006).

The total number of chemical compounds in tars has been estimated as high as 10,000 (most are organic aromatic compounds), a figure that can account for as much as 70% of the tar mass. The composition of tars is a function of the gas manufacturing process from which they were produced. For example, the percentage of naphthalene is greater in the coal tars produced at high temperatures. The water-gas and oil-gas tars contain almost no tar acids. In comparison, low-temperature tars produced in Germany contain from 20 to 50% tar acids (Birak and Miller 2009). Early efforts to quantify individual constituents in tar demonstrated that most constituents were not present at appreciable concentrations; however, naphthalene was the most abundant compound, an aromatic hydrocarbon consisting of two fused benzene rings. Phenanthrene, on the other hand was the only compound that was not previously recognized for its abundance in tar. The composition of water-gas and oil-gas tars is expected to contain a similar list of compounds as coal tars, absent the tar acids and bases (Birak and Miller 2009). Wide ranges of trace minerals such as cyanides, sulfur, and some heavy metals such as arsenic, chromium and lead are also found in tars. Table 2.5 lists the chemical classes and common wastes/chemicals in each class encountered at former MGP sites (Biyani 2003).

2.5 Dissolution of Coal Tar and Release of Contaminants

Dissolution is defined as the transfer of soluble organics from an immiscible liquid (such as DNAPLs) to the water (Bedient et al. 1999). Dissolution of the DNAPL occurs as groundwater flows through the residual DNAPL zone. Within layers or pools of free-phase DNAPL, the contaminants may occupy up to 70% of the pore space and may substantially reduce the groundwater flow throughout these zones (Feenstra and Guiguer

1996). It is very important to be able to estimate the dissolution of individual chemical species in order to understand the risks posed by tars in the subsurface. This involves an understanding of both equilibrium concentrations and the amount of time required to reach equilibrium, or the rate of mass transfer (Birak and Miller 2009). There is, however, considerable uncertainty involved because of the complexity of the tar source, both spatially and temporally due to substantial spatial and temporal variability in hydrogeochemical parameters and uncertainty in geochemical reactions (Herold et al. 2011). Therefore, the exact relationship between aqueous and tar phase concentrations is not completely understood, but it is generally accepted that the aqueous phase concentration for an individual chemical species in equilibrium with tar will be less than the solubility for the pure species (Birak and Miller 2009).

The equilibrium dissolution was empirically described by some researchers using a partitioning coefficient as:

$$\mathrm{Knw}i = \frac{\mathrm{C}_i^{\mathrm{n}}}{\mathrm{C}_{ei}^{\mathrm{a}}} \qquad (2.1)$$

Where:

Knw$i$ = Partitioning coefficient

$\mathrm{C}_i^{\mathrm{n}}$ = Concentration of the ith species in the NAPL phase (mol/L)

$\mathrm{C}_{ei}^{\mathrm{a}}$ = Equilibrium concentration of the ith species in the aqueous phase (mol/L)

A more rigorous approach to predicting equilibrium concentrations based on thermodynamics is Raoult's Law which describes dissolution by the effective solubility:

$$C_{ei}^{a} = \mathcal{X}_i^n \, \mathcal{S}_i \qquad (2.2)$$

Where:

C_{ei}^{a} = Equilibrium concentration of the ith species in the aqueous phase (mol/L)

$\mathcal{S}_i$ = Species' subcooled pure liquid solubility (mol/L)

$\mathcal{X}_i^n$ = Mole fraction in the nonaqueous phase

Birak and Miller (2009) plotted experimentally determined values for C_{ei}^{a} versus predicted values calculated based on Raoult's Law for several tar samples. The plot shows uncertainity in the application of Raoult's Law. This deviation is related to non-ideal behavior, analytical limitations, and uncertainty in chemical properties of tar chemical compounds, such as the subcooled liquid solubility. Particularly, measuring aqueous phase concentrations of PAHs was found to be confounded by losses in sample preparation, including volatilization, photodegradation, and sorption. Higher molecular weight PAHs, such as benzo(a)pyrene, are of particular concern from a risk perspective due to their relatively high toxicity and possible increased mole fraction as tar ages, however, little data are available to evaluate the dissolution behavior of these compounds. In Brown et al. (2006) close inspection of data plots reveal that equilibrium aqueous phase concentrations were not determined for PAHs with a molecular weight greater than 202 g/mol. Further, in Lee et al. (1998), the most significant deviations from Raoult's

Law were for the highest molecular weight compound measured (e.g. benzo(a)anthracene) and these deviations were attributed to analytical limitations (Lee et al. 1998; Brown et al. 2005).

In a study by Fraser et al. (2008), a model of source dissolution for an emplaced creosote source using Raoult's Law adequately predicted the dissolution of several chemical compounds analyzed at the Borden research aquifer. Mass transformation has limited the extent of the plumes as groundwater flowed more than 500 m over 14 years yet the plumes were no longer than 50 m. Plumes of dissolved chemicals were produced by the essentially horizontal groundwater flowing at about 9 cm/day. Many chemicals were extensively sampled using a monitoring network. For less soluble chemicals the bulk of the mass removal apparently occurred in the source zone. However, the greatest mass loss is in the plume, especially for mobile compounds having high solubility and low partitioning coefficients such as xylenes, phenols and naphthalene. The study noted the complex evolution nature of the plumes and the difficulty of understanding the controlling transformation processes (Fraser et al. 2008).

2.6 Characterization and Groundwater Monitoring of Former MGPs

The most important factor to consider in choosing the proper remediation technique for any former MGP site is to adequately assess the risks associated with coal tar and other former MGP releases onsite. This requires effective monitoring of subsurface soil as well as groundwater, mainly through sampling methods. The primary objectives in characterizing a site are to obtain information to identify the risk posed by actual or

potential contamination, and to collect data necessary to select remedial alternatives. The information necessary to satisfy these objectives includes an understanding of the contaminants present and their properties, chemical compounds and concentrations, plume extent and migration pathways, and understanding the geologic and hydrologic factors that control the transport of contaminants (Nielsen 2006).

The primary tools used for site characterization are hollow stem auger drilling and direct push technologies (DPTs). Hollow stem auger drilling can be used to collect continuous soil samples and to install monitoring wells with a filter pack and 50 mm diameter casing and well screen. Note that care must be taken to avoid cross contamination. DPTs are commonly used to collect soil and groundwater samples, since they offer cost effective, minimally invasive and accurate data acquisition methods to better recognize the contaminant plume characteristics and impacts of subsurface geology and hydrogeology on the plume, and can also provide data about remediation progress and natural attenuation development (Nielsen 2006). A set of tools and sensors are pushed or driven into the ground to collect depth-discrete soil and groundwater samples and continuous information about subsurface properties such as stratigraphy and contaminant distribution (Biyani 2003). Some very useful direct push sensor systems are: cone penetration tests (CPTs), laser induced fluorescence (LIF) devices, electric conductivity probes (EC) and membrane interface probe (MIP).

The CPT was initially developed for geotechnical engineering applications. With the development of geoenvironmental engineering, adaptations to the equipment along with additional contaminant sensors have made the CPT a valuable tool for environmental site

characterization (Nielsen 2006). The common modern use of the CPT utilizes the mass (9000 to 36000 kg) of supporting vehicles along with hydraulic rams to advance an electric cone into the soil to provide soil behavior type. The basic measurements employ tip stress, sleeve friction and pore pressure to determine soil behavior type. The CPT rig has the capability to log stratigraphic soil characteristic information that leads to understanding preferred contaminant migration pathways, as well as the ability to install piezometers and monitoring wells as large as 51 mm diameter. One of the main drawbacks for the CPT is site accessibility of the larger 36000kg vehicle. However, smaller percussion probing rigs equipped with similar sensor systems, such as those supplied by Geoprobe Systems, can be utilized to overcome this limitation. Overall, CPT and percussion probing equipment with their specialized probes have the capability of cost effectively collecting large amounts of former MGP high resolution site stratigraphy, pore-pressure distribution, moisture content, porosity, hydraulic conductivity, the presence and concentration of soil and groundwater contaminant site data (Nielsen, 2006).

Laser induced fluorescence (LIF) are devices that normally combine with CPTs drilling tools to detect contaminant concentrations within subsurface soil and groundwater. The LIF systems incorporate a tunable wavelength dye laser or a fixed wavelength nitrogen laser to send a pulse wave of ultraviolet light through fiber optic cable. The device is normally placed immediately behind the CPT cone in order to retrieve accurate stratigraphic profile. As pulses are sent through subsurface soils, petroleum hydrocarbons emit fluorescence. The emitted light is sent back through the optical cable

and measured as function of wavelength. The wavelength is then compared to standard curves to determine the type of hydrocarbons present. Intensity of the fluorescence is used to determine the existing concentrations within the soil or groundwater. The operator retrieves the result in real time, allowing for alterations to be made to better allocate time and resources of the environmental investigation. The LIF devices require competent operators for careful calibration to avoid errors that reduce the quality of the investigation (Nielsen 2006).

Another important direct push tool is electric conductivity tests at which soil conductivity and resistivity are used to classify soils. The power of this tool stems from the fact that higher electrical conductivities are representative of finer grained sediments, such as silts or clays, while sands and gravels are characterized by distinctly lower electrical conductivities. A few site specific core samples, either from discrete depths or a continuous core, can be used to verify the lithology interpreted from electrical conductivity values at a former MGP site. The electrical conductivity logs are then correlated across the site to show changes in thickness or elevation of lithologic units of interest. Soil conductivity logging continues to increase in usage because conductivity logging can be efficiently performed with the highly mobile and cost-effective percussion probing equipment. Electrical conductivity logs can be used to define hydraulic conductivity zones which help to predict the movement of contaminants in the subsurface and to facilitate the proper placement of DPT monitoring wells (Nielsen, 2006).

The membrane interface probe (MIP) is a direct push technology-based sampling method

used for detecting and quantifying volatile organic contaminants within subsurface soils and groundwater. Generally these devices are incorporated with DPT probing. The MIP sensor systems are capable of collecting the required contaminant information from both saturated and unsaturated soils (Sara 2003). The MIP system consists of a thin film fluorocarbon polymer membrane mounted on a stainless-steel drive point. The drive point is advanced in the targeted push location, subsequently, the membrane is heated to approximately 100°C to 120°C and a clean carrier gas (nitrogen, helium, or purified air) is circulated across the internal surface of the membrane. Volatile organic compounds (VOCs) that partition across the membrane are subsequently measured by a conventional detector system (e.g. gas chromatograph, mass spectrometer and flame ionization detectors) at the ground surface. A continuous log of VOC detections versus depth is generated. Soil electrical conductivity and penetration rate information are also provided by use of a conductivity dipole and other sensors, providing real-time lithology-based data for interpretation (Sara 2003).

Groundwater monitoring is defined by the American Society of Civil Engineers (ASCE) as testing of groundwater over an extended time period in order to document groundwater conditions, including the collection of chemical data, such as contaminant concentrations. The objectives of groundwater monitoring are to collect representative groundwater samples from a target monitoring zone for chemical analysis to detect the release of contaminants, determine the extent of contamination from a suspected or known source, obtain accurate water level data at specific locations to construct water table or potentiometric surface contour maps, determine groundwater flow directions, and design

a remedial strategy and monitor the efficiency of an applied remediation option (USEPA 2007; ASCE 2003).

Sealed groundwater samplers (Figure 2.2) and exposed groundwater samplers (Figure 2.3) are pushed into the ground using DPTs to collect groundwater samples. Exposed samplers can be used to collect multi-level samples with a single push. However, exposed samplers can drag down contaminants or contaminated soil and/or groundwater as the tool advances into the ground, and the exposed screen may be clogged by silt and clay particles as the sampler advances through fine grained layers. Sealed-screen samplers, where the well screen is not exposed to soil while the tool is being pushed to the targeted depth, typically consist of a short screen nested within a sealed water-tight tool body which mitigates plugging of the screen and/or the contamination of samples (Biyani 2003).

The BAT Permeameter is commonly used for in-situ testing of hydraulic conductivity in unsaturated and saturated low-permeable soils. Typical applications are: control of hydraulic conductivity values for compacted clay liners, control of hydraulic conductivity values of in-situ slurry walls and general geotechnical investigations. The test is based on measurement of flow into or out of a test container which is connected to a filter tip. The type of test is a "falling head" test. By using the logging function of a BAT IS Sensor, pressure data from the test container are automatically collected at a preselected time interval. The recorded pressure data can be translated into a volume change or flow (Nielsen 2006).

Drilling methods are used to install monitoring wells with preference of casing the hole during drilling such as hollow stem augers. The hollow stem auger consists of a hollow auger bit, generally with carbide teeth that disturbs soil material when rotated, whereupon spiral flights transport the cuttings to the surface. This method is best suited for soils in which an unsupported borehole will not stay open, such as sands. A monitoring well can be installed inside of hollow-stem augers with little or no concern for the caving potential of the soils. Boreholes can be augered to depths of 46 m or more (depending on the auger size), but generally boreholes are augered to depths less than about 30 m (USEPA 2008). Alternatively, direct push rigs are used to install groundwater monitoring wells to allow short-term or long-term monitoring of groundwater by collecting samples from wells that are usually 51 mm in diameter or less and are made of PVC and/or stainless steel.

Since monitoring wells are installed for periods of several months to several years, the annulus of the boring around the well casing above the screen and filter pack is sealed to prevent migration of contaminants. A slotted or screened section permits groundwater to flow into the well under ambient hydrostatic pressure. Groundwater may be collected from monitoring wells using bailers, various pumps, or passive sampling devices (USEPA 2005).

The groundwater monitoring program should be designed to monitor solute plume behavior over time and to verify that natural attenuation is occurring at rates sufficient to protect potential downgradient receptors (Nielsen 2006). It is very important to be able to

understand the 3-D plume configuration. This objective requires setting up a network of monitoring wells with transects across the entire plume extent. However, in many real sites the number of monitoring wells is limited due to economical or geological reasons. Under such restricted conditions, it is difficult to develop a reliable understanding of a 3-D plume configuration or to detect a trend of contaminant mass flux in flow direction (Bockelman et al. 2003). This supports to a large degree the importance of using the data to create groundwater flow models to simulate existing receptor exposure pathways and to accurately predict future plume migration, remediation effectiveness, and attenuation rates in order to assess risks and to take necessary further remediation actions whenever required (Nielsen 2006). Therefore, placement of a limited number of monitoring wells and frequency of sampling must yield useful data and allow detection of significant changes in plume configuration and reveal trends in contaminant concentrations over time. In many cases it may be possible to utilize some of the available monitoring wells at a specific site, thereby reducing the cost of implementing the long-term monitoring plan. However, it is important that these wells are located in appropriate locations (Nielsen 2006).

Two types of wells are used for groundwater monitoring, these are performance monitoring and compliance wells (PMWs) and contingency wells. Located upgradient from and within a known source area, and just downgradient from the plume as shown in Figure 2.4, the PMWs are placed along the plume centerline and beyond the plume longitudinal and transverse extents to understand plume trends and to verify the predictions during the evaluation of natural attenuation. Contingency monitoring wells

are placed beyond the maximum predicted lateral and downgradient boundaries of the plume, and typically upgradient from known or possible receptor exposure points to observe the groundwater chemical concentrations for early detection of any possible plume expansion (Nielsen 2006).

2.7 Remediation of Former MGP Sites

Several remediation approaches that can be applied at former MGP sites are available with an overall goal to reduce the mass flux from the source zone. The selection of a technique or a combination of methods generally depends upon many factors that include technical, socioeconomic, regulatory, risk, liability, and financial (EPRI 2003).

2.7.1 Source Zone Remediation

Birak and Miller (2009) state that simple pump-and-treat approaches are not an effective or efficient alternative for remediation of former MGP contaminated sites. They emphasize the importance of source remediation in reducing source-longevity and resistance of plumes to remediation techniques such as monitored natural attenuation.

As a result, the first goal of a cleanup strategy should be to remediate the areas of highest contamination (source area) in order to prevent additional releases to the environment. Therefore, Birak and Miller (2009) categorize methods currently used to remediate former MGP sites into three general groups: source-zone removal, source-zone containment and source-zone treatment.

Source Removal

Being frequently used as the sole alternative for dealing with the presence of former MGP contaminant plumes and subsurface coal tars, source removal refers to excavation or dredging of contaminated soil and sediments. Excavation is defined as the removal of sediment from shallow-water contaminated sites using typical earth moving equipment such as track or wheel-mounted excavators and backhoes operating from exposed land. In contrast, dredging is the removal of subaqueous contaminated sediment utilizing mechanical or hydraulic removal techniques operated over-water from a barge or other floating vessel (EPRI 2007).

Source removal was applied in line with the Wisconsin regulatory framework for remediation of two former MGP sites in Wiconsin. Impacted soil was excavated, transported to a remote facility for thermal treatment, backhauled and then backfilled in the excavation area. As a result, the potential for direct contact with coal tar impacted soils has been significantly reduced. Consequently, addressing the dissolved-phase contamination was adequately accomplished by means of monitored natural attenuation (Lingle and Brehm 2003).

For contaminants located within the saturated zone, removal is usually achieved by physically extracting the contaminants from the subsurface. Multiphase extraction, for example, employs a vacuum or pump to extract NAPL, vapor, and aqueous phase tar contaminants from the subsurface, which may then be disposed of or treated. Alternatively, similar to pump and treat, surfactant and co-solvent flushing can be used to

introduce a liquid within the subsurface into which the contaminant partitions, and then the mixture is extracted from the subsurface and subsequently treated (National Research Council 2005).

Source Containment

Source containment includes the use of capping, slurry walls, sheet piling, and in situ stabilization applied as a remedial option to limit future migration of contaminants into the environment. Therefore, the process is not considered as source reduction (Birak and Miller 2009). Published research indicates that containment via capping and vertical containment barriers provides one of the most cost-effective and environmentally-effective site remediation methods (EPRI 2007).

Subsurface vertical containment barriers such as slurry walls and sheet-pile cut-off walls are used either alone or in conjunction with surficial caps or groundwater pump-and-treat systems to contain soil and groundwater contaminants. When used alone, vertical containment barriers are usually designed as permeable reactive barriers that allow a flux out of the containment system at a rate that limits migration of constituents of concern (COCs), but allows groundwater to flow out of the system. Pump-and-treat systems are usually used with containment barriers that are keyed into confining layers, for active treatment. Extraction wells are located upgradient of the containment barrier to discharge contaminated groundwater to a treatment facility (EPRI 2007).

Groundwater modeling is necessary during the design of containment systems, because the flow of groundwater will be affected by the barrier, and also, nearby sites could be affected as water diverts around the barrier, and some groundwater mounding can occur upgradient of the barrier. Groundwater modeling provides early predictions of these barrier effects (National Research Council 2005).

Source Treatment

Source-zone treatment technologies applied at former MGP sites include thermal treatment, chemical treatment as well as biodegradation applied at sites where applying physical or chemical means to remove free or residual tars is not possible (Birak and Miller 2009). The following sections detail each technology and its potential for application for different situations.

Thermal Treatment

Thermal treatment processes involve the use of steam or electricity to raise the temperature of the subsurface and mobilize the contaminants either in the liquid or vapor phase. In situ thermal treatment includes using a network of thermal wells to destroy contaminants in place to achieve the soil clean-up standards within the target treatment zone, while in situ thermal desorption (ISTD) is a soil remediation process by which heat and a vacuum are applied simultaneously to remove organic contaminants from the subsurface (EPRI 2007). ISTD application desorbs and subsequently destroys organic compounds by combustion. Heat is applied to the soil with an array of vertical or horizontal heaters, under an imposed vacuum. Heat transfer into the soil occurs primarily

by thermal conduction from a network of electrically powered heating elements (heater wells). Three levels of heating have been developed to apply thermal in situ treatment at Former MGP sites, including: gentle heating (below 100°C), moderate heating (to approximately 100°C), and elevated heating (to about 325°C) (Baker et al. 2006).

Chemical Treatment

In situ chemical oxidation (ISCO) is a chemical oxidation process involving oxidation-reduction (redox) reactions, which are essentially an exchange of electrons between chemical species. This exchange of electrons affects the oxidation state (valence) of the chemical species. Consequently, carbon bonds are broken and the organic compounds are either completely destroyed or converted to smaller and typically less hazardous compounds. Advances in the development of this technology include systems that effectively deliver and inject reagents into subsurface soil and ground water so that in situ chemical oxidation can be achieved (Huling and Pivetz 2006). The process involves adding strong oxidants such as hydrogen peroxide, ozone, permanganate, or persulfate to the subsurface. These compounds can oxidize a wide variety of contaminants at former MGP sites to relatively less harmful compounds, thereby promoting mass transfer from sorbed or NAPL phases to the aqueous phase and consequently shrinking the tar source mass. However, the rate of reaction is highly variable, depending on the compound being treated and the oxidant that is applied (Huling and Pivetz 2006; National Research Council 2005). The primary costs associated with implementing an ISCO system (apart from site characterization costs) include delivery system design and installation costs, defining mass of tar contaminants to treat, and the quantity of reagent needed for

complete oxidation. In general, the operation and maintenance (O&M) costs associated with ISCO are expected to be significantly less than O&M costs for traditional "physical" remediation technologies such as pump and treat, due to reduced treatment times and equipment requirements (Huling and Pivetz 2006; ITRC 2000).

Chemical injection coupled with extraction, known as surfactant/co-solvent flushing, is a chemical enhancement technology that increases removal efficiency through injection of chemicals to solubilize and/or mobilize contaminant compounds that can then be extracted from the subsurface, separated and treated aboveground (USEPA 2004). Although the main mechanisms underlying surfactant/co-solvent flushing are usually considered as being either solubilization or mobilization, an alternate approach, super-solubilization fits between these two extremes. In this process, further solubility enhancement can be achieved using a mixture of surfactants, alcohols and/or other co-solvents while still maintaining a suitably high interfacial tension so as to mitigate the potential for mobilization and vertical migration. The chemicals typically used are aqueous surfactant solutions, co-solvents that lower the interfacial tension (including alcohols such as ethanol or isopropyl alcohol), or electrolytes that aid in contaminant solubilization (National Research Council 2005; USEPA 2004).

Biodegradation

Considered as an emerging technology for treatment of source-zone contaminated areas, in situ bioremediation (ISB) is the use of microorganisms in the subsurface to degrade contaminants in place metabolically. In general, microbial metabolism requires a source

of carbon, an electron donor, an electron acceptor, appropriate nutrients, and suitable environmental conditions. The process is based on injecting electron donor substrates such as lactate into the subsurface, stimulating existing native microbes to degrade contaminants. Non-aboriginal microbes also have been introduced into the subsurface; this is referred to as bioaugmentation (ITRC 2008; USEPA 2004). The major advantage associated with in situ bioremediation is that the contaminants are destroyed largely in place, minimizing contaminant extraction to the surface for subsequent treatment or disposal (National Research Council 2005).

It was believed that high concentrations of contaminants in the source zone would be poisonous to microorganisms until the 1990's. Since then, many researchers have shown that microorganisms degrade the subsurface contaminants at high concentrations, and at a faster rate in the source area than in the plume (Moretti 2005). As with other source zone remediation methods, in situ bioremediation may reduce the duration for which a former MGP site remains impacted by contamination. Although complete remediation is not likely to be achieved in a short time period, by reducing the prolonged existence of contaminants above regulatory levels at a site, the risk of exposure and the cost of treatment often are significantly minimized (Moretti 2005).

Bioremediation processes take place during natural attenuation, which is considered as an appropriate remediation technology when it results in contaminants degrading more rapidly than they migrate, resulting in a stable or shrinking contaminant plume. When natural biodegradation occurs too slowly or is inhibited by a lack of substrates or

nutrients or by some other condition, enhanced bioremediation (Figure 2.5) is considered a suitable technology to follow and it engages stimulation of contaminant-degrading microorganisms within a subsurface aquifer by delivering chemical amendments to the contamination zone. Stimulation of microorganisms can be achieved by delivery of substrates, electron acceptors, and/or nutrients by means of subsurface injection or surface infiltration (National Research Council 2005). For remediation via natural attenuation to be a practical option, it is important to verify current attenuation of contaminants and understand the length of time required for these processes. Therefore, it is important to understand the factors controlling biodegradation as the primary mechanism for natural attenuation (Birak and Miller 2009). With the complex nature of biodegradation process and uncertainty involved in long term estimates, the development of multi-phase, multi-component groundwater flow and contaminant transport models becomes an important tool to appropriately understand the process complexity and to estimate time scales necessary for natural attenuation to achieve acceptable levels of contaminant concentrations as well as impacts on source reduction (Birak and Miller 2009).

2.7.2 Contaminant Plume Remediation

Figure 2.6 shows a simplified scenario of a tar contaminant source- plume system. After the DNAPL contaminant source is released into the aquifer, and before the contamination is discovered and cleanup efforts begin, the contaminant mass is transferred via dissolution from the DNAPL source into the contaminant plume. The factors affecting the mass release rate include the groundwater flow rate through the source area, which

could be impacted by the regional groundwater flow and flow induced by plume cleanup efforts, the spatial distribution of the contaminant mass and hydraulic conductivity distribution within the source area, and the chemical composition of the source. Once the contaminant mass has entered the plume via dissolution, the spatial and temporal behavior of the plume is again controlled by the groundwater flow rate and hydraulic conductivity distribution, and also attenuation factors, including dispersion, sorption and degradation reactions (Mayer and Endres 2007).

Although there is a tradeoff between the level of effort and funds dedicated to source remediation versus the cleanup of the groundwater plume originating from the source, plume remediation can begin at the same time as the DNAPL source removal, although it occurs over a much longer time period. Analytical solutions presented by Falta et al. (2005) show that partial DNAPL removal from the source zone likely leads to large reductions in plume concentrations and mass, and reduces the longevity of the plume. When the mass discharge from the source zone is linearly related to the DNAPL mass, it is shown that partial DNAPL source depletion leads to linearly proportional reductions in the plume mass and concentrations (Mayer and Endres 2007; Falta et al. 2005). Contaminant mass in the plume is removed via physical means (e.g. pump and treat) or biochemical means (e.g. bioremediation). In either case, since the source removal is likely to be incomplete, mass will continue to transfer from the source into the plume.

The amount of mass entering the subsurface after source removal is dependent on the efficiency of the source removal efforts and the physical and chemical properties of the source area (Mayer and Endres 2007).

In an attempt to study plumes from DNAPL contamination and assess the impacts of partial mass depletion, Falta et al. (2005) developed a power function source strength model coupled with a simple plume transport model that assumes steady homogeneous flow and retardation, but neglects hydrodynamic dispersion. Because the effects of dispersion are neglected, this model will tend to over-predict the actual plume concentrations at points directly downgradient of the source. More comprehensive analytical solutions that couple the full set of source functions with a flux-based advection dispersion model have been developed, and numerical based modeling programs are increasingly being used to provide more realistic plume scenarios (Falta et al. 2005).

2.8 Fate and Transport of Former MGP Site Contaminants and Estimation of Parameters for Modeling

The analysis of the fate and transport of site-related contaminants is critical to the evaluation of risk and the development of potential remedial alternatives. Coal tar as a major DNAPL contaminant is the most widespread subsurface contaminant detected at former MGP sites and moves in a complicated manner above and within saturated zones (USEPA 1991). Because of their relatively low solubility, high density, and relatively high viscosity, tar compounds at former MGP sites do not readily mix with the groundwater and remain as separate phases. Their high density provides a driving force that can carry them vertically until they pool above low permeability strata (USEPA 1991). However, the fate and transport of tar compounds is governed by many different factors such as tar chemical composition and physical properties (e.g. specific gravity and

viscosity), conventional groundwater transport mechanisms (advection, dispersion, sorption and biodegradation), soil characteristics (pore size distribution of subsurface soils), stratigraphic layer distribution and site lithology. For example, the properties that can affect the fate and transport of organic contaminants in groundwater are water solubility, vapor pressure, molecular weight, Henry's Law constant, and specific gravity. These properties can determine how contaminants behave under certain conditions and can be useful for evaluating the fate and transport of contaminants associated with a site, and for evaluating applicable remedial technologies (USEPA 2006). Changes in tar compositions in space and time, and changes in hydrogeologic systems are factors adding to the complexity of understanding contaminant transport at former MGP contaminated sites (Birak and Miller 2009).

2.8.1 Hydrogeologic Parameters

Investigating existing or possible groundwater pollution sources should include a sufficient characterization of site hydrogeology. Typically, an evaluation includes a three-dimensional assessment of the underlying geologic materials and the movements of groundwater within the aquifer (USEPA 2006). Hydrogeologic parameters such as groundwater seepage velocity, hydraulic conductivity, hydraulic gradient, storage properties, and hydraulic head records for a specific site are important data required as inputs for groundwater numerical modeling.

Seepage velocity ($\mathcal{V}_x$) is the average velocity at which the water flows through the interconnected soil pores. The hydraulic gradient (i) is the measure of the difference in

energy potential between two points which drives the flow of water through the aquifer material. It is expressed as a change in total hydraulic head divided by the distance along the flow path between the two points. Hydraulic conductivity (k), an aquifer property, can be defined as a measure of the ease with which a medium transmits water. Higher hydraulic conductivity values will have higher seepage velocities given a specified hydraulic gradient resulting in a more rapid solute transport (Schwartz and Zhang 2003). Effective porosity (n_e) is a dimensionless storage parameter that describes the percentage of volume of the aquifer material through which flow can occur. An increase in n_e increases the volume through which groundwater flow occurs and decreases the seepage velocity and the rate of solute transport (Ingebritsen and Sanford 1999).

The relationship between groundwater seepage velocity, hydraulic conductivity, hydraulic gradient and effective porosity is as follows:

$$v_x = \frac{k \, . \, i}{n_e} \qquad (2.3)$$

Where:

v_x = Groundwater seepage velocity (m/s)

k = Hydraulic conductivity (m/s)

i = Hydraulic gradient (m/m)

n_e = Effective porosity

Slug tests are usually used to measure in situ hydraulic conductivity at contaminated sites. The test involves instantaneous injection or withdrawal of a volume of water or a slug within a monitoring well casing and measurement of recovery or drawdown of the water level within the casing. In addition to the ability of performing the tests quickly at relatively low cost, another advantage is that hydraulic conductivity is measured while avoiding errors incurred in laboratory testing of disturbed soil samples (Nielsen 2006).

Specific storage (S_s) and specific yield (S_y) are material physical properties that characterize the capacity of an aquifer to release groundwater from storage in response to a decline in hydraulic head. For that reason they are sometimes referred to as "storage properties". For confined aquifers, the following mathematical formulas obtained from Schwartz and Zhang (2003) are used to calculate specific storage (Equation 2.4) and specific yield (Equation 2.5):

$$S_s = \rho_w.g\ (\beta_p+n\beta_w) \qquad (2.4)$$

Where:

S_s = Specific storage (1/m)

n = Porosity of the aquifer

ρ_w = Water density (1000kg/m^3)

g = Gravitational constant (9.81 m/s^2)

β_w = Compressibility of water (4.8 x 10^{-10} m^2/N)

β_p = Vertical compressibility of soil matrix (m^2/N)

$$S_y = \frac{V_{wd}}{V_T} \quad (2.5)$$

Where:

S_y = Specific yield

V_{wd} = Volume of water drained (m^3)

V_T = Total rock or material volume (m^3)

Table 2.6 obtained from Schwartz and Zhang (2003) lists specific yield values for different soils and some rock types.

2.8.2 Coal Tar Source Term

An understanding of coal tar dissolution and subsurface transport processes affecting contaminant movement plays an important role in former MGP source zone characterization, remediation and prediction of long-term plume behavior. The rate of contaminant dissolution to groundwater over time, for example, is a crucial factor governing the feasibility and effectiveness of engineered remediation or natural attenuation at former MGP sites (Xu and Wu 2011; Parker and Park 2004). Determining source-zone mass release flux has proven to be difficult, even in the case of single component models which simulate transport of contaminants from a single tar source in a confined aquifer unit or layer under the effect of one fate and transport process (e.g. biodegradation). This difficulty is directly related to the variability in tar composition and properties, especially the notable lack of data related to high molecular weight PAHs in studies of equilibrium dissolution, mass transfer, and biodegradation, and lack of

information on how tars might change spatially across a given site. There is clear uncertainty involved in such estimates along with the complexity of the subsurface systems being modeled (Birak and Miller 2009).

Herold et al. (2011), in conducting reactive transport model simulations for a former gasworks (MGP) site in Southern Germany, emphasized that their field data indicate substantial spatial and temporal variability of hydrogeochemical parameters. Further, their simulations highlight the uncertainties that result from the insufficient characterization of the hydrogeochemical heterogeneities and the complication in defining the tar source and dissolution of individual tar compounds which vary temporally and spatially. This is also accepted even for well-characterized systems and is likely to be more pronounced when models are applied to larger highly variable field sites. Despite the numerous simplifications made in their conceptualization and numerical modeling study of microbial dynamics, their models demonstrated the ability of a model-based analysis to detect key processes that can be crucial for assessing effectiveness of a remediation scheme (Herold et al. 2011).

D'Affonseca et al. (2008) studied the coal tar source composition by using three composite and two individual constituents in a source term definition as part of simulating contaminant release from a coal tar source zone using a three-dimensional steady-state groundwater flow model. The source zone model domain was defined such that it covered all locations where DNAPL was observed at monitoring well and direct-push locations and the entire lateral extent of the existing contaminant plume originating from the DNAPL source zone downgradient of the source area. The contaminant

concentrations for source term definition were determined using analysis of groundwater samples from wells that best correspond to the original coal tar composition at the site (D'Affonseca et al. 2008). The importance of coal tar source definition is demonstrated by the research conducted at the Canadian Forces Base (CFB) Borden site. The site is an example of a fairly well defined source composition with known mass/volume of the source placed for several field-based subsurface transport studies conducted over many years. The controlled spills and emplaced sources of various contaminants were also analyzed for testing a variety of remediation technologies (Sudicky and Illman 2011)

2.8.3 Contaminant Transport Parameters

The physical, chemical, and biological processes that reduce the contaminant concentration in groundwater include dilution, dispersion, sorption, volatilization, and biodegradation. Although each process has relative influence according to different specific conditions at different former MGP sites, when explicitly evaluated, and reasonably quantified, they can be considered with solute-transport models that integrate hydrogeologic, geochemical, and microbiological factors to predict future behavior of a tar contaminant plume (Zhang and Heathcote 2003). Further, the accuracy of modeling results rely heavily on the dispersion, retardation and biodegradation values used in the model. These parameters have a direct influence on the rate at which the contamination migrates through the subsurface (Zhang and Heathcote 2003). Following is a brief overview of the main processes and parameters affecting contaminant transport in the subsurface. Note that the effects of thermal processes and thermal gradients are not considered in this research study.

Mechanical Dispersion

Mechanical dispersion is the spreading of the dissolved contaminant front in the direction of groundwater flow (longitudinal) and in directions transverse to the direction of groundwater flow. It occurs due to variations in seepage velocity within the porous medium (Figure 2.7). Molecular diffusion is negligible compared to the dominant process of mechanical dispersion for an advecting dissolved contaminant mass. The mechanical dispersive flux can be expressed as:

$$J_{\mathbf{M}} = - D_m \, n \, \frac{dC}{dX} \qquad (2.6)$$

Where:

$J_{\mathbf{M}}$ = Mechanical dispersive flux (mg/m^2·s)

D_m = Mechanical dispersion coefficient (m^2/s)

n = Porosity

$\frac{dC}{dX}$ = Concentration gradient (mg/ m^4)

The mechanical dispersion coefficient (D_m) is assumed to be a function of seepage velocity (v_x) according to the following formula:

$$D_m = \alpha_x \, v_x^{\beta} \qquad (2.7)$$

Where:

D_m = Mechanical dispersion coefficient (m^2/s)

α_x = Longitudinal dispersivity of the porous medium in the direction of transport (m)

β = Empirically determined constant between 1 and 2

v_χ = Groundwater seepage velocity (m/s)

The two effects of hydrodynamic dispersion are dilution of contaminant concentrations and volume increase of the dissolved plume, therefore, contaminant concentrations in a sample obtained from a monitoring well downstream of a source zone may be significantly less than the aqueous solubility of the contaminant compound of interest (Alvarez and Illman 2006; Pretorius et al. 2008).

Due to the impracticability of measuring dispersion in the field, dispersivity values are often estimated for transport modeling based on plume length or travel distance of the contaminants. Gelhar et al. (1992) note that dispersivity values vary between two to three orders of magnitude due to natural variation in hydraulic conductivity. Therefore, dispersivity values can be estimated within a large range and still be within the range of real field values observed at former MGP sites (USEPA 2007).

For transport modeling purposes, the dispersivity estimates can be calculated using the following formulas recommended by the U.S. Environmental Protection Agency (2007):

$$\alpha_x = 0.83 \left[\log(L_p)\right]^{2.312} \qquad (2.8)$$

$$\alpha_t = 0.2\,\alpha_x \quad \text{and} \quad \alpha_v = 0.1\,\alpha_t \qquad (2.9)$$

Where,

α_x = Longitudinal dispersivity of the porous medium in the direction of transport (m)

L_p = Plume length (m)

α_t = Transverse dispersivity (m)

α_v = Vertical dispersivity (m)

Sorption and Retardation

Sorption refers to bonding of contaminant particles to soil mineral particle surfaces or to organic matter surfaces in the soil. This bonding is usually temporary and is accomplished through ionic exchange, ligand, dipole, hydrogen, or Van der Wall's bonds. Sorption causes aqueous concentrations of contaminants to be lower than expected at a certain time and location (Alvarez and Illman 2006; Liu and Liptak 2000).

Retardation refers to the effect of slowing the apparent contaminant velocity relative to the groundwater seepage velocity, and thereby increasing travel times between source and receptor. This may provide additional time for destructive attenuation processes to occur, or for alternative risk-management strategies to be developed (Smith and Lerner 2011). The commonly accepted equation used to calculate the retardation factor using bulk dry density, porosity, and the solute partition coefficient is described by Liu and Liptak (2000):

$$R_f = 1 + \frac{(\rho_b) \cdot K_d}{n} \qquad (2.10)$$

Where:

R_f = Retardation factor

ρ_b = Soil bulk dry density (g/L)

n = Porosity

K_d = Partition coefficient of the solute between adsorbed and dissolved phases (L/g)

With a limited solubility in water because of their nonpolarity and increasing molecular size, tar contaminant compounds dissolved in water results in a homogeneous solution regardless of the proportions that are mixed. Nonpolar organic compounds interact with soil organic matter through a process known as "hydrophobic sorption".

Organic molecules of increasing size, decreasing polarity and therefore decreasing water solubility, are said to exhibit increasing hydrophobicity, which can be quantified by the octanol-water partition coefficient (K_{ow}). It is a measure of the distribution of a chemical between water and an organic (octanol) phase with which it is in contact. The more hydrophobic the contaminant, the more likely it is to partition into the octanol phase. The octanol-water partition coefficient (K_{ow}) as a measurement of hydrophobicity can be used to determine the chemical-specific partition coefficient between soil organic carbon and the aqueous phase (K_{oc}). Larger values of (K_{oc}) indicate affinity of contaminants for the organic carbon fraction of soil (Alvarez and Illman 2006).

By measuring organic carbon content for soil samples collected during site characterization activities, the partition coefficient (K_d) can be estimated based on the soil

adsorption coefficient for soil organic carbon (K_{oc}) and the fraction of soil organic carbon (f_{oc}) as:

$$K_d = f_{oc} \cdot K_{oc} \qquad (2.11)$$

Where:

K_d = Partition coefficient of the solute between adsorbed and dissolved phases (L/g)

f_{oc} = Fraction of soil organic carbon

K_{oc} = Soil adsorption coefficient for soil organic carbon (L/g)

The soil adsorption coefficient for soil organic carbon (K_{oc}) for different classes of organic compounds can be correlated to the octanol-water partition coefficient (K_{ow}). Examples of such correlations are presented in Table 2.7 (Alvarez and Illman 2006). The retardation factor (R_f) obtained from Equation (2.10) can be expressed as:

$$R_f = \frac{\mathcal{V}_x}{\mathcal{V}_c} \qquad (2.12)$$

Where:

$\mathcal{V}_c$ = Velocity of a contaminant moving within groundwater (m/s)

$\mathcal{V}_x$ = Groundwater seepage velocity (m/s)

A high value of the retardation factor, in other words, high sorption, significantly retards the movement of contaminants in groundwater.

Biodegradation

Biodegradation is the most important subsurface destructive mechanism applicable to attenuation of dissolved contaminants at former MGP sites. It refers to the microbial breakdown of complex tar contaminants into simpler byproducts. The mechanisms of microbial degradation (biodegradation) include redox transformation (oxidation-reduction reactions), hydrolytic and other biotransformations not involving redox processes, such as hydrolysis and synthetic reactions. Most of the contaminants found at former MGP sites are degraded by oxidation-reduction reactions. The most common reaction is biodegradation, in which microorganisms consume energy from an electron transfer process during oxidation (Alvarez and Illman 2006).

The biodegradation rate coefficient (λ) is the parameter that describes the rate at which a contaminant is being degraded. One of the most commonly accepted expressions for representing the biodegradation of an organic compound involves the use of an exponential decay relationship which depends on the average time it takes for a typical contaminant compound to react (i.e. the half-life of a reaction). Therefore, first-order rate constants for MAHs and PAHs are often expressed in terms of a half-life time (first order kinetics) for a contaminant compound. The relationship between the half-life ($t_{1/2}$) and λ is: $t_{1/2} = \ln 2/\lambda = \frac{0.693}{\lambda}$.

Analytical fate and transport models usually describe biodegradation rates in a half-life or a first-order decay regime with respect to contaminant concentration (Alvarez and Illman 2006):

$$\frac{dC}{dt} = -\lambda \cdot C \qquad (2.13)$$

Where:

λ = Biodegradation rate coefficient (1/d)

$\frac{dC}{dt}$ = Concentration change with respect to time (mg/L·d)

C = Concentration of contaminant (mg/L)

There are several different methods to determine a site-specific λ. These methods include mass balances, the method of Buscheck and Alcantar, normalization of contaminant concentrations to those of a recalcitrant contaminant that was present in the initial release, the use of in situ microcosms and direct push tests (Alvarez and Illman 2006; Zhang and Heathcote 2003).

Based on an analytical solution for one-dimensional, steady-state contaminant transport, the method of Buscheck and Alcantar (1995) is frequently used to determine the biodegradation rate coefficient according to the following equation:

$$\lambda = \left(\frac{v_c}{4\alpha_x}\right) . \left\{\left[1 + 2\alpha_x\left(\frac{\mathcal{K}}{v_x}\right)\right]^2 - 1\right\} \qquad (2.14)$$

Where:

λ = Biodegradation rate coefficient (1/d)

$\mathcal{V}_c$ = Velocity of a contaminant moving within groundwater (m/s)

α_x = Longitudinal dispersivity of the porous medium in the direction of transport (m)

$\mathcal{K}$ = Bulk attenuation rate (1/d)

$\mathcal{V}_\mathcal{X}$ = Groundwater seepage velocity (m/s)

In addition to defining longitudinal dispersivity and contaminant retarded velocity, to determine the biodegradation rate coefficient using this approach, a negative slope of a regression line can be obtained from a log-linear plot of the contaminant concentration versus distance downgradient along the plume centerline flow path corresponding to the $\left(\frac{\mathcal{K}}{\mathcal{V}_x}\right)$ part of the equation (Alvarez and Illman 2006).

Stenback et al. (2004) estimated first-order degradation rate constants that include degradation in both the aqueous and solid phases unlike the method by Buscheck and Alcantar (1995) in which the solid phase and aqueous phase degradation rate constants are arbitrarily assumed to be equal. A 2-D analytical model was utilized to simulate dissolved contaminant plumes using a least squares fitting of selected model parameters to minimize the differences between the observed data and the modeled concentrations. Data from all monitoring wells downgradient of the source area were utilized in their model fitting exercise to account for transverse dispersivity (Stenback et al. 2004).

Bulk Attenuation Rate

The overall impact of natural attenuation processes at a given site can be assessed by evaluating the rate at which contaminant concentrations are decreasing either spatially or temporally. Estimated from plotting concentration versus distances, bulk attenuation rate constants ($\mathcal{K}$) are used for estimating if a plume is expanding, showing relatively little change, or shrinking due to the combined effects of dispersion, biodegradation, and other attenuation processes (Newell et al. 2002).

For many BTEX plumes, $\mathcal{K}$ will be similar to λ (within a range of 0.001 to 0.01 per day) as the effects of dispersion and sorption will be small compared to biodegradation (Newell et al. 2002). On the other hand, the main processes affecting the attenuation of PAH compounds are sorption and biodegradation as indicated by Rogers et al. (2002). Rogers et al. (2002) also indicate the lack of understanding of some former MGP contaminant related characteristics such as the solubility and dissolution of contaminants, the interactions and effects of the more soluble low molecular weight contaminants on the sparingly soluble high molecular weight contaminants, and the utilization of electron acceptors other than oxygen during microbial degradation of PAHs under complex mixture conditions.

If compound-specific total mass fluxes (M_d) have been quantified at different distances from the source zone and if the average travel time between two existing control planes is known, it is possible to quantify the bulk attenuation rate ($\mathcal{K}$) using the following formula (Bockelmann et al. 2003):

$$\mathcal{K} = -\ln\left(\frac{M_{d2}}{M_{d1}}\right)\frac{1}{t} \qquad (2.15)$$

Where:

$\mathcal{K}$ = Bulk attenuation rate (1/d)

M_{d2} = Compound-specific mass flux at control plane 1 (g/d)

M_{d1} = Compound-specific mass flux at control plane 2 (g/d)

t = Average time travel of contaminants between the two control planes (d)

Equation 2.15 assumes constant contaminant mass fluxes from the source zone and equilibrium conditions for sorption process (i.e. R_f = 1). With a linear sorption assumption, the time component of Equation 2.15 needs to be adjusted with the value of the retardation factor for the contaminant compound being measured.

2.9 Flux Based Site Management Principles

The goal of groundwater remediation is to reduce the risk posed to human and environmental receptors by contaminants in the subsurface. Therefore, when cleaning up a source of groundwater contamination or evaluating the movement of contaminants in a groundwater plume, the focus should be on the contaminant concentration as well as the rate with which contaminant mass is transported toward receptors, known as the contaminant mass flux (Yoon 2008). Flux-based site management is a new approach that has been developed and implemented to characterize, manage, and remediate contaminated sites at which mass discharge and flux estimates are used to quantify source or plume strength at a given time and location (Annable et al. 2008).

Consideration of the strength of a source or solute plume (i.e., the contaminant mass moving in the groundwater per unit of time) improves evaluation of natural attenuation and assessment of risks posed by contamination to downgradient receptors, such as supply wells or surface water bodies. Therefore, considering contaminant mass discharge and mass flux can improve former MGP contaminated site remediation decisions. Flux-based management is not used normally as an exclusive source of information, instead, common experience is to measure mass flux and discharge at a site to improve the overall conceptual site model (CSM) for a better understanding of the potential risks and to help managers identify the highest-priority segments of a site (ITRC 2010).

For contaminant fate and transport modeling purposes, boundary conditions are normally specified in terms of contaminant concentrations and/or fluxes. Being able to measure contaminant flux is critical to the ability of properly quantifying a source term in a proposed model, thereby allowing simulation of contaminant fate and transport at a specific site. Appropriate quantification of the source flux will result in improved modeling simulations and eventually, better management decisions at any former MGP contaminated site (Goltz et al. 2007).

By definition, mass flux is specific to a defined area, and when used for contaminant plumes, the area that is sampled to determine mass flux is usually small compared to the overall dimensions of the plumes. Furthermore, the critical issue is not the mass flux across some particular subsurface area at a former MGP site. Rather, it is the total mass transmitted by the plume to some point along its length. Hence, a common objective is to

measure the mass discharge "total mass flux" across the entire plume, which can be estimated by measuring contaminant concentrations and groundwater fluxes along a monitoring well transect perpendicular to groundwater flow. Mass flux is expressed as mass/time/area (e.g. g/d/m^2). On the other hand, mass discharge is an integrated mass flux estimate (the sum of all mass fluxes measured across an entire plume) and thus represents the total mass of any solute conveyed by groundwater through a defined plane. Mass discharge is therefore expressed as mass/time. The three basic methods to measure mass flux and/or mass discharge are the transect method, well capture/pump test method and passive flux meters. For the transect method, individual monitoring points (i.e. wells) distributed in planes along the length of a contaminant plume are used to integrate concentration and flow data to compute the mass flux (Figures 2.8 and 2.9). This method is based on the assumption that the hydraulic conductivity and hydraulic gradient are constant across a control plane (Annable et al. 2008; ITRC 2010).

2.9.1 Monitoring Well Control Planes - Transect Method

A control plane is composed of a number of monitoring wells located along a plane perpendicular to the groundwater flow direction that cuts across the contaminant plume. Control planes can be installed along the length of the plume. The purpose of these control planes is to allow measurement of the mass flux and changes in mass flux along the length of the contaminant plume. A single-screen monitoring well or multi-level groundwater monitoring wells can be utilized to collect groundwater samples at various points in control planes (Figure 2.8). As described in section 2.6 and shown in Figure 2.4 the monitoring well configuration should cover the entire width and depth of the plume in

order to determine total contaminant mass discharge through the control planes and also include background, source and compliance and contingency monitoring wells. This, however, is not possible at most former MGP sites given the limited number of available monitoring wells due to economic or geologic reasons (Bocklemann et al. 2003; Goltz et al. 2007). Monitoring well transects (control planes) are used to measure the contaminant flux at different locations along the contaminant plume (Figure 2.8). Typically the first control plane is located immediately downgradient of a coal tar source zone, while other control planes are located downgradient at reasonable interval distances to reduce uncertainty of characterizing the plume trends (Wood 2008).

2.9.2 Mass Flux Calculations

With a control plane area just large enough to completely inscribe the dissolved plume width (Figure 2.8), the cross sectional area of the plane is divided into subareas representing different concentration values measured at different depths (Figure 2.9) to determine the mass flux for each well. Flux can be determined for each local area through multiplying contaminant concentration from a groundwater sample collected from the monitoring well by the groundwater discharge velocity. The total flux at the control plane can then be computed by summing all the local fluxes (Rao 2008). The total contaminant mass flux across a transect is calculated as follows:

$$M_d = \sum_{i=1}^{i=n} \mathrm{C}_i \, q_i \, A_i \qquad (2.16)$$

Where:

M_d = Total mass flux (mass discharge) across the transect (g/d)

C_i = Concentration of constituent at flow area in transect (mg/L)

q_i= Specific flow area discharge associated with an individual measurement i (m/s)

The specific flow area discharge (q_i) can be calculated using Darcy's Law:

$$q_i = k \cdot i \qquad (2.17)$$

Where:

k = Hydraulic conductivity (m/s)

i = Hydraulic gradient (m/m)

A conversion factor is applied to Equation 2.16 to obtain mass flux in units of g/d.

2.9.3 Assessment of Attenuation Rate from Mass Flux Measurements

Measuring changes in mass flux are useful in the sense of determining natural attenuation as well as evaluating the effectiveness of a remediation technology. Several researchers reported that mass flux measurement is a powerful tool that can be used to evaluate natural attenuation at contaminated former MGP sites (Bockelmann et al. 2001; Zamfirescue and Grathwohl 2001; Rogers et al. 2002; Neuhauser et al. 2009). In the paper by Goltz et al. (2007), Borden et al. (1997) used mass flux measurements to demonstrate methyl tert-butyl ether (MTBE) and BTEX natural attenuation in a shallow aquifer contaminated by leaking underground storage tanks that contained gasoline and diesel fuel. Flux measurements demonstrated that natural attenuation was higher near the source area than downgradient and that natural attenuation of the BTEX compounds was

greater than natural attenuation of MTBE (Goltz et al. 2007).

The work by Zamfirescue and Grathwohl (2001) focused on the identification of recalcitrant compounds and determining contaminant attenuation rates using point concentrations along the plume centerline. MAHs were found to be degrading at the highest rate and the degradation rates decreased with increase in the number of carbon atoms in alkyl chains. Bockelmann et al. (2001) developed an integral groundwater investigation approach to quantify natural attenuation rates at field scale. In their approach, monitoring wells were installed along two control planes perpendicular to the mean groundwater flow direction at specific distances downstream of a contaminant source zone at a former MGP site in the Neckar valley near Stuttgart, Germany. BTEX and PAH compounds were detected on site. At the control planes, compound-specific concentrations were measured from groundwater samples and mass fluxes were estimated and used for the estimation of first-order natural attenuation rates. To derive the relative contribution of contaminant degradation and sorption on mass flux reduction between the control planes, Bockelmann et al. (2001) recommended integrating the groundwater investigation with numerical reactive transport modeling which explicitly simulates the attenuation of contaminant compounds. Equation 2.15 was used by Bockelmann et al. (2001) to estimate the natural attenuation rates from quantified mass fluxes between control planes. Then, an analytical solution with simplified assumptions was applied to estimate contaminant mass fluxes using a relatively small number of monitoring wells. With comparison of results, Bockelmann et al. (2001) recommended utilizing numerical flow and transport models that include spatially variable aquifer properties, asymmetrical

well capture zones, retardation, specific boundary conditions and other site specific factors into mass flux calculation.

2.10 Visual MODFLOW

Developed by Schlumberger Water Services, Visual MODFLOW is a computer- based modeling program that is capable of producing 3-D groundwater flow and contaminant transport simulations. It combines MODFLOW, a 3-D finite-difference groundwater flow engine with MODPATH, a 3-D particle-tracking engine that computes the path a particle takes in a steady state or transient flow field over a given time period and MT3DMS, a three-dimensional transport engine that solves coupled partial differential equations describing reactive-flow and transport of multiple mobile and/or immobile species in a 3-D saturated porous media (Schlumberger Water Services 2010). This integrated modeling environment has the capability for the user to graphically design the model grid, to visualize the model input parameters and boundary conditions in two or three dimensions, to run the groundwater flow, pathline and contaminant transport simulations. It is also capable of automatically calibrating the model using the WINPEST component of the program, and to display and interpret the modeling results in three-dimensional space using the Visual MODFLOW 3-D explorer (Kumar 2006).

2.10.1 Groundwater Flow Modeling

Numerical models are used to simulate the rate and direction of groundwater flow through the subsurface. This requires a comprehensive understanding of the hydrogeologic system and other modeling input parameters. With a 3-D finite difference

formulation, Visual MODFLOW simulates steady and non-steady flow patterns in irregularly shaped flow systems with aquifers being confined, unconfined, or a combination of both aquifer types (Biyani 2003; USEPA 2007).

The Visual MODFLOW menu structure allows editing and refining the model domain, selecting units, conveniently assigning model properties and boundary conditions, running groundwater model simulations, calibrating the model, and visualizing the results with line contours or color shading. The model grid, input parameters and results can be visualized in cross-section or plan view at any time during the development of the groundwater flow model or while displaying the results (Schlumberger Water Services 2010).

To produce groundwater model simulations, Visual MODFLOW utilizes a numerical solution for the following equation that governs groundwater flow (Arlen et al. 2000):

$$\frac{\delta}{\delta x}\left[k_{xx}\,\frac{\delta h}{\delta x}\right] + \frac{\delta}{\delta y}\left[k_{yy}\,\frac{\delta h}{\delta y}\right] + \frac{\delta}{\delta z}\left[k_{zz}\,\frac{\delta h}{\delta z}\right] + W = S_s\,\frac{\delta h}{\delta t} \qquad (2.18)$$

Where:

k_{xx} , k_{yy} , k_{zz} = Hydraulic conductivity along x, y, and z coordinates (m/s)

h = Hydraulic head (m)

W = Volumetric flux per unit volume (sources and/or sinks of water) (1/s)

S_s = Specific storage (1/m)

t = Time (s)

The outputs from model simulations include hydraulic heads and groundwater flow rates, which are in equilibrium with hydrogeologic conditions (boundaries, initial and transient conditions, hydraulic properties, and sources or sinks) for the modeled area. Models can also be used to simulate possible future changes to hydraulic head or ground water flow rates as a result of future changes in stresses on a ground water zone (USEPA 2007).

2.10.2 Contaminant Transport Modeling

Developed by Zheng and Wang in June 1998 for the US Army Corps of Engineers, MT3DMS is a modular three-dimensional multi-species transport engine for simulation of advection, dispersion, and chemical reactions of contaminants in groundwater systems. The following general equation that describes the fate and transport of aqueous phase species is solved (Kurniawan and Jinno 2006):

$$\frac{\delta}{\delta t}\left(\mathrm{C}_k\right) = \frac{\delta}{\delta x_i}\left[\mathrm{D_{ij}}\frac{\delta\,\mathrm{C}_k}{\delta x_j}\right] - \frac{\delta}{\delta x_i}\left(V_i'\,\mathrm{C}_k\right) + \frac{q_s}{\theta}\mathrm{C}_k' + r_k \qquad (2.19)$$

Where: k = 1, 2…m

m = Total number of aqueous species

C_k = Aqueous phase concentration of the k^{th} species (g/L)

C_k' = Solid-phase concentration of the k^{th} species (g/L)

$\mathrm{D_{ij}}$ = Hydrodynamic dispersion coefficient (m^2/s)

V_i' = Pore velocity = seepage velocity, $\mathcal{V}_x$ (m/s)

q_s = Volumetric flux of water per unit volume of aquifer sources and sinks (1/s)

r_k = Reaction rate ($g/m^3/s$)

θ = Porosity.

MT3DMS contains the following components (Schlumberger Water Services 2010):

- A third-order total-variation-diminishing system for solving the advection term, which is an iterative solver based on generalized conjugate gradient methods and the Lanczos/ORTHOMIN acceleration scheme,
- Options for accommodating non-equilibrium sorption and dual-domain advection-diffusion mass transport, and
- A multi-component program structure to accommodate add-on reaction packages.

The basic chemical reactions included in the MT3DMS model are equilibrium-controlled or rate-limited linear or non-linear sorption, and first-order irreversible or reversible kinetic reactions. MT3DMS can accommodate very general spatial discretization schemes and transport boundary conditions including: confined, unconfined or variably confined/unconfined aquifer layers; inclined model layers and variable cell thickness within the same layer; specified concentration or mass flux boundaries; and the solute transport effects of external hydraulic sources and sinks such as wells, drains, rivers, areal recharge and evapotranspiration (Zheng and Wang 1999).

2.10.3 Calibration of Model Including Use of PEST

The calculated hydraulic head values produced by the groundwater flow model with initial boundary conditions and subsurface properties usually do not match the observed head values measured onsite. Groundwater flow model output from Visual MODFLOW includes a “Calculated Vs Observed Head” plot that can be used to determine how close the simulated hydraulic heads are to the observed hydraulic head inputs at monitoring

well locations in the model domain. Calibrating the model by varying the values of the model input parameters in an attempt to match field conditions within acceptance criteria is an important part of the modeling process. This requires that field conditions at a site be properly characterized. Lack of proper site characterization may result in a model that is calibrated to a set of conditions which are not representative of actual field conditions (USEPA 2007).

Automated calibration using Non-Linear Parameter Estimation and Predictive Analysis (PEST) is frequently used to minimize the discrepancy between model results and field observation values. WINPEST, a fully functional version of the PEST program, is a statistical engine built into the Visual MODFLOW modeling environment to aid calibration of the groundwater flow model. WINPEST can be used to adjust the hydrogeologic parameters in order to reduce the average of hydraulic head residuals. Therefore, during the calibration process, it is recommended to focus on varying the hydraulic conductivity values and recharge rates gradually. Further, it is always best to start the calibration simply by varying one parameter only, and increase the complexity only if needed (Doherty 2005; Schlumberger Water Services 2010).

In addition to matching simulated hydraulic heads and field-observed hydraulic head values, groundwater flow calibration iterations should include comparison of the simulated groundwater flow direction and the groundwater flow direction interpreted from observed site data. Contaminant concentrations, migration rates and plume

directions can be calibrated with realistically varying contaminant transport parameter values at the input platform of Visual MODFLOW.

2.10.4 Particle Tracking

Modpath is a component of Visual MODFLOW which uses the calculated hydraulic heads and the flow terms within the domain cells in addition to the soil porosity to compute the movement of particles released from an assumed source zone under the sole effect of the advection process throughout the modeled area. It uses a semi-analytical particle-tracking scheme. The method is based on the assumption that each directional velocity component varies linearly within a grid cell in its own coordinate direction. This assumption allows an analytical expression to be obtained describing the flow path within a grid cell. Given the initial position of a particle anywhere in a cell, the coordinates of any other point along its path line within the cell and the time of travel between them can be computed (Biyani 2003; Schlumberger Water Services 2010).

An area or line of particles can be placed at the source-zone area within the model domain to examine the routes contaminants will follow towards potential receptors. The output of Modpath can be displayed in the pathlines map which defines the flow path and travel time of particles due to advective groundwater flow. Pathlines represent a historical travel log of the groundwater particles. Forward tracking pathlines are used to predict where groundwater is flowing, and how long it will take to reach a given location if it starts from a known location at a known time. Backward tracking pathlines are used to predict where groundwater at a given location and time is coming from, and how long it took to get there (Schlumberger Water Services 2010).

2.11 Summaries of Relevant Case Studies

Following are summaries of key former MGP site case studies with a focus on remediation technologies such as natural attenuation, as well as field scale characterization and modeling the migration of contaminants from a coal tar source zone.

2.11.1 Case Study 1

Former MGP site in Neckar Valley, Southern Germany:

Zamfirescu and Grathwohl (2001) investigated the contaminant varying characteristics in relation to the travelled distance in the anaerobic groundwater plume downstream from an extended zone containing residual NAPL at a former MGP situated in the Neckar Valley, Germany. The study showed there are many aromatic compounds apart from the usual expected BTEX and PAH compounds present in the plume and need to be taken into account when studying the overall groundwater contamination. According to Zamfirescu and Grathwohl (2001), the overall groundwater contamination in the plume can be seriously underestimated if only BTEX and PAHs are monitored. For example, O- and N-heterocyclic aromatic compounds are enriched with increasing distance in the plume relative to the usually assessed coal tar constituents (MAHs and PAHs). These compounds are found to be original coal tar constituents or their degradation products, and many of them are toxic and still present in high concentrations even after long distances down-gradient from the contaminant source. Therefore, an aim of the study was to identify those recalcitrant compounds and determine their attenuation rates using point concentrations along the plume centerline. It was noted that almost all compounds investigated are attenuated in the groundwater plume at different rates and the overall

attenuation of most compounds along the plume centerline could be described as a first order decay process. MAHs were found to be degrading at the highest rate and the degradation rates decreased with increase in the number of carbon atoms in alkyl chains. Degradation rates for benzene and related MAHs (methyl-indene, acridine, methyl-quinolinol and methyl benzofuran) were in range of 0.013 to 0.068 (1/d). Finally, the paper concluded that for heterogeneous systems it is advisable to rely on integral groundwater investigations, as in such systems, conclusions based on point measurements are expected to be influenced by the well positioning off the plume centre line and by heterogeneous flow fields.

Bockelmann et al. (2001) and (2003) demonstrated the applicability of using limited monitoring wells to determine field scale attenuation rates and utilized a new integral groundwater investigation approach to quantify natural attenuation rates at field scale. They calculated the contaminant mass fluxes at four pumping wells positioned along two control planes perpendicular to the mean groundwater flow direction at distances of 140 and 280 m downgradient of a contaminant source zone at the Neckar Valley former MGP site. Reduction of contaminant mass with transport distance from the source, together with an increase of dissolved iron (Fe^{2+}) mass flux and a reduction in sulfate mass flux, all indicated the presence of microbial degradation activity. Therefore, it was assumed that the contaminant plumes are biodegraded under anaerobic conditions. Based on the quantified changes in total contaminant mass fluxes and the average non retarded groundwater travel time between the two control planes, first-order natural attenuation rate constants were calculated. The attenuation rates for BTEX compounds (benzene, toluene, ethylbenzene, o-xylene and p-xylene) ranged from 0.014 to 0.13 (1/d) and for

PAH compounds (naphthalene, acenaphthene, fluorene, anthracene, fluoranthene and pyrene) the attenuation rates ranged from 0.00037 to 0.031 (1/d).

Herold et al. (2011), at the same former MGP site located in the Neckar River, used a reactive transport model to analyze the fate of a contaminant plume containing acenaphthene, methylbenzofurans and dimethylbenzofurans prior to applying an active remediation scheme and to analyze an enhanced remediation experiment during which oxygen (O_2) and hydrogen peroxide (H_2O_2) were added to the contaminated groundwater through a recirculation well. The numerical model developed by Herold et al. (2011) considered the primary contaminant microbially mediated degradation redox reactions as well as secondary and competing mineral precipitation/dissolution reactions that affect the site's hydrochemistry and contaminant fate. The model was calibrated using a variety of constraints to test the uncertainty on model predictions resulting from the undocumented presence of reductants such as pyrite.

To illustrate the effect of the reductive minerals on the effectiveness of the remediation scheme, Herold et al. (2011) carried out comparative simulations for two alternative conceptual models where pyrite, acting as the model reductant, was either present or absent in the aquifer. For the investigated scenarios the calibrated aerobic degradation constants differed considerably between the two alternative conceptual models, as pyrite consumed a significant fraction of the injected oxidation capacity. This shows that enhanced natural remediation via O_2/H_2O_2 injection is highly sensitive to the reductive capacity of the aquifer, in other words, to the concentrations and reactivity of reductants

such as pyrite or sedimentary organic matter. This conclusion highlights the important role of reactive transport modeling in the development of a comprehensive process understanding. Despite the numerous simplifications made in the conceptualization and numerical modeling of microbial dynamics, the Herold et al. (2011) modeling study demonstrated the ability of a model-based analysis to detect key processes that can be crucial for the effectiveness of an enhanced natural attenuation remediation scheme.

2.11.2 Case Study 2

Field Scale Characterization and Modeling of Contaminant Release from a Coal Tar Source Zone:

A coal tar contaminated site located 40 km south of the city of Hamburg in Buchholz, Germany used to be a former wood treatment plant that operated from 1904 to 1986. D'Affonseca et al. (2008) noted that the site was characterized using traditional and innovative investigation methods. The study followed careful interpretation of hydrogeological and hydrogeochemical data allowing for the conceptualization of the heterogeneous coal tar distribution in the subsurface. Past and future contaminant release from the coal tar source zone was calculated using a modeling framework consisting of a three-dimensional steady-state groundwater flow model (MODFLOW) and two MIN3P hydrogeochemical models. Computational time of long-term simulations was reduced by simplifying the coal tar composition using 3 composite and 2 individual constituents and sequential application of a 2-D centerline model (for calibration and predictions) and a 3-D model (only for predictions). Predictions were carried out for a period of 1000 years.

The results reveal that contaminant mass flux is governed by the geometry of zones containing residual coal tar, amount of coal tar, its composition and the physicochemical properties of the constituents. The long-term predictions made using the 2-D model show source depletion will be small with respect to phenanthrene of which 89% initial mass will be still available after 1000 years, and for the moderately and sparingly soluble composite constituents, 60% and 98%, respectively after the same time period. Both the 2-D and 3-D source depletion model simulations indicate that only the mass fluxes of naphthalene and its high solubility constituents have achieved the maximum after a 60 year simulation time and follow a decreasing trend. Time series of naphthalene concentrations also indicate a decreasing trend of concentrations in a few wells located downgradient of the source zone.

D'Affonseca et al. (2008) concluded that partial source removal will have only a minor impact on the total lifetime of the contamination and might slightly reduce the total mass flux and the length of the contaminant plume. Hence, monitored natural attenuation (MNA) is currently applied as an appropriate remediation strategy for the site due to the identified immobile condition of the contaminant plume and the active bioremediation in the plume.

Landmeyer et al. (1998) assessed the natural attenuation of MAHs in shallow anaerobic groundwater near a former MGP site located in Charleston, South Carolina, U.S. A combination of field, laboratory, and numerical flow and transport model investigations were made to assess natural attenuation processes affecting the contaminant distributions.

Adsorption isotherm experiments were run for naphthalene, toluene and benzene using the Schwarzenbach and Westall (1981) method and microbial degradation rates were determined by quantifying the production of radio-labeled $^{14}CO_2$ over time from a known amount of uniformly labeled ^{14}C-napthalene, ^{14}C-toluene and ^{14}C-benzene added to microorganism incubations at the aquifer. The laboratory measured adsorption coefficients were determined as 10 L/kg for toluene and 137 L/kg for naphthalene. The first order biodegradation rates of toluene, benzene and naphthalene in aerobic and anaerobic aquifer environments were found to be 0.84, 0.002, 0.03 (1/d) and 0.00014, 0.88 and 0.000046 (1/d), respectively.

Numerical-model simulations that incorporated field and laboratory measurements accurately depicted naphthalene, toluene, and benzene transport from the time of release in the mid-1800s to current conditions. Predictive simulations of toluene and benzene indicate that maximum distances of toluene and benzene transport have been primarily limited by intrinsic bioremediation (natural attenuation), and that the concentration distribution of benzene is at steady state. Landmeyer et al. (1998) relate the differences in MAH and PAH behavior in part to differences in the rates of microbial degradation of naphthalene (PAH), toluene, and benzene (MAHs) in aquifer sediments.

2.11.3 Case Study 3

Borden Site Emplaced Creosote Source Zone Experiments:

A site at the Canadian Forces Base (CFB) Borden, located approximately 80 km northwest of Toronto, Ontario, has been subject to several field-based studies of

subsurface contaminant transport conducted over many years. The field research initially consisted of extensive monitoring and analytical and numerical modeling of a leachate plume from an abandoned landfill. Sources of contaminants were then emplaced to observe their subsurface movement, distribution and for testing various remediation technologies (Sudicky and Illman 2011).

In August of 1991, 74 kg of coal tar creosote was mixed with 5800 kg of sand and emplaced in two 1.5 m deep, 2 m wide and 0.5 m thick blocks oriented perpendicular to the groundwater flow. The blocks were placed 1 m apart and 0.5 to 1.5 m below the water table. Sand coarser than Borden sand was used to ensure hydraulic conductivity was not decreased by the addition of creosote. The creosote source was placed upgradient of an existing monitoring network that was installed in the early 1980s for a previous plume study. The evolution of plumes from the coal tar creosote source has been monitored and the distribution of the contaminants was determined over a ten year period using an extensive multilevel monitoring network with up to 2400 samples being collected. Soluble chemicals (e.g. phenol) were rapidly leached from the source and biotransformation caused essentially complete attenuation of the soluble chemicals within 600 days. Plumes of less soluble chemicals (e.g. xylene) appeared to contract and were essentially completely attenuated within 1000 days. Among the dissolved contaminants, naphthalene, formed the largest plume and was found to be the dominant dissolved compound. A funnel-and-gate remedial system was implemented at the site to control naphthalene migration. Subsequently the naphthalene plume began to shrink as the rate of biotransformation exceeded the rate of naphthalene dissolution from the source (Sudicky and Illman 2011; Martin et al. 2002).

The release and transport behavior of naphthalene, m-xylene, phenol, phenanthrene, dibenzofuran, 1-methyl naphthalene, carbazole, biphenyl, fluorine, anthracene and acenaphthene plumes was studied by Fraser et al. (2008). They found that a model developed for multi-component source dissolution based on Raoult's Law adequately predicted the dissolution of nine of the eleven examined tar creosote compounds. It was documented that mass transformation limited the extent of the plumes. Some compound plumes reached an apparent steady state (e.g. naphthalene) while plumes of the other compounds (e.g. dibenzofuran and phenanthrene) continued to expand due to an increasing mass flux and limited degradation. Through the long term monitoring, Fraser et al. (2008) found that biotransformation was the major process controlling natural attenuation at the site. The greatest organic mass lost was linked to the high solubility and low partitioning coefficient compounds. However, the majority of the mass loss for most compounds occurred in the source zone at less than residual saturation. Although the complex evolution of the plumes has been well documented in their research study, it was concluded that understanding the controlling biotransformation processes is still unclear.

2.11.4 Case Study 4

Monitored Natural Attenuation of Former MGP Tar MAHs and PAHs in Groundwater:

Neuhauser et al. (2009) describe a 14-year study of dissolved MAH and PAH plumes created by the disposal of former MGP tar into a shallow sandy aquifer located in upstate New York in South Glens Falls. In the summer of 1991, 15,000 tons of tar-impacted soil representing the source area was removed, and clean soil was backfilled into the excavation. Following source removal, the 14-year ground water study was

implemented to evaluate MNA of the plumes with the source removed. A network of 32 monitoring wells was installed along six transects set perpendicular to the longitudinal axis of the plume centerline. Screen lengths were selected to intercept the groundwater in discrete layers so that higher concentration zones were defined with at least three different well screens (one above, one below, and one within the highest concentration zone). MAH and PAH samples were collected over the 14-year period and shipped to laboratories for analysis. Naphthalene was found to decrease to less than 99% of the original dissolved mass, with degradation rates of 0.00082 (1/d). Bulk attenuation rate constants for plume centerline concentrations over time ranged from 0.000904 (1/d) for toluene and 0.00132 (1/d) for naphthalene. The collective evidence of decreased groundwater concentrations, shrinking areal extent of the plume, contaminant mass reduction, and point decay rates demonstrates that MNA is a viable remedial strategy once the source area is removed.

Product	Time period	Process	Tar properties and composition
Coal gas (coke plants)	1800s–1918	Bituminous coal was heated in beehive ovens to create coke. Coal gas was not captured.	Negligible tar production.
	1892–1918	Facilities upgraded to by-product coke ovens, allowing the capture of off-gases and operating from 850–900 °C.	Primarily unsubstituted aromatic compounds. Contain tar acids, tar bases. Water content 3–7%.
Coal gas (gas plants)	Before 1850	Bituminous coal was heated in cast iron horizontal retorts from 600–800 °C.	Similar to coal tar from carbonization. Lower temperatures resulted in more heterocyclics and tar acids.
	After 1850	Facilities switched to clay retorts allowing temperatures > 900 °C.	Higher temperatures resulted in more aromatics and less acids.
	After 1910	Facilities switched to vertical retorts. Operating temperatures lower than horizontal retorts.	More heterocylics. Tar acids 5–10%.
Carburetted water gas	Before 1910	Coke or anthracite coal was heated in the presence of steam. Oil was sprayed into emissions to crack the oil. Oil was predominantly paraffinic.	Primarily aromatics. Absent of tar acids and bases. Water content 50–90% but easily separated.
	After 1910	Most facilities switched to heavier, asphaltic oils mostly from Texas.	Higher density. 68% of these facilities reported problems separating emulsions.
	1910–1930	Many facilities switched to bituminous coal.	Higher density. 100% of these facilities reported problems separating emulsions. Composition more closely resembled coal tar.
Oil gas	After 1940	Many facilities forced to use heavy fuel oil fractions. Oils were heated to crack hydrocarbons into smaller molecules.	Higher density and continued difficulty separating emulsions.
	Before 1919	Mostly used in the West. Used raw crude.	Primarily aromatics. Almost no tar acids and bases. Some problems with emulsions.
	After 1919	Facilities forced to use heavier residual oil.	Increased emulsions. More difficult to break.

Table 2.1: Impact of manufactured gas process on tars produced in the U.S. (Birak and Miller 2009).

By-product or Waste	Coal Carbonization	Carburetted Water Gas	Oil Gas
Coal Tar	X	X	-
Oil Tar	-	X	X
Lampblack	-	-	X
Tar/Oil/Water Emulsions	-	X	X
Tar Decanter Sludge	X	-	-
Ammonia Saturator Sludge	X	-	-
Acid/Caustic Hydrocarbon Treatment Sludges	X	-	-
Wastewater Treatment Sludges	X	X	X
Coke	X	-	-
Ash	X	X	X
Spent Oxide/Lime	X	X	X
Sulfer Scrubber Blow Downs	X	X	X
Ammonium Sulfate	X	-	-

Table 2.2: Wastes or by-products from different gas manufacturing processes (Biyani 2003)

Tar	Type	Specific gravity	Kinematic viscosity	Engler viscosity	Dynamic viscosity
		15.5/15.5 °C	35 °C cSt	40 °C	35 °C cP
Coal	VR	1.103	237		$2.6 \cdot 10^2$
	CO	1.180	316		$3.7 \cdot 10^2$
	CO	1.196		163	$2.0 \cdot 10^3$
	CO	1.198			$1.4 \cdot 10^3$
	CO	1.226	2850		$3.5 \cdot 10^3$
	HR	1.240			$1.6 \cdot 10^3$
	HR	1.249	14,090		$1.8 \cdot 10^4$
Water-gas	L	1.061		1.7	$9.1 \cdot 10^0$
	L	1.089		2.0	$1.5 \cdot 10^1$
	L	1.125		11.8	$1.8 \cdot 10^2$
	H	1.212			$5.0 \cdot 10^3$
	FO	1.227			$2.1 \cdot 10^4$
Oil–gas	MT	1.206		13.2	$2.0 \cdot 10^2$
	FO	1.256			$1.2 \cdot 10^4$
	HT	1.297			$7.6 \cdot 10^4$
	FO	1.317			$5.0 \cdot 10^5$
	HT	1.334			$6.6 \cdot 10^5$

Viscosity related data were converted to Dynamic viscosity using a linear interpolation of data in Phelan and Rhodes (1966) Table 15-13.
VR = vertical retort; CO = coke oven; HR = horizontal retort; L = light; H = heavy; FO = fuel oil. MT = medium temperature; HT = high temperature.

Table 2.3: Specific gravity and viscosity data for manufactured gas tars (after Birak and Miller 2009)

Coal tar MAH/PAH chemical compositions		Coal tar samples											
Compounds	Formula	1	2	3	4M	4H	5	6	7	8	9	10	Average
Benzene	C_6H_6	47.5	984	491	514	3390	523	964	986	1690	1360	233	1016.6
Toluene	$C_6H_5CH_3$	210	3690	2020	3100	11900	1000	3330	2840	6370	4270	458	3562.5
Ethylbenzene	$C_6H_5C_2H_5$	48.4	2920	1330	901	1990	251	647	1760	2590	3790	134	1487.4
m/p-Xylenes	$C_6H_4(CH_3)_2$	284	3120	1720	2920	8100	1160	3020	2100	4620	3400	638	2825.6
Styrene	$C_6H_5C_2H_3$	183	954	122	2450	7480	467	508	1110	3410	337	265	1571.5
o-Xylene	$C_6H_4(CH_3)_2$	148	1610	728	1600	4170	440	1620	1060	2180	1590	264	1400.9
1,2,4-Trimethylbenzene	$C_6H_3(CH_3)_3$	323	1950	884	1830	3680	705	2650	1130	2710	2410	168	1676.4
Naphthalene	$C_{10}H_8$	10000	32700	7770	20600	35700	27500	28800	13900	56100	68200	22200	29406.4
2-Methylnaphthalene	$C_{11}H_{10}$	4660	19000	5270	12300	17600	6860	27000	8620	24000	38300	4230	15258.2
1-Methylnaphthalene	$C_{11}H_{10}$	2870	16200	3330	8900	1390	3930	17400	5530	14000	24300	2420	9115.5
Acenaphthlylene	$C_{12}H_8$	1710	9520	567	4730	8220	4050	6600	2430	8040	20000	2410	6207.0
Acenaphthene	$C_{12}H_{10}$	430	1880	1150	612	1030	928	1330	559	959	2300	808	1089.6
Dibenzofuran	$C_{12}H_80$	1520	1030	185	1000	1830	5250	1040	180	421	2505	1800	1523.7
Fluorene	$C_{13}H_{10}$	2420	6320	716	2730	4440	2960	4540	1370	2540	9510	1770	3574.2
Phenanthrene	$C_{14}H_{10}$	5570	17300	2160	8010	12400	10400	14200	4080	9830	27200	7220	10760.9
Anthracene	$C_{14}H_{10}$	1670	5170	634	2780	4600	3090	4020	1210	2970	8310	2000	3314.0
Fluoranthene	$C_{16}H_{10}$	2870	5240	572	2550	4150	6220	2390	1330	3070	8690	4230	3755.6
Pyrene	$C_{16}H_{10}$	2100	7150	762	3200	5190	5110	4260	2200	4750	11400	3980	4554.7
Benz[*a*]anthracene	$C_{18}H_{12}$	1110	3600	347	1680	2720	2440	1210	1020	1950	4390	1800	2024.3
Chrysene	$C_{18}H_{12}$	802	3930	339	1430	2380	2250	1080	979	1840	3850	1720	1872.7
Benzo[*b*]fluoranthene	$C_{18}H_{12}$	481	1170	136	638	980	1630	329	389	735	1930	1040	859.8
Benzo[*k*]fluoranthene	$C_{20}H_{12}$	695	1650	156	712	1280	1780	413	419	1060	2420	1240	1075.0
Benzo[*a*]pyrene	$C_{20}H_{12}$	678	2610	268	1150	1940	2340	816	864	1960	4100	1570	1663.3
Indeno[1,2,3-cd]pyrene	$C_{22}H_{12}$	311	797	85.4	371	629	1270	202	295	671	1530	1110	661.0
Dibenz[*a,h*]anthracene	$C_{22}H_{14}$	93.9	346	33.7	151	254	366	80.4	124	222	463	79.1	201.2
Benzo[g,h,i]perylene	$C_{22}H_{12}$	351	1000	100	465	787	1400	251	487	898	1930	759	766.2

Units are in mg/kg

Table 2.4: Coal tar MAH/PAH chemical compositions (Brown et al. 2006)

Inorganics	Metals	Volatile Aromatics	Phenolics	PAHs
Ammoina Cynide Nitrate Sulfate Sulfide Thiocyanates	Aluminum Antimony Arsenic Barium Cadmium Chromium Copper Iron Lead Manganese Mercury Nickel Selenium Silver Vanadium Zinc	Benzene Ethylbenzene Toluene Xylenes	Phenol 2-Methylphenol 4-Methylphenol 2,4-Dimethylphenol	Acenaphthene Acenaphthylene Anthracene Benzo(a)anthracene Benzo(a)pyrene Benzo(b)fluoranthene Benzo(g,h,i)perylene Benzo(k)fluoranthene Chrysene Dibenz(a,h)anthracene Dibenzofuran Fluoranthene Fluorene Naphthalene Phenanthrene Pyrene 2-Methylnaphthalene

Table 2.5: Typical chemicals found at former MGP sites (Biyani 2003)

Material	Specific Yield (%)
Gravel, coarse	23
Gravel, medium	24
Gravel, fine	25
Sand, coarse	27
Sand, medium	28
Sand, fine	23
Silt	8
Clay	3
Sandstone, fine-grained	21
Sandstone, medium-grained	27
Limestone	14
Dune sand	38
Loess	18
Siltstone	12
Till, predominantly silt	6
Till, predominantly sand	16
Till, predominantly gravel	16

Table 2.6: Specifc yield values for differet soils and some rock types (Schwartz and Zhang 2003)

Equation	Chemical Class Represented
(1) $\log K_{oc} = 0.544 \log K_{ow} + 1.377$	Wide variety, mostly persticides
(2) $\log K_{oc} = 0.937 \log K_{ow} - 0.006$	Aromatics, polynuclear aromatics, triazines, and dinitroaniline herbicides
(3) $\log K_{oc} = 1.00 \log K_{ow} - 0.21$	Mostly aromatic or polynuclear aromatics
(4) $\log K_{oc} = 0.94 \log K_{ow} + 0.02$	Two chlorinated s-Triazines and dinitroaniline herbicides
(5) $\log K_{oc} = 1.029 \log K_{ow} - 0.18$	Variety of insecticides, herbicides, and fungicides
(6) $\log K_{oc} = 0.524 \log K_{ow} + 0.855$	Substitued phenylureas and alkyl-*N*-phenylcarbamates
(7) $\log K_{oc} = 0.72 \log K_{ow} + 0.5$	Haloginated hydrocarbons, both aliphatics and aromatics

Table 2.7: Correlations to estimate K_{oc} from K_{ow} (Alvarez and Illman 2006)

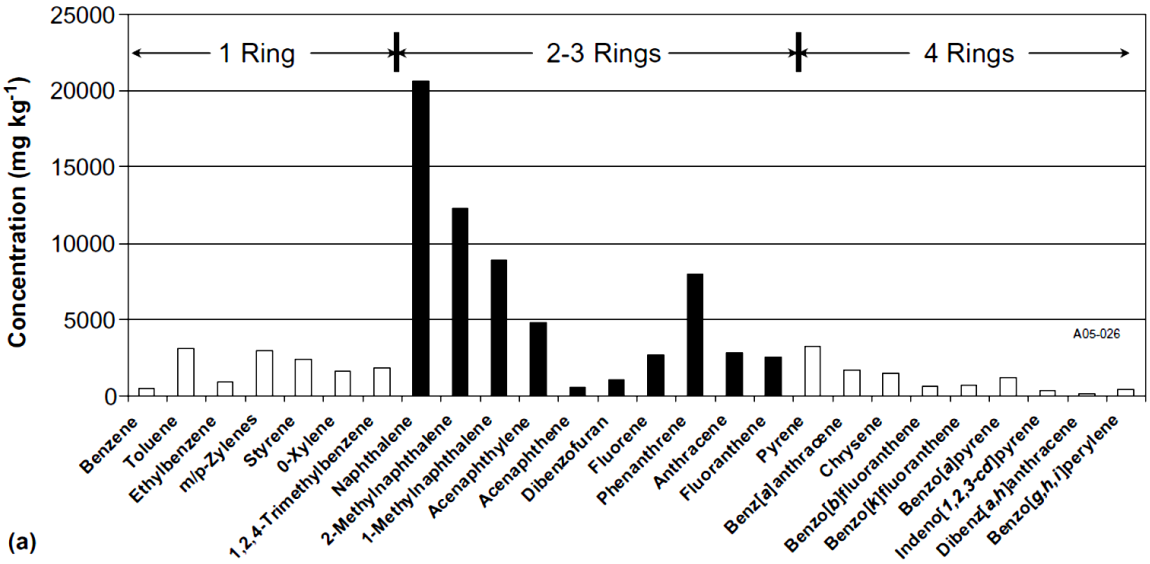

Figure 2.1: MAH/PAH analysis showing enhanced concentrations of the naphthalenes & phenanthrene (Brown et al. 2006)

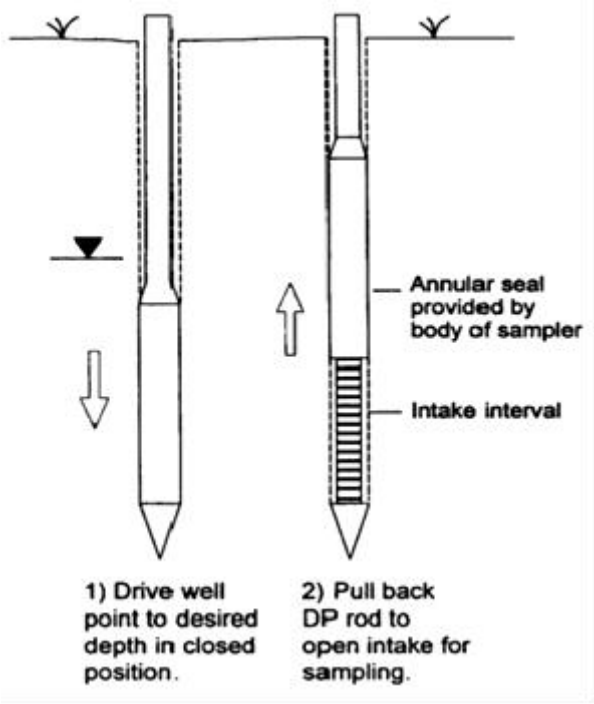

Figure 2.2: Groundwater Sealed-Screen Sampler (USEPA 2005)

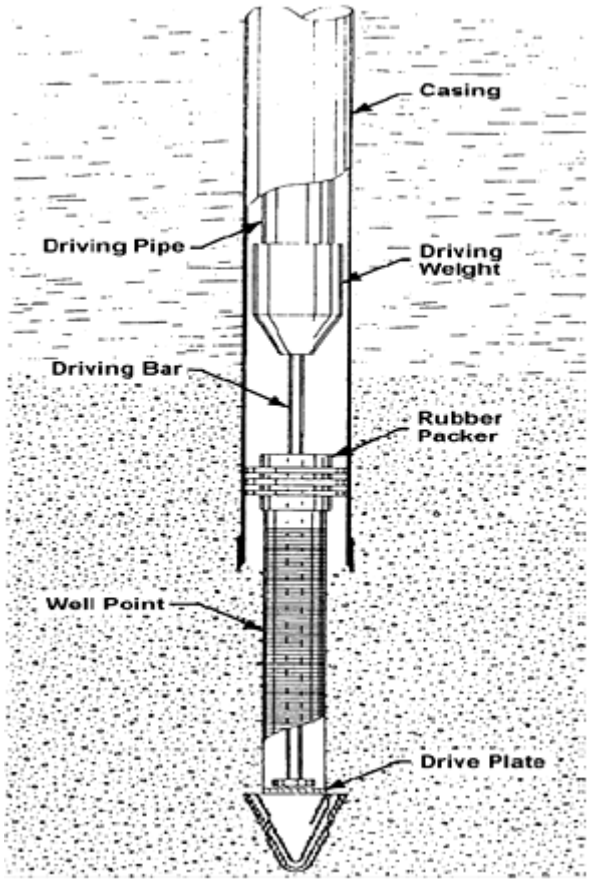

Figure 2.3: Exposed-Screen Sampler, Well Point Driven below the Base of a Borehole (USEPA 2005)

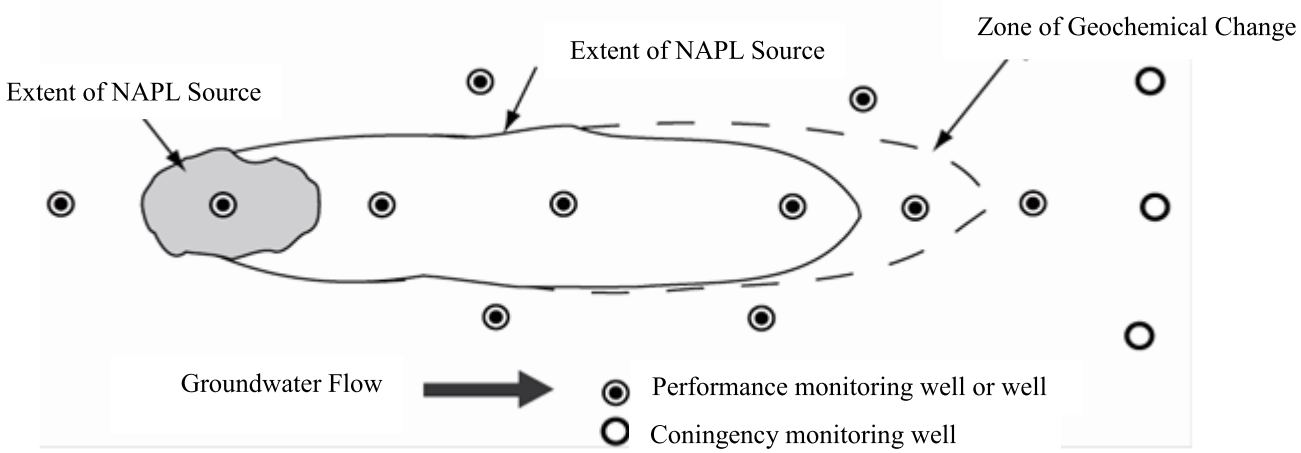

Figure 2.4: Conceptual diagram of monitoring point locations (Nielsen 2006)

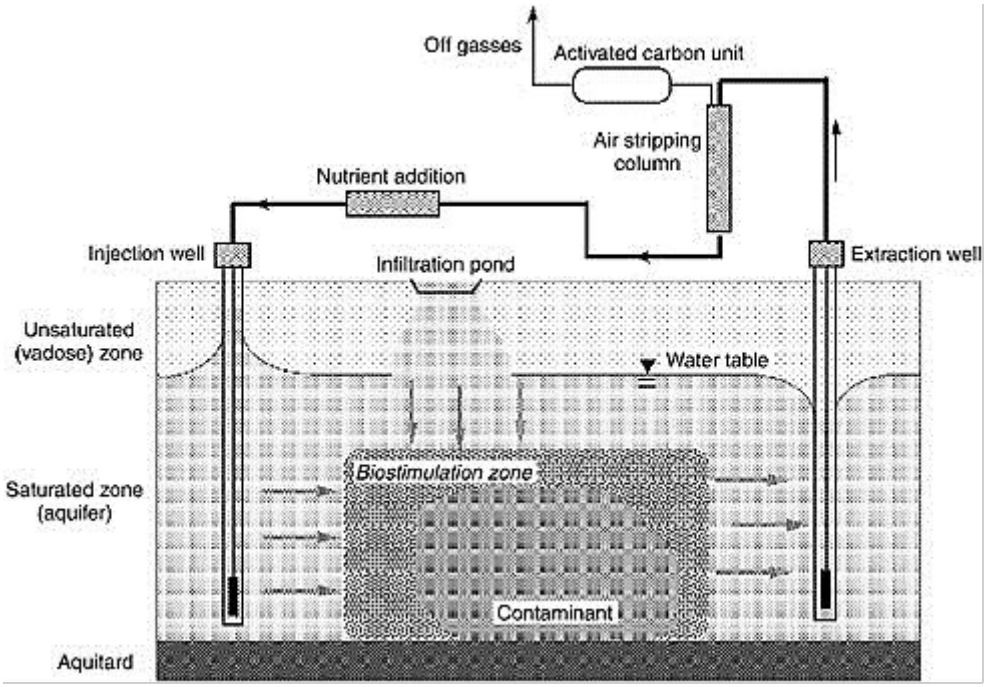

Figure 2.5: Enhanced bioremediation: injection well and infiltration pond for nutrient delivery and air stripping with activated carbon for treatment of extracted water (NRC 2005).

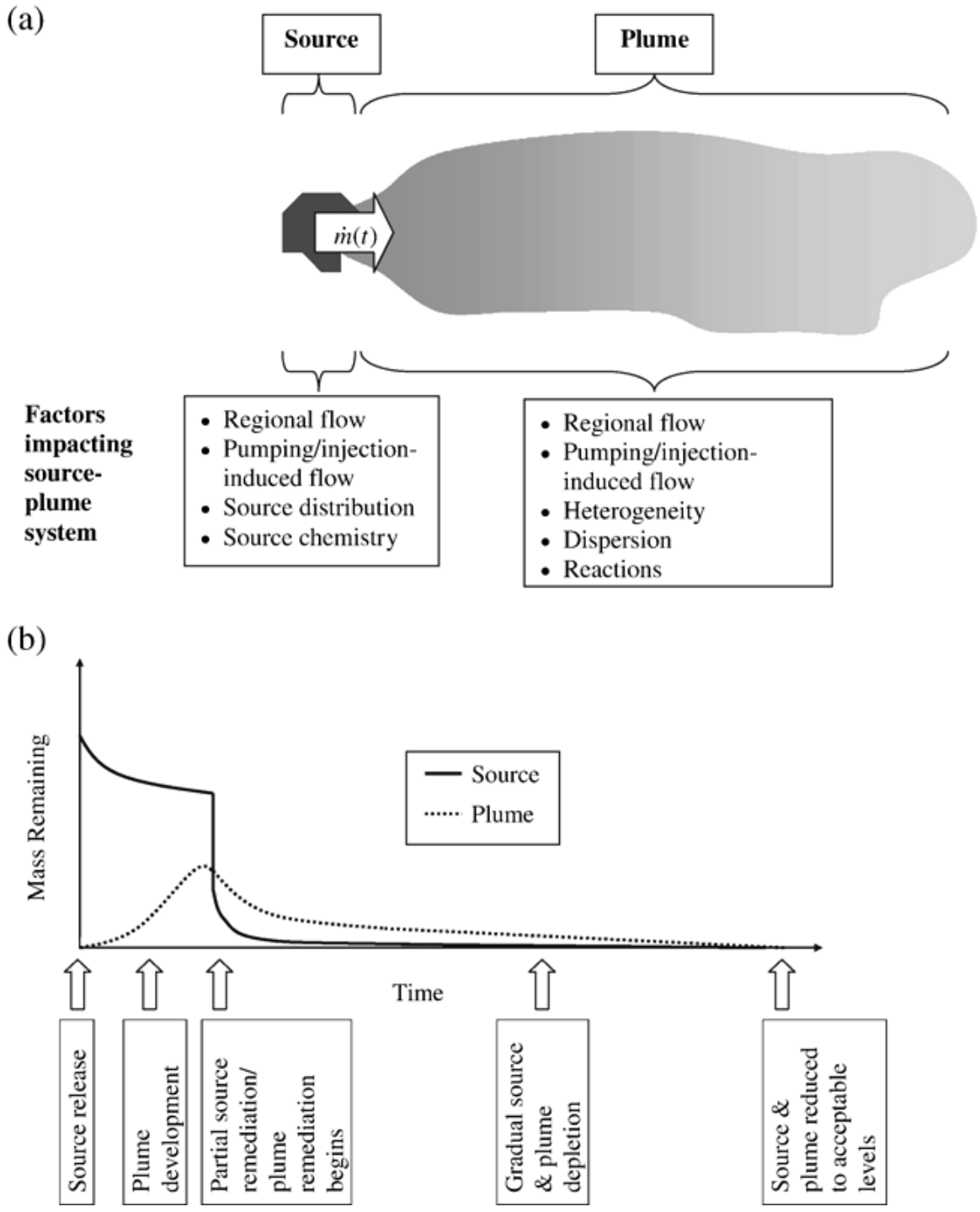

Figure 2.6: Contaminant source-plume scenario (a) schematic illustration and factors influencing behavior of source and plume; (b) sequence of events and contaminant mass history (Mayer and Endres 2007).

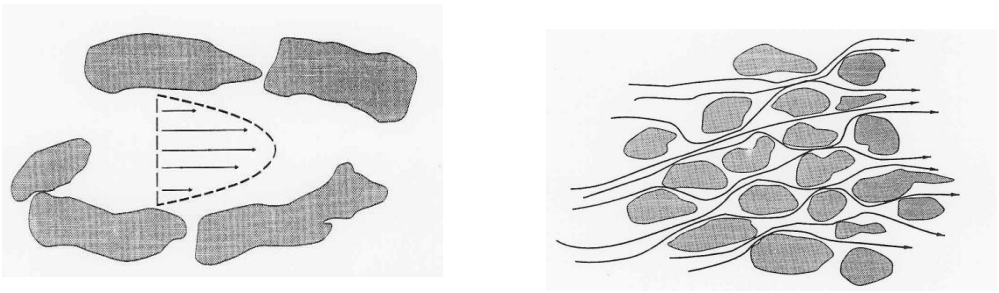

Figure 2.7: Mechanical dispersion and velocity distribution (Daniel 1993)

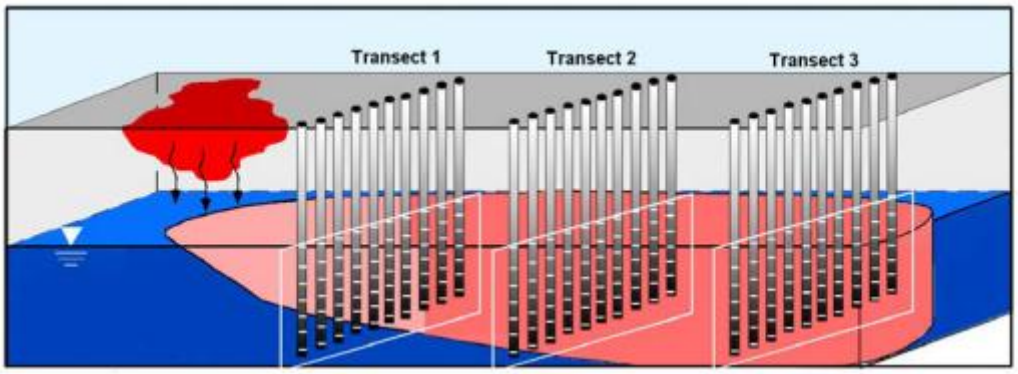

Figure 2.8: Example transects through 3D plume delineation (API 2003)

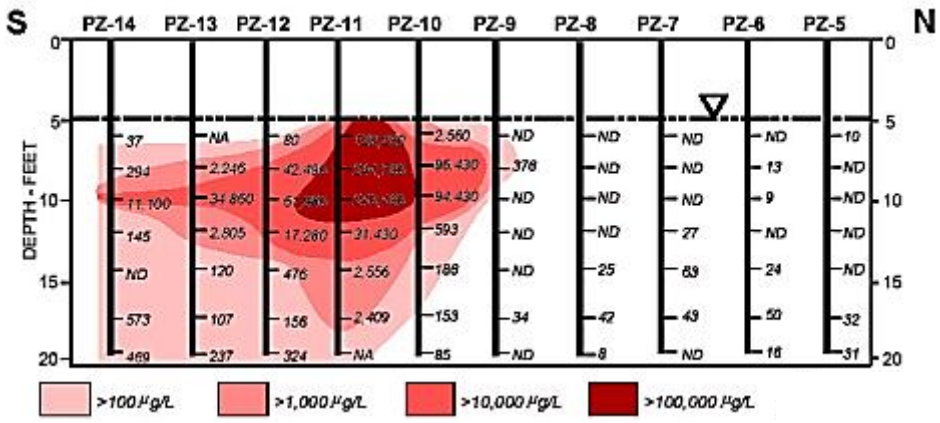

Figure 2.9: Concentration profile for transects (API 2003)

Chapter 3 Former MGP Site Characteristics

3.1 Site Description and History

The former MGP site in the Midwestern U.S. is located in a mix of light industrial and residential buildings. Figure 3.1 illustrates a plan view of the former MGP site showing the original layout of the MGP-related buildings, gas holder, storage tanks, coal tar cisterns, oil tanks, and coal storage areas as well as the location of the site monitoring wells. Bounded by railroad tracks to the west and northwest, residential areas to the north and northeast, and a river about 180 m to the southeast, the ground surface slightly slopes from north to south towards the river. The site ground cover consists of grass, dirt roads, and few trees. The site climate is typical continental with an average seasonal snowfall of 81.3 cm and annual precipitation of 71.1 cm (Rogers et al. 2007a).

A carbureted water gas plant was operated from 1905 to 1936. Over the years, coal tar PAH and BTEX contamination resulting from the gas manufacturing operations and possible gasoline spillage pervaded the aquifer underlying the former MGP site (Rogers et al. 2007a; Biyani 2003). The history of investigating the contamination started in 1984 when soil contaminated with coal tar was first observed during sewer line installation, after which preliminary investigation activities began in 1986 followed by preliminary site assessment in 1991. A subsurface investigation was then conducted at the site late in 1997 to further characterize and delineate the dissolved phase contamination downgradient of the former MGP site and to gain baseline information for evaluating the groundwater plume. Contaminated soils were excavated and backfilled with clean sand following 1997 site characterization

activities (Biyani 2003; Black and Veatch 1998). Since then, the site has been extensively investigated and anlyzed through several research studies (e.g. Kjartanson et al. 2002; Biyani 2003; Stenback and Ong 2003, Stenback et al. 2004; Rogers et al. 2007a; Rogers et al. 2007b). Black and Veatch (2004) summarizes field observations and measurements and the analytical results for groundwater samples that were collected in March and September 2003 in support of a monitored natural attenuation (MNA) study as well as the results of Iowa State University research projects conducted at the site. Black and Veatch (2008) summarizes the results of characterization activities conducted at the site since 2004 including further soil probing, membrane interface probing and monitoring well installation activities conducted to delineate the extent of the DNAPL present in the granular alluvium overlying glacial till, to evaluate DNAPL recoverability, and to evaluate ground water contamination levels and plume stability.

3.2 Site Geology

The site geology was defined using borehole and electrical conductivity logs for monitoring well installations and soil samples collected as part of direct push technologies (DPT) activities (Rogers et al. 2007a). The general site soil stratigraphy comprises four primary geologic units as shown by the cross-section in Figure 3.2: a highly transmissive coarse alluvium layer confined in depth by glacial till and overlain by a fine-grained silty alluvial layer and loess (Rogers et al. 2007a). The thickness of the glacial till underneath the alluvium layer and the nature of materials below the till are not known. However, the till has been described as a stiff to very stiff clay with low to high plasticity and occasional silt or trace of sand or gravel. As a relatively low permeability layer, the glacial till is restricting the vertical migration of

groundwater and contaminants (Biyani 2003; Rogers et al. 2007a; Black & Veatch 1994).

Pinching of the coarse alluvium by the overlying fine-grained silty alluvial layer from approximately 90 m to 140 m longitudinal distance along the flow path cross section (see Figure 3.2) is a prominent feature of the site geology. The pinch zone thickness varies and has more silty and fine-grained clayey soil. Running across the site more or less from east to west, the pinch zone has a lower hydraulic conductivity (Biyani 2003; Golchin et al. 2004). The coarse alluvium layer is about 9 m thick in the northern portion of the site and narrows to as low as 0.91 m in the pinch zone and increases thickness again to approximately 8 m near the river. The overlying fine loess is almost absent in the areas north of the former MGP site, however, its thickness increases to about 8 m over the pinch zone (Biyani 2003; Golchin et al. 2004). As discussed in section 3.3, this pinch zone has a prominent effect on the site hydrogeology.

Grain size analyses were carried out for soil samples obtained during site characterization activities (Biyani 2003). Out of the nine samples collected, four samples were from the loess layer (primarily silt) overlying the pinch zone. All four samples showed high sand and silt contents with sand content generally found more than silt in most of sampled locations. The samples collected from the alluvium layer in locations close to the pinch zone showed sand content slightly higher than silt indicating grading of loess into alluvium. The samples collected from locations close to the river were found to be of a non-plastic soil and showed approximately 97%

sand content. Soil samples were dried and weighed for dry soil weight to determine soil porosity and dry bulk density (Table 3.1).

Biyani (2003) carried out separate tests to determine total carbon and inorganic carbon content in soil samples collected from the loess and alluvium units at different locations within the former MGP site. Organic carbon content was then found by taking the difference between the total and inorganic carbon content. Dry combustion tests for some of the samples collected from the loess unit reflected high total carbon content indicating high inorganic carbon content in the soil. Organic carbon content was generally lower for deeper samples (between 0.15% to 0.3%), with soil samples collected from the pinch zone showing high organic carbon content (between 2.6% to 3.9%) suggesting high sorptive nature of the soil (Biyani 2003; Kjartanson et al. 2002).

3.3 Site Hydrogeology and Recharge

As shown in Figure 3.3, monitoring wells have been installed at 28 locations to monitor the groundwater hydraulic head changes and groundwater quality across the site. Table 3.2 summarizes the measured hydraulic heads at monitoring wells at different times to interpret head variations and groundwater flow patterns across the site as part of the groundwater monitoring program. Figure 3.4 is a plot of the hydraulic head data for monitoring wells organized from the upgradient wells near the former MGP location to the furthest downgradient wells. The groundwater elevations in the monitoring wells near and north of Main Street generally have not shown significant hydraulic head variations across several years while the wells in the south region of the site have shown some variations. Water levels in wells nearest to the

river have varied as much as 1.82 m and appeared to be highly influenced by the river seasonal elevations. This variation in water levels has no significant impact on the overall hydraulic gradient and groundwater flow patterns in the southern part of the site at the times of groundwater monitoring as shown in Figure 3.4. The hydraulic gradient pattern in Figure 3.4 is highly correlated to the potentiometric surface in Figure 3.2 which further demonstrates the minimal impact of the water levels variation near the river on the overall hydraulic gradient.

Biyani (2003) notes that hydraulic heads were between 2.7 to 4.57 m below the ground surface downgradient of MW-6 (the region south of the former MGP site). However, the hydraulic heads were about 0.06 m below ground surface in MW-6 and the upgradient wells (the region north of the former MGP) and remain almost constant with time. Because of the relatively small hydraulic head and gradient variations over the time period from April 2002 to June 2007, the March 2003 data set has been used to represent the groundwater flow conditions. This is a more complete data set than the June 2007 data set (see Table 3.2). In addition, the March and September 2003 groundwater elevation data in Table 3.2, for example, show that most of the nested wells in the alluvium do not indicate a significant vertical hydraulic gradient.

The groundwater potentiometric surface defined using groundwater elevations measured in March 2003 (Table 3.2) (Black and Veatch 2004) along with the general groundwater flow direction in the alluvial layer are shown in Figure 3.5 (Biyani 2003; Golchin et al. 2004). An average hydraulic head drop of about 4.0 m occurs between MW6 and MW-9 in a general southern direction and between MW-6 and MW-8 in in a general eastern direction. The likely cause of the hydraulic gradient increase is the pinch in the coarse alluvium layer running in a general east-west direction across the

site. The groundwater is flowing in a generally southeast direction, perpendicular to the potentiometric surface contours as shown in Figure 3.5.

The site monitoring wells have been slug tested and slug tests have been carried out as a part of soil and groundwater sampling activities. Table 3.2 also lists the monitoring well top of casing elevation, screen elevation and screen geologic unit.

Hydraulic conductivity values measured onsite were found to vary between 9.2×10^{-9} to 3.2×10^{-7} m/s in the loess zone with an average of 5.29×10^{-7} m/s, and between 2.10×10^{-7} to 9.98×10^{-3} m/s in the coarse alluvium layer and were as low as 2.5×10^{-7} m/s in the pinch zone. Based on the hydraulic conductivity values and with the glacial till layer effectively acting as a barrier for flow, the alluvium layer has the greatest potential for flow. To this end, the hydraulic conductivity value variation across the alluvium layer is shown in Figure 3.6, and the monitoring well hydraulic conductivity values are listed in Table 3.3. A recharge rate of 278.3 mm/yr downgradient of MW-6 was used by Biyani (2003) for modeling purposes.

3.4 Soil and Groundwater Contamination

Coal tar PAH and BTEX contamination resulting from gas manufacturing operations and possible gasoline spillage pervades the aquifer underlying the former MGP site. Coal tar DNAPLs and the resultant plumes are primarily confined to the alluvial sediments (Rogers et al. 2007b). Water samples collected from the nested monitoring wells showed zonation of contaminant concentrations between the upper and the lower portions of the aquifer. A deep well often showed greater contaminant concentration than a shallow well. However, some shallow wells showed greater

concentrations than nested deeper wells. Free-phase coal tar source material located under the former gas-holder tanks and shallow source contaminated soils were excavated in 1997 to depths of 2.4 m but no deeper than the water table elevation. The excavations were then backfilled with clean sand up to 0.8 m of the original ground surface, capped with a 0.6 m layer of clay and then topped with gravel. Subsequent soil investigations near the former gas holder and coal tar tanks have revealed additional coal tar DNAPLs smeared between approximately 3 m below ground surface to the confining glacial till, upon which a thin layer of coal tar was assumed to be pooling. Analysis of soil and groundwater samples indicated no evidence of former MGP site contamination entering the river (Stenback and Ong 2003; Rogers et al. 2007a).

Soil probing and monitoring well installation were conducted in April and June of 2004 to further delineate the extent of tar compounds present near the former MGP site area (Black and Veatch 2008). DPT probes were advanced, continuously sampled and logged to the granular alluvium/glacial till interface. Varying degrees of tar DNAPL staining and free product were present at specific depths in each of the push locations. Tar DNAPL was pooled at the base of the alluvium and/or suspended within the alluvium.

Intervals of pooling DNAPL tars were present at the alluvium/glacial till interface with an approximate thicknesses greater than 1.27 cm at all push locations. Pushes located closer to the former MGP process areas contained a significant quantity of free saturated tars overlying the till surface with thicknesses greater than about 1.5 cm, and approximately 70 cm of tar coated alluvium soils directly overlaying it.

A membrane interface probe (MIP) was pushed at two locations at the former MGP site to evaluate whether this technology would be useful in detecting DNAPL in the subsurface. DNAPL contamination was not identified at either of the two push locations when visually logging the pushes. This was related to "increasing the detection limits while calibrating the MIP in anticipation of encountering DNAPL in the subsurface, or because the probe is primarily designed to detect VOCs and does not accurately detect the heavier compounds of which DNAPL is typically composed" (Black and Veatch 2008). Combining the entire direct push probes and groundwater monitoring results with historic soil boring data, Black and Veatch (2008) describes the coal tar DNAPL contamination extent along with the extent of the coal tar DNAPL suspended plume representing a smear zone in the alluvium (Figure 3.7).

Black and Veatch (2008) report the analysis of groundwater samples collected in June 2007 for PAH and MAH (BTEX) compounds. BTEXs were detected in 10 out of 19 monitoring wells sampled in 2007, with concentrations generally decreasing with increasing distance from the former MGP site. Downgradient of the site, BTEX concentrations increased with depth at only one well location. While all compounds were detected, benzene was detected at the highest concentrations. Lower levels of BTEXs were detected in deep wells MW-6, MW-20, and MW-27B, which are located laterally from the wells with elevated BTEX detections. No BTEXs were detected in wells MW-7, MW-8, MW-9, MW-10, MW-12, and MW-28. On the other hand, PAHs were detected in 15 out of 19 monitoring wells sampled in 2007. As with the BTEXs, PAH concentrations decreased with increasing distance from the former MGP site, however, unlike the BTEX results, concentrations increased with depth at all nested

well locations. Elevated concentrations of naphthalene, 1-methylnaphthalene, acenaphthylene, and acenaphthene were detected approximately 80 m downgradient of the primary source region in several monitoring locations screened both in the fine-grained alluvium and the overlying loess. Concentrations in MW-7, MW-10, MW-12, MW-13B, MW-20, and MW-28 ranged from 0.0124 µg/L of acenaphthene to 1.18 µg/L of naphthalene. No PAHs were detected in wells MW-8 and MW-9.

Table 3.4 (Black and Veatch 2008) details the compliance standards for protected groundwater and summarizes the wells with contaminant concentrations exceeding the groundwater compliance standards at the former MGP site in June 2007. As shown in the table, benzene and ethylbenzene are the only BTEXs with concentrations above the compliance standards. Nine wells exceed the standard for benzene, while only one well exceeds the standard for ethylbenzene. PAHs including benzo(a)anthracene, benzo(a)pyrene, benzo(b)fluoranthene, benzo(k)fluoranthene, chrysene, dibenzo(a,h)anthracene, indeno(1,2,3-cd)pyrene, and naphthalene were found to exceed compliance standards in well MW-5B (Black and Veatch 2008).

Three compounds were selected to be the focus for this study; benzo(a)pyrene represents the heavy weight PAH contaminants, naphthalene represents the medium weight PAHs and benzene represents the MAHs. In addition to representing different contamination groups, the foresaid contaminants were consistently detected in monitoring wells at the site with concentrations well above regulatory limits (see Table 3.5). Benzo(a)pyrene, a high molecular weight compound, is not very mobile in the subsurface, but has a high risk due to its relatively high toxicity and possible increased mole fraction as the tar ages (Birak and Miller 2009). With a minimal

number of contaminants to be modeled, this selection scheme provides a distinction in the flow and transport behavior of different weight compounds. The concentrations of benzene, benzo(a)pyrene and naphthalene measured in monitoring well samples between 1992 and 2007 are listed in Tables 3.5, 3.6 and 3.7, respectively. Concentration versus time scatter plots have been prepared for benzene, benzo(a)pyrene and naphthalene at selected monitoring wells. The monitoring wells were selected because they are either close to or within the former MGP area. These plots are meant to give a general sense of the three contaminant concentration variations with time at some monitoring wells in the site. Figures 3.8 to 3.11 show the benzene concentration versus time at the selected monitoring wells, Figures 3.12 to 3.15 show the benzo(a)pyrene concentration versus time at the selected monitoring wells and finally, Figures 3.16 to 3.19 show the naphthalene concentration versus time at those selected monitoring wells.

The contaminant concentration data given in Tables 3.5, 3.6 and 3.7 were used to illustrate the approximate extent of the BTEX and PAH contaminant plumes where concentrations exceeded the drinking water regulatory limits (5 μg/L or 0.005 mg/L for benzene, 20 μg/L or 0.020 mg/L for naphthalene and 0.2 μg/L or 0.0002 mg/L for benzo(a)pyrene). For nested wells, the maximum concentration measured was used to define the plume extents. September 2003 concentration data were used because they are the most inclusive recent measured data set for the contaminants in comparison to other data sets shown within the tables. Non-detect samples were given a concentration equal to the detection limit of the contaminants. Figure 3.20 displays approximate plume locations and extents used as the basis for calibrating the contaminant transport model. Another set of concentration data measured in March

2002 (Tables 3.5, 3.6 and 3.7) was used to produce plume contours for the three contaminants (see Figure 3.21). Comparing the plumes of Figure 3.20 with the plumes shown in Figure 3.21 indicate that the plumes are of about the same extent. Analysis of the limited concentration data for June 2007 indicates that the benzene, naphthalene and benzo(a)pyrene plumes have approximately the same extents as in September 2003. This supports the utilization of September 2003 concentration data and Figure 3.20 as the basis for calibrating the contaminant transport model.

Sample id	Location	Depth (bgs) m	Expected Layer	Porosity (%)	Dry Bulk Density (g/L)
SS IA	Upgradient of the source area	3.4	alluvium	22.49	2.054
		5.8	alluvium	28.85	1.886
SS 2	Upgradient of the source area	4.1	alluvium	26.22	1.955
		6.7	alluvium	32.68	1.694
		7.8	alluvium	17.25	2.192
SS 6	Downgradient of the source area	2.3	loess	44.26	1.5
		4.0	alluvium/loess	53.11	1.265
		5.2	alluvium	32.5	1.43
SS 8	Downgradient of the source area	2.7	alluvium/loess	40.58	1.604
		4.0	alluvium	22.35	2.058
SS 10	In the pinch zone	4.3	loess	50.72	1.33
		5.3	loess	59.92	1.08
SS 12	In the pinch zone	3.5	loess	51.62	1.306
		4.3	loess	53.47	1.256
		6.7	alluvium/loess	52.5	1.282

Table 3.1: Porosity and dry bulk density of soil (Biyani 2003)

Monitoring Well	TOC (m)	Geologic Unit	Screen Elevation (m)	Groundwater Elevation (m)					
				Apr-02	Nov-02	Mar-03	Sep-03	Apr-04	Jun-07
MW-1	362.00	Alluvium	358.54	358.43	358.56	358.43	358.53	358.59	358.59
MW-2	361.44	Alluvium	351.68	358.42	358.55	358.43	358.52	358.57	NM
MW-3	359.60	Alluvium	355.69	358.42	358.56	358.41	358.51	358.57	NM
MW-3A	359.48	Alluvium	NA	358.38	358.56	358.41	358.52	358.55	NM
MW-3B	359.53	Alluvium	NA	358.49	358.57	358.42	358.54	358.57	NM
MW-3C	359.41	Alluvium	NA	358.43	358.57	358.41	358.53	358.55	NM
MW-4	362.32	Alluvium	354.62	358.43	358.56	358.43	358.54	NM	NM
MW-5A	359.80	Alluvium	357.03	358.44	358.57	358.44	358.54	358.59	358.59
MW-5B	359.88	Alluvium	352.36	358.44	358.57	358.44	358.54	358.59	358.59
MW-6	358.59	Alluvium	353.64	358.46	358.58	358.44	358.55	358.60	358.59
MW-6A	358.55	Alluvium	354.73	358.45	358.56	358.37	358.53	358.55	NM
MW-6B	358.53	Alluvium	352.59	358.46	358.58	358.38	358.61	358.53	NM
MW-6C	358.49	Alluvium	353.61	358.46	358.58	358.40	358.54	358.55	NM
MW-7	357.69	Alluvium	347.93	353.48	353.11	353.13	352.97	NM	353.93
MW-8	358.01	Alluvium	348.69	354.57	354.53	354.53	354.06	355.25	354.68
MW-9	357.76	Alluvium	349.23	353.73	353.35	353.36	353.21	353.99	354.14
MW-10	357.37	Alluvium	345.61	353.09	352.71	352.79	352.53	353.26	353.53
MW-11	357.54	Alluvium	345.46	353.09	352.70	352.78	352.53	353.26	353.53
MW-12	357.44	Alluvium	347.23	353.11	352.72	352.79	352.54	353.27	353.60
MW-13A	358.05	Loess	353.02	355.41	355.34	355.34	355.41	355.86	355.73
MW-13B	358.00	Loess	350.22	354.93	354.77	354.73	354.66	355.25	355.27
MW-13C	357.98	Alluvium	349.41	NI	354.74	354.72	354.65	355.22	NM
MW-14	358.16	Alluvium	NA	356.23	356.11	356.06	356.16	356.66	NM
MW-14A	358.15	Alluvium	351.60	NI	355.45	356.34	356.43	356.42	356.64
MW-15A	358.64	Alluvium	NA	358.43	358.58	358.37	358.55	358.63	358.42
MW-15B	358.67	Alluvium	352.42	358.44	358.57	358.32	358.57	358.66	NM
MW-16A	359.51	Alluvium	354.78	358.43	358.57	358.43	358.57	358.59	358.58
MW-16B	359.63	Alluvium	352.17	358.43	358.56	358.46	358.59	358.61	358.63
MW-17	358.25	Alluvium	NA	357.16	356.86	356.98	357.07	356.86	NM
MW-18	359.76	Alluvium	354.74	358.44	358.56	358.42	358.56	358.59	354.63
MW-19A	360.47	Alluvium	NA	358.42	358.55	358.42	358.57	358.58	NM
MW-19B	360.60	Alluvium	NA	358.47	358.54	358.42	358.58	358.58	NM
MW-20	357.94	Alluvium	348.95	354.28	354.11	354.09	353.90	354.78	354.63
MW-21	358.16	Alluvium	NA	355.74	355.92	355.84	355.86	356.29	NM
MW-22	357.00	Alluvium	NA	353.07	352.70	352.80	352.56	353.25	NM
MW-23	357.55	Alluvium	349.61	NI	352.73	352.78	352.89	355.77	NM
MW-24	359.36	Alluvium	351.08	NI	355.09	354.24	355.23	356.22	NM
MW-25	358.59	Alluvium	351.40	NI	355.38	355.79	355.94	357.14	NM
MW-26	359.72	Alluvium	356.63	NI	358.58	358.43	358.58	358.61	NM
MW-27A	358.44	Alluvium	354.74	NI	358.32	358.41	358.54	358.44	NM
MW-27B	358.43	Alluvium	353.25	NI	358.34	358.43	358.51	358.44	358.43
MW-28	357.97	Alluvium	349.58	NI	354.06	354.03	353.85	354.73	354.58
The River	360.06	NA	NA	352.83	352.58	352.73	353.11	353.28	NM

TOC Top of casing elevation in meters
NA Not available
NI well not yet installed at the time of measurement
NM Not measured

Table 3.2: Monitoring wells and corresponding elevations (Black and Veatch 2008)

id	k(ft/d)	k(m/s)
MW1	2.27E+02	8.01E-04
MW2	1.76E+02	6.21E-04
MW3	9.07E+01	3.20E-04
MW3A	1.02E+01	3.60E-05
MW3B	3.69E+01	1.30E-04
MW3C	1.36E+01	4.80E-05
MW4	1.73E+02	6.10E-04
MW5B	1.81E+02	6.39E-04
MW6	2.83E+01	9.98E-05
MW6A	2.52E+00	8.89E-06
MW6B	9.35E-01	3.30E-06
MW6C	2.83E+01	9.98E-05
MW7	1.16E+01	4.09E-05
MW8	1.28E+01	4.52E-05
MW9	4.54E+01	1.60E-04
MW10	3.69E+02	1.30E-03
MW11	2.83E+03	9.98E-03
MW12	3.40E+01	1.20E-04
MW13C	8.79E+00	3.10E-05
MW14A	1.50E-01	5.29E-07
MW14	4.54E-01	1.60E-06
MW15A	3.69E+01	1.30E-04
MW15B	3.12E+01	1.10E-04
MW16A	4.54E+01	1.60E-04
MW16B	4.54E+01	1.60E-04
MW17	6.80E-02	2.40E-07
MW18	1.67E+01	5.89E-05
MW19A	7.09E+01	2.50E-04
MW19B	1.56E+01	5.50E-05
MW20	2.30E+01	8.11E-05
MW21	1.22E+00	4.30E-06
MW22	5.10E+01	1.80E-04
MW23	1.19E+01	4.20E-05
MW24	5.95E-02	2.10E-07
MW25	7.65E-02	2.70E-07
MW26	1.02E+01	3.60E-05
MW27A	1.53E+01	5.40E-05
MW27B	8.79E+00	3.10E-05
MW28	9.35E+00	3.30E-05

Table 3.3: Hydraulic conductivity test results (Stenback and Ong 2003)

Chemical of Concern	Compliance Standard (µg/L)	Monitoring Wells Exceeding Standards
Benzene	5	MW-5A, MW-5B, MW-13B, MW-14A, MW-15B, MW-16A, MW-16B, MW-20,MW-27B
Toluene	1,000	None
Ethylbenzene	700	MW-16B
Total Xylenes	10,000	None
Acenaphthene	420	None
Acenaphthylene	210	None
Anthracene	2,100	None
Benzo(a)anthracene	0.24	MW-5B, MW-16B
Benzo(a)pyrene	0.2	MW-5B
Benzo(b)fluoranthene	0.24	MW-5B
Benzo(g,h,i)perylene	210	None
Benzo(k)fluoranthene	2.4	MW-5B
Chrysene	24	MW-5B
Dibenzo(a,h)anthracene	0.024	MW-5B
Fluoranthene	280	None
Fluorene	280	None
Indeno(1,2,3-cd)pyrene	0.24	MW-5B
Naphthalene	100	MW-5B, MW-15B, MW-16A, MW-16B
Phenanthrene	210	MW-5B
Pyrene	210	None
Abbreviation: µg/L micrograms per liter		

Table 3.4: Summary of groundwater compliance standards and monitoring wells exceeding the standards in June 2007 at the former MGP (Black and Veatch 2008)

Well	Concentration (µg/L)																						
	Dec-92	Nov-93	Mar-94	Aug-95	Mar-96	Jun-96	Sep-96	Dec-96	Mar-98	Jun-98	Sep-98	Jun-99	Nov-99	Jun-00	Nov-00	Jun-01	Aug-01	Nov-01	Mar-02	Nov-02	Mar-03	Sep-03	Jun-07
MW-1	-	-	-	-	-	-	-	-	-	-	-	-	-	-	-	-	-	-	-	-	-	-	-
MW-2	-	-	-	-	-	-	-	-	-	-	-	-	-	-	-	-	3.9	-	<1	<1	<0.32	<0.32	-
MW-3	34	11	10	11	39	62	480	25	27	32	14.6	7.5	8.7	3.1	27	-	8	-	6.4	5	8.3	9.9	6.5
MW-3A	-	-	-	-	-	-	-	-	-	-	-	-	-	-	-	-	-	-	15.1	20.4	5.9	14.3	-
MW-3B	-	-	-	-	-	-	-	-	-	-	-	-	-	-	-	-	-	-	36.8	14.5	7.2	10.8	-
MW-3C	-	-	-	-	-	-	-	-	-	-	-	-	-	-	-	-	-	-	8.3	12.1	6.5	-	-
MW-4	-	1	1	1	1	1	1	1	5	1	0.05	1	1	1	1	ND	ND	-	ND	ND	ND	ND	-
MW-5A	-	-	-	-	-	-	-	-	-	-	-	-	-	-	-	-	26.7	-	<5.0	30.4	2.2	48.1	335
MW-5B	-	2400	800	-	-	-	-	-	510	380	529	280	430	260	580	560	511	490	382	402	472	687	338
MW-6	-	2.7	52	38	5.4	4.1	1.1	3.2	5	1.4	29.9	4.7	57	6.2	1	<0.57	<1.0	-	37	<1	1.98	10.4	<0.32
MW-6A	-	-	-	-	-	-	-	-	-	-	-	-	-	-	-		<1	<2	<1	<5	0.38	<0.32	<0.33
MW-6B	-	-	-	-	-	-	-	-	-	-	-	-	-	-	-	-	1.1	-	<1.0	<1	0.39	2	-
MW-6C	-	-	-	-	-	-	-	-	-	-	-	-	-	-	-	-	1.5	-	<1	1.14	11.2	-	-
MW-7	-	-	31	6.1	10	7.1	1	1	5	1	0.5	1	1	1	1	ND	ND	-	ND	ND	ND	ND	ND
MW-8	-	-	-	-	-	-	-	-	5	1	0.5	1	1	1	1	ND	ND	-	ND	ND	ND	ND	ND
MW9	-	-	-	-	-	-	-	-	5	1	0.5	1	1	1	1	ND	ND	-	ND	ND	ND	ND	ND
MW-10	-	-	-	-	-	-	-	-	5	1	0.5	1	1	1	1	ND	ND	-	ND	ND	ND	ND	ND
MW-11	-	-	-	-	-	-	-	-	5	1	0.5	1	1	1	1	ND	ND	ND	ND	ND	ND	ND	-
MW-12	-	-	-	-	-	-	-	-	-	-	-	-	-	-	-	-	-	-	<1	<1	0.51	<0.32	<0.32
MW-13A	-	-	-	-	-	-	-	-	-	-	-	-	-	-	-	-	7.7	-	6	<5	5.9	6.9	<0.32
MW-13B	-	-	-	-	-	-	-	-	-	-	-	-	-	-	-	-	1220	-	313	571	610	574	524
MW-13C	-	-	-	-	-	-	-	-	-	-	-	-	-	-	-	-	-	-	-	29.8	<0.32	21.9	-
Protection Standard	5	5	5	5	5	5	5	5	5	5	5	5	5	5	5	5	5	5	5	5	5	5	5

Table 3.5: Benzene concentrations measured and drinking water regulatory standard (regulatory standard exceedences are highlighted)

	Concentration (µg/L)																						
Well	Dec-92	Nov-93	Mar-94	Aug-95	Mar-96	Jun-96	Sep-96	Dec-96	Mar-98	Jun-98	Sep-98	Jun-99	Nov-99	Jun-00	Nov-00	Jun-01	Aug-01	Nov-01	Mar-02	Nov-02	Mar-03	Sep-03	Jun-07
MW-14	-	-	-	-	-	-	-	-	-	-	-	-	-	-	-	-	-	-	10.3	<5	7	5.4	-
MW-14A	-	-	-	-	-	-	-	-	-	-	-	-	-	-	-	-	-	-	-	10.1	9.4	10.3	7.48
MW-15A	-	-	-	-	-	-	-	-	-	-	-	-	-	-	-	-	-	-	168	88.6	691.8	269	-
MW-15B	-	-	-	-	-	-	-	-	-	-	-	-	-	-	-	-	-	-	1010	1000	832	34.5	880
MW-16A	-	-	-	-	-	-	-	-	-	-	-	-	-	-	-	-	-	-	263	1270	33.2	595	1200
MW-16B	-	-	-	-	-	-	-	-	-	-	-	-	-	-	-	-	-	-	650	243	590	327	312
MW-17	-	-	-	-	-	-	-	-	-	-	-	-	-	-	-	-	-	-	8.1	4.99	5.3	4.9	-
MW-18	-	-	-	-	-	-	-	-	-	-	-	-	-	-	-	-	-	-	<1.0	<1.0	<0.32	<0.32	<0.32
MW19A	-	-	-	-	-	-	-	-	-	-	-	-	-	-	-	-	-	-	ND	ND	ND	ND	-
MW19B	-	-	-	-	-	-	-	-	-	-	-	-	-	-	-	-	-	-	ND	ND	ND	ND	-
MW-20	-	-	-	-	-	-	-	-	-	-	-	-	-	-	-	-	-	-	74.6	85	<0.32	<1.6	5
MW-21	-	-	-	-	-	-	-	-	-	-	-	-	-	-	-	-	-	-	-	-	-	-	-
MW-23	-	-	-	-	-	-	-	-	-	-	-	-	-	-	-	-	-	-		ND	ND	ND	-
MW-24	-	-	-	-	-	-	-	-	-	-	-	-	-	-	-	-	-	-	-	-	-	-	-
MW-25	-	-	-	-	-	-	-	-	-	-	-	-	-	-	-	-	-	-	-	-	-	-	-
MW-26	-	-	-	-	-	-	-	-	-	-	-	-	-	-	-	-	-	-	-	ND	ND	ND	-
MW-27A	-	-	-	-	-	-	-	-	-	-	-	-	-	-	-	-	-	-	-	<5	0.37	8	-
MW-27B	-	-	-	-	-	-	-	-	-	-	-	-	-	-	-	-	-	-	-	76.9	3.9	204	16.6
MW-28	-	-	-	-	-	-	-	-	-	-	-	-	-	-	-	-	-	-	-	<1	<0.32	0.33	<0.32
Protection Standard	5	5	5	5	5	5	5	5	5	5	5	5	5	5	5	5	5	5	5	5	5	5	5

Table 3.5: Benzene concentrations measured and drinking water regulatory standard (continued) (regulatory standard exceedences are highlighted)

	Concentration (µg/L)																						
Well	Dec-92	Nov-93	Mar-94	Aug-95	Mar-96	Jun-96	Sep-96	Dec-96	Mar-98	Jun-98	Sep-98	Jun-99	Nov-99	Jun-00	Jun-01	Aug-01	Nov-01	Nov-00	Mar-02	Nov-02	Mar-03	Sep-03	Jun-07
MW-1	-	-	-	-	-	-	-	-	-	-	-	-	-	-	-	-	-	-	-	-	-	-	-
MW-2	-	-	-	-	-	-	-	-	-	-	-	-	-	-	-	-	-	-	-	-	-	-	-
MW-3	12	48	11	95	4.8	0.22	4.6	19	60	12	0.1	2.077	0.022	1.7	0.6	<0.1	3	0.36	0.24	-	0.266	-	-
MW-3A	-	-	-	-	-	-	-	-	-	-	-	-	-	-	-	-	-	-	-	-	-	-	-
MW-3B	-	-	-	-	-	-	-	-	-	-	-	-	-	-	-	-	-	<0.19	<0.19	<0.26	0.082	-	-
MW-3C	-	-	-	-	-	-	-	-	-	-	-	-	-	-	-	-	-	-	-	-	-	-	-
MW-4	-	0.19	0.19	1.6	0.19	0.19	0.19	0.27	10	12	0.1	0.03	0.025	0.021	0.01	<0.10	0.29	<0.19	-	<0.048	<0.05	-	-
MW-5A	-	-	-	-	-	-	-	-	-	-	-	-	-	-	-	<0.1	-	<0.19	<0.19	<0.051	<0.05	0.0293	0.0293
MW-5B	-	280	110	-	-	-	-	-	200	12	0.1	4.2	14	18	4	-	47	<9.5	<19	13.5	11	38.5	38.5
MW-6	-	0.95	1.9	1.9	1.9	1.9	3.8	0.31	10	12	0.1	0.222	0.021	0.21	<0.005	<0.1	0.81	<0.19	<0.19	-	<0.05	<0.0156	<0.0156
MW-6A	-	-	-	-	-	-	-	-	-	-	-	-	-	-		-		-	-	-	-		
MW-6B	-	-	-	-	-	-	-	-	-	-	-	-	-	-	-	-	-	-	-	-	-	-	-
MW-6C	-	-	-	-	-	-	-	-	-	-	-	-	-	-	-	-	-	-	-	-	-	-	-
MW-7	-	-	0.19	0.19	0.19	0.19	0.19	0.19	10	12	0.1	0.021	0.03	0.021	0.02	<0.1	0.028	<0.19	<0.19	<0.051	<0.05	<0.0209	<0.0209
MW-8	-	-	-	-	-	-	-	-	10	12	0.1	0.02	0.02	0.022	<0.005	<0.1	0.023	<0.19	<0.19	<0.049	<0.05	<0.014	<0.014
MW9	-	-	-	-	-	-	-	-	10	12	0.1	0.0618	0.02	0.021	<0.005	<0.1	0.031	<0.19	<0.19	<0.053	<0.05	<0.014	<0.014
MW-10	-	-	-	-	-	-	-	-	10	12	0.1	0.02	0.02	0.022	<0.005	<0.1	0.049	<0.19	<0.19	<0.051	<0.05	<0.014	<0.014
MW-11	-	-	-	-	-	-	-	-	10	12	0.1	0.021	0.02	0.022	-	-	-	-	-	-	-	-	-
MW-12	-	-	-	-	-	-	-	-	-	-	-	-	-	-	-	-	-	<0.19	<0.19	<0.046	<0.05	0.0162	0.0162
MW-13A	-	-	-	-	-	-	-	-	-	-	-	-	-	-	-	-	-	-	-	-	-	-	-
MW-13B	-	-	-	-	-	-	-	-	-	-	-	-	-	-	-	-	-	-	-	-	-	-	-
MW-13C	-	-	-	-	-	-	-	-	-	-	-	-	-	-	-	-	-	-	-	-	-	-	-
Protection Standard	0.2	0.2	0.2	0.2	0.2	0.2	0.2	0.2	0.2	0.2	0.2	0.2	0.2	0.2	0.2	0.2	0.2	0.2	0.2	0.2	0.2	0.2	0.2

Table 3.6: Benzo(a)pyrene concentrations measured and drinking water regulatory standard (regulatory standard exceedences are highlighted)

	Concentration (µg/L)																						
Well	Dec-92	Nov-93	Mar-94	Aug-95	Mar-96	Jun-96	Sep-96	Dec-96	Mar-98	Jun-98	Sep-98	Jun-99	Nov-99	Jun-00	Jun-01	Aug-01	Nov-01	Nov-00	Mar-02	Nov-02	Mar-03	Sep-03	Jun-07
MW-14	-	-	-	-	-	-	-	-	-	-	-	-	-	-	-	-	-	-	-	-	-	-	-
MW-14A	-	-	-	-	-	-	-	-	-	-	-	-	-	-	-	-	-	-	-	-	-	-	-
MW-15A	-	-	-	-	-	-	-	-	-	-	-	-	-	-	-	-	-	-	-	-	-	-	-
MW-15B	-	-	-	-	-	-	-	-	-	-	-	-	-	-	-	-	-	<0.19	<0.19	<0.49	<0.05	0.166	0.166
MW-16A	-	-	-	-	-	-	-	-	-	-	-	-	-	-	-	-	-	<0.19	0.3	0.27	0.26	0.0176	0.0176
MW-16B	-	-	-	-	-	-	-	-	-	-	-	-	-	-	-	-	-	<0.19	2.03	<4.6	1.18	0.154	0.154
MW-17	-	-	-	-	-	-	-	-	-	-	-	-	-	-	-	-	-	-	-	-	-	-	-
MW-18	-	-	-	-	-	-	-	-	-	-	-	-	-	-	-	-	-	<0.19	<0.19	0.35	0.226	0.11	0.11
MW19A	-	-	-	-	-	-	-	-	-	-	-	-	-	-	-	-	-	-	-	-	-	-	-
MW19B	-	-	-	-	-	-	-	-	-	-	-	-	-	-	-	-	-	ND	ND	ND	ND	-	-
MW-20	-	-	-	-	-	-	-	-	-	-	-	-	-	-	-	-	-	-	-	-	-	-	-
MW-21	-	-	-	-	-	-	-	-	-	-	-	-	-	-	-	-	-	-	-	-	-	-	-
MW-23	-	-	-	-	-	-	-	-	-	-	-	-	-	-	-	-	-	-	-	-	-	-	-
MW-24	-	-	-	-	-	-	-	-	-	-	-	-	-	-	-	-	-	-	ND	ND	ND	-	-
MW-25	-	-	-	-	-	-	-	-	-	-	-	-	-	-	-	-	-	-	ND	ND	ND	-	-
MW-26	-	-	-	-	-	-	-	-	-	-	-	-	-	-	-	-	-	-	-	-	-	-	-
MW-27A	-	-	-	-	-	-	-	-	-	-	-	-	-	-	-	-	-	-	-	-	-	-	-
MW-27B	-	-	-	-	-	-	-	-	-	-	-	-	-	-	-	-	-	-	-	-	-	-	-
MW-28	-	-	-	-	-	-	-	-	-	-	-	-	-	-	-	-	-	-	-	-	-	-	-
Protection Standard	0.2	0.2	0.2	0.2	0.2	0.2	0.2	0.2	0.2	0.2	0.2	0.2	0.2	0.2	0.2	0.2	0.2	0.2	0.2	0.2	0.2	0.2	0.2

Table 3.6: Benzo(a)pyrene concentrations measured and drinking water regulatory standard (continued) (regulatory standard exceedences are highlighted)

	Concentration (µg/L)																						
Well	Dec-92	Nov-93	Mar-94	Aug-95	Mar-96	Jun-96	Sep-96	Dec-96	Mar-98	Jun-98	Sep-98	Jun-99	Nov-99	Jun-00	Nov-00	Jun-01	Aug-01	Nov-01	Mar-02	Nov-02	Mar-03	Sep-03	Jun-07
MW-1	-	-	-	-	-	-	-	-	-	-	-	-	-	-	-	-	-	-	-	-	-	-	-
MW-2	-	-	-	-	-	-	-	-	-	-	-	-	-	-	-	-	1.86	-	4.69	<0.1	0.12	<0.054	-
MW-3	190	350	210	120	90	18	110	22	190	18	95	250	0.1	270	220	19	276	14	35.5	186	-	53.2	-
MW-3A	-	-	-	-	-	-	-	-	-	-	-	-	-	-	-	-	-	-	1550	2920	1890	1100	-
MW-3B	-	-	-	-	-	-	-	-	-	-	-	-	-	-	-	-	-	-	35.7	25.1	29.6	13.4	-
MW-3C	-	-	-	-	-	-	-	-	-	-	-	-	-	-	-	-	-	-	-	604	472	42.2	-
MW-4	-	1.2	0.19	0.89	0.21	0.19	0.19	1.5	10	12	0.1	0.13	0.11	0.46	0.06	0.03	<0.1	<0.028	<0.1	-	<0.071	<0.054	-
MW-5A	-	-	-	-	-	-	-	-	-	-	-	-	-	-	-	-	<0.1	-	<0.1	<0.1	2.9	4.61	10.7
MW-5B	-	26000	7200	-	-	-	-	-	1400	360	2800	2100	0.99	1400	2000	820	-	760	1050	1900	2050	1650	957
MW-6	-	23	1.9	1.9	4.4	4.6	6.6	2.5	10	12	0.7	1.332	0.095	0.95	1.9	0.1	0.46	<0.56	<0.1	1.39	-	0.224	0.211
MW-6A	-	-	-	-	-	-	-	-	-	-	-	-	-	-	-	-	<0.1	-	<0.1	<0.1	<0.07	0.844	-
MW-6B	-	-	-	-	-	-	-	-	-	-	-	-	-	-	-	-	3.67	-	0.41	0.49	<0.37	0.278	-
MW-6C	-	-	-	-	-	-	-	-	-	-	-	-	-	-	-	-	1.76	-	<0.1	<0.1	-	0.597	-
MW-7	-	-	0.19	0.19	0.19	0.34	0.19	0.19	10	12	0.1	0.126	0.13	0.096	0.06	<0.028	0.85	0.032	0.6	<0.1	<0.074	<0.054	<0.018
MW-8	-	-	-	-	-	-	-	-	10	12	0.1	0.121	0.09	0.097	0.096	<0.028	0.85	0.039	<0.1	<0.1	0.15	<0.054	<0.018
MW9	-	-	-	-	-	-	-	-	10	12	0.1	0.0824	0.09	0.096	0.098	<0.013	<0.1	0.029	<0.1	<0.1	<0.037	<0.034	-
MW-10	-	-	-	-	-	-	-	-	10	12	0.1	0.121	0.09	0.097	0.067	<0.013	<0.1	0.035	<0.1	<0.1	<0.036	<0.034	-
MW-11	-	-	-	-	-	-	-	-	10	12	0.1	0.123	0.09	0.098	0.092	0.03	<0.10	<0.028	<0.1	<0.1	<0.075	<0.054	-
MW-12	-	-	-	-	-	-	-	-	-	-	-	-	-	-	-	-	-	-	-	-	-	-	-
MW-13A	-	-	-	-	-	-	-	-	-	-	-	-	-	-	-	-	-	-	-	-	-	-	-
MW-13B	-	-	-	-	-	-	-	-	-	-	-	-	-	-	-	-	0.57	-	2.41	4.76	3.6	2.43	0.894
MW-13C	-	-	-	-	-	-	-	-	-	-	-	-	-	-	-	-	-	-	-	62.20	<0.077	21.5	-
Protection Standard	20	20	20	20	20	20	20	20	20	20	20	20	20	20	20	20	20	20	20	20	20	20	20

Table 3.7: Naphthalene concentrations measured and drinking water regulatory standard (regulatory standard exceedences are highlighted)

	Concentration (µg/L)																						
Well	Dec-92	Nov-93	Mar-94	Aug-95	Mar-96	Jun-96	Sep-96	Dec-96	Mar-98	Jun-98	Sep-98	Jun-99	Nov-99	Jun-00	Nov-00	Jun-01	Aug-01	Nov-01	Mar-02	Nov-02	Mar-03	Sep-03	Jun-07
MW-14	-	-	-	-	-	-	-	-	-	-	-	-	-	-	-	-	-	-	2.6	1.48	0.84	0.933	-
MW-14A	-	-	-	-	-	-	-	-	-	-	-	-	-	-	-	-	-	-	-	1.85	<0.087	1.17	0.604
MW-15A	-	-	-	-	-	-	-	-	-	-	-	-	-	-	-	-	-	-	118	19.6	4	43.1	-
MW-15B	-	-	-	-	-	-	-	-	-	-	-	-	-	-	-	-	-	-	3310	4780	3220	386	1910
MW-16A	-	-	-	-	-	-	-	-	-	-	-	-	-	-	-	-	-	-	1070	2020	788	556	662
MW-16B	-	-	-	-	-	-	-	-	-	-	-	-	-	-	-	-	-	-	4720	8110	7200	5260	4970
MW-17	-	-	-	-	-	-	-	-	-	-	-	-	-	-	-	-	-	-	246	42.2	<0.091	<0.06	-
MW-18	-	-	-	-	-	-	-	-	-	-	-	-	-	-	-	-	-	-	<0.1	0.56	<0.08	<0.054	0.3
MW19A	-	-	-	-	-	-	-	-	-	-	-	-	-	-	-	-	-	-	0.48	<0.1	0.19	<0.054	-
MW19B	-	-	-	-	-	-	-	-	-	-	-	-	-	-	-	-	-	-	ND	ND	ND	ND	-
MW-20A	-	-	-	-	-	-	-	-	-	-	-	-	-	-	-	-	-		-	<0.1	<0.081	0.081	
MW-20	-	-	-	-	-	-	-	-	-	-	-	-	-	-	-	-	-	-	0.91	1.98	<0.079	1.76	1.18
MW-21	-	-	-	-	-	-	-	-	-	-	-	-	-	-	-	-	-	-	<0.1	<0.1	0.98	0.086	-
MW-22	-	-	-	-	-	-	-	-	-	-	-	-	-	-	-	-	-	-	<0.1	<0.1	<0.08	0.078	
MW-23	-	-	-	-	-	-	-	-	-	-	-	-	-	-	-	-	-	-	-	<0.1	1.7	0.117	-
MW-24	-	-	-	-	-	-	-	-	-	-	-	-	-	-	-	-	-	-	-	ND	ND	ND	-
MW-25	-	-	-	-	-	-	-	-	-	-	-	-	-	-	-	-	-	-	-	ND	ND	ND	-
MW-26	-	-	-	-	-	-	-	-	-	-	-	-	-	-	-	-	-	-	-	<0.1	0.47	<0.054	-
MW-27A	-	-	-	-	-	-	-	-	-	-	-	-	-	-	-	-	-	-	-	4.86	4.3	0.915	-
MW-27B	-	-	-	-	3.25	8.3	5.57	1.55	-	-	-	-	-	-	-	-	-	-	-	3.25	8.3	5.57	1.55
MW-28	-	-	-	-	<0.1	0.076	<0.054	0.0347	-	-	-	-	-	-	-	-	-	-	-	<0.1	0.076	<0.054	0.0347
Protection Standard	20	20	20	20	20	20	20	20	20	20	20	20	20	20	20	20	20	20	20	20	20	20	20

Table 3.7: Naphthalene concentrations measured and drinking water regulatory standard (continued) (regulatory standard exceedences are highlighted)

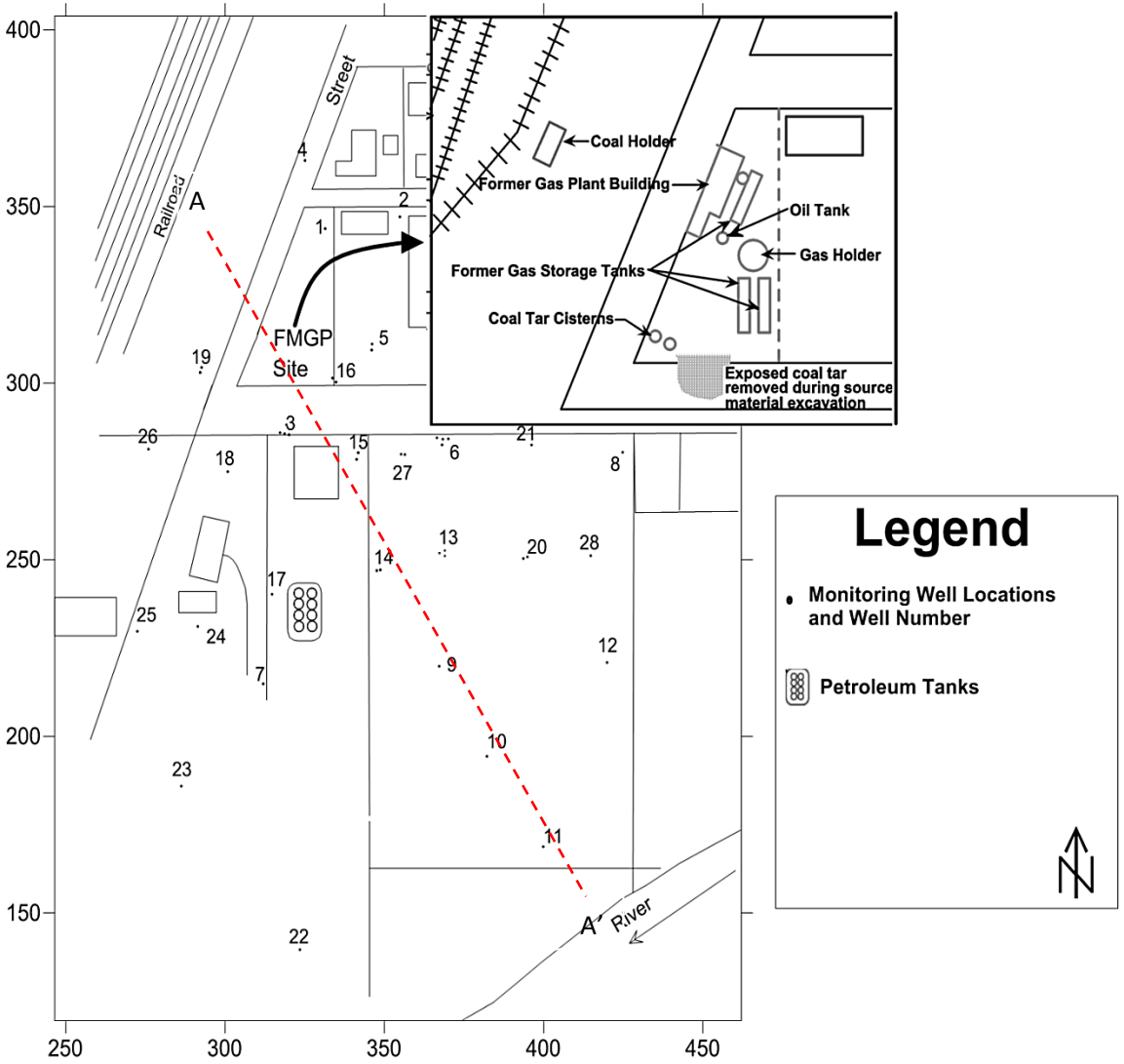

Figure 3.1: Plan view of the site showing general features of the Former MGP; horizontal and vertical scales are in meters (after Rogers et al. 2007a)

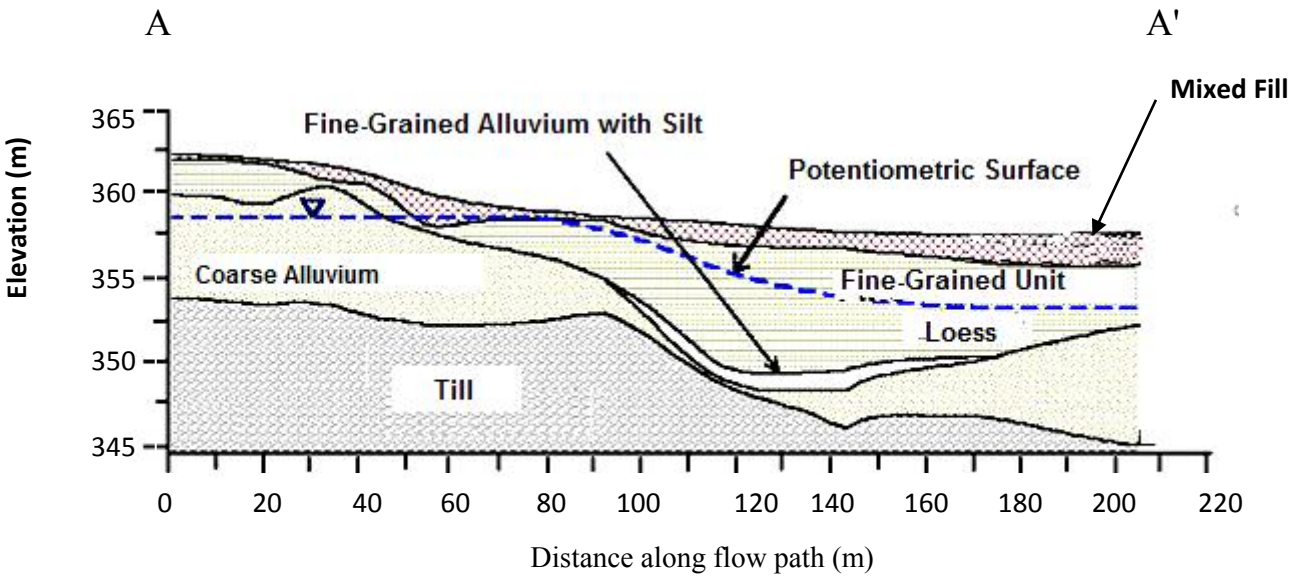

Figure 3.2: Cross-section along A-A' shown in Figure 3.1 (Rogers et al. 2007a)

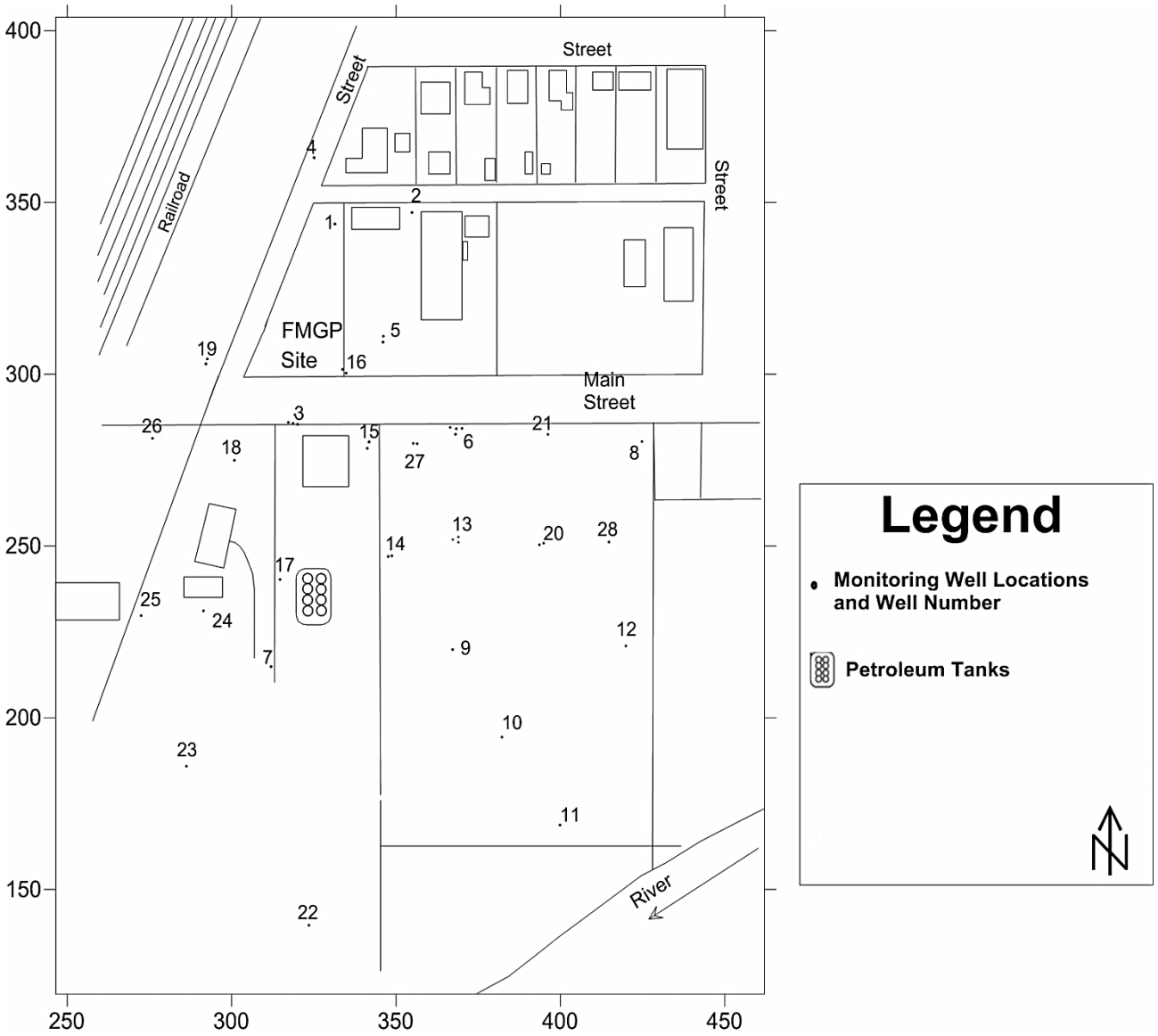

Figure 3.3: Plan view of the site showing the monitoring wells at the Former MGP; horizontal and vertical scales are in meters (Stenback and Ong 2003)

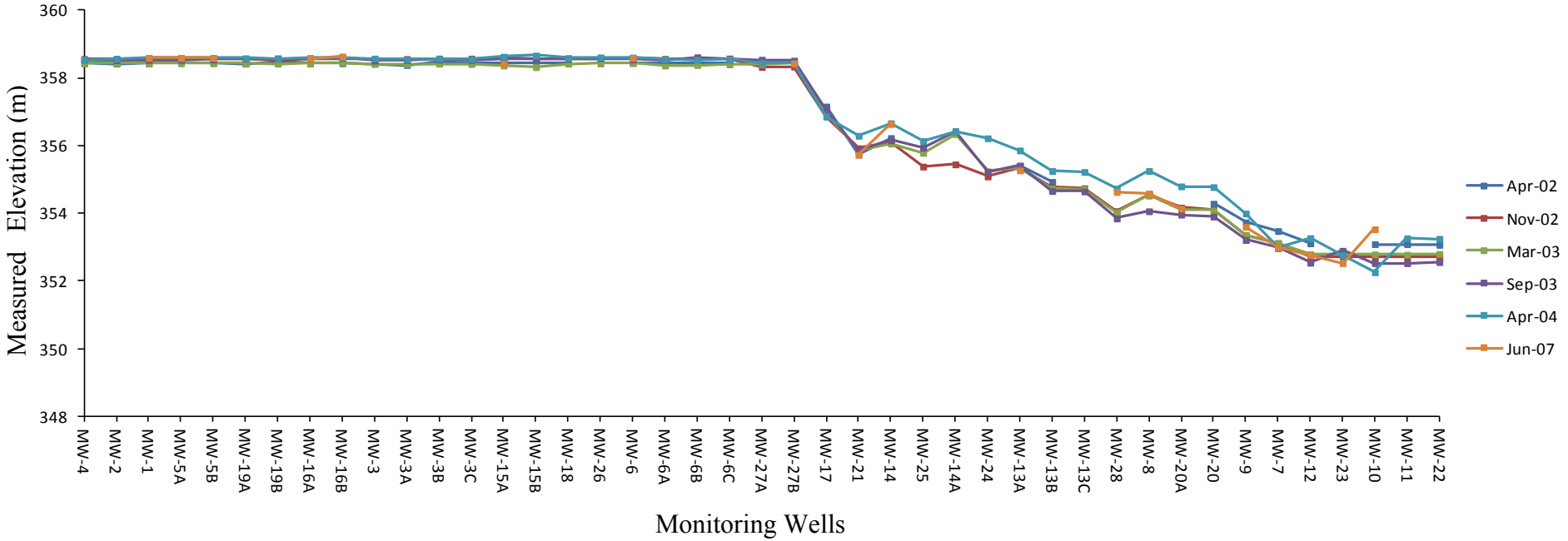

Figure 3.4: Seasonal variation of measured hydraulic heads at monitoring wells

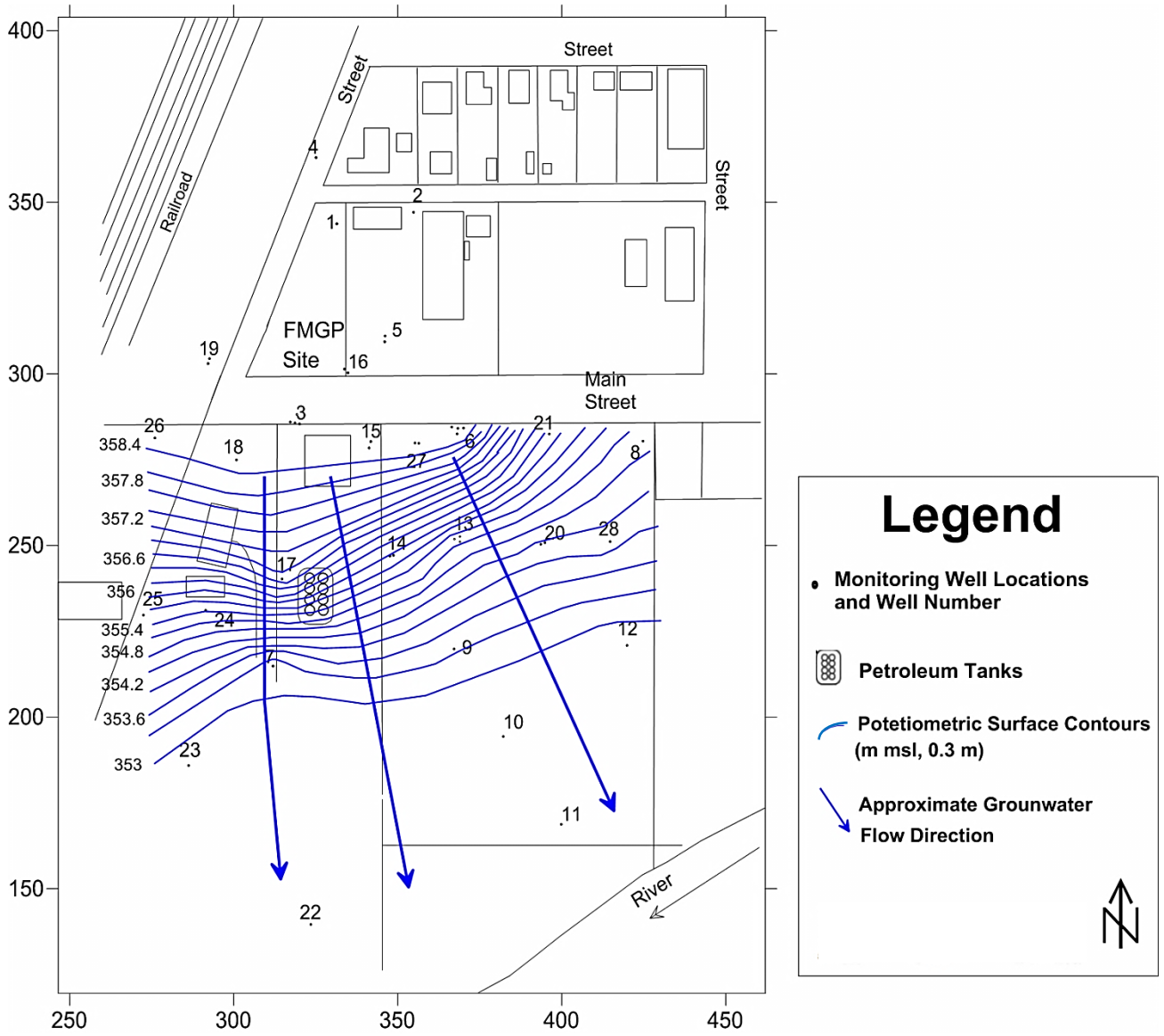

Figure 3.5: Plan showing March 2003 alluvium ground water potentiometric surface contours; horizontal and vertical scales are in meters

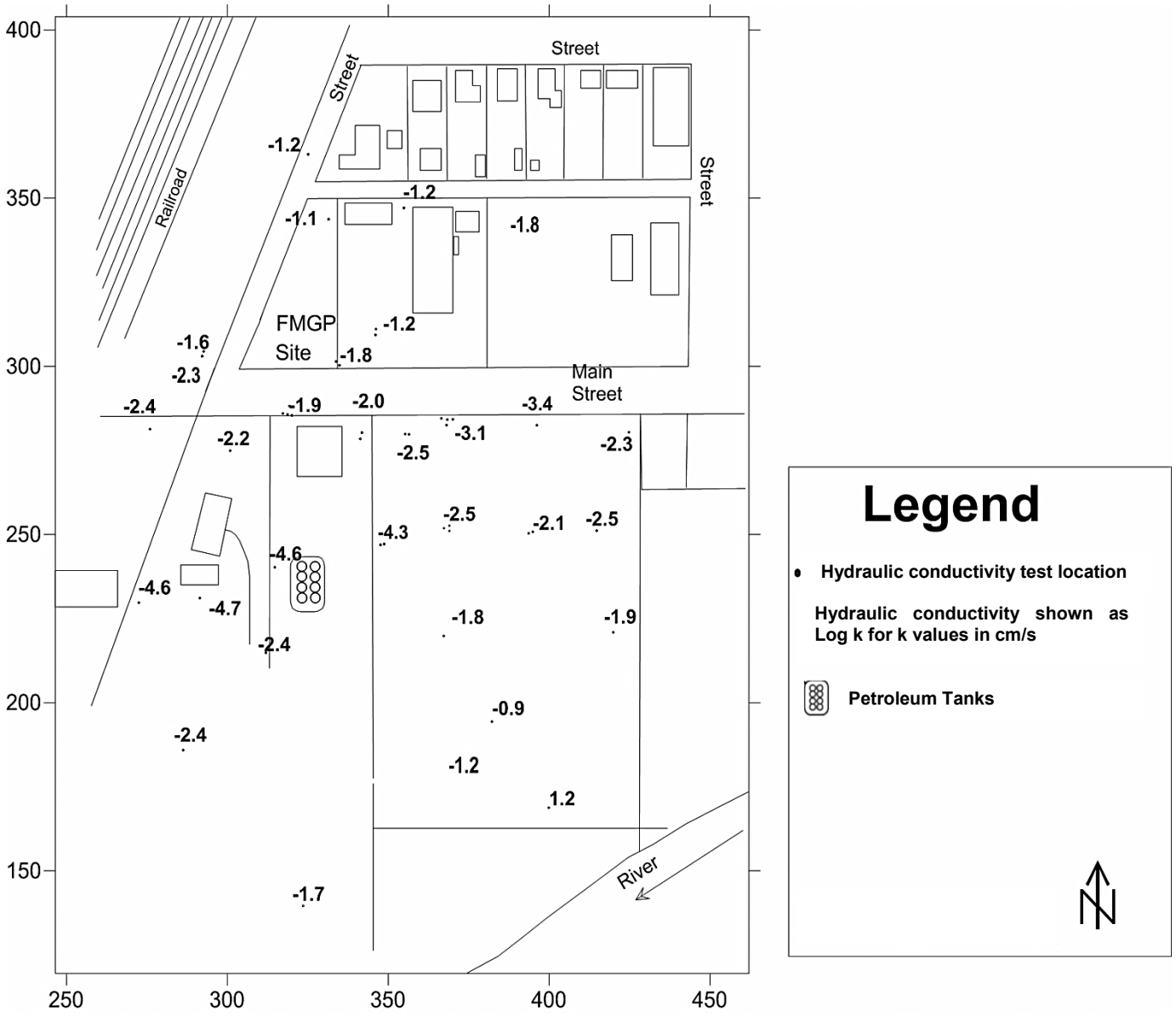

Figure 3.6: Alluvium Hydraulic Conductivity results; horizontal and vertical scales are in meters (Stenback and Ong 2003)

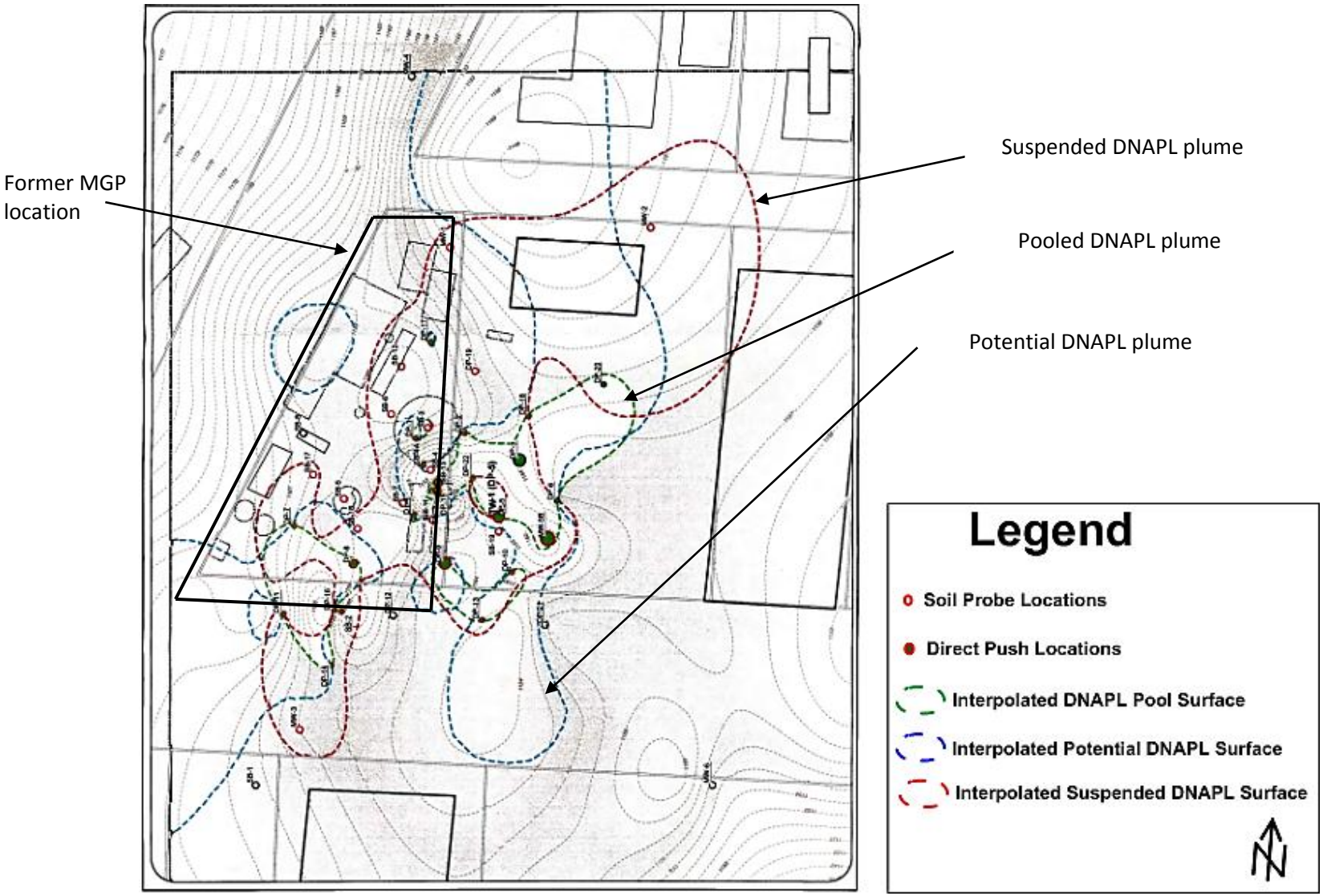

Figure 3.7: Extent of DNAPL overlying the glacial till (Black and Veatch 2008)

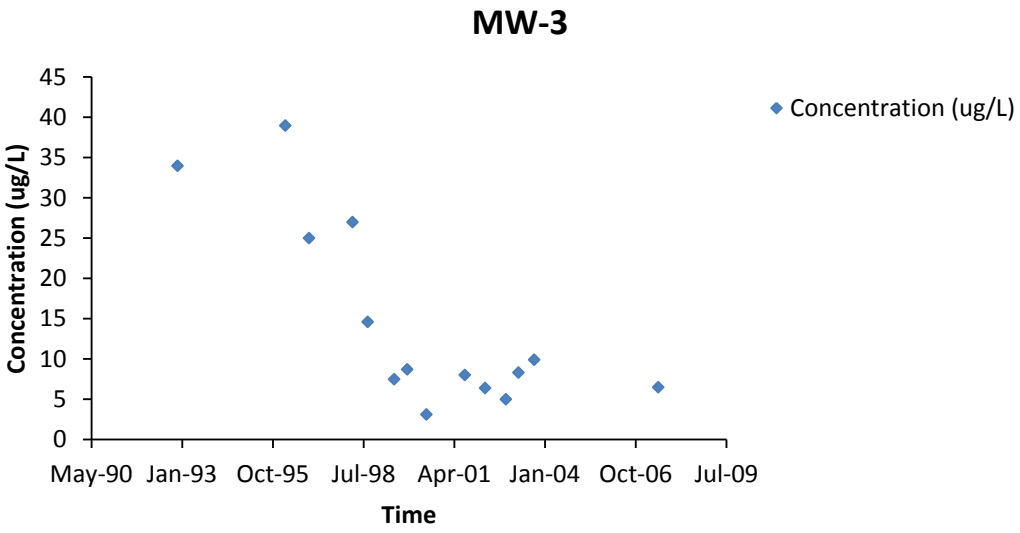

Figure 3.8: Benzene concentration versus time for MW-3

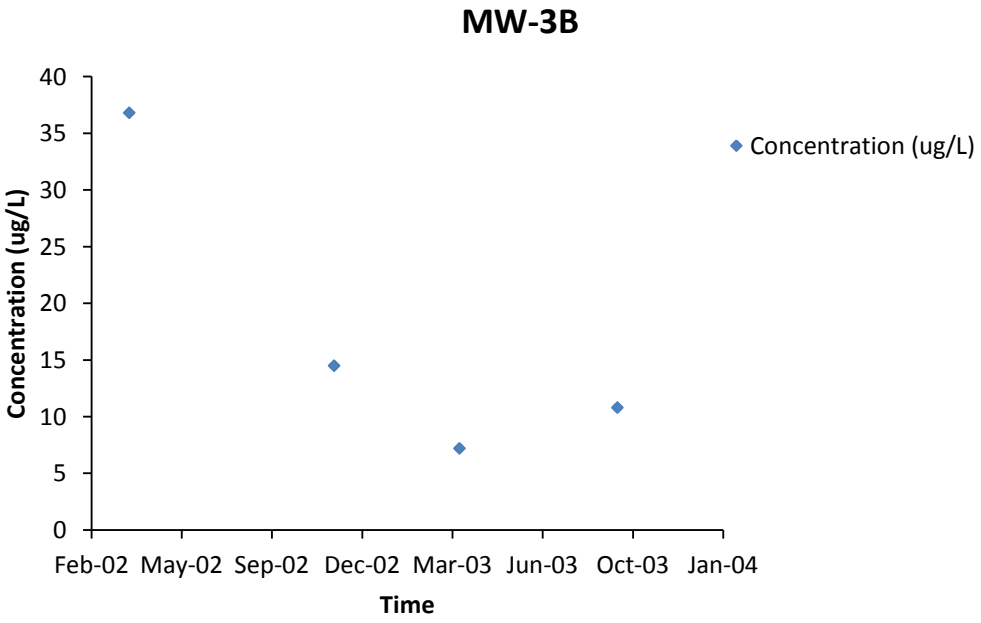

Figure 3.9: Benzene concentration versus time for MW-3B

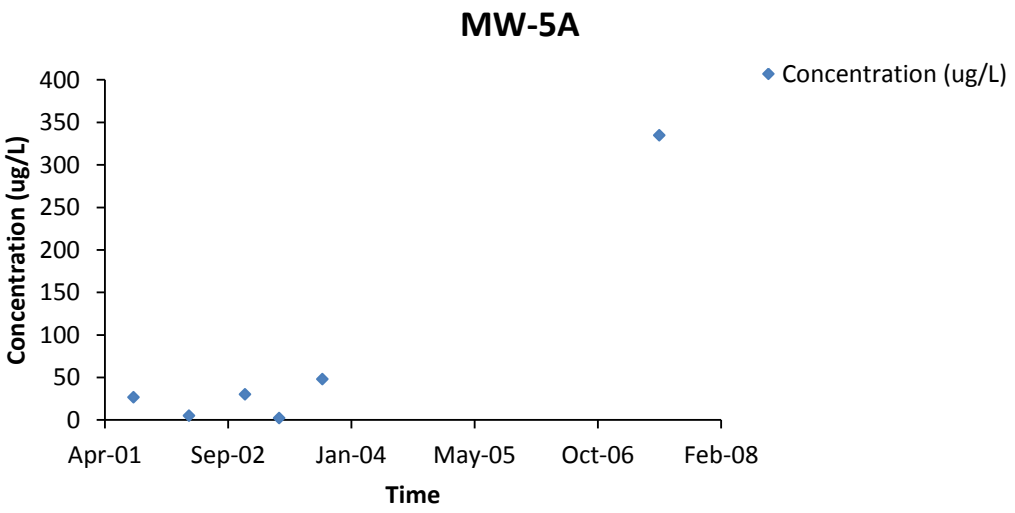

Figure 3.10: Benzene concentration versus time for MW-5A

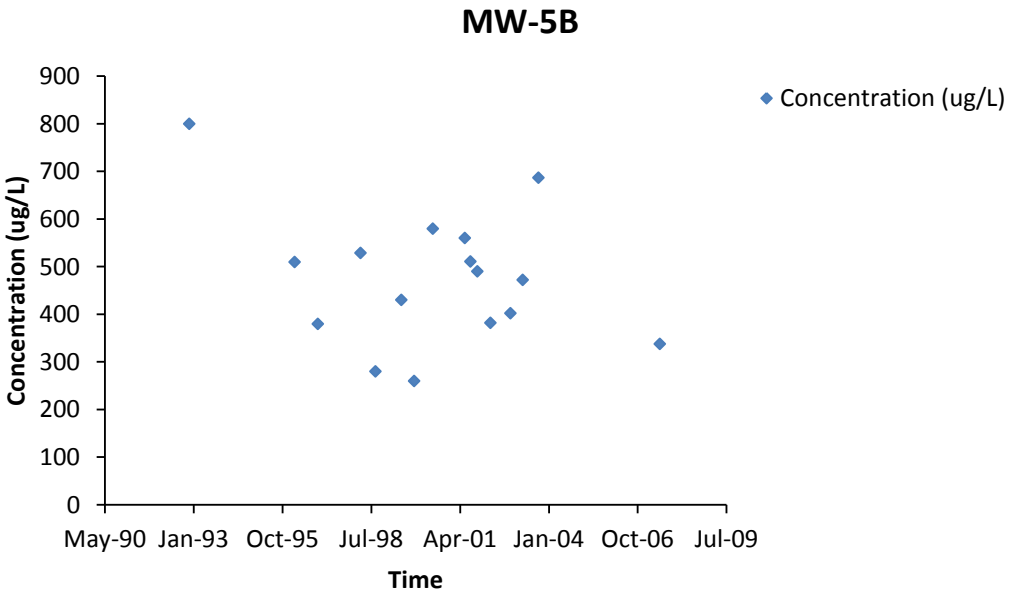

Figure 3.11: Benzene concentration versus time for MW-5B

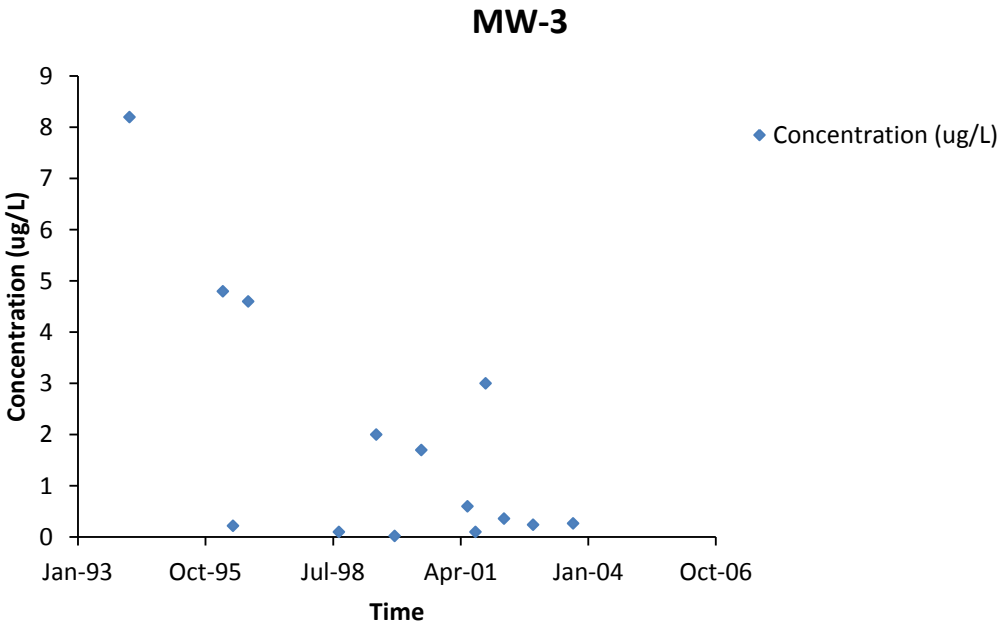

Figure 3.12: Benzo(a)pyrene concentration versus time for MW-3

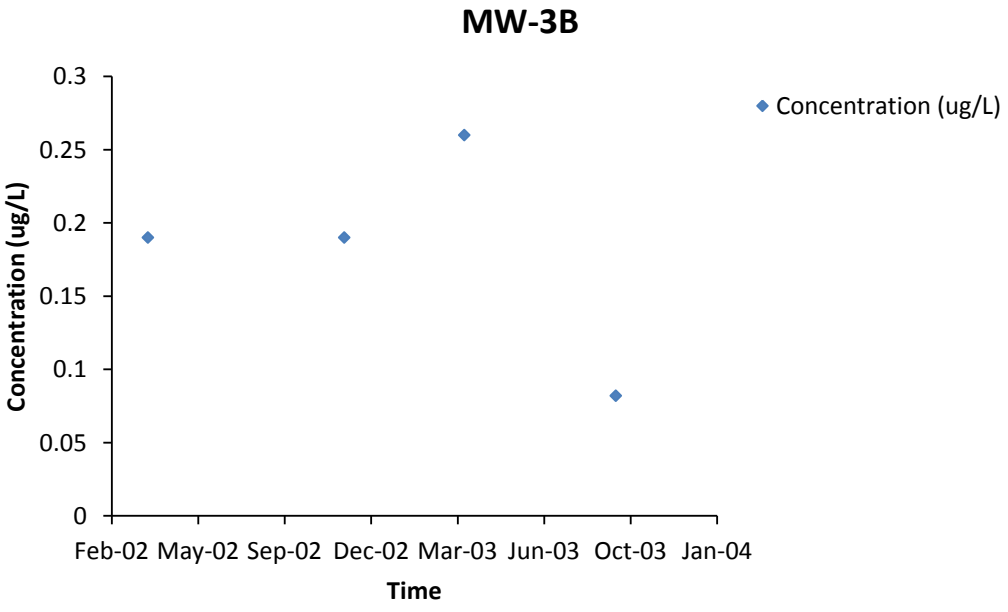

Figure 3.13: Benzo(a)pyrene concentration versus time for MW-3B

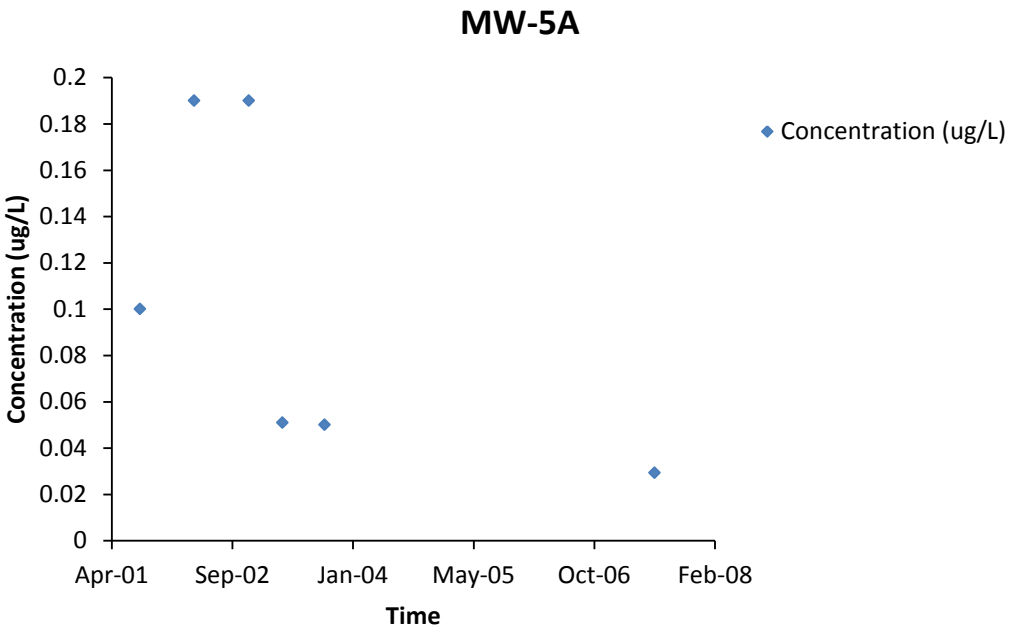

Figure 3.14: Benzo(a)pyrene concentration versus time for MW-5A

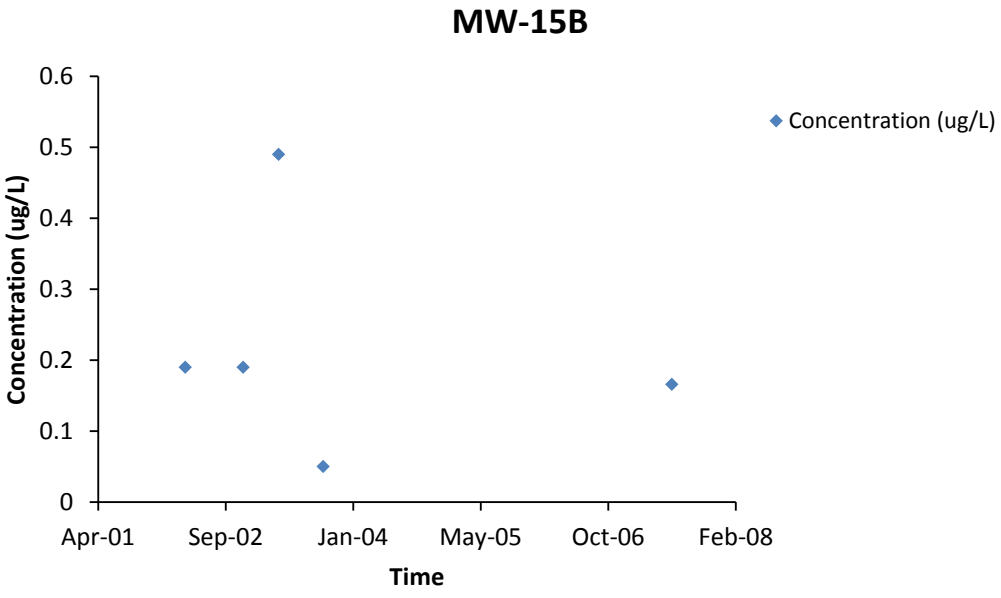

Figure 3.15: Benzo(a)pyrene concentration versus time for MW-15B

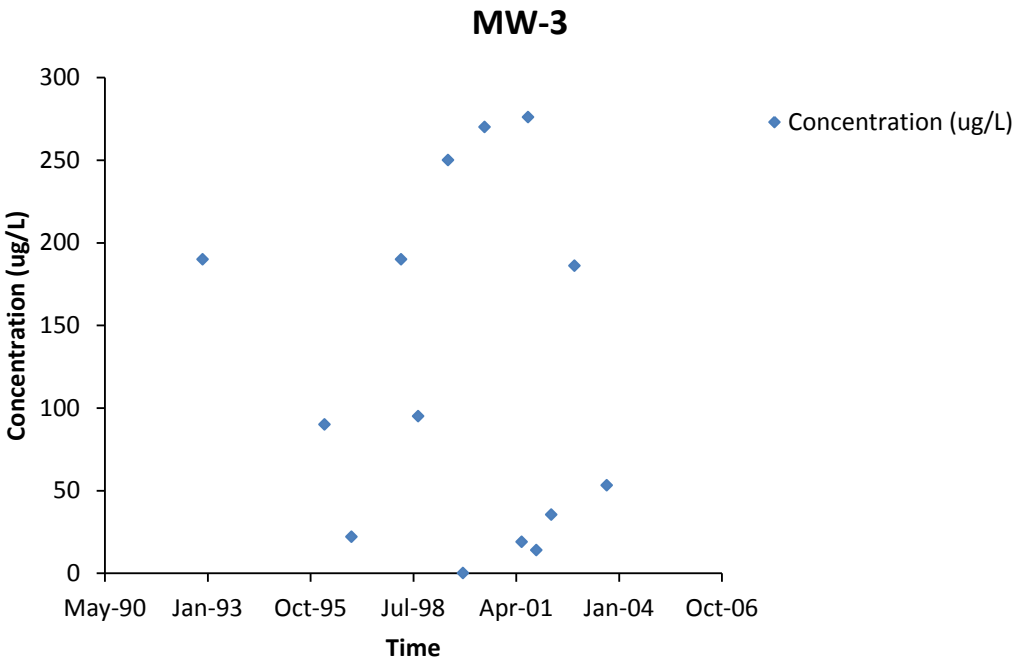

Figure 3.16: Naphthalene concentration versus time for MW-3

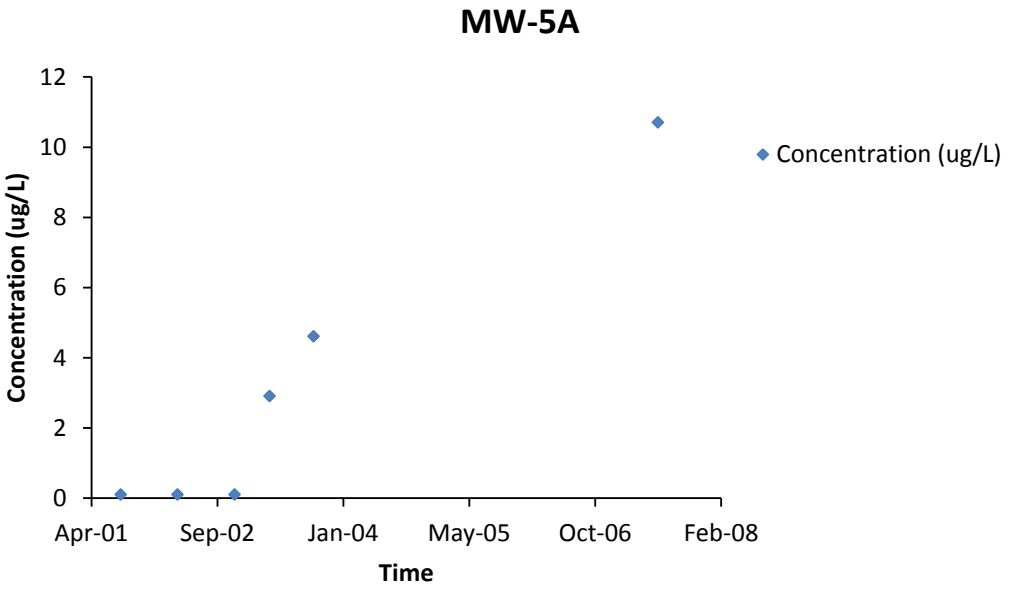

Figure 3.17: Naphthalene concentration versus time for MW-5A

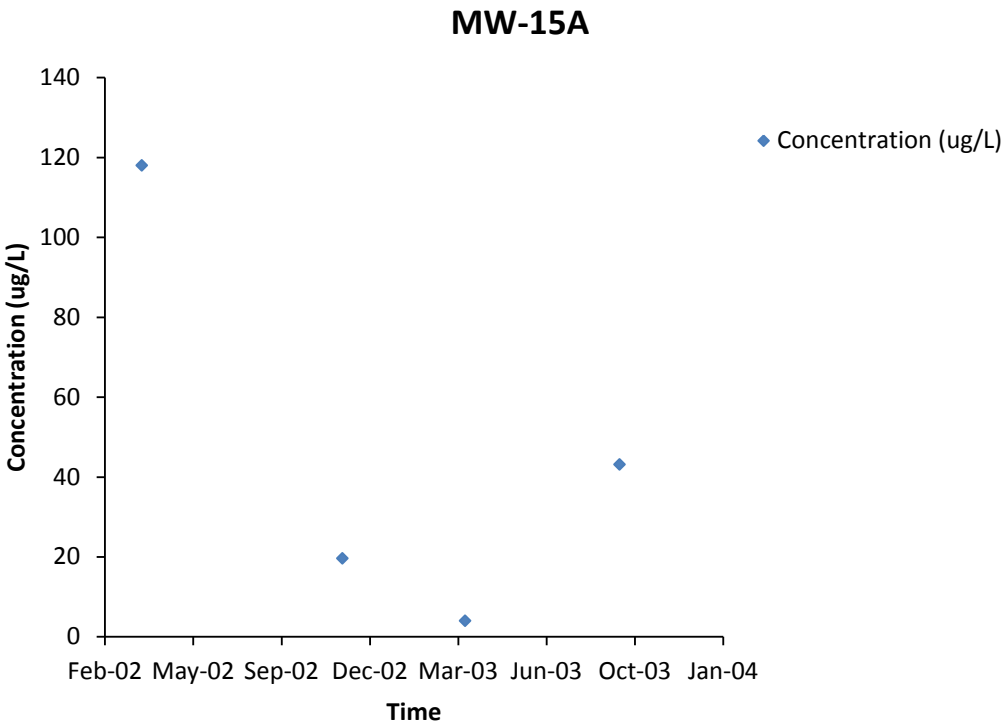

Figure 3.18: Naphthalene concentration versus time for MW-15A

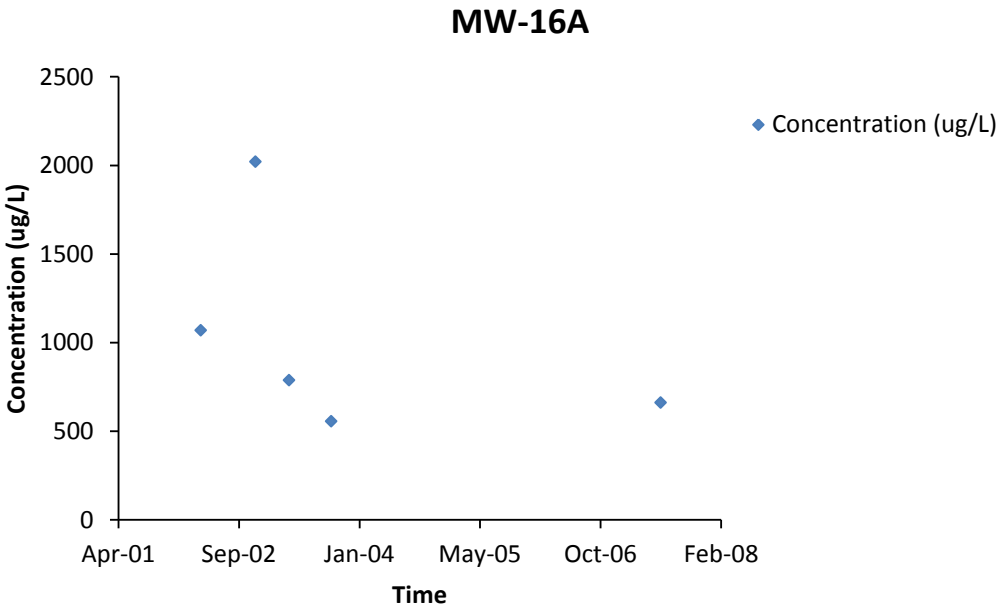

Figure 3.19: Naphthalene concentration versus time for MW-16A

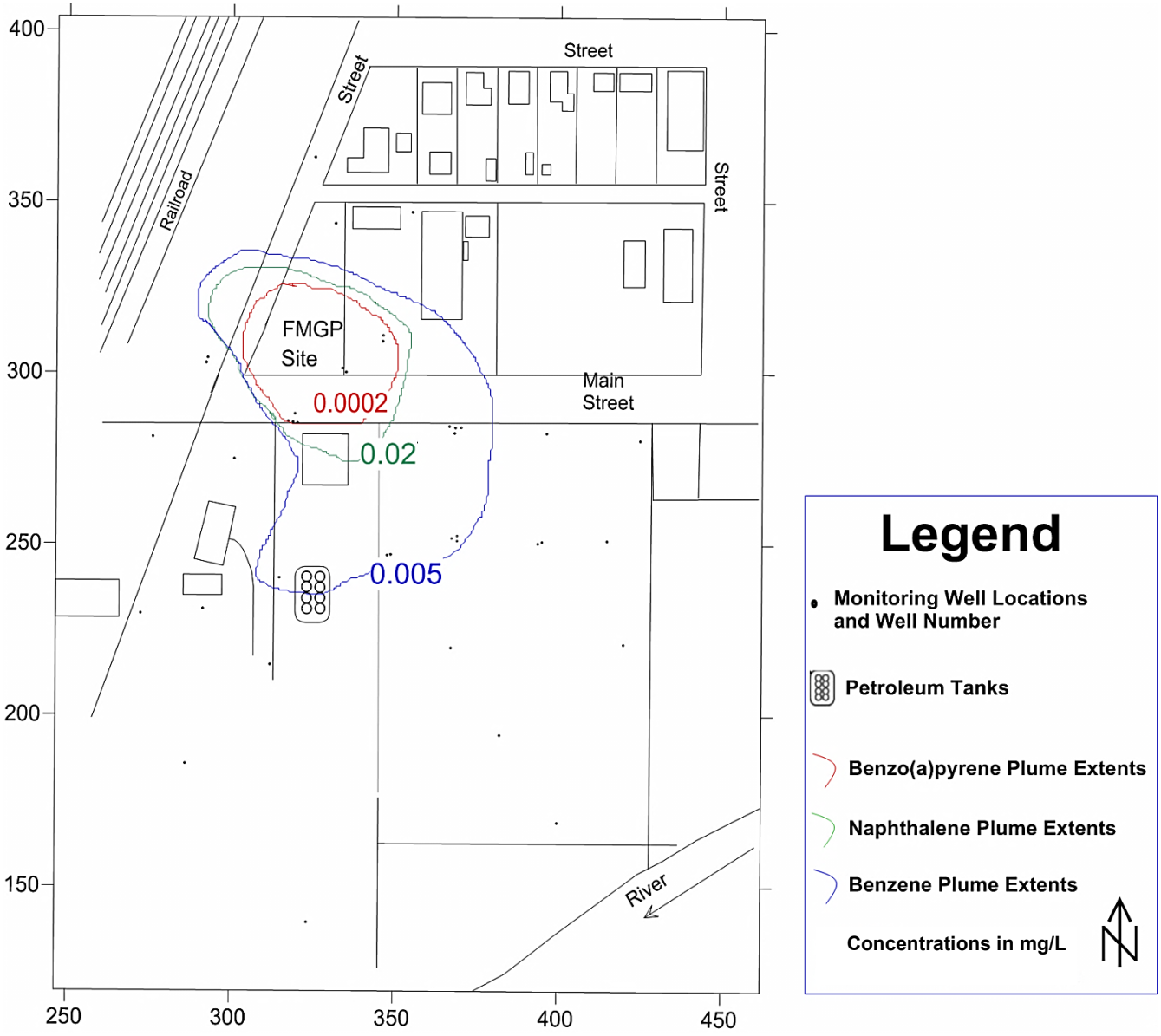

Figure 3.20: Approximate BTEX and PAH plume extents using September 2003 concentration data; horizontal and vertical scales are in meters

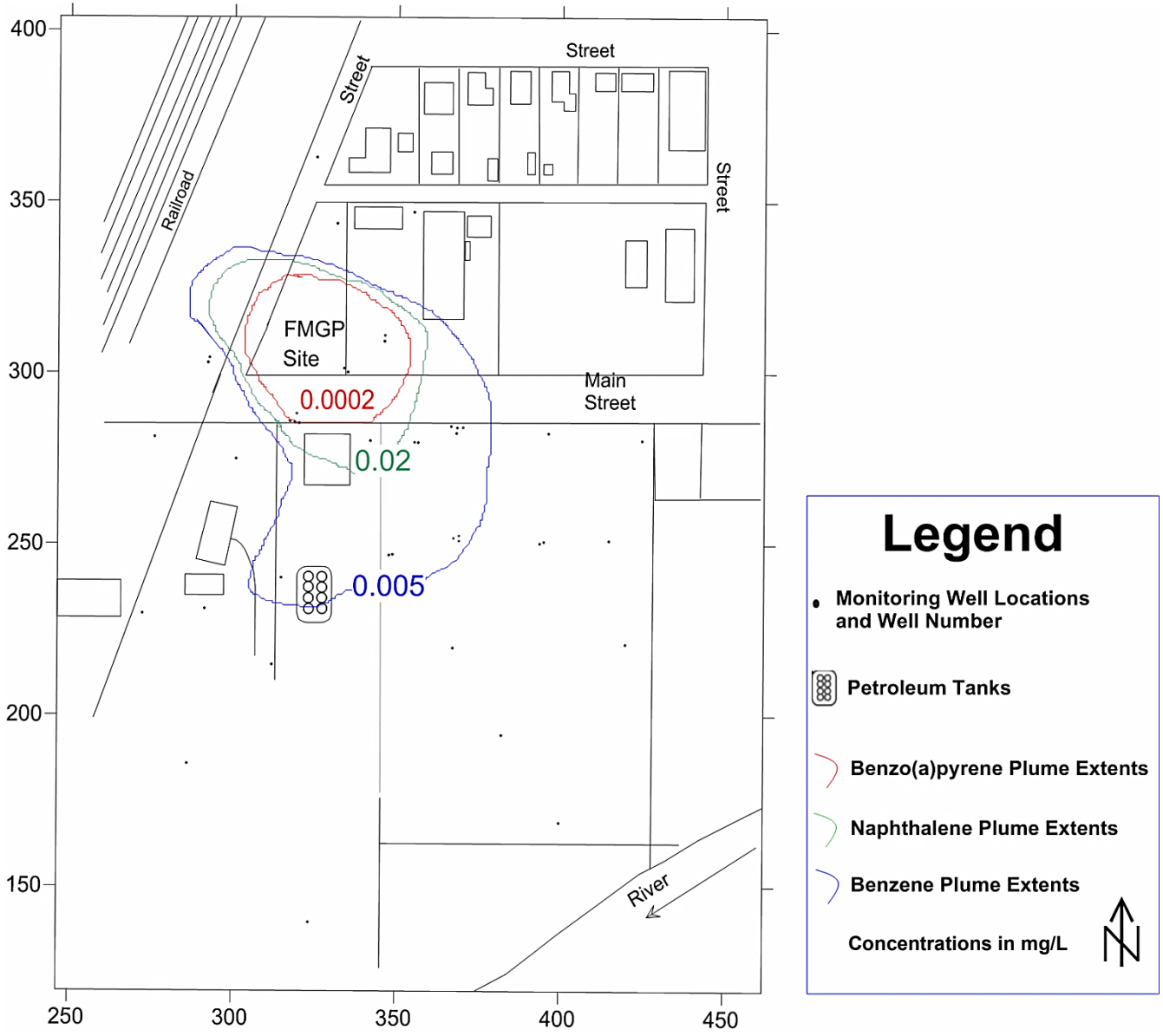

Figure 3.21: Approximate BTEX and PAH plume extents using March 2002 concentration data; horizontal and vertical scales are in meters

Chapter 4 Groundwater Flow Modeling

Models for simulating groundwater flow and solute transport can be classified according to the mathematical method employed to solve the groundwater flow and contaminant transport governing partial differential equations described in section 2.10. The two common methods are analytical and numerical methods. This study uses a numerical solution methodology for modeling.

4.1 Modeling Methodology

A flow chart after Downs and Webster (2007) describes the steps in setting up and running a groundwater flow and contaminant transport model (Figure 4.1). The first stage of the modeling process entails defining the objectives of the groundwater flow and contaminant transport modeling. These objectives are described in section 1.2. The site data and other applicable information are compiled in Chapter 3.

In the Visual MODFLOW platform, four information windows guide the user to generate the initial model characteristics. These windows are titled: project outline, flow option, transport option, and model domain. For steady state flow in a confined aquifer, the main features for modeling this site, the user can select the MODFLOW 2005 engine because this is the latest version of the groundwater flow engine available, after which flow options can be outlined. These flow options include: the time the user wants to run the simulation in days or years, hydraulic conductivity, storage, porosity and recharge values for the groundwater flow model, and bulk density, species parameters and transport properties (dispersion, sorption and biodegradation coefficients) for the contaminant transport modeling. These values can

be modified after creating the model at any time during the process.

After the model basic information input has been accomplished, the process continues with determining the areal extent of the site that needs to be modeled. The user at this point divides the site into a finite difference grid and inputs various geological data (e.g. number of model layers, geological layer contact elevations and grid locations. these data are provided in Appendix A). The user then inputs the flow boundary conditions such as constant head, river/stream, or drain that provide the initial head values and the observation wells. Next, the groundwater flow model is run and the simulated hydraulic heads are compared with the measured hydraulic heads at the observation wells. To improve the match between calculated and observed hydraulic heads, calibration with the PEST engine can be initiated by adjusting the boundary conditions or hydrogeologic input parameters (mainly hydraulic conductivity and recharge rate) throughout different zones of the model domain to minimize the hydraulic head residuals (differences between model calculated heads and site observed hydraulic head values). Successful calibration should also result in the modeled potentiometric surface closely matching the observed potentiometric surface and groundwater flow patterns at the site.

4.2 Model Construction, Inputs and Boundary Conditions

4.2.1 Groundwater Flow Model Construction

A finite difference grid was set up to cover the former MGP site and potential plume extents (Figure 4.2). The model display area, oriented approximately parallel to the NNW - SSE groundwater flow direction (see Figure 3.5), as well as the observation wells, was created with Auto-Cad and imported into Visual MODFLOW, forming the

basemap for the modeling activities. The grid is 260 m wide (ΔX = 130 columns, at spacing of 2 m) by 280 m long (ΔY = 140 rows, at spacing of 2 m). As modeling of the site progressed, the grid was coarsened by a factor of two to end up with domain cell dimensions of 4 m × 4 m. This facilitated contaminant transport modeling and had no impact on the groundwater flow model results.

The model was divided into three zones to represent the different soil layers and site stratigraphy shown in Figure 3.2. The detailed stratigraphic contact data are given in Appendix A. The top layer represents the surficial fill covering most of the site. The second layer represents the loess layer (poorly graded silt and clay size particles), and the third layer is the coarse alluvium layer. In the model, the glacial till underlying the alluvium is not defined since the thickness of the glacial till layer is unknown. Furthermore, the alluvium layer will carry the bulk of the groundwater flow and the contaminants as described in section 3.2. Hence, the glacial till layer nature and thickness are not considered part of model construction or any subsequent modeling activities. Observation wells and hydraulic head data measured in March 2003 were imported into the constructed model and used as the basis for calibrating the simulated hydraulic heads.

As described in Chapter 3 and illustrated in Figure 3.2, the geology and hydrogeology of this site are relatively complex. Figure 3.2 indicates that the coarse alluvium is a confined aquifer in the region downgradient of the source area, with the loess being considered as a confining layer. As this alluvium is considered the primary migration pathway for contaminants released from the coal tar source, the groundwater monitoring program has focused on the alluvium unit; very few monitoring wells have

been screened in the overlying loess, as indicated in Table 3.2. Moreover, the March and September 2003 groundwater elevation data in Table 3.2, for example, show that most of the nested wells in the alluvium do not indicate a significant vertical hydraulic gradient. Given this, plus the uncertainty of the spatial variation of hydraulic heads in the loess unit, it is assumed for the groundwater modeling conducted for this research that there is no vertical hydraulic gradient in the alluvium and loess units. The groundwater modeling approach for this research, therefore, is phenomenological whereby the primary goal and focus is to match the alluvium layer simulated hydraulic heads (i.e. potentiometric surface elevations), potentiometric contours and groundwater flow patterns with the alluvium layer measured conditions. In addition, while the change in thickness and lateral variations of hydraulic conductivity of the alluvium layer are accounted for in this modeling, the alluvium is modeled as one continuous layer across the site. The alluvium geologic and hydrogeologic data that are available do not warrant a systematic subdivsion of the alluvium into sublayers. This is the basis of the groundwater flow modeling conducted for this site for this research.

4.2.2 Groundwater Flow Input Parameters

The groundwater flow model requires defining the following input parameters: hydraulic conductivity, recharge rate, starting heads, geologic layer top and bottom elevations and storage. Hydraulic conductivity values for the alluvium layer, shown in Table 4.1 (obtained from Stenback and Ong 2003), were imported into the model and then interpolated using the Visual MODFLOW kriging function to create conductivity zones covering the entire layer as shown in Figure 4.3. Kriging is a geostatistical method that can be used to produce an interpolation map from irregularly spaced data.

Anisotropy and underlying trends suggested in the raw data can be incorporated in an efficient manner through kriging. However, it was discovered that using piecewise constant hydraulic conductivity zones rather than the kriging zones better represented the alluvium hydraulic conductivity (Figure 4.4) and gave simulated hydraulic head values closer to the observed values than the kriging method. The loess layer was assigned a uniform hydraulic conductivity value of 5.29×10^{-7} m/s, obtained from site characterization activities conducted by Biyani (2003), whereas the top fill layer was assigned a uniform hydraulic conductivity value of 1.0×10^{-7} m/s. A recharge rate of 278.3 mm/yr was applied downgradient of MW-6. The northern part of the site (upgradient of MW-6) is largely developed while the southern part of the site (downgradient of MW-6) is open field.

The elevation data for the layers were obtained from site investigation data including direct push technologies (DPT) (Stenback and Ong 2003). Layer elevation files were imported and interpolated to create elevations throughout the model domain. Figure 4.5 shows cross-section B-B' of the model grid (see Figure 4.2 for cross section location) detailing the three layer stratigraphy and the pinch zone (thinning of the alluvium layer).

A specific storage (S_s) value of 2.0×10^{-4} (1/m) was calculated using Equation (2.4) and assigned to both layer 2 (loess) and layer 3 (alluvium). Specific yield parameters were determined using Table 2.6 (Schwartz and Zhang 2003). For layer 3, knowing that the alluvium is mainly sand, a specific yield (S_y) value of 0.28 was used as input. Layer 2, on the other hand was assigned an S_y value of 0.18. Table 4.2 summarizes the input parameters used for modeling groundwater flow.

4.2.3 Groundwater Flow Boundary Conditions

Because monitoring well water elevations have not shown significant variations between April 2002 and June 2007 (see Figure 3.4), the water level data from March 2003 were used to define the observed hydraulic heads and boundary conditions because they represent a relatively complete set of hydraulic head data for all monitoring wells located across the site (see Table 4.3).

Constant head boundary conditions are the total head values input into the cells on the northern and southern boundaries of the site model (Figure 4.6). At the model northern end, a constant head value of 358.9 m was initially assigned. As the northern end of the grid is beyond the northern most monitoring well (MW-4), a hydraulic gradient of approximately 0.01 m/m was used to calculate the hydraulic head to be used as the model northern boundary condition. Biyani (2003) notes that the river level varied from 352.96 m to 353.28 m along the river flow direction from east to west. The lower value of 352.96 m was used as an initial constant head along the entire south boundary condition because groundwater flow simulation trials indicated that varying the boundary condition head value from east to west had minimal impact on the simulation results. The model eastern and western boundaries were assumed as no flow boundaries. These boundaries are approximately perpendicular to the measured potentiometric surface contours, indicating a no flow condition is most appropriate along these boundaries.

4.3 Groundwater Flow Modeling Results

4.3.1 Initial Runs

Initial Visual MODFLOW model runs were conducted using the kriging interpolated

hydraulic conductivity values for the alluvium layer. Figure 4.7 shows the resulting potentiometric contour distribution in the alluvium layer. The simulated contour heads show a poor match to the measured potentiometric contours shown in Figure 3.5. It was noticed, however, that the simulated contours show a clear indication of the pinch zone area where there is a sudden drop of about 4 m of head. Figure 4.8 shows the 32 data points (i.e. monitoring/observation wells) of calculated heads plotted in relation to the corresponding observed head values. This run gave a maximum residual head value (i.e. difference between calculated and observed) of more than one meter at monitoring well 14A and a calculated heads absolute residual mean of 0.413 m. Potentiometric contours for layer 2 (loess) are presented in Figure 4.9. Most of the northern site area was found to be composed of dry cells in this layer. The implications of this are discussed in section 4.3.2.

With such large variations of calculated versus observed head values, it was decided to run the model using the piecewise alluvium conductivity zones shown in Figure 4.4. This run resulted in values of hydraulic heads and potentiometric contours more closely matching the measured values (compare Figure 4.8 with Figure 4.10). Furthermore, this run gave a maximum residual head value of 0.865 m (for MW-6B) as well as a calculated heads absolute residual mean of 0.334 m (see Figure 4.11). These were considered promising initial values that can be further optimized with the WINPEST component of Visual MODFLOW during calibration runs.

4.3.2 Groundwater Flow Calibration Using WINPEST

The purpose of calibration is to define the distribution of parameters and boundary conditions that provide the best fit between calculated and observed hydraulic heads

and groundwater flow patterns. Therefore, several hydraulic conductivity, constant boundary and recharge rate values were altered across the model zones during calibration using WINPEST to obtain better correlation between observed and calculated head values and groundwater flow patterns.

Visual MODFLOW assigns a default head value for each dry cell as a flag to indicate it is dry, and this value is typically a very large negative number (e.g. -1.0×10^{30} m). The presence of large negative head values in dry cells caused problems for parameter estimation simulations because this large negative value is used to calculate the calibration residual (calculated head minus observed head) at a grid cell that has become dry during one of the WINPEST iterations. In such a case, the Visual MODFLOW manual (Schlumberger Water Services 2010) recommends that the hydraulic head value in such a model cell be set equal to the cell bottom elevation (rewetting option). This was done for all dry cells to complete the WINPEST runs.

The calibration process was approached by decreasing both the recharge rate and the model southern hydraulic head boundary (river) slightly and progressively, until calculated head values more closely matching the measured values were achieved. After this, hydraulic conductivity zone values were altered by varying one hydraulic conductivity zone value and monitoring the impact on hydraulic head residuals, and then adjusting other hydraulic conductivity zone values accordingly. In addition, during calibration runs, the final conductivity values obtained from a complete run were used as a starting point for the next calibration run until the final calibration run produced acceptable maximum residual head values, acceptable calculated head values, and a groundwater flow pattern that closely matches that obtained from

observed head values. The final results obtained from WINPEST were then re-entered by the user to rerun the model in order to conclude the calibration process.

The southern boundary condition (river) head was decreased by 0.2 m to a final calibrated value of 352.7 m, and the final recharge rate obtained after calibration was 98 mm/yr. Figure 4.12 details the calibrated model potentiometric contours in the alluvium layer and the general groundwater flow pattern. These closely match the observed conditions as shown in Figure 3.5. Additionally, the potentiometric contours for the loess layer are shown in Figure 4.13 and correspond quite closely to the alluvium layer potentiometric contours. This follows the assumption that there is no vertical hydraulic gradient in the alluvium and loess layers. The calculated versus observed head graph for the calibrated model is shown in Figure 4.14; a maximum residual head value of 0.245 m at monitoring well 27B and an absolute residual mean of head residuals of 0.116 m were achieved. Table 4.4 presents a comparison between measured and simulated hydraulic head values for the monitoring/observation wells for the calibrated model. The root mean square error between observed and calibrated hydraulic heads is 0.133 m. MW-6, MW-6A, MW-6B and MW-6C along with MW-27B have the highest residual head values that contribute to increasing the root mean square error. This could be related to the fact that the MW-6 wells were occasionally artesian, as described by Kjartanson et al. (2002).

The calibrated hydraulic conductivity values obtained from the Visual MODFLOW conductivity database are shown in Table 4.5 together with the initial values of conductivity for the 12 conductivity zones, for comparison purposes. Most of the zonal hydraulic conductivity values were calibrated to within a maximum of one order

of magnitude from the initial zonal hydraulic conductivity values. The calibrated hydraulic conductivity zones are shown in Figure 4.15. Note that zones 1 and 2 represent the fill and loess layers, respectively.

4.4 Particle Tracking

Modpath was used to track the flowpath of particles released from the former MGP contaminant source area. Several particle lines were added in layer 3 (alluvium) within the upstream source area cells, the area believed to be the most impacted by the MGP process tar residuals (Figure 4.16).

The distribution of calibrated hydraulic conductivity zones in the alluvium, shown in Figure 4.15, has directly affected the trend of the particle pathlines. The higher hydraulic conductivity area on the eastern side of the pinch zone is a preferred pathline area for the particles to travel toward the river boundary. On the other hand, in the western part of the pinch zone (zone 6 and zone 8, Figure 4.15), the lower hydraulic conductivity area was modestly used by the particles in their migration downgradient. The pathlines produced with Modpath for a steady state condition presented in Figure 4.16 indicate that the flow of contaminants in the alluvium layer would be mainly in a south-south east direction heading towards the river at the model south boundary. A minimum number of particles were able to pass throughout the western part of the pinch zone. This is due to the lower hydraulic conductivity values throughout this part of the pinch zone. This indicates that contaminants released from the MGP source will be less likely to migrate through this part of the pinch zone.

id	k(ft/d)	k(m/s)
MW1	2.27E+02	8.01E-04
MW2	1.76E+02	6.21E-04
MW3	9.07E+01	3.20E-04
MW3A	1.02E+01	3.60E-05
MW3B	3.69E+01	1.30E-04
MW3C	1.36E+01	4.80E-05
MW4	1.73E+02	6.10E-04
MW5B	1.81E+02	6.39E-04
MW6	2.83E+01	9.98E-05
MW6A	2.52E+00	8.89E-06
MW6B	9.35E-01	3.30E-06
MW6C	2.83E+01	9.98E-05
MW7	1.16E+01	4.09E-05
MW8	1.28E+01	4.52E-05
MW9	4.54E+01	1.60E-04
MW10	3.69E+02	1.30E-03
MW11	2.83E+03	9.98E-03
MW12	3.40E+01	1.20E-04
MW13C	8.79E+00	3.10E-05
MW14A	1.50E-01	5.29E-07
MW14	4.54E-01	1.60E-06
MW15A	3.69E+01	1.30E-04
MW15B	3.12E+01	1.10E-04
MW16A	4.54E+01	1.60E-04
MW16B	4.54E+01	1.60E-04
MW17	6.80E-02	2.40E-07
MW18	1.67E+01	5.89E-05
MW19A	7.09E+01	2.50E-04
MW19B	1.56E+01	5.50E-05
MW20	2.30E+01	8.11E-05
MW21	1.22E+00	4.30E-06
MW22	5.10E+01	1.80E-04
MW23	1.19E+01	4.20E-05
MW24	5.95E-02	2.10E-07
MW25	7.65E-02	2.70E-07
MW26	1.02E+01	3.60E-05
MW27A	1.53E+01	5.40E-05
MW27B	8.79E+00	3.10E-05
MW28	9.35E+00	3.30E-05

Table 4.1: Hydraulic conductivity values for monitoring wells screened within the alluvium layer (Stenback and Ong 2003)

Parameter	Value
Extent of model in X-direction	260 m
Extent of model in Y-direction	280 m
Cell dimensions (ΔX) = (ΔY)	2 m x 2 m
Specific storage S_S	2.0E-4 1/m
Specific yield (Loess)	0.18
Specific yield (alluvium)	0.28
Hydraulic Conductivity:	
Layer 1 – Fill	1.0 E-7 m/s (uniform)
Layer 2 – Loess	5.29 E-7 m/s (uniform)
Layer 3 – Alluvium	Varied (See table 4.1)
Recharge Rate at Layer 1 – Fill	278.3 mm/yr

Table 4.2: Input parameters for groundwater flow modeling

id	X	Y	Screen Elevaiton (m)	Observed Head, March 2003 (m)
MW1	331.147	343.446	358.536	358.43
MW2	354.562	346.804	351.678	358.43
MW3	318.973	287.92	355.686	358.414
MW4	324.844	362.752	354.62	358.43
MW5A	345.716	309.092	357.027	358.445
MW5B	345.854	310.795	352.364	358.439
MW6	368.058	283.863	353.644	358.436
MW6A	366.199	284.253	354.726	358.366
MW6B	369.783	283.961	352.593	358.381
MW6C	367.814	282.254	353.614	358.399
MW7	311.719	214.604	347.929	353.126
MW8	424.51	280.154	348.691	354.525
MW9	366.937	219.566	349.225	353.364
MW10	381.908	194.091	345.613	352.788
MW11	399.587	168.503	345.46	352.779
MW12	419.63	220.629	347.228	352.791
MW13A	368.714	252.344	353.019	355.339
MW13B	368.71	250.823	350.215	354.729
MW13C	367.037	251.612	349.414	354.717
MW14A	347.35	246.656	351.599	356.342
MW15B	341.495	280.005	352.422	358.32
MW16A	334.561	300.024	354.784	358.43
MW16B	333.473	301.148	352.166	358.457
MW18	300.569	274.652	354.735	358.42
MW20	394.631	250.546	348.95	354.086
MW23	285.951	185.651	349.606	352.782
MW24	291.166	230.843	351.075	354.239
MW25	272.208	229.463	351.401	355.787
MW26	275.673	281.026	356.631	358.427
MW27A	354.967	279.575	354.741	358.408
MW27B	356.131	279.496	353.245	358.427
MW28	414.485	250.875	349.584	354.028

Table 4.3: Screen elevations and observed head data (Black and Veatch 2004)

id	Observed Head (m)	Calculated Head (m)	Difference	Square of Difference
MW1	358.43	358.322	0.108	0.012
MW3	358.414	358.325	0.089	0.008
MW4	358.43	358.306	0.124	0.015
MW5A	358.445	358.345	0.100	0.010
MW5B	358.439	358.350	0.089	0.008
MW6	358.436	358.639	-0.203	0.041
MW6A	358.366	358.555	-0.189	0.036
MW6B	358.381	358.591	-0.210	0.044
MW6C	358.399	358.604	-0.205	0.042
MW7	353.126	353.213	-0.087	0.008
MW8	354.525	354.417	0.108	0.012
MW9	353.364	353.458	-0.094	0.009
MW10	352.788	352.754	0.034	0.001
MW11	352.779	352.794	-0.015	0.000
MW12	352.791	352.601	0.190	0.036
MW13A	355.339	355.357	-0.018	0.000
MW13B	354.729	354.637	0.092	0.008
MW13C	354.717	354.627	0.090	0.008
MW14A	356.342	356.345	-0.003	0.000
MW15B	358.32	358.242	0.078	0.006
MW16A	358.43	358.270	0.160	0.026
MW16B	358.457	358.299	0.158	0.025
MW18	358.42	358.246	0.174	0.030
MW20	354.086	354.011	0.075	0.006
MW23	352.782	352.681	0.101	0.010
MW24	354.239	354.047	0.192	0.037
MW25	355.787	355.865	-0.078	0.006
MW26	358.427	358.229	0.198	0.039
MW27A	358.408	358.487	-0.079	0.006
MW27B	358.427	358.672	-0.245	0.060
MW28	354.028	354.079	-0.051	0.003
Total square of difference =				0.552
Mean square of difference =				0.018
Root mean square of difference =				0.133

Table 4.4: Comparison of simulated and observed hydraulic heads for the calibrated groundwater model

Zone	Model Layer	Geologic Unit	Monitoring Wells	Hydraulic Conductivity (m/s)	
				Initial Value	Calibrated Value
1	1	Fill	N/A	6.60E-06	8.036E-06
2	2	Loess	MW13A and MW13B	1.30E-06	2.771E-07
3	3	Alluvium	MW1, MW2, MW4 and MW5B	1.20E-04	7.139E-05
4	3	Alluvium	MW6, MW6A, MW6B, MW6C, MW8 and MW21	5.00E-05	6.245E-05
5	3	Alluvium	MW3, MW3A, MW3B, MW3C, MW15A, MW15B, MW16A, MW16B, MW19A and MW19B	6.00E-03	4.487E-03
6	3	Alluvium	MW18 and MW26	2.00E-06	1.050E-05
7	3	Alluvium	MW13C, MW20, MW27A, MW27B and MW28	1.00E-04	9.891E-05
8	3	Alluvium	MW14, MW14A, MW17, MW24 and MW25	4.00E-07	2.358E-07
9	3	Alluvium	MW7 and MW 23	5.00E-05	3.546E-04
10	3	Alluvium	MW9 and MW12	5.50E-04	1.954E-04
11	3	Alluvium	MW10 and MW11	4.50E-04	6.789E-04
12	3	Alluvium	MW22	4.70E-04	6.414E-05

Table 4.5: Hydraulic conductivity values at monitoring wells by zone before and after calibration

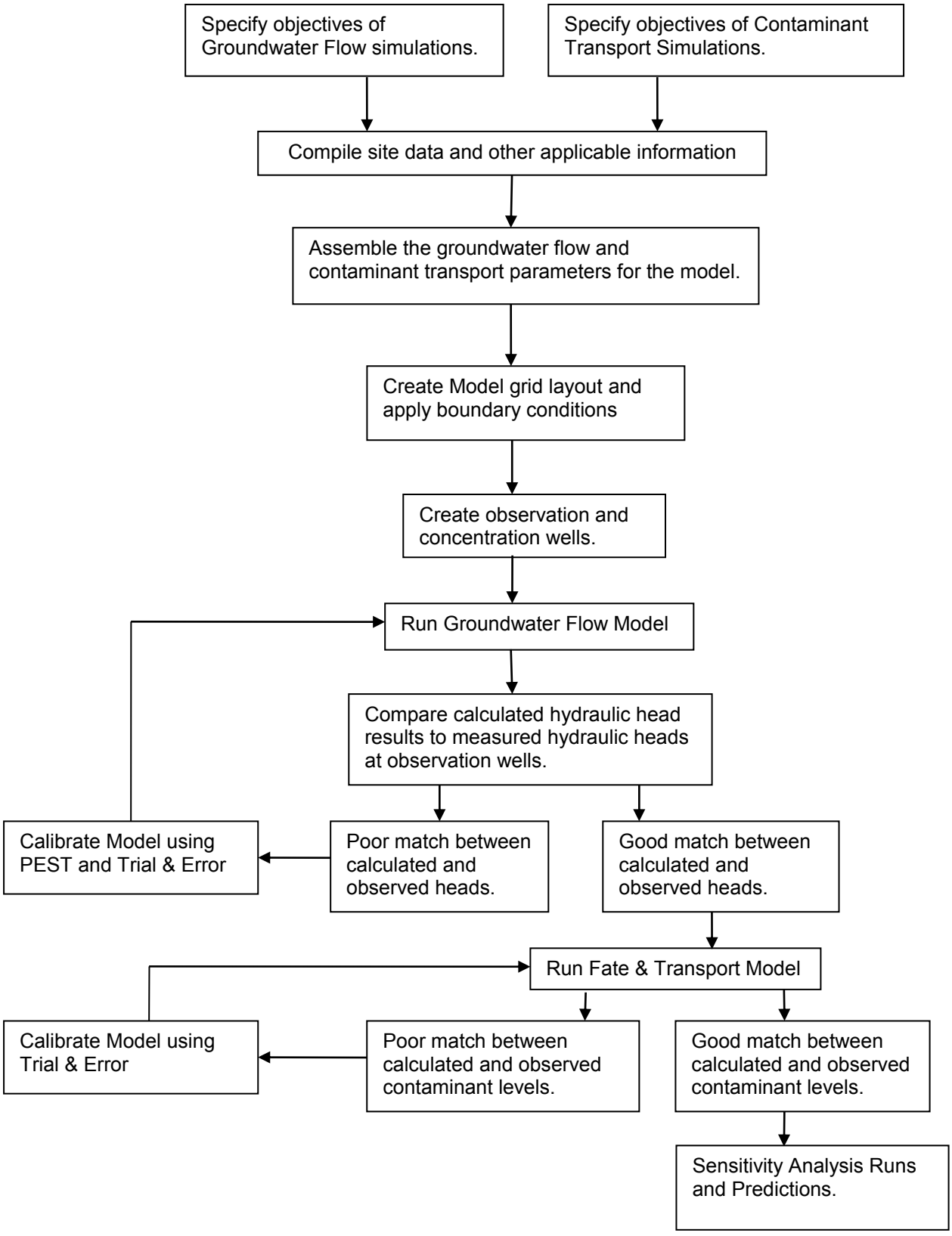

Figure 4.1: Flowchart of the groundwater flow and contaminant transport modeling process (after Downs and Webster 2007)

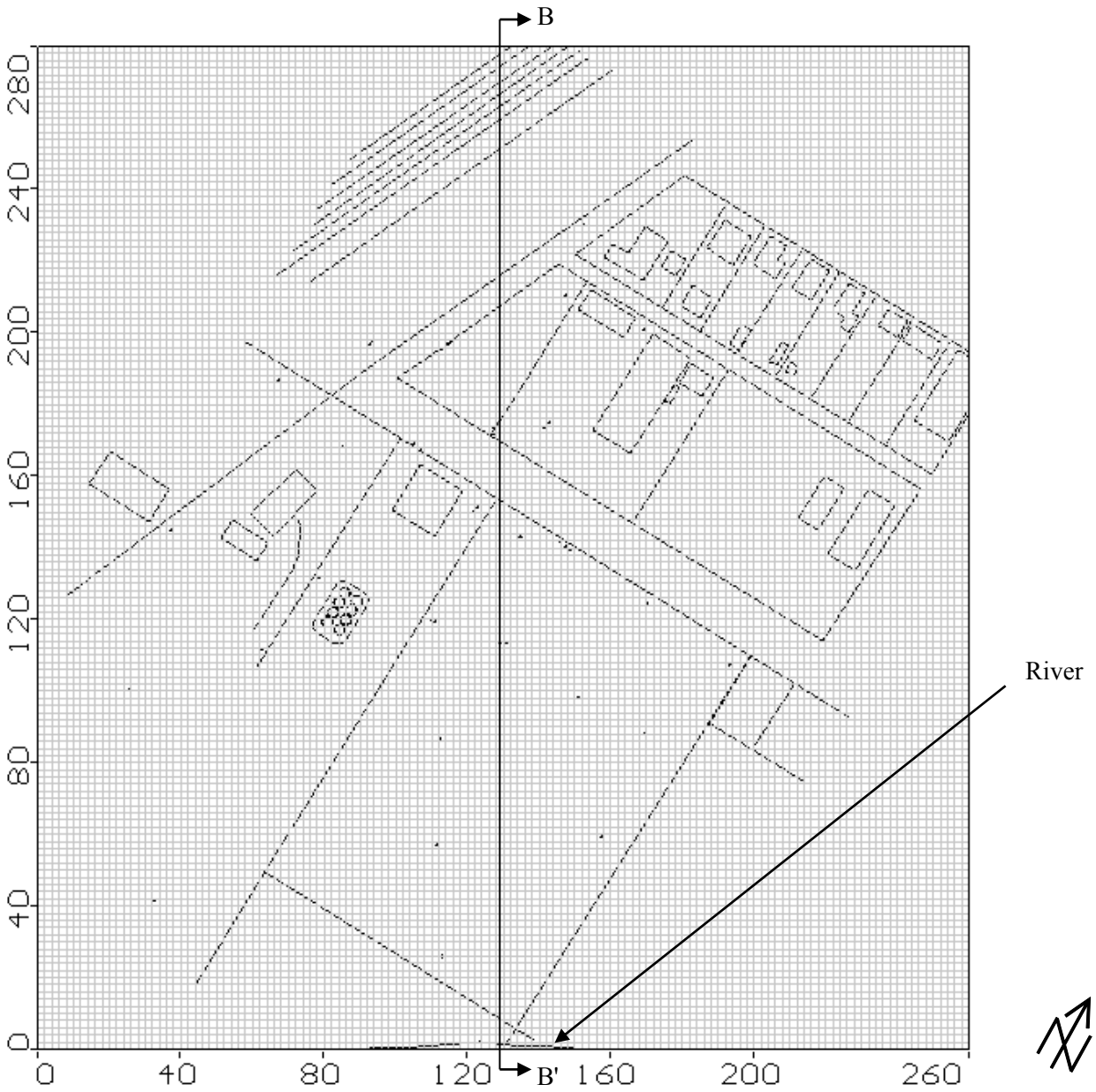

Figure 4.2: Midwestern U.S. former MGP site model on grid layout

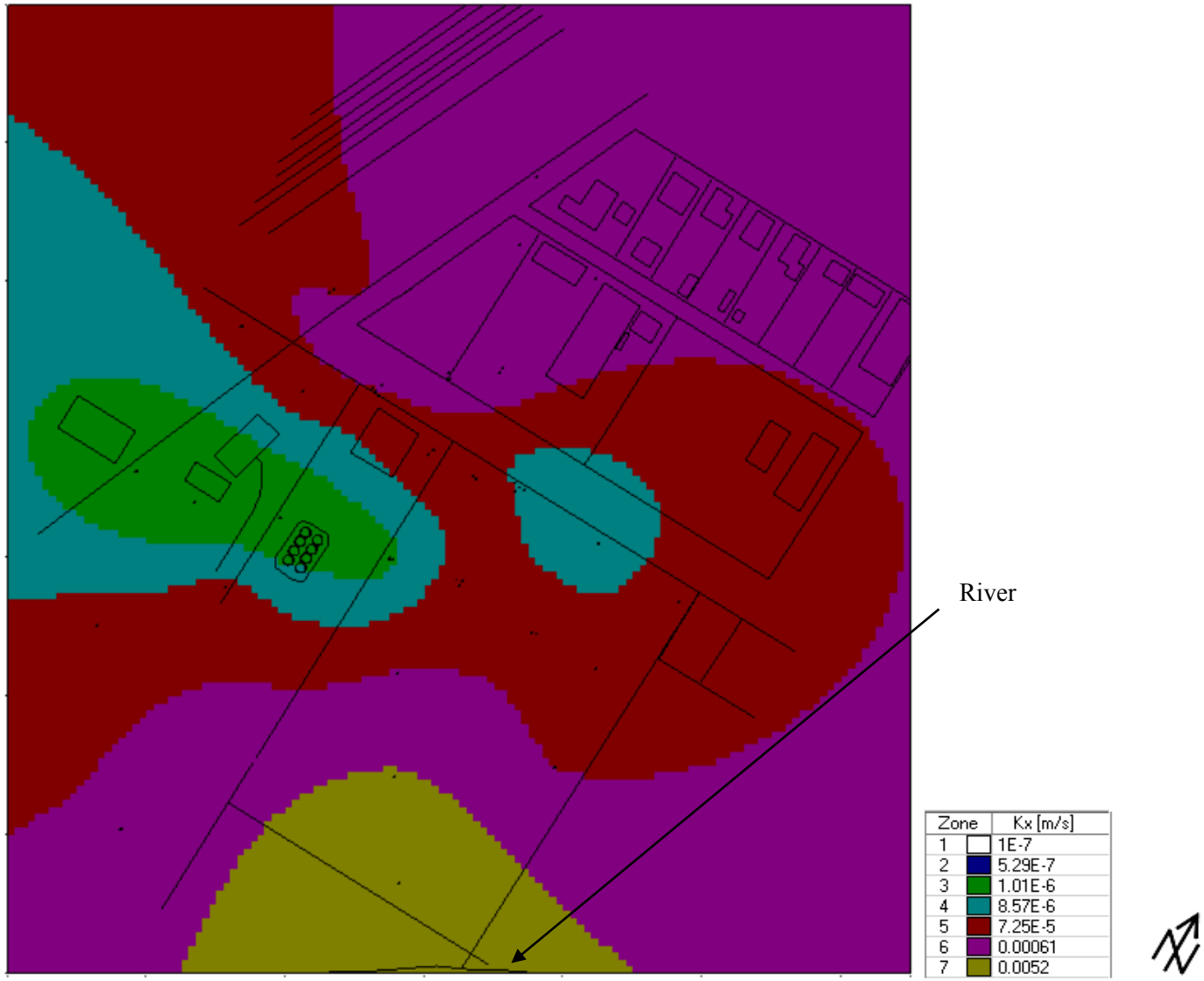

Figure 4.3: Kriging interpolated hydraulic conductivity zones for alluvium layer

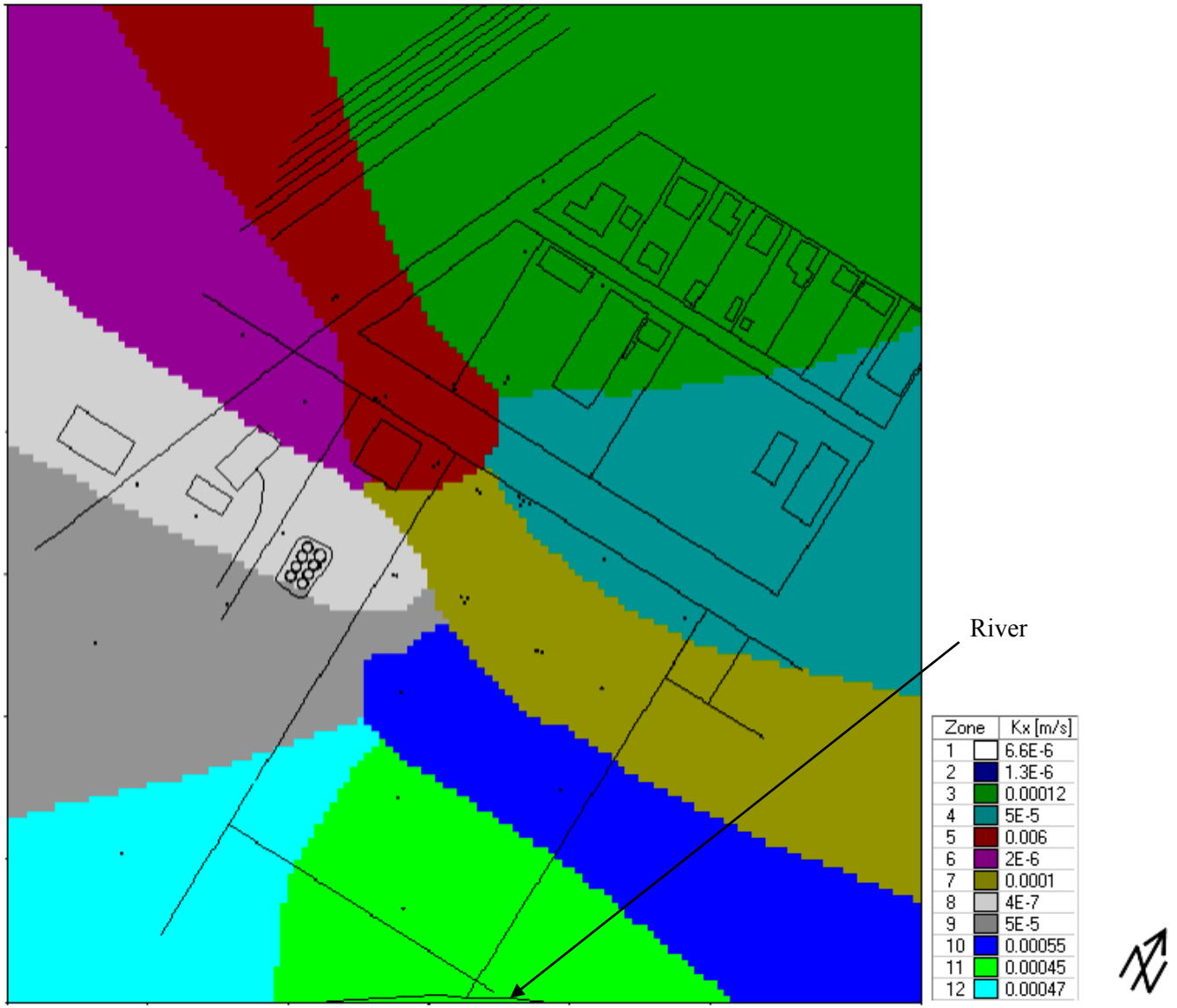

Figure 4.4: Piecewise hydraulic conductivity zones for alluvium layer

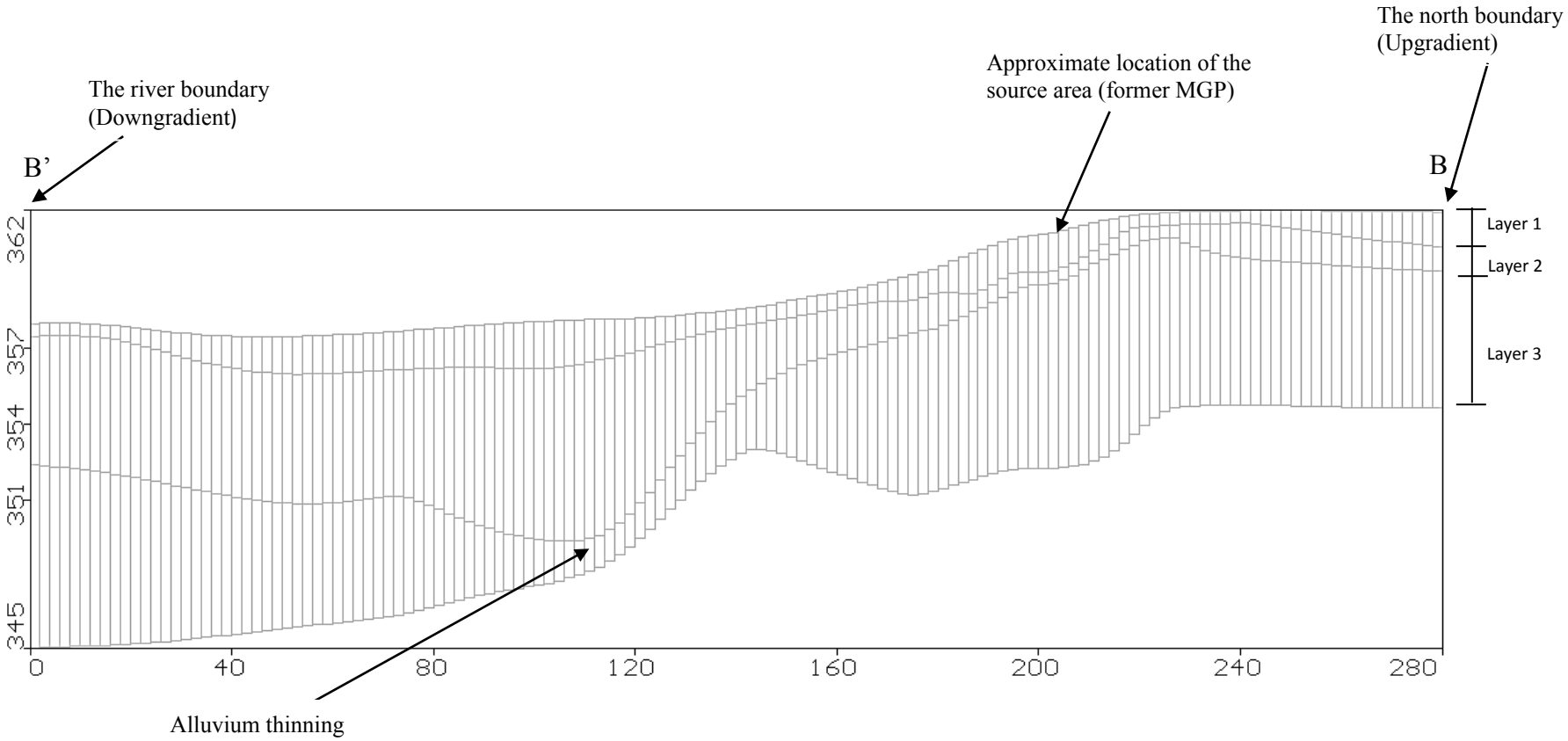

Figure 4.5: Cross section BB' showing the alluvium pinch zone

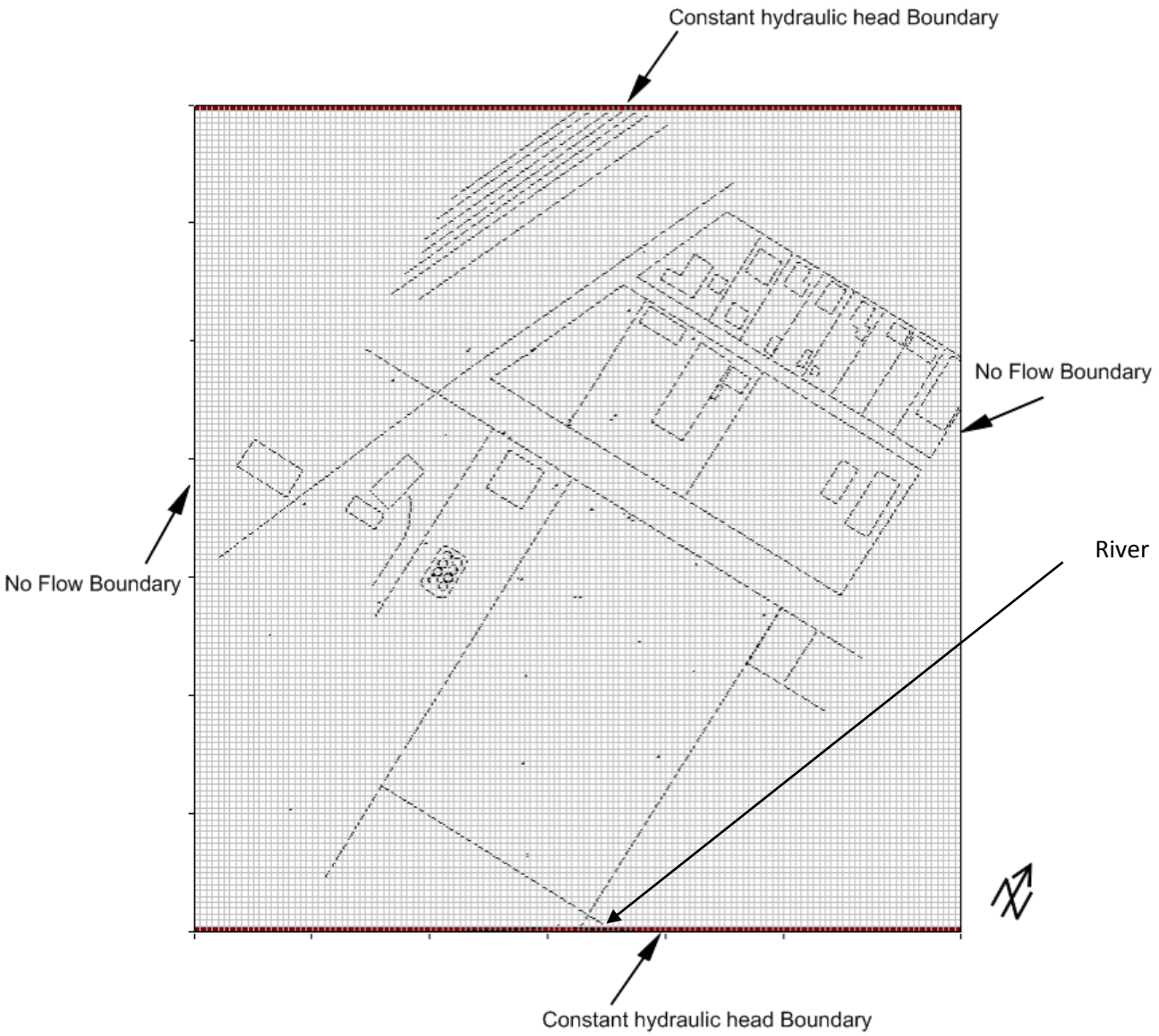

Figure 4.6: Boundary conditions for the site model domain

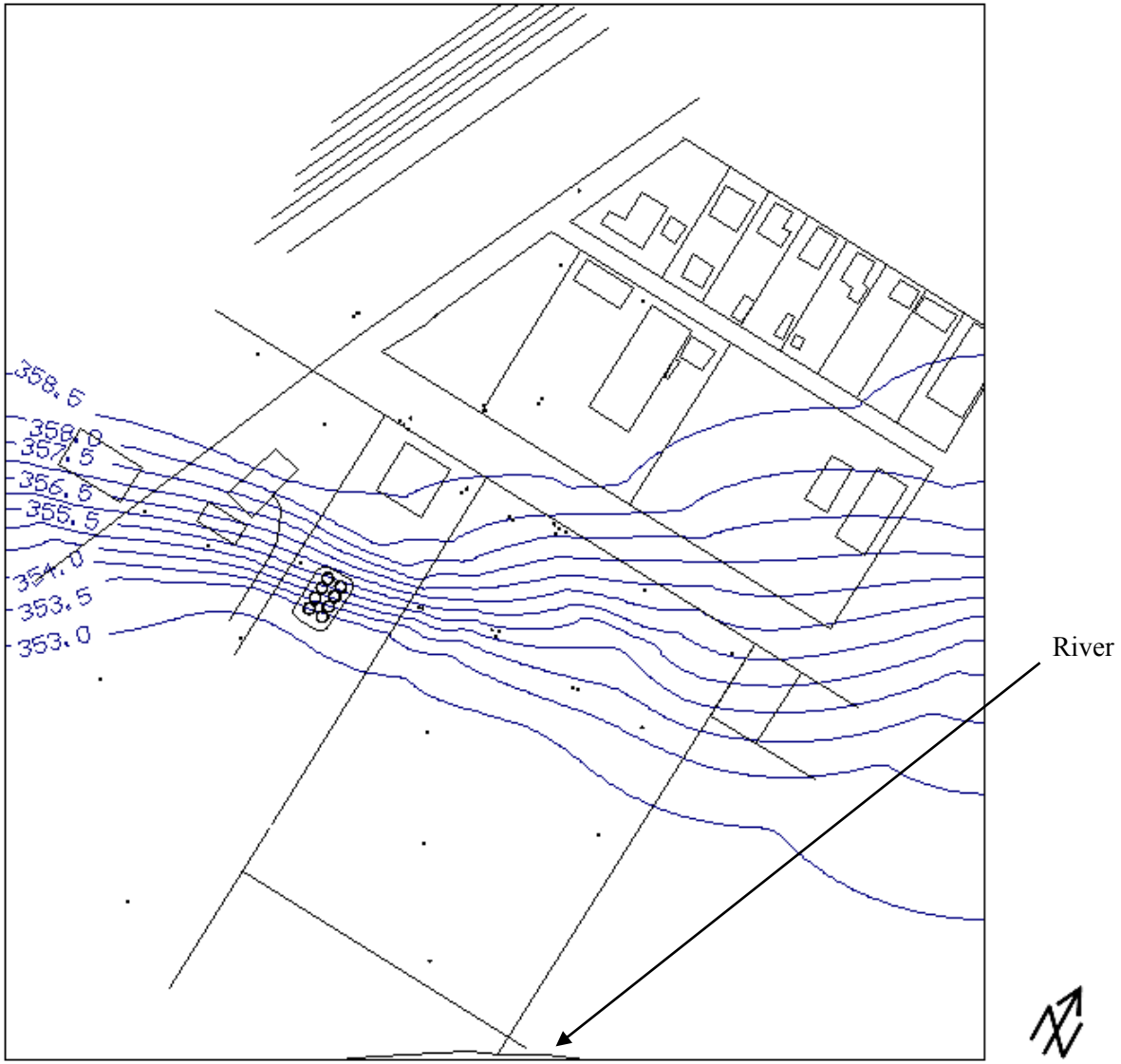

Figure 4.7: Initial run potentiometric contours for the alluvium layer, contour elevations are in meters

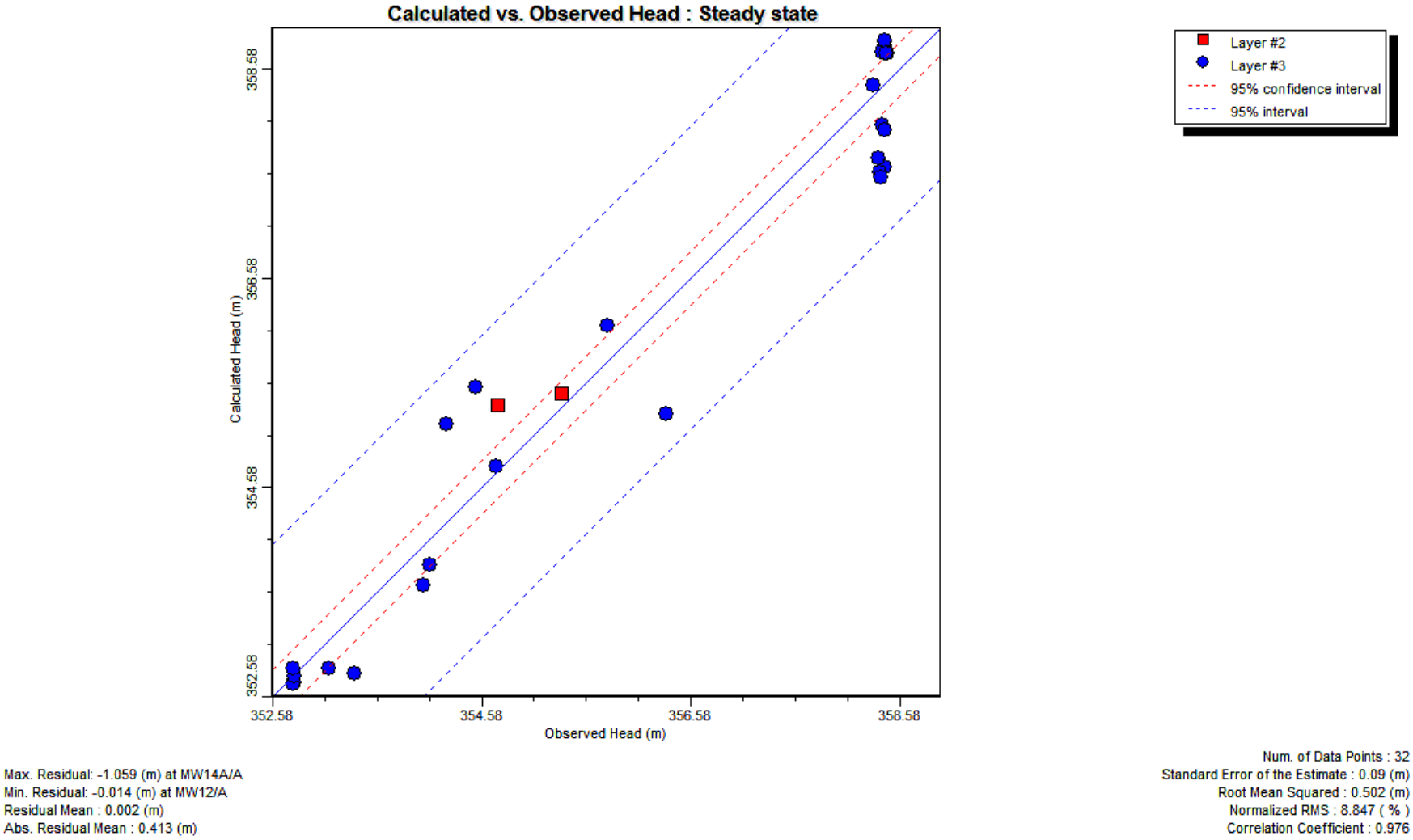

Figure 4.8: Initial run calculated versus observed heads graph

Figure 4.9: Initial run potentiometric contours for the loess layer, contour elevations are in meters

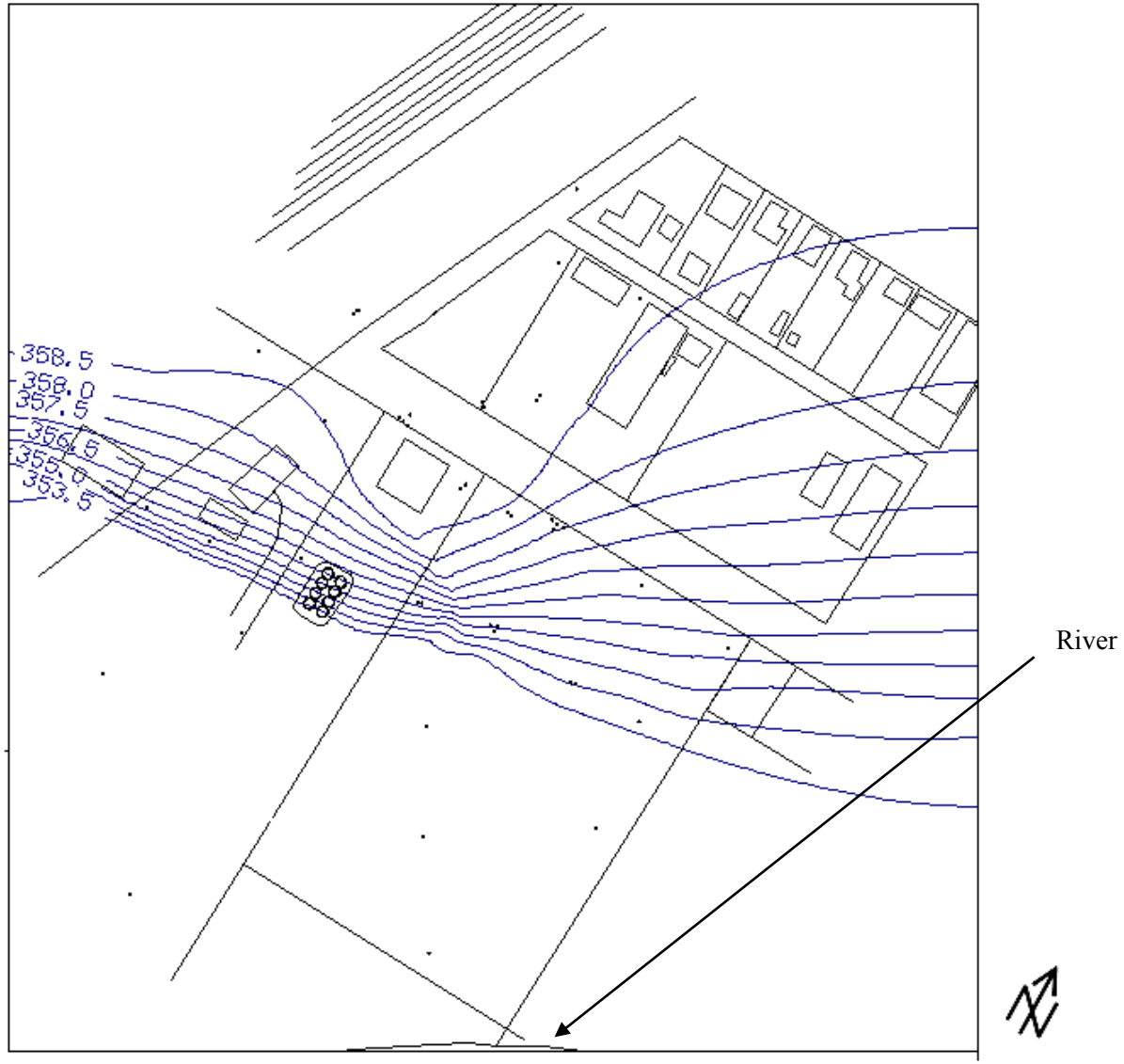

Figure 4.10: Potentiometric contours within the alluvium layer using piecewise hydraulic conductivity zones, contour elevations are in meters

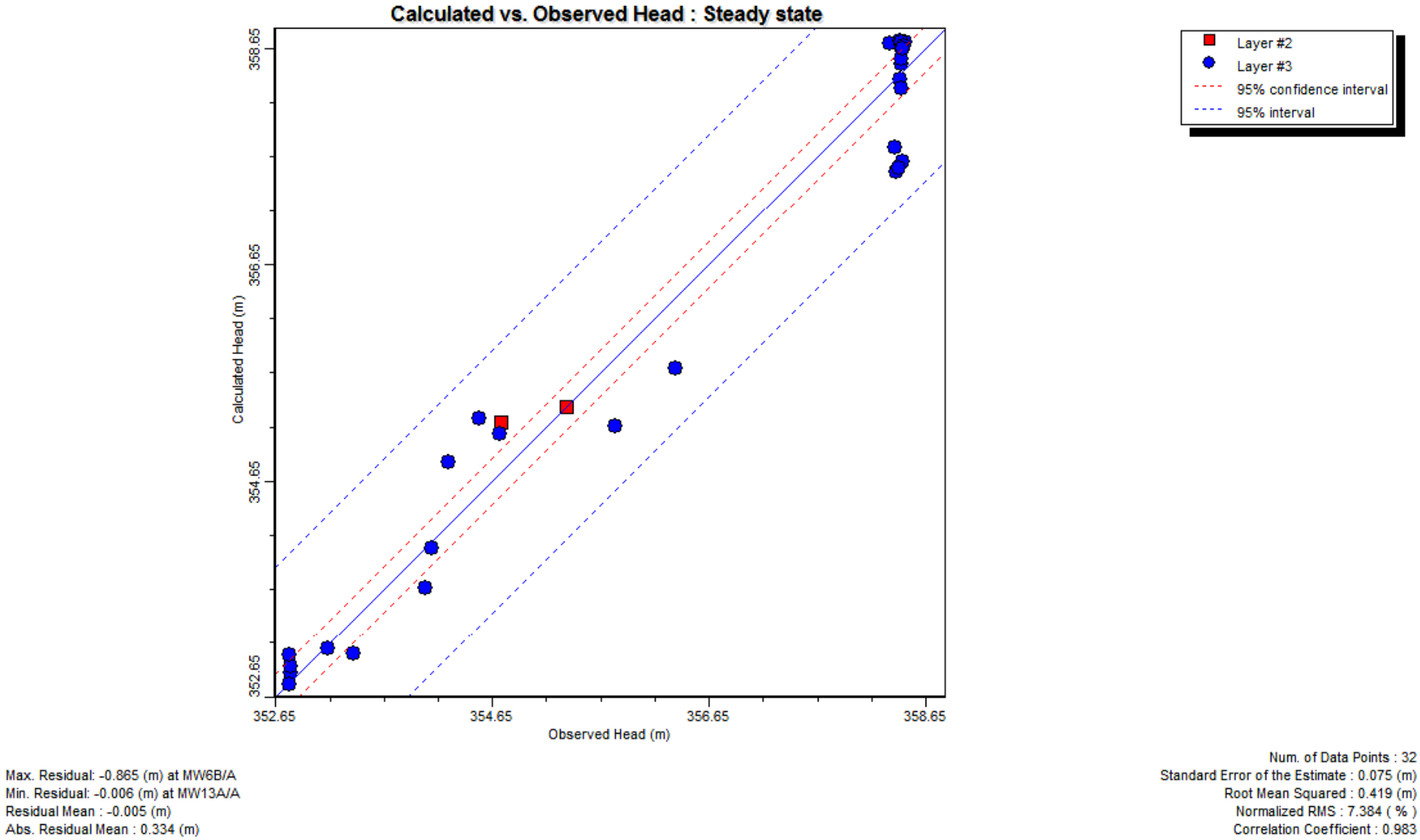

Figure 4.11: Calculated versus observed heads for the run with piecewise hydraulic conductivity zones

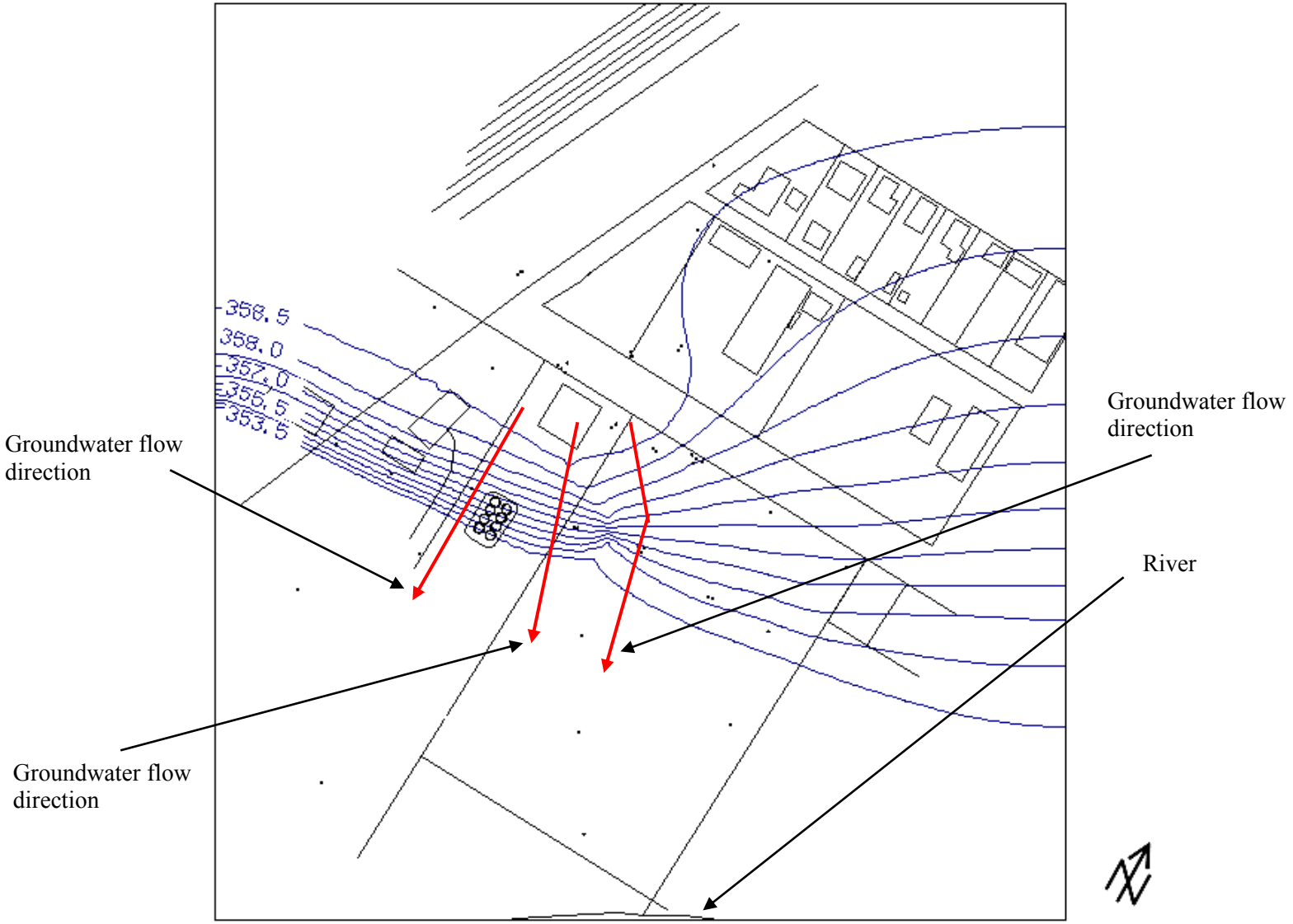

Figure 4.12: Alluvium layer calibrated potentiometric contours and groundwater flow directions, contour elevations are in meters

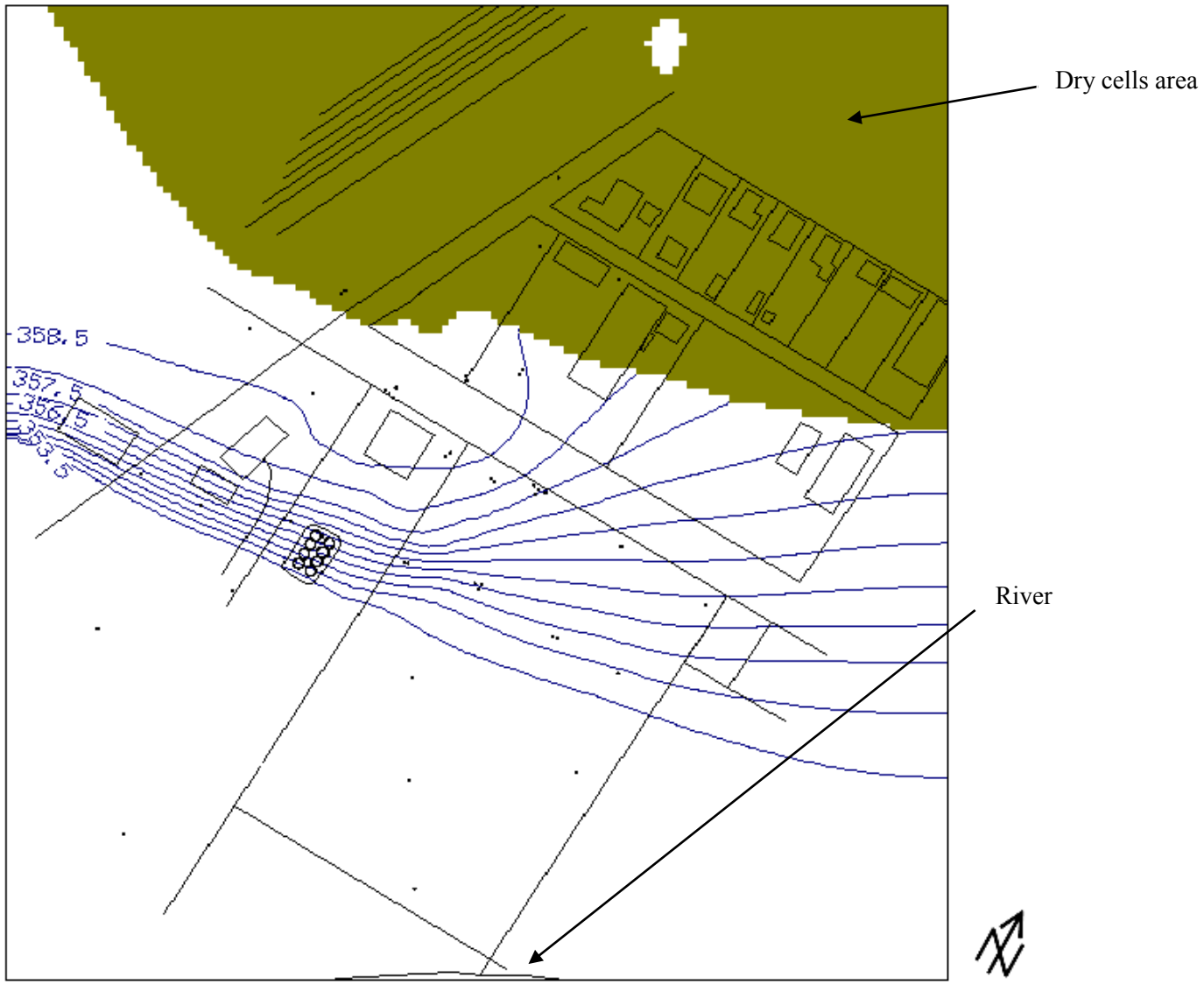

Figure 4.13: Loess layer calibrated potentiometric contours, contour elevations are in meters

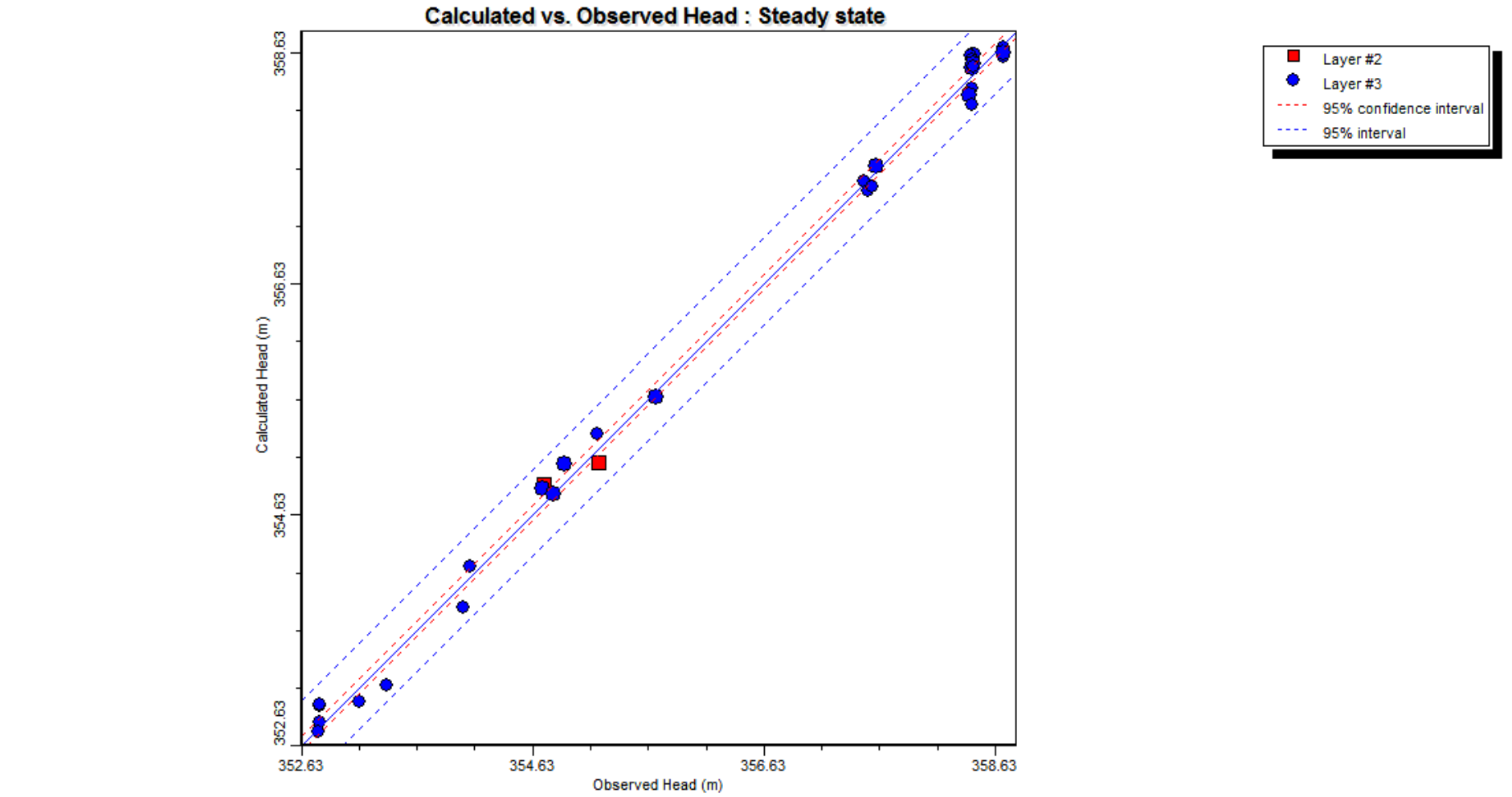

Figure 4.14: Calculated versus observed heads for the calibrated run

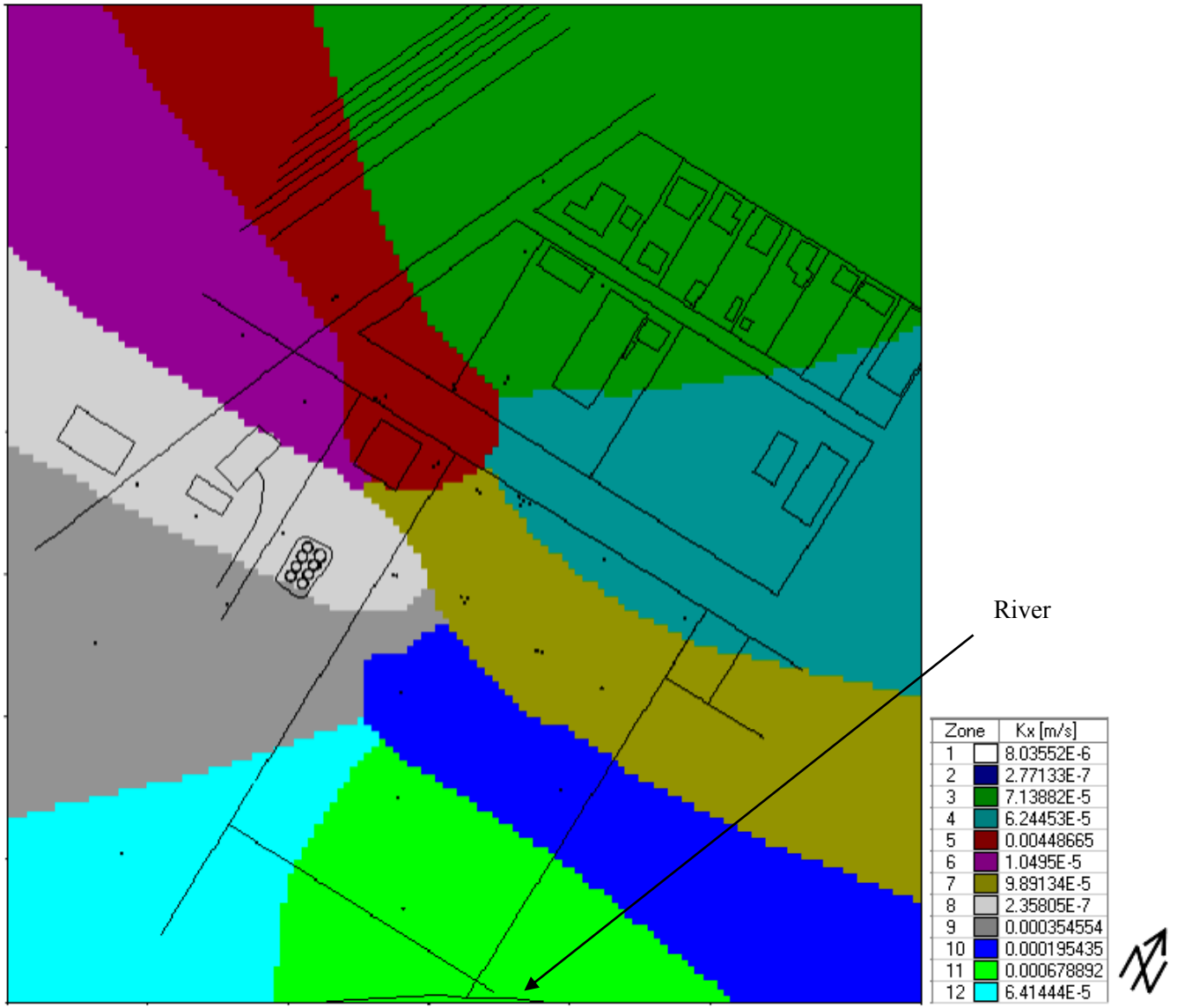

Figure 4.15: The calibrated hydraulic conductivity zones for alluvium layer

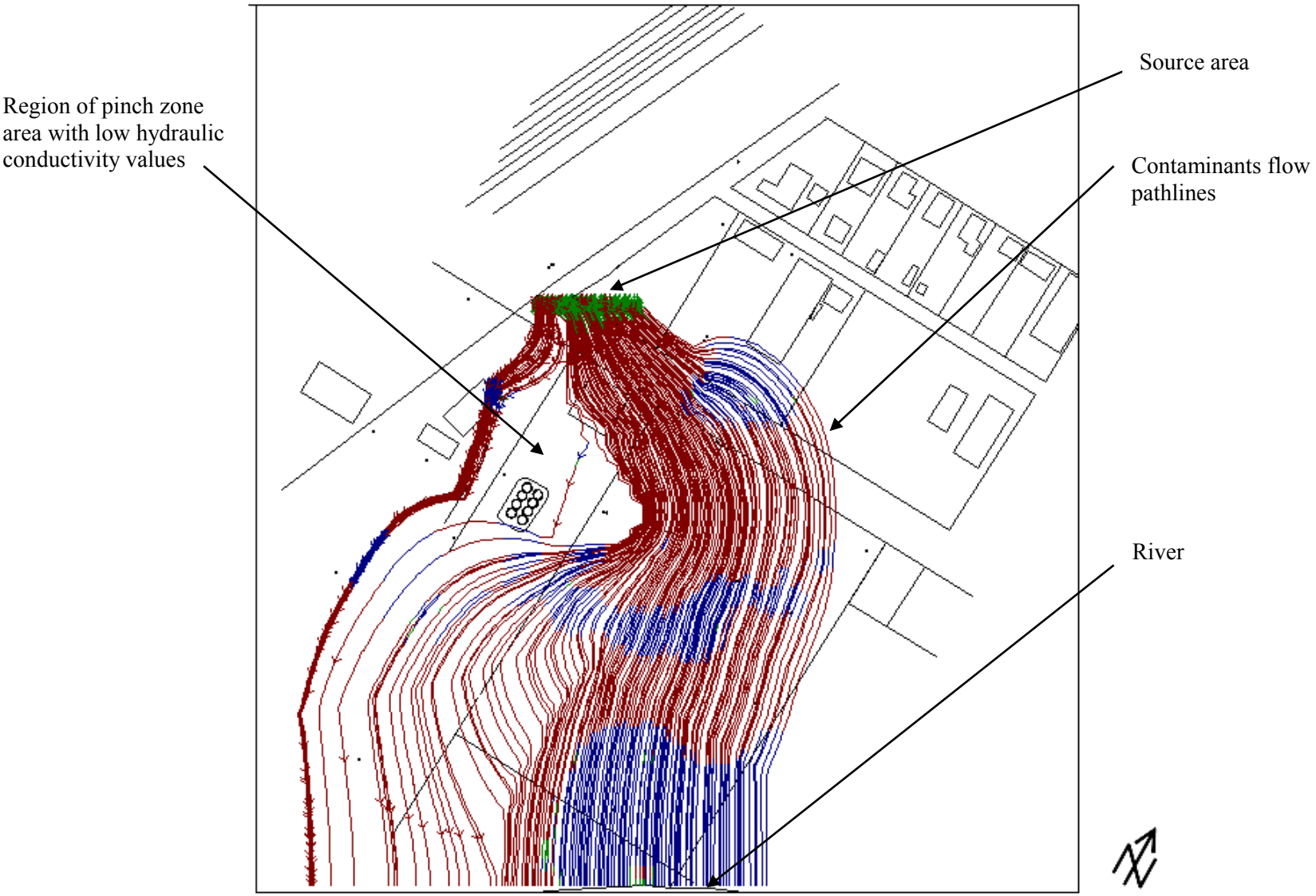

Figure 4.16: Pathlines of particles released from the source area tracked with Modpath

Chapter 5 Contaminant Transport Modeling

5.1 Modeling Methodology

The methodology for modeling the fate and transport of contaminants using the MT3DMS transport engine follows the modeling process flow chart shown in Figure 4.1. As shown in Figure 4.1, the transport model utilizes the calibrated groundwater flow model. The potentiometric contours and groundwater flow directions are shown in Figure 4.12. As described in section 3.4, the contaminant transport modeling focuses on three contaminants released from the coal tar DNAPL: benzene, naphthalene and benzo(a)pyrene. The transport model was run for a time period of 75 years to simulate site conditions at the time of conducting this research study, as the MGP was operated from 1905 to 1936. The plume extent at 75 years is taken to represent that model run with the particular set of input parameters.

To assess the impact of natural attenuation and individual transport processes on plume evolution, selective MT3DMS runs were made for advection and dispersion only; then advection, dispersion and sorption; and finally, advection, dispersion, sorption and biodegradation. The plume extents with the September 2003 concentration data, shown in Figure 3.20 were used as the observed plumes for comparison with simulated plumes. Table 5.1 was set up to document systematic changes made to each parameter and the outcome of each run. This allowed for efficient transport parameter alteration and to monitor the impacts of transport parameter variation on plume shape and extent until a good match between the simulated and observed plumes was achieved.

Using the calibrated plumes as a baseline condition, sensitivity analysis runs were

conducted by systematically adjusting one of the input transport parameters, dispersion (α_x), sorption (K_d) and biodegradation (λ) by one order of magnitude while keeping the others constant to monitor the influence on the extent of the contaminant plumes. Small changes to a particular transport parameter with significant impact on the contaminant plume indicate high sensitivity and vice versa.

5.2 Model Construction, Contaminant Transport Properties, Model Boundary Conditions and Source Term

5.2.1 Model Construction

The construction of the transport model requires defining hydrogeologic parameters (soil porosity, dry bulk density and dispersivities), contaminant species parameters (sorption and biodegradation coefficients), as well as the source extent and contaminant concentrations, according to the site soil and groundwater contamination detailed in section 3.4.

For contaminant transport modeling for the former MGP site in the Midwestern U.S., the model grid was coarsened from cell dimensions of 2 m × 2 m (see Table 4.2) to 4 m × 4 m following several initial transport simulation failures. The transport simulation failures were caused by the model grid cell dimensions being too small to allow the proper operation of the MT3DMS transport engine. Coarsening the model grid by a factor of two had no effect on the calibrated groundwater model used for transport simulations.

5.2.2 Contaminant Transport Input Properties

Dispersion

Contaminant transport models require dispersivity terms to account for the mechanical dispersion process. Longitudinal dispersivity (α_x) was estimated using Equation 2.8. The plume length (L_p) in Equation 2.8 was defined using the benzene dissolved plume length of about 100 m from the source area to slightly upgradient of MW-9 (see Figure 3.20). Transverse dispersion (α_t) and vertical dispersion (α_v) values were entered under layer options as fractions of the longitudinal dispersion (α_x) in units of meters using Equation 2.9. The initial estimated dispersivity values are shown in Table 5.1 under Run #1.

Sorption

Linear partition coefficient (K_d) values were estimated using the fraction of soil organic carbon content (f_{oc}) measured for several soil samples collected during the August 2001 site characterization activities (Biyani 2003-see Table 5.2). Values of the octanol-water partition coefficient (K_{ow}) for benzene, naphthalene and benzo(a)pyrene were taken from Alvarez and Illman (2006). Chemical-specific organic carbon partition coefficient (K_{oc}) values were calculated using Equation 2 from the list of correlations presented in Table 2.7 to estimate K_{oc} from K_{ow} for benzene, naphthalene and benzo(a)pyrene. Equation 2.11 was used to calculate K_d values for the soil samples and these values are given in Table 5.2. Average values of the calculated K_d for each contaminant in the alluvium and loess layers were used as initial sorption inputs (for the Run #6, Table 5.1). Average soil porosity values of 0.3 and 0.5 and average bulk dry density values of 1.9 and 1.3 (g/cm^3) were defined for the alluvium

and loess layers, respectively (see Table 3.1). These values were used as inputs into Equation 2.10 to estimate the retardation factors (R_f) for the three contaminant compounds, which were then employed in Equation 2.12 to define the velocity of the contaminants (see Table 5.3).

Biodegradation and attenuation rates

Mass fluxes of benzene and naphthalene were estimated using monitoring well transects A-A' and B-B', shown in Figure 5.1. Since the plume for benzo(a)pyrene did not extend far enough downgradient to cross the transects, mass flux calculations were not conducted for benzo(a)pyrene. Transect A-A' is through MW-8, MW-21, MW-6, MW-27, MW-15, MW-3, MW-18 and MW-26 (see the cross section in Figure 5.2). Transect B-B' is through MW-28, MW-20, MW-13, MW-14, MW-17, MW-24 and MW-25 (see the cross section in Figure 5.3). Groundwater contaminant concentrations measured in November 2002, September 2003 and June 2007 (shown in Tables 3.5 to 3.7) were used for mass flux estimations across the two transects to assess changes in mass flux at the transect location with time and to assess changes in mass flux between transect A-A' and B-B' at a given time. Non-detects and unmeasured results for the monitoring wells at the ends of the transects were assumed to have a value of the detection limit for benzene and naphthalene.

The mass discharge for benzene and naphthalene at each transect was quantified using Equation 2.16. Following the approach of Stenback and Ong (2003), the groundwater Darcy's discharge velocity for transect B-B' was estimated using the measured potentiometric contours shown in Figure 3.5. An average hydraulic gradient (i) of 0.076 m/m was used for the region of alluvium thinning in which a drop of

approximately 5.5 m occurs over a distance of around 72.5 m. Assuming steady state conditions and continuity of the flow, and that flow is predominantly through the alluvium, the groundwater Darcy's velocity for transect A-A' was estimated by adjusting the groundwater Darcy's velocity across transect B-B' to account for the difference in the average thickness of the alluvium along the two transects. Therefore, the Darcy's velocity across transect A-A' was estimated by multiplying the Darcy's velocity across transect B-B' by a factor of 0.576, the ratio of the thickness of transect B-B' to transect A-A'. The areas associated with the monitoring wells along the transects (Ai in Equation 2.16) were approximated using Figures 5.2 and 5.3 for transect A-A' and transect B-B', respectively.

The mass flux and mass discharge calculation results for the two transects are shown in Tables 5.4 to 5.9. Further, the trends of benzene and naphthalene mass discharges across the transects throughout the years are presented in Figures 5.4 and 5.5. A general trend of decrease in mass discharge with time is apparent. The mass discharge estimation for transect A-A' using November 2002 concentration data shows that around 73 grams of benzene per year migrated downgradient away from the source area. Mass discharge is reduced to about 59 grams of benzene per year using March 2003 data. A slight increase of benzene mass discharge to about 63 grams of benzene per year was estimated using the June 2007 concentration data. The naphthalene mass discharge calculated for transect A-A' using the June 2007 concentration data shows a significantly lower amount of about 133 grams per year compared with the September 2003 and the November 2002 concentration data that yielded mass discharges of approximately 225 and 346 grams of naphthalene per year, respectively. This indicates either increasing attenuation of naphthalene or a reduction in the release of

naphthalene emanating from the source area.

Flux calculations for benzene for transect B-B' for all three years of data show consistently decreasing mass discharges. The benzene mass discharge for June 2007 of approximately 18 grams per year is less than the September 2003 and November 2002 benzene mass discharges of approximately 22 and 28 grams per year, respectively. Naphthalene mass discharges showed the same trend. The approximately 0.19 grams of naphthalene discharge per year in June 2007 is less than the approximate naphthalene mass discharges of 0.4 and 9 grams per year in September 2003 and November 2002, respectively.

The mass discharge results were used to estimate bulk attenuation rates ($\mathcal{K}$) using Equation 2.15 in which the time was estimated from the distance between the two transects for each contaminant velocity shown in Table 5.3. Bulk attenuation rates for each contaminant compound were then used in Equation 2.14 to estimate values of biodegradation coefficients (λ). Tables 5.10, 5.11 and 5.12 summarize mass discharge, bulk attenuation and biodegradation rate estimates for benzene and naphthalene using mass discharge data for the two transects. The data show that the bulk attenuation and biodegradation rates for benzene for all three years of mass discharge data are approximately equal. This indicates that the primary attenuation process for benzene is biodegradation. For naphthalene, the bulk attenuation rate is higher than the biodegradation rate for all three years, indicating that other attenuation processes, such as sorption, are active.

Biodegradation rate estimates are compared to different published studies conducted

at the former MGP site in Table 5.13 to formulate a general understanding of biodegradation rate variations and to assist with calibration of the transport model. The biodegradation rates estimated in previous research studies conducted at the site were determined using the methods described in section 2.8.3. The biodegradation rates determined from the mass flux analysis are generally within about one order of magnitude of the biodegradation rates determined by the other researchers. The average of the values listed in Table 5.13 for the two contaminants (benzene and naphthalene) are used as initial inputs for the transport modeling simulations.

Because no benzo(a)pyrene biodegradation rate constant information was available from previous research studies, and with the lack of data for estimation of benzo(a)pyrene mass fluxes as described earlier, the benzo(a)pyrene biodegradation rate constant for this research is based on its decay rate or half-life as described in section 2.8.3.

The half-life of benzo(a)pyrene can range from 2 to 693 days corresponding to a biodegradation rate constant ranging between 0.346 and 0.001 (1/d) (Downs and Webster 2007). The lower biodegradation rate constant value of 0.001 (1/d) was used as the initial value for the transport simulations because it corresponds to the 693 days believed to better represent the condition at the former MGP site. This value of biodegradation rate constant for benzo(a)pyrene is within about one order of magnitude when compared to the value of biodegradation rate constant for benzo(a)pyrene reported by Rogers et al. (2002) (0.028 (1/d)) as well as other PAHs biodegradation rate constant values reported by Rogers et al. (2007a).

5.2.3 Contaminant Transport Boundary Conditions and Source Term

The boundary conditions for the transport modeling can be defined using contaminant concentrations in the model as either constant concentrations or point sources. The point source boundaries facilitate entry and exit of contaminants through a groundwater flow boundary such as contaminated waterways (e.g. streams and rivers). This is not the case of the former MGP site in the Midwestern U.S. given that no evidence of contamination entering the river was detected (Stenback and Ong 2003; Rogers et al. 2007a). For the contaminant source, a constant concentration boundary condition was defined by a source polygon acting as a contaminant source providing solute mass to the model domain. The polygon location within the model domain was based on the source definition described in section 3.4.

Stenback and Ong (2003) used the MW-13 location as a point source for analytical contaminant plume modeling purposes. Figures 5.6 to 5.10 show the measured concentration versus time at MW-13A, MW-13B and MW-13C for benzene and naphthalene. While MW-13B has an anomalously high benzene concentration for this location relative to the coal tar source, the MW-13 location is not included as a source location to run the transport modeling simulations for this research. The MW-13B benzene concentrations remain relatively high through to the last available monitoring event in June 2007 and this should continue to be monitored and assessed.

The coal tar source area concentration for benzene, naphthalene and benzo(a)pyrene was determined using the average value of concentrations measured at the monitoring wells MW-3, MW-5 and MW-16 located within the area covered by the source polygon as shown in Figure 5.11. As discussed in section 2.8.2, modeling the actual

release of the compounds from the coal tar source into the groundwater is not possible at this site because the chemical composition of the coal tar source has not been fully characterized. The average concentration for each contaminant, 0.28 mg/L for benzene, 1.438 mg/L for naphthalene and 0.0097 mg/L for benzo(a)pyrene, was assigned to the model cells in layer 3 (the alluvium layer) covering the total depth of the layer to account for the suspended coal tar filtering throughout layer 3 and feeding the free product pooling on top of the till at the bottom of layer 3. The average values of contaminant historical concentrations were used to define the source term for the transport simulations because they account for variability due to any sampling error, the effects of remediation (removal of contaminated soil in 1997), potential seasonal variability (changes in recharge can affect release of contaminants from the source), and other factors that may be responsible for variations such as contaminant mass losses due to degradation or volatilization (natural attenuation processes). In addition, Black and Veatch (2008) indicate a general stable trend of the contamination plume. Considering all foresaid points, using the average concentration values was assumed to be rational for conducting the contaminant transport modeling.

5.3 Contaminant Transport Modeling Results

5.3.1 Calibration of Simulated Results with Observed Contaminant Plumes

Separate groups of transport simulation runs were carried out to evaluate the cumulative effect of individual natural attenuation processes on the evolution of the contaminant plumes, and to calibrate the model by systematically altering the transport parameter values to produce simulated contaminant plumes that closely match the observed plumes for the three contaminants shown in Figure 3.20. The

transport runs are documented in Table 5.1. The process commenced by running advection and dispersion only with the baseline dispersivities. The advection dispersion outcome from Run #1 (Figures 5.12) shows the plumes of benzene, naphthalene and benzo(a)pyrene extending well beyond the source area towards the south, south-east and south-west of the former MGP area.

The calibration process involved adjusting dispersivity values to better match observed plume shapes. Dispersivity values were reduced to narrow the width and length of the contaminant plumes. After Run #2 (Table 5.1), for Runs #3, #4 and #5 the transverse dispersivity was held at 10% of the longitudinal dispersivity and the vertical dispersivity was held at 10% of the transverse dispersivity. By decreasing the dispersivity values, the plume spreading was somewhat reduced. Run #5 (Figure 5.13) shows a slight shrinking of the three contaminant plumes relative to Run #1 (Figure 5.12). Further adjustments to the dispersivity values used for Run #5 produced no observable plume changes. Thus, Run #5 is considered final for the advection-dispersion only analysis. The contaminant plumes, however, were far larger than the measured plumes. The advection-dispersion process only runs indicate that attenuation processes are active at this site; otherwise the observed plumes for all three contaminants would extend to the river. Figures 3.20 and 3.21 indicate that the longest plume, benzene, extends to about MW-9.

For the advection, dispersion and sorption runs, the average partition coefficient (K_d) values for the contaminants (described in section 5.2.2 with Tables 5.2 and 5.3) were added as initial sorption parameter values in Runs #6 and #7 to determine the effects of sorption on the contaminant plume (see Table 5.1). The resulting plume in Figure

5.14 shows that benzene still extends well off the site. This is because benzene has higher solubility and lower relative sorption compared to naphthalene and benzo(a)pyrene. Conversely, the naphthalene and benzo(a)pyrene simulated plumes have shrunk relative to the advection-dispersion only Run #5 (Figure 5.13), with the benzo(a)pyrene plume considerably minimized and the naphthalene plume size reduced as shown in Figure 5.14. The K_d value was increased for benzene by one order of magnitude in Run #8, followed by another one order of magnitude increment in Run #9. As a result, the benzene plume shrank further as shown in Figure 5.15 compared to that exhibited in Figure 5.14 (Run #7).

In general, adding the sorption process resulted in considerable shrinkage of the benzo(a)pyrene plume due to its strong sorption characteristic (i.e. high K_d value). The benzene plume only shrank slightly despite increasing the benzene partition coefficient by two orders of magnitude. Comparison of Figure 5.15 with Figures 3.20 and 3.21 indicates that the strong sorption tendency of benzo(a)pyrene can fairly well explain the small plume size and not much migration from the source area. Note, however, that even with the sorption process, the benzene and naphthalene plumes still extend well beyond the observed plumes to the river. This indicates that degradation processes, such as biodegradation, are playing a role in attenuation of benzene and naphthalene.

The effect of biodegradation on the contaminant plumes became apparent following the addition of the biodegradation process in Run #10. Figure 5.16 shows the significant influence that the biodegradation process has on reducing the contaminant plume sizes. The benzene and naphthalene plumes have significantly shrunk and are

closer to the former MGP source area. The biodegradation rate of benzene was increased by one order of magnitude in Run #11. This increase was high enough to bring the benzene plume closer to the former MGP source area than the observed extent of the measured benzene plume (see Figure 5.17). Combining the dispersivity and partition coefficient values from Run #8 with an adjustment of biodegradation rates from Run #10 has resulted in expansion of the benzene plume and shrinkage of the naphthalene plume (see Figure 5.18). The benzene biodegradation rate was then decreased along with slightly decreasing the partition coefficient value for benzo(a)pyrene. A reasonable match between the simulated plumes and the observed plumes was achieved in Run #13 as shown by comparing Figure 5.19 with Figure 3.20.

The benzene calibrated run (Run #13) partition coefficient is one order of magnitude greater than the initial value used when the sorption process was added to the transport parameters. Benzo(a)pyrene and naphthalene calibrated run partition coefficients are within the same order of magnitude as the initial values used in Run # 10. In addition, the biodegradation rate coefficients for the three contaminants for the calibrated run (Run #13) were within the same order of magnitude as the initial run that included all transport parameters (Run #10). It is noticed that the calibrated value of the partition coefficient for benzene is very small when compared to the benzo(a)pyrene calibrated value of partition coefficient (see Run #13 in Table 5.1). This indicates the significant impact sorption has on limiting the benzo(a)pyrene plume to near the source area location. Naphthalene calibrated value of partition coefficient is slightly larger than the partition coefficient of benzene and significantly smaller than the partition coefficient of benzo(a)pyrene, indicating that naphthalene

transport is less impacted by the sorption process than benzo(a)pyrene transport, but more impacted than benzene transport by the sorption process. For the calibrated values of the biodegradation rate constant (Run #13) for the three contaminants, the benzene biodegradation rate constant value is about one order of magnitude greater than naphthalene and benzo(a)pyrene biodegradation rate constant values. This indicates that the biodegradation process likely has significant influence on the benzene contaminant plume attenuation.

There is some difference between the simulated and observed benzene plumes in the south-western portion of the plume. As shown in Figure 3.20, the observed benzene plume extends to the west crossing the petroleum tanks location and including MW-17. The simulated benzene plume extent within this area, however, was limited by the low hydraulic conductivity part of the pinch zone as discussed in section 4.3. As indicated in Table 3.6, the September 2003 concentrations of benzene for MW-14 and MW-17 are 10.3 and 4.9 μg/L, respectively, so the observed extent of the plume in this region has concentrations close to the limit of 5 μg/L (0.005 mg/L).

During the calibration of the transport model, the effect of varying the transport parameter values was noted. Reducing dispersivity coefficients has resulted in a slight decrease of the contaminant plume extents, indicating the limited effect that dispersivity appears to have on the contaminant plume extents. Increasing partition coefficient (K_d) values shrinks the simulated plumes as shown by comparing Figure 5.15 with Figure 5.14 for the transport Runs #9 and #7, respectively. The contaminant most affected by the sorption mechanism is benzo(a)pyrene. The biodegradation process seems to have the greatest effect on the extent of the benzene and naphthalene

plumes. Benzene has a much higher sensitivity to varying biodegradation rates than benzo(a)pyrene. The naphthalene plume was affected by varying both the partition and biodegradation rate coefficients. These observed trends of the three contaminants to varying transport parameter values during calibration runs were taken into account for further sensitivity analysis discussed in the following section.

5.3.2 Parameter Sensitivity Analysis

Several contaminant transport simulations were run using the MT3DMS engine to carry out the sensitivity analysis. By adjusting one transport parameter value while keeping the other transport parameters constant, the effect of that parameter on the contaminant plumes can be observed. The sensitivity analysis was conducted using the final calibrated transport model parameter values (Run #13) as the basis for varying the transport parameters. Increasing and decreasing dispersivity values by one order of magnitude shows no observable effect on the contaminant plumes. This can be related to the other transport parameters having a more noticeable influence on the contaminant plume extent than dispersivity. Decreasing the partition coefficients from Run #13 by one order of magnitude has resulted in expansion of the three contaminant plumes. The benzo(a)pyrene plume expands considerably as shown by comparing Figure 5.20 with Figure 5.19. Decreasing the biodegradation rates from Run #13 by one order of magnitude has resulted in significant expansion of the benzene and naphthalene plumes while the benzo(a)pyrene plume was not affected by decreasing the biodegradation rate; this is shown by comparing Figure 5.21 with Figure 5.19. The sensitivity analysis shows that of the three contaminants, benzene is the most sensitive to changes in biodegradation and sorption rates. This is because benzene has a much lower partition coefficient and higher solubility than benzo(a)pyrene. Benzo(a)pyrene

was more sensitive to changes in the partition coefficient and not very sensitive to variations in biodegradation rate. The naphthalene plume extent was affected by variations in biodegradation rates as well as partition coefficients. However, it was less sensitive than benzene to both process parameters.

The hydraulic conductivity in zone #8 (see Figure 4.15) was increased by one order of magnitude as part of the sensitivity analysis, to assess the impact on the benzene and naphthalene plumes within the western part of the pinch zone in the petroleum tanks area. Figure 5.22 details the resulting potentiometric contours in the alluvium layer. The potentiometric contours were not greatly changed as indicated by comparison to Figure 4.12. The calculated versus observed heads graph is presented in Figure 5.23. The maximum residual head value is increased to 0.76 m at MW-24 compared to 0.245 m at MW-27B in the calibrated groundwater flow model. The absolute residual mean of head residuals is also increased to 0.16 m compared to 0.116 m in the calibrated groundwater flow model. This increase of hydraulic conductivity has not noticeably changed the benzene plume (compare the benzene plume of Figure 5.24 with the benzene plume of Figure 5.19). As discussed in section 5.3.1, the benzene concentrations at MW-14 and MW-17 are close to the limit of 5 μg/L (0.005 mg/L) which is being used to define the benzene plume extent. Moreover, there may be seams or small layers of higher hydraulic conductivity within this region of the pinch zone which can facilitate contaminant transport and are not captured by the model.

5.4 Assumptions and Limitations of the Model

Although the groundwater flow and contaminant transport model for the former MGP in the Midwestern U.S. was carried out as accurately as possible to best simulate the

observed site conditions, several assumptions were involved during the modeling activities leading to limitations of the model. All modeling related data were collected from several academic sources and site reports conducted for previous modeling and site characterization and monitoring efforts at the former MGP site. Although a close and critical assessment was carried out to validate the accuracy of these data, they may not represent the site conditions at the time of this study. The ideal scenario would be to conduct site characterization activities to obtain more recent data representing the site. However, this was not possible, and therefore, it is assumed that all available previous data are applicable and are used to conduct the modeling and simulation study.

Because the groundwater monitoring data did not indicate a significant vertical hydraulic gradient in the alluvium and because of the uncertainty of the spatial variation of hydraulic heads in the loess unit, it is assumed that there is no vertical hydraulic gradient in the alluvium and loess units for the groundwater modeling conducted for this research.

Steady-state conditions are assumed for the groundwater flow system of the model area. In a steady-state condition, long-term equilibrium between groundwater inflow and groundwater outflow is established and groundwater levels remain largely constant with time. The application of steady state hydrogeologic water balance provides a crude approach of the hydrogeologic gains and losses of the aquifer, and therefore it has its own limitation. As a lumped parameter approach it does not represent either spatial variation or time dependent effects of precipitation, evapotranspiration, recharge and discharge. Hence, for better accuracy of the water

balance, it is necessary to have as much hydrogeologic data as possible for the former MGP site for groundwater modeling and calibration purposes (Kumari 2007).

Other uncertainties that also limit the ability to develop an absolutely accurate numerical model are:

1. Source area and source concentrations: it was assumed that a main coal tar source exists close to where the manufactured gas process facilities existed. This assumption follows the well-defined source in the Black and Veatch (2008) report. Because it is not possible to model the time dependent dissolution and release of compounds from the coal tar source, average source area monitoring well concentrations were used to represent the source. Although MW-13 contaminant concentrations show a clear decreasing trend (see graphs in Figures 5.6 to 5.10), there is uncertainty associated with using this location as a secondary source of contamination following the approach of Stenback and Ong (2003).

2. Soil sorption and retardation coefficients: the sorption coefficients were estimated based on the measured soil organic carbon on site and estimated K_{ow} and K_{oc} values. However, actual sorption depends on the type of sorbing soils present. The site geology has noticeable soil type variations and overlapping at different regions. This might affect the sorption coefficients used for modeling, and in turn, can impact the contaminant transport simulations.

3. Decay and attenuation coefficients: first-order biodegradation rates were assumed for the contaminant simulation runs to simplify the complex biodegradation process. Because of uncertainties associated with estimates of first-order biodegradation rates, it is considered as a limitation to produce an accurate contaminant transport model.

4. Boundary conditions: the study assumed constant heads at the upstream and

downstream model boundaries, and no flow boundaries on the east and west model sides. This does not represent the real site conditions since the groundwater heads will not be constant with time and will have seasonal variations (e.g. river boundary).

5. Transport simulation time of 75 years: the contaminant transport run for a maximum period of 75 years was to simulate current conditions at the site, and was based on the assumption that the contaminant plumes are stable after the 75 year period with no further contaminant plume expansion/shrinking. However, additional source releases, if any, could further increase contaminant concentrations and expand the plumes. In contrast, decrease in source releases and/or increases in natural attenuation process rates would shrink the contaminant plumes closer to the source area.

Figure	Run	Dispersivity (m)			Partition Coefficient (K_d) (L/mg)			Biodegradation Rate (λ) (d^{-1})			Run Details
		α_x	α_t	α_V	Benzene	Benzo(a) pyrene	Naphthalene	Benzene	Benzo(a) pyrene	Naphthalene	
		Advection and Dispersion									
5.12	1	4.120	0.824	0.0824	-	-	-	-	-	-	Base Dispersion values
	2	4.120	0.618	0.0618	-	-	-	-	-	-	Changed transverse to 15% of α_x
	3	4.120	0.412	0.0412	-	-	-	-	-	-	Changed transverse to 10% of α_x
	4	3.520	0.352	0.0352	-	-	-	-	-	-	Repeat Run #3, except changed α_x to 3.52 m
5.13	5	3.120	0.312	0.0312	-	-	-	-	-	-	Repeat Run #4, except changed α_x to 3.12 m
		Advection, Dispersion & Sorption									
	6	4.120	0.824	0.0824	8.715E-07	5.775E-02	1.365E-05	-	-	-	Added base K_d values to Run #1
5.14	7	4.120	0.618	0.0618	8.715E-07	5.775E-02	1.365E-05	-	-	-	Added base K_d values to Run #2
	8	4.120	0.618	0.0618	8.715E-06	5.775E-02	1.365E-05	-	-	-	Increased benzene K_d value by one order of magnitude from Run #7
5.15	9	4.120	0.618	0.0618	8.715E-05	5.775E-02	1.365E-05	-	-	-	Increased benzene K_d values by one order of magnitude from Run #8
		Advection, Dispersion, Sorption & Degradation									
5.16	10	4.120	0.618	0.0618	8.715E-07	5.775E-02	1.365E-05	1.89E-02	1.00E-03	2.10E-03	Added base λ values to Run #7
5.17	11	4.120	0.618	0.0618	8.715E-07	5.775E-02	1.365E-05	1.89E-01	1.00E-03	2.10E-03	Increased λ value of benzene by one order of magnitude from Run #10
5.18	12	4.120	0.618	0.0618	8.715E-06	5.775E-02	1.365E-05	1.89E-01	2.30E-03	3.00E-03	Combining Run # 8 with Run # 11but increasing λ for naphthalene and benzo(a)pyrene from Run #10
5.19	13	4.120	0.618	0.0618	8.715E-06	4.775E-02	1.365E-05	2.89E-02	2.30E-03	3.00E-03	Adjusting benzene λ value and benzo(a)pyrene K_d value from Run #12

Table 5.1: Summary of the transport analysis runs

Location			SS 2 (alluvium)	SS 2 (alluvium)	SS 5 (alluvium)	SS 5 (alluvium)	SS 6 (alluvium)	SS 10 (alluvium)	HC 5 (alluvium)
f_{oc} (%)			0.25	0.2	0.8	0.3	2.6	2.9	0.3
Compound	log Kow	Koc (ml/g)	K_d (ml/g)						
Benzene	2.13	83	0.21	0.17	0.66	0.25	2.16	2.41	0.249
Naphthalene	3.29	1300	3.25	2.60	10.40	3.90	33.80	37.70	3.9
Benzo(a)pyrene	6.06	5500000	13750	11000	44000	16500	143000	159500	16500
Location			SS 2 (loess)	SS 6 (loess)	SS 8 (loess)	SS 10 (loess)	SS 12 (loess)	SS 12 (loess)	HC 5 (loess)
f_{oc} (%)			0.29	3.05	0.3	2.6	0.7	3.9	0.35
Compound	log Kow	Koc (ml/g)	K_d (ml/g)						
Benzene	2.13	83	0.24	2.53	0.249	2.158	0.581	3.237	0.2905
Naphthalene	3.29	1300	3.77	39.65	3.9	33.8	9.1	50.7	4.55
Benzo(a)pyrene	6.06	5500000	15950	167750	16500	143000	38500	214500	19250

Table 5.2: Partition coefficients in ml/g units for the selected contaminants using the samples measured by Biyani (2003)

Contaminant	Average K_d (ml/g)	Retardation Factor (R_f)	*Contaminants Velocity (m/d)
Benzene	0.872	6.52	3.13E-3
Naphthalene	13.65	87.45	2.33E-4
Benzo(a)pyrene	57750	365751	5.58E-8

*Contaminants velocity was estimated based on seepage velocity of 0.0204 m/d (Golchin et al. 2004)

Table 5.3: Average partition coefficients (K_d), retardation factors and velocity of the contaminants in the alluvium layer

MW No.	Benzene (µg/L)	Hydraulic Gradient (m/m)	Hydraulic Conductivity (m/yr)	Darcy's velocity (m/yr)	Mass flux ($g/m^2 \cdot yr$)	Area (m^2)	Mass discharge (g/yr)
MW-25	0.32	0.076	39.735	3.020	0.001	20	0.019
MW-24	0.32	0.076	39.735	3.020	0.001	20	0.019
MW-17	4.99	0.076	39.735	3.020	0.015	45	0.678
MW-14	7.55	0.076	39.735	3.020	0.023	45	1.026
MW-13	201.93	0.076	39.735	3.020	0.610	32.5	19.819
MW-20	85	0.076	39.735	3.020	0.257	25	6.417
MW-28	1	0.076	39.735	3.020	0.003	20	0.060
						Total benzene mass discharge =	28.04
MW No.	Naphthalene (µg/L)	Hydraulic Gradient (m/m)	Hydraulic Conductivity (m/yr)	Darcy's velocity (m/yr)	Mass flux ($g/m^2 \cdot yr$)	Area (m^2)	Mass discharge (g/yr)
MW-25	0.02	0.076	39.735	3.020	0.0001	20	0.001
MW-24	0.02	0.076	39.735	3.020	0.0001	20	0.001
MW-17	42.2	0.076	39.735	3.020	0.1274	45	5.735
MW-14	1.85	0.076	39.735	3.020	0.0056	45	0.251
MW-13	33.48	0.076	39.735	3.020	0.1011	32.5	3.286
MW-20	1.98	0.076	39.735	3.020	0.0060	25	0.149
MW-28	0.1	0.076	39.735	3.020	0.0003	20	0.006
						Total naphthalene mass discharge =	9.43

Table 5.4: Transect B – B' mass flux estimations using November 2002 concentration data

MW No.	Benzene (µg/L)	Darcy's velocity (m/yr)	Mass flux ($g/m^2 \cdot yr$)	Area (m^2)	Mass discharge (g/yr)
MW-26	0.32	1.739	0.001	50	0.028
MW-18	1	1.739	0.002	40	0.070
MW-3	0.24	1.739	0.000	40	0.017
MW-15	1000	1.739	1.739	40	69.578
MW-27	76.9	1.739	0.134	30	4.013
MW-6	1	1.739	0.002	30	0.052
MW-21	0.32	1.739	0.001	40	0.022
MW-8	0.32	1.739	0.001	60	0.033
				Total benzene mass discharge =	73.81
MW No.	Naphthalene (µg/L)	Darcy's velocity (m/yr)	Mass flux ($g/m^2 \cdot yr$)	Area (m^2)	Mass discharge (g/yr)
MW-26	0.1	1.739	0.000	50	0.009
MW-18	0.56	1.739	0.001	40	0.039
MW-3	186	1.739	0.324	40	12.942
MW-15	4780	1.739	8.315	40	332.584
MW-27	3.25	1.739	0.006	30	0.170
MW-6	1.39	1.739	0.002	30	0.073
MW-21	0.1	1.739	0.000	40	0.007
MW-8	0.1	1.739	0.000	60	0.010
				Total naphthalene mass discharge =	345.83

Table 5.5: Transect A – A' mass flux estimations using November 2002 concentration data

MW No.	Benzene (µg/L)	Hydraulic Gradient (m/m)	Hydraulic Conductivity (m/yr)	Darcy's velocity (m/yr)	Mass flux ($g/m^2 \cdot yr$)	Area (m^2)	Mass discharge (g/yr)
MW-25	0.32	0.076	39.735	3.020	0.001	20	0.019
MW-24	0.32	0.076	39.735	3.020	0.001	20	0.019
MW-17	5.3	0.076	39.735	3.020	0.016	45	0.720
MW-14	9.4	0.076	39.735	3.020	0.028	45	1.277
MW-13	205.4	0.076	39.735	3.020	0.620	32.5	20.159
MW-20	0.32	0.076	39.735	3.020	0.001	25	0.024
MW-28	0.32	0.076	39.735	3.020	0.001	20	0.019
					Total benzene mass discharge =		22.24
MW No.	Naphthalene (µg/L)	Hydraulic Gradient (m/m)	Hydraulic Conductivity (m/yr)	Darcy's velocity (m/yr)	Mass flux ($g/m^2 \cdot yr$)	Area (m^2)	Mass discharge (g/yr)
MW-25	0.02	0.076	39.735	3.020	0.0001	20	0.001
MW-24	0.02	0.076	39.735	3.020	0.0001	20	0.001
MW-17	0.091	0.076	39.735	3.020	0.0003	45	0.012
MW-14	0.087	0.076	39.735	3.020	0.0003	45	0.012
MW-13	3.6	0.076	39.735	3.020	0.0109	32.5	0.353
MW-20	0.079	0.076	39.735	3.020	0.0002	25	0.006
MW-28	0.076	0.076	39.735	3.020	0.0002	20	0.005
					Total naphthalene mass discharge =		0.39

Table 5.6: Transect B – B' mass flux estimations using March 2003 concentration data

MW No.	Benzene (µg/L)	Darcy's velocity (m/yr)	Mass flux ($g/m^2 \cdot yr$)	Area (m^2)	Mass discharge (g/yr)
MW-26	0.32	1.739	0.001	50	0.028
MW-18	0.32	1.739	0.001	40	0.022
MW-3	8.3	1.739	0.014	40	0.577
MW-15	832	1.739	1.447	40	57.889
MW-27	3.9	1.739	0.007	30	0.204
MW-6	1.98	1.739	0.003	30	0.103
MW-21	0.32	1.739	0.001	40	0.022
MW-8	0.32	1.739	0.001	60	0.033
				Total benzene mass discharge =	58.88
MW No.	Naphthalene (µg/L)	Darcy's velocity (m/yr)	Mass flux ($g/m^2 \cdot yr$)	Area (m^2)	Mass discharge (g/yr)
MW-26	0.47	1.739	0.00082	50	0.041
MW-18	0.08	1.739	0.00014	40	0.006
MW-3	0.02	1.739	0.00003	40	0.001
MW-15	3220	1.739	5.60105	40	224.042
MW-27	8.3	1.739	0.01444	30	0.433
MW-6	0.02	1.739	0.00003	30	0.001
MW-21	0.98	1.739	0.00170	40	0.068
MW-8	0.15	1.739	0.00026	60	0.016
				Total naphthalene mass discharge =	224.61

Table 5.7: Transect A – A' mass flux estimations using March 2003 concentration data

MW No.	Benzene (µg/L)	Hydraulic Gradient (m/m)	Hydraulic Conductivity (m/yr)	Darcy's velocity (m/yr)	Mass flux ($g/m^2 \cdot yr$)	Area (m^2)	Mass discharge (g/yr)
MW-25	0.32	0.076	39.735	3.020	0.001	20	0.019
MW-24	0.32	0.076	39.735	3.020	0.001	20	0.019
MW-17	0.32	0.076	39.735	3.020	0.001	45	0.043
MW-14	0.32	0.076	39.735	3.020	0.001	45	0.043
MW-13	174.88	0.076	39.735	3.020	0.528	32.5	17.164
MW-20	5	0.076	39.735	3.020	0.015	25	0.377
MW-28	0.32	0.076	39.735	3.020	0.001	20	0.019
						Total benzene mass discharge =	17.690
MW No.	Naphthalene (µg/L)	Hydraulic Gradient (m/m)	Hydraulic Conductivity (m/yr)	Darcy's velocity (m/yr)	Mass flux ($g/m^2 \cdot yr$)	Area (m^2)	Mass discharge (g/yr)
MW-25	0.02	0.076	39.735	3.020	0.0001	20	0.001
MW-24	0.02	0.076	39.735	3.020	0.0001	20	0.001
MW-17	0.02	0.076	39.735	3.020	0.0001	45	0.003
MW-14	0.02	0.076	39.735	3.020	0.0001	45	0.003
MW-13	0.894	0.076	39.735	3.020	0.0027	32.5	0.088
MW-20	1.18	0.076	39.735	3.020	0.0036	25	0.089
MW-28	0.0347	0.076	39.735	3.020	0.0001	20	0.002
						Total naphthalene mass discharge =	0.19

Table 5.8: Transect B – B' mass flux estimations using June 2007 concentration data

MW No.	Benzene (µg/L)	Darcy's velocity (m/yr)	Mass flux ($g/m^2 \cdot yr$)	Area (m^2)	Mass discharge (g/yr)
MW-26	0.32	1.739	0.001	50	0.028
MW-18	0.32	1.739	0.001	40	0.022
MW-3	6.5	1.739	0.011	40	0.452
MW-15	880	1.739	1.531	40	61.229
MW-27	16.6	1.739	0.029	30	0.866
MW-6	0.32	1.739	0.001	30	0.017
MW-21	0.32	1.739	0.001	40	0.022
MW-8	0.32	1.739	0.001	60	0.033
				Total benzene mass discharge =	62.67
MW No.	Naphthalene (µg/L)	Darcy's velocity (m/yr)	Mass flux ($g/m^2 \cdot yr$)	Area (m^2)	Mass discharge (g/yr)
MW-26	0.02	1.73946	0.00003	50	0.002
MW-18	0.3	1.73946	0.00052	40	0.021
MW-3	0.02	1.73946	0.00003	40	0.001
MW-15	1910	1.73946	3.32236	40	132.894
MW-27	1.55	1.73946	0.00270	30	0.081
MW-6	0.211	1.73946	0.00037	30	0.011
MW-21	0.02	1.73946	0.00003	40	0.001
MW-8	0.018	1.73946	0.00003	60	0.002
				Total naphthalene mass discharge =	133.01

Table 5.9: Transect A – A' mass flux estimations using June 2007 concentration data

Contaminant	Mass discharge A-A' (g/yr)	Mass discharge B-B' (g/yr)	Bulk attenuation rate (1/d)	Biodegradation rate (1/d)
Benzene	73.81	28.04	2.90E-02	3.06E-02
Naphthalene	345.83	9.43	8.04E-03	2.41E-04
Benzo(a)pyrene	N/A	N/A	N/A	N/A

Travel time (t) was determined using contaminants velocity (see Table 5.3)

Table 5.10: Attenuation rates for November 2002 flux estimations

Contaminant	Mass discharge A-A' (g/yr)	Mass discharge B-B' (g/yr)	Bulk attenuation rate (1/d)	Biodegradation rate (1/d)
Benzene	58.88	22.24	2.92E-02	3.09E-02
Naphthalene	224.61	0.39	1.42E-02	6.26E-04
Benzo(a)pyrene	N/A	N/A	N/A	N/A

Travel time (t) was determined using contaminant velocity (see Table 5.3)

Table 5.11: Attenuation rates for March 2003 flux estimations

Contaminant	Mass discharge A-A' (g/yr)	Mass discharge B-B' (g/yr)	Bulk attenuation rate (1/d)	Biodegradation rate (1/d)
Benzene	62.67	17.69	3.79E-02	5.04E-02
Naphthalene	133.01	0.19	1.47E-02	6.63E-04
Benzo(a)pyrene	N/A	N/A	N/A	N/A

Travel time (t) was determined using contaminants velocity (see Table 5.3)

Table 5.12: Attenuation rates for June 2007 flux estimations

Source	Biodegradation rate (1/d)	
	Benzene	Naphthalene
Rogers et al. (2007a)	8.40E-03	5.80E-03
Stenback and Ong (2003)	4.10E-03	5.40E-03
Biyani (2003)	1.50E-03	8.00E-05
Miller (2000)	6.30E-03	1.90E-03
November 2002 flux estimations	3.06E-02	2.41E-04
March 2003 flux estimations	3.09E-02	6.26E-04
June 2007 flux estimations	5.04E-02	6.63E-04
Average	1.89E-02	2.10E-03

Table 5.13: Biodegradation rates reported in different studies in comparison to the estimated rates with mass flux calculations

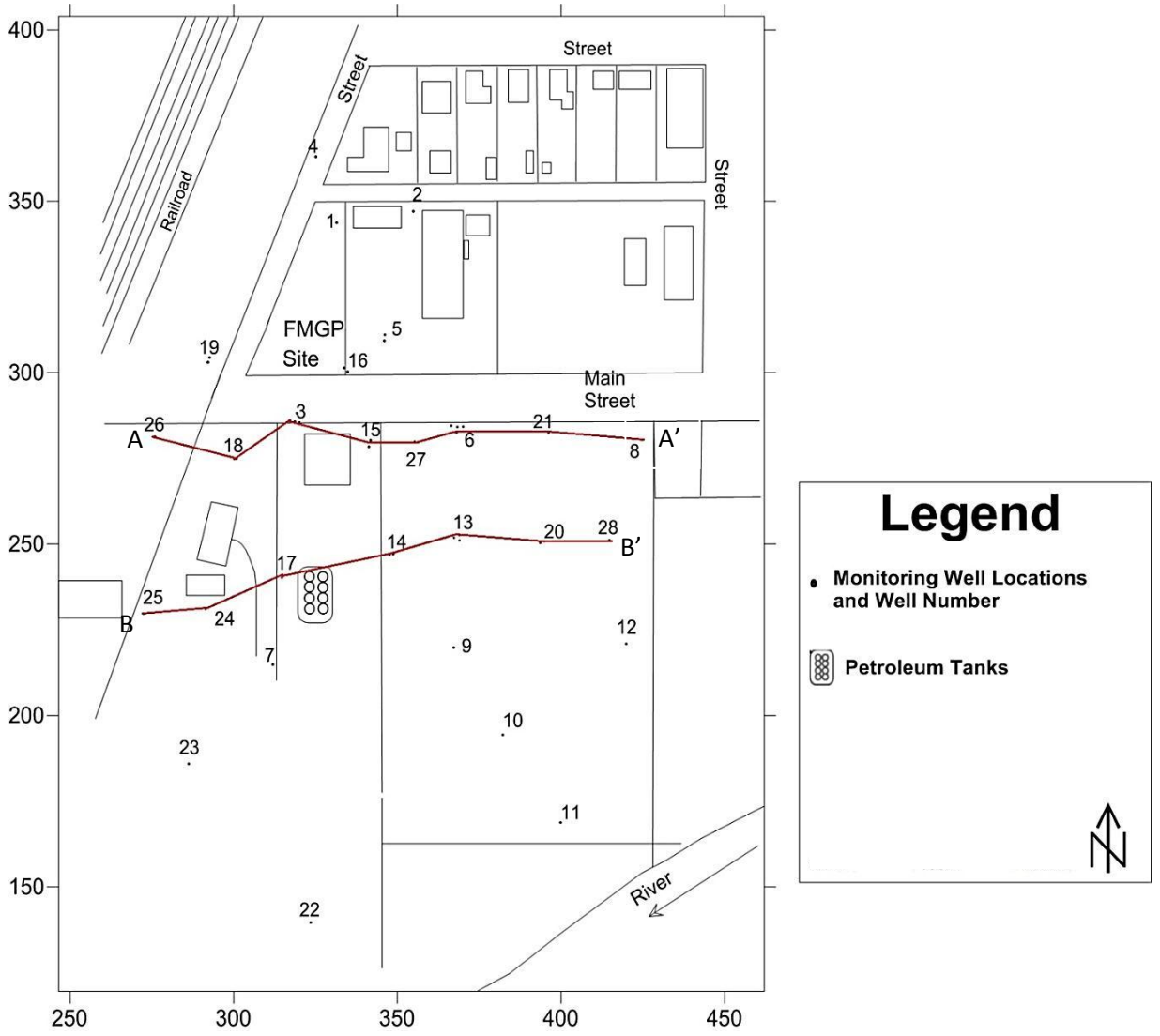

Figure 5.1: Site plan showing the selected transects; horizontal and vertical scales are in meters

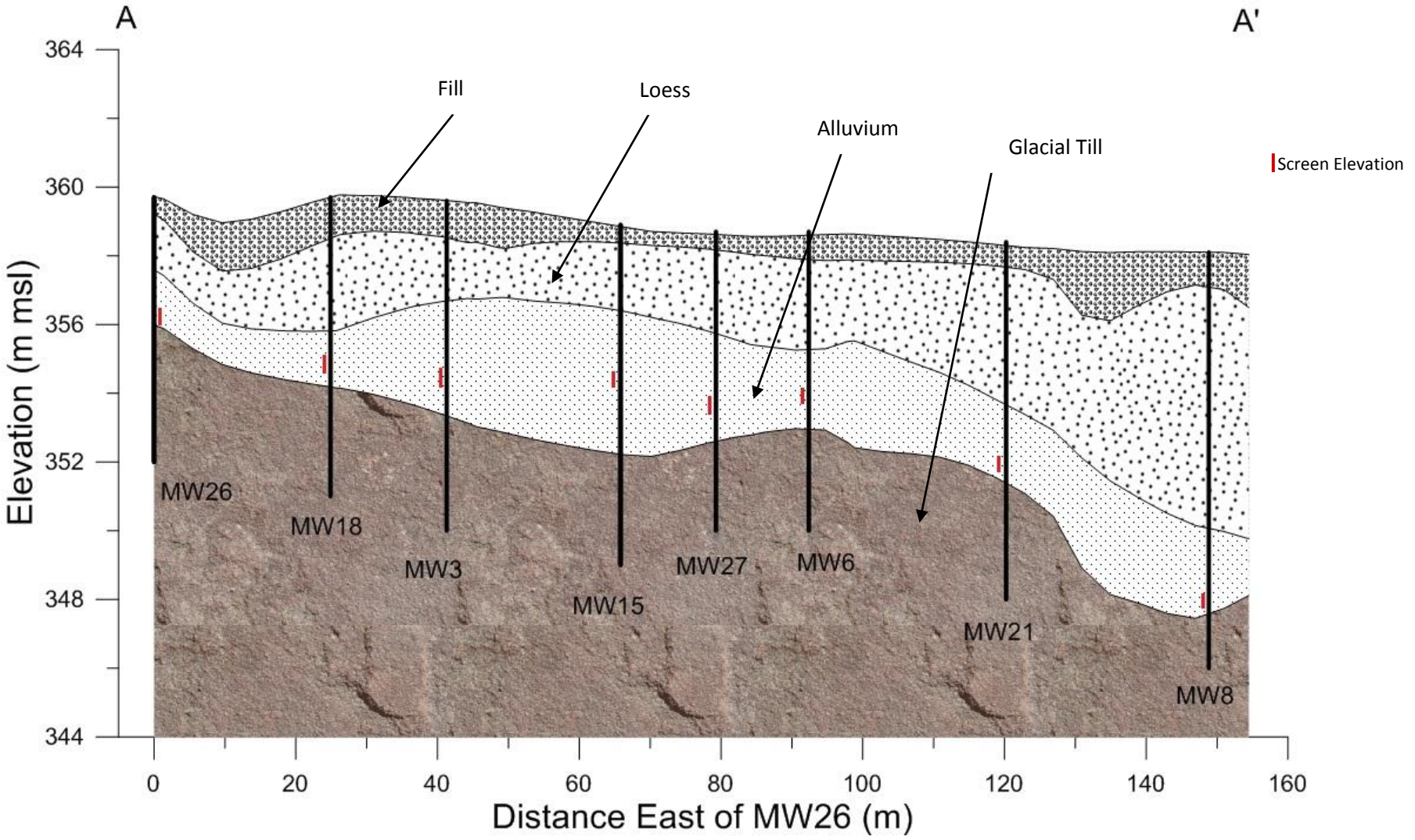

Figure 5.2: Transect A-A'

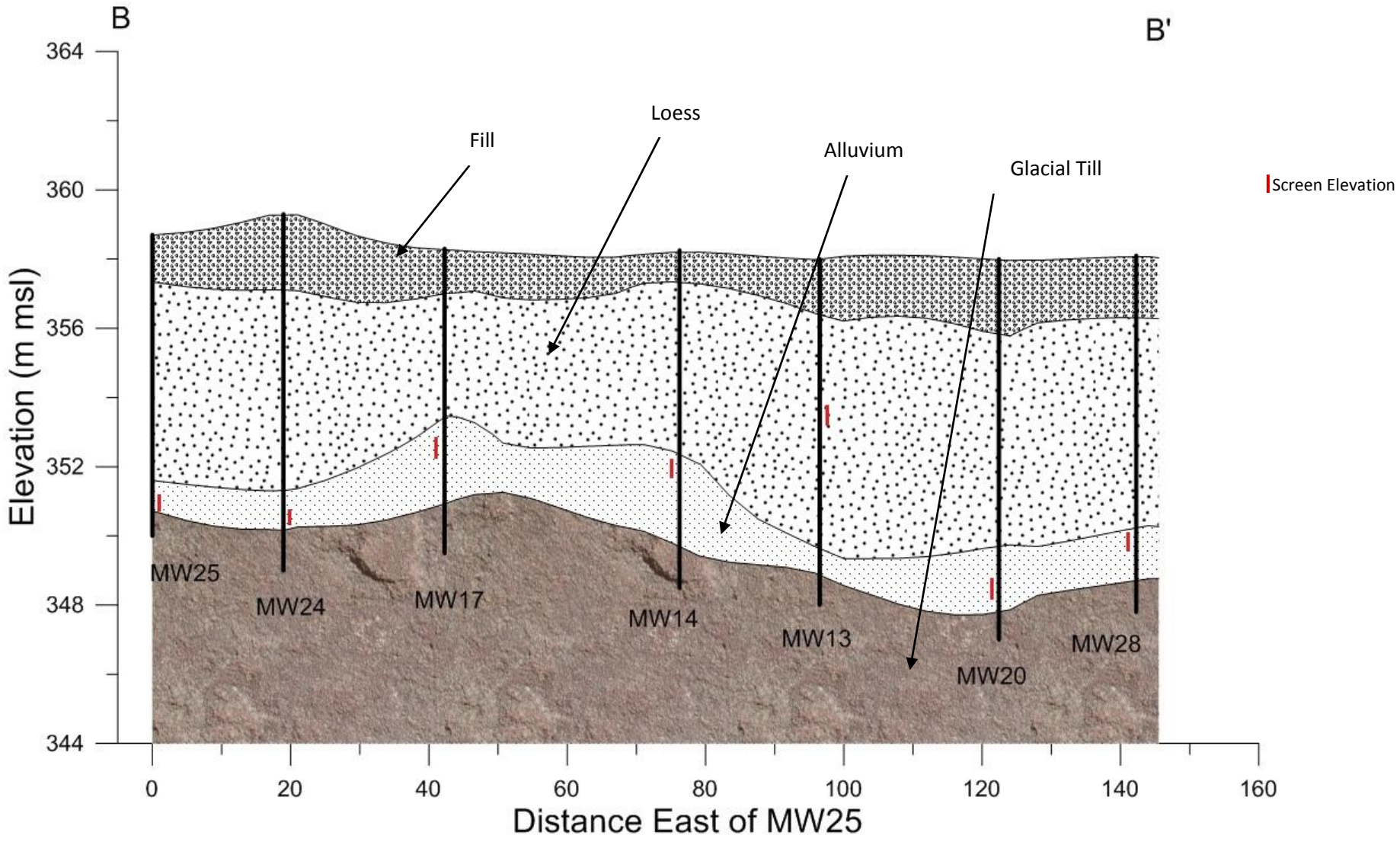

Figure 5.3: Transect B-B'

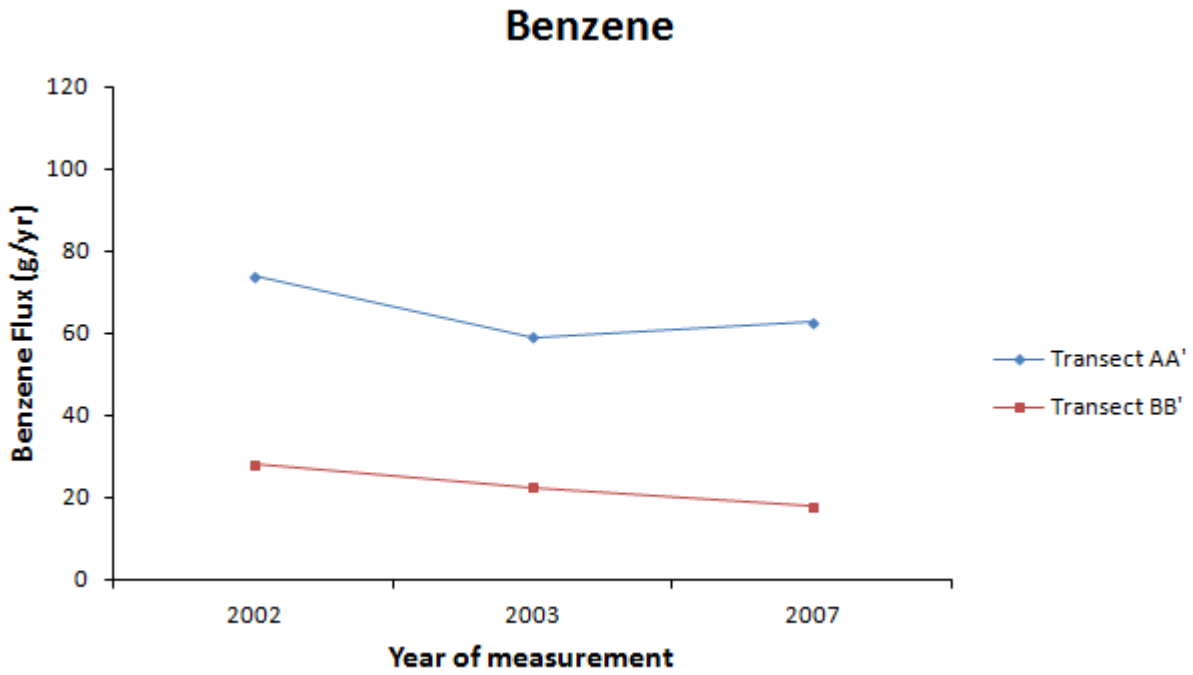

Figure 5.4: Benzene mass discharge variation with time across the transects

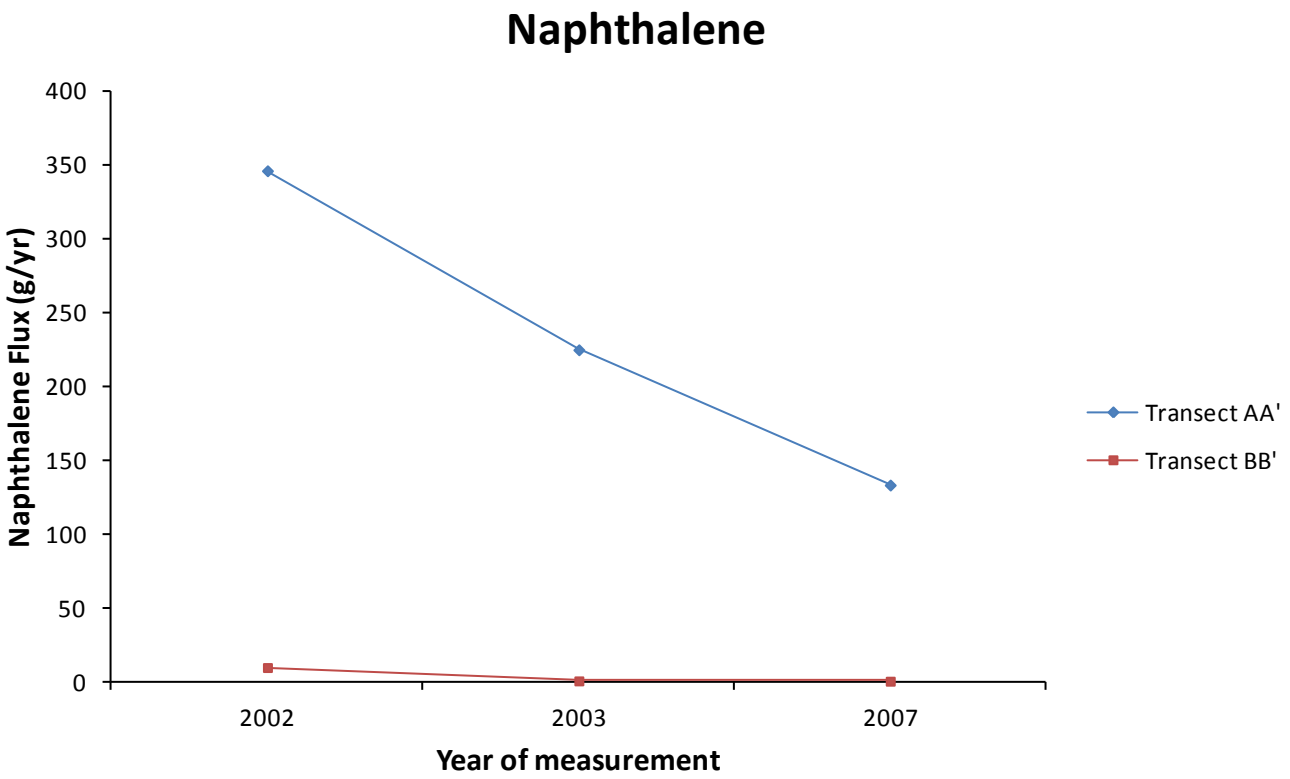

Figure 5.5: Naphthalene mass discharge variation with time across the transects

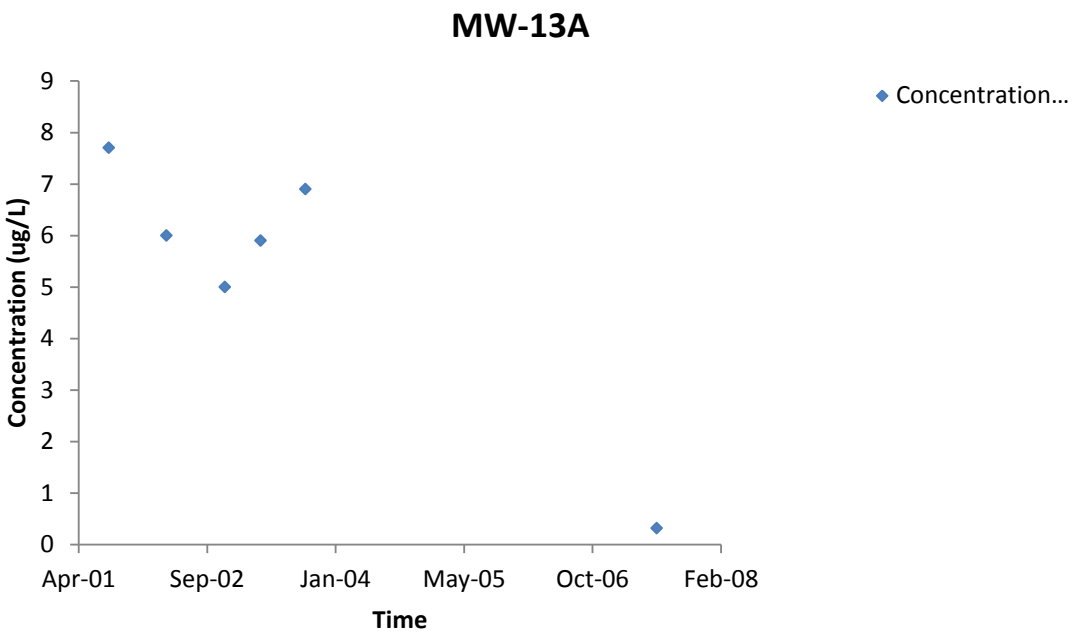

Figure 5.6: Benzene concentration versus time for MW-13A

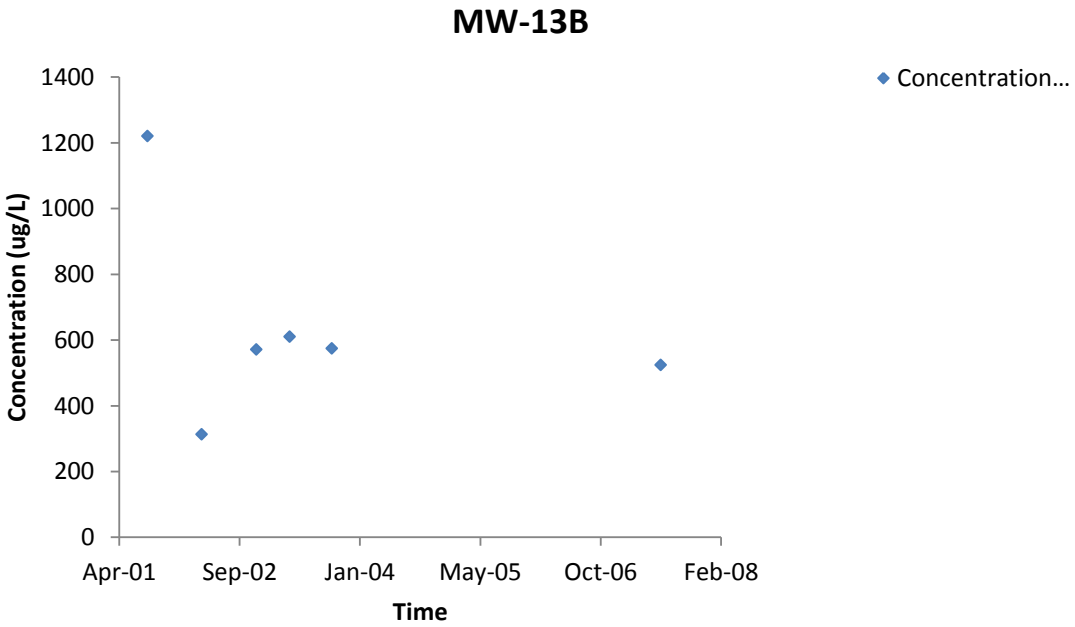

Figure 5.7: Benzene concentration versus time for MW-13B

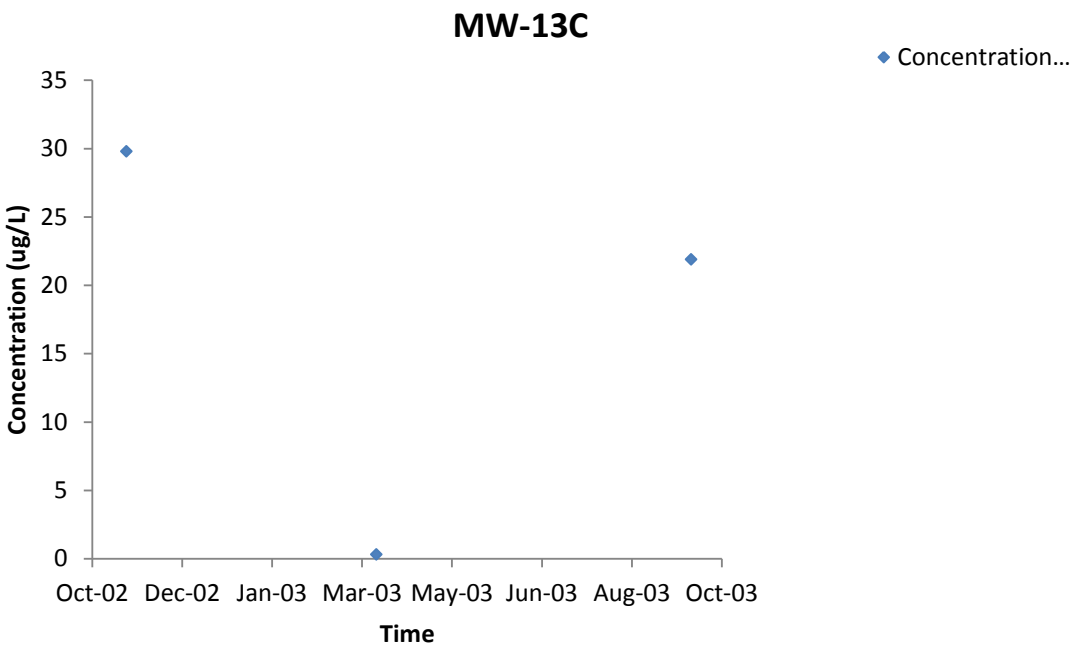

Figure 5.8: Benzene concentration versus time for MW-13C

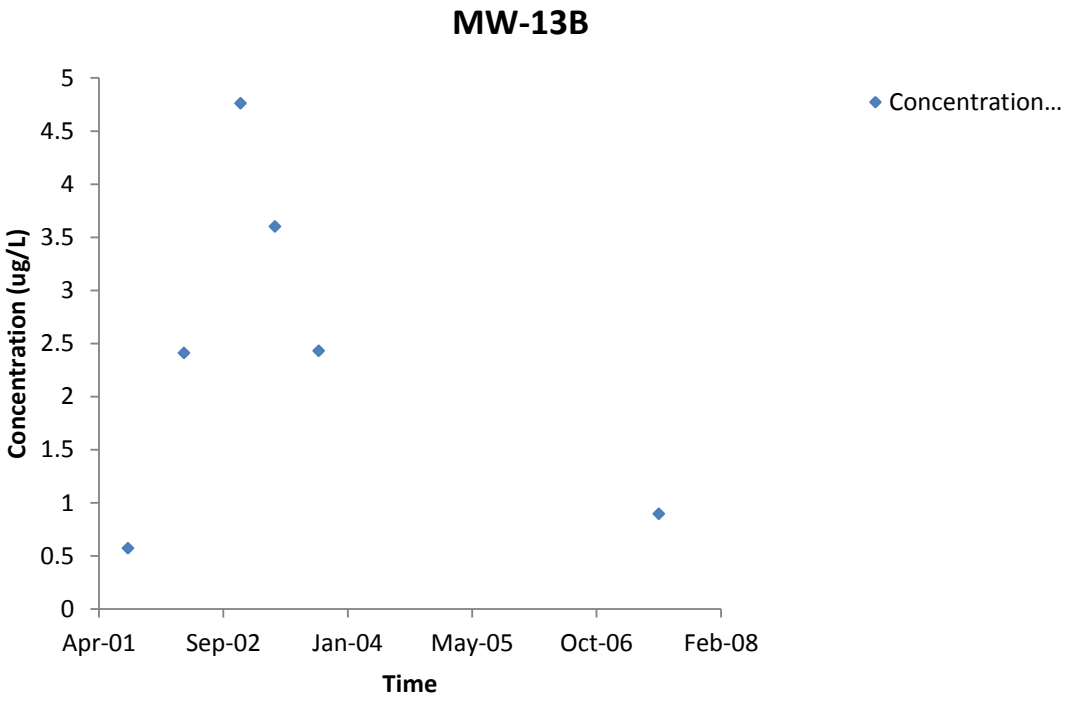

Figure 5.9: Naphthalene concentration versus time for MW-13B

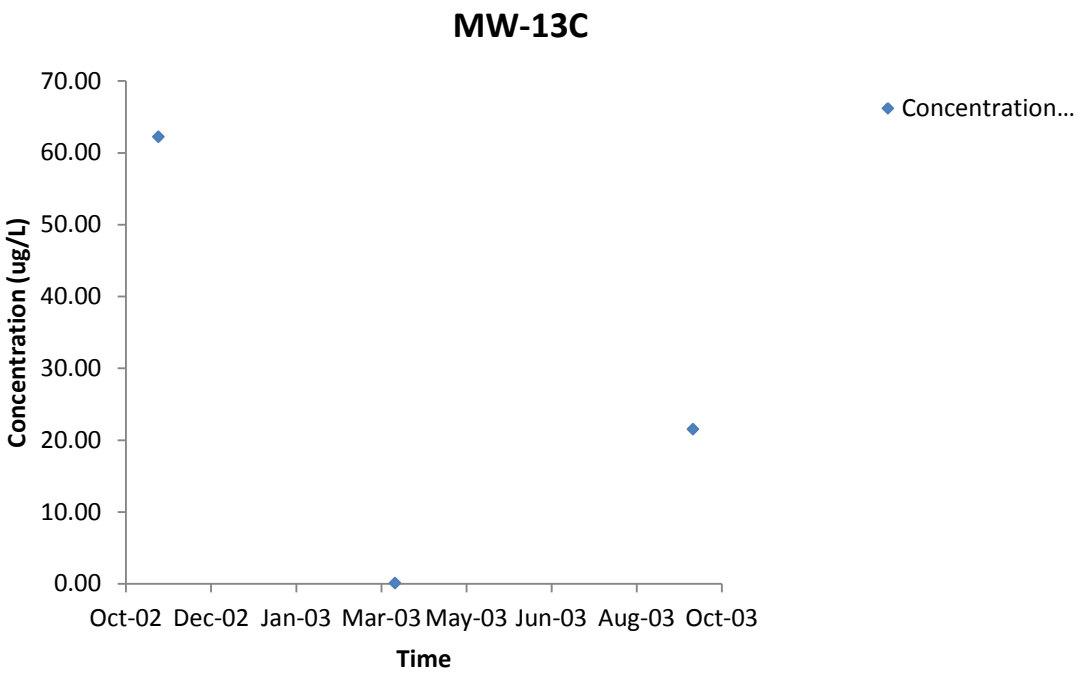

Figure 5.10: Naphthalene concentration versus time for MW-13C

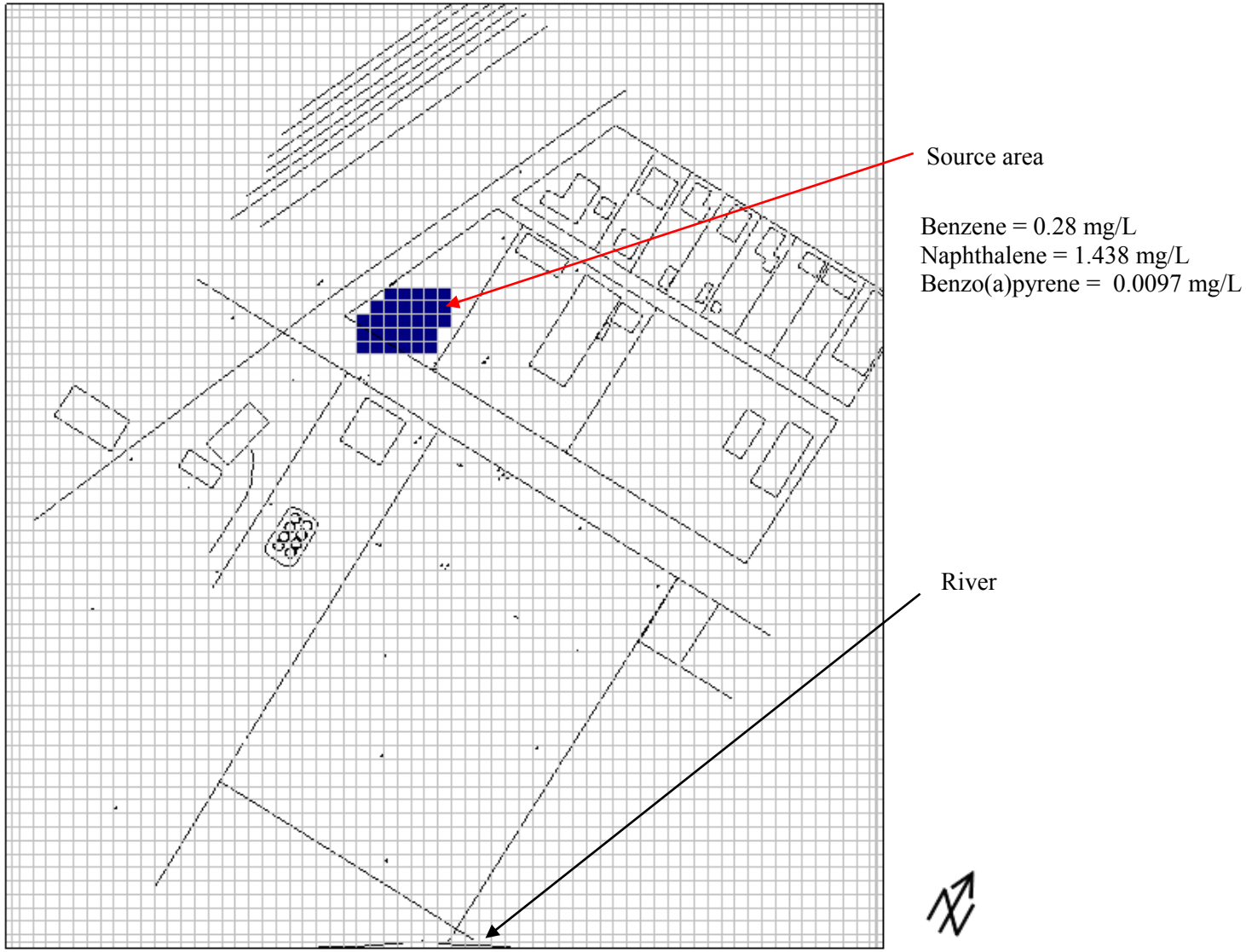

Figure 5.11: Source area displayed within layer 3 of the model

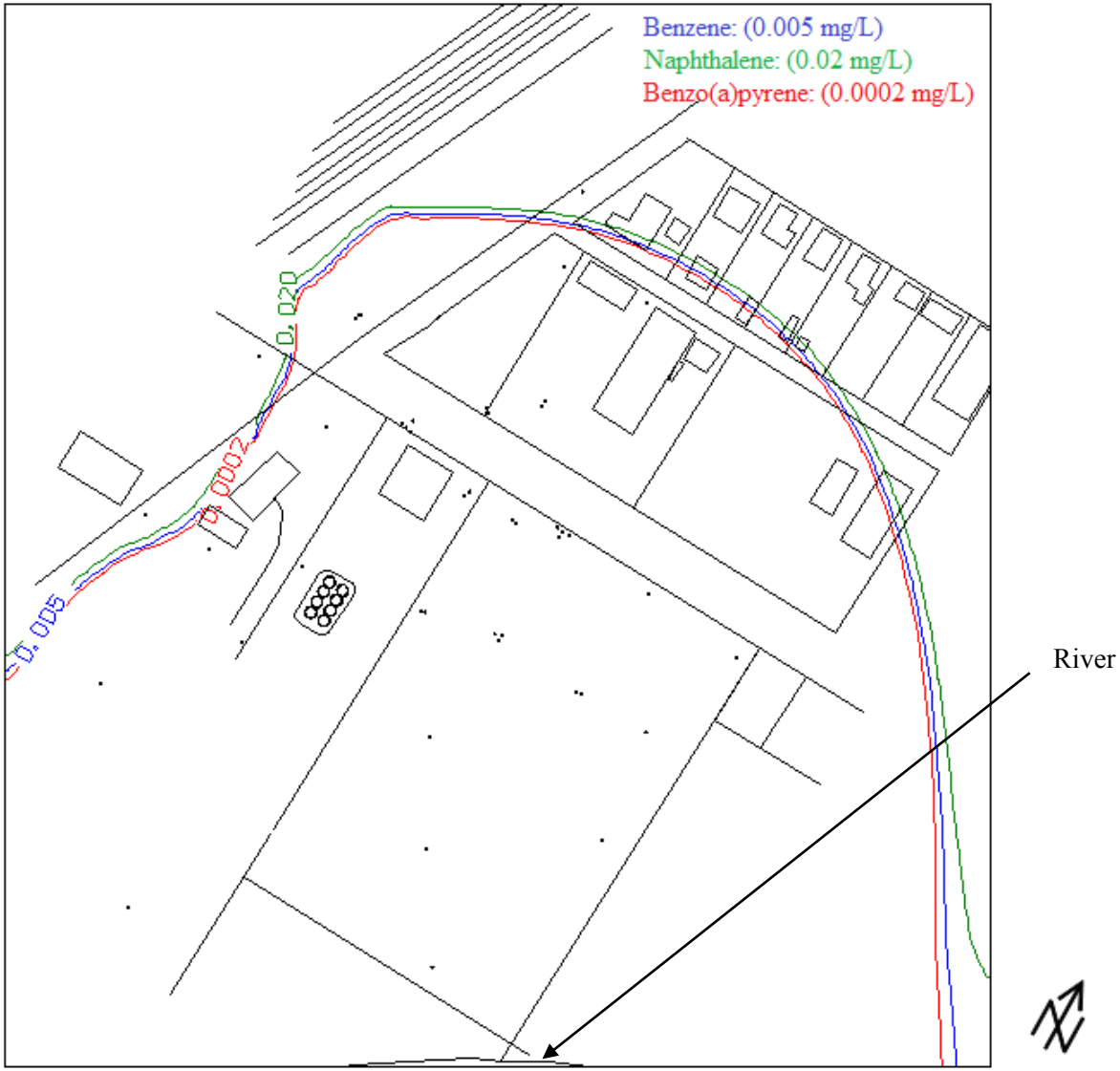

Figure 5.12: Plume at 75 years with advection and dispersion transport processes, parameters used for Run # 1 (see Table 5.1)

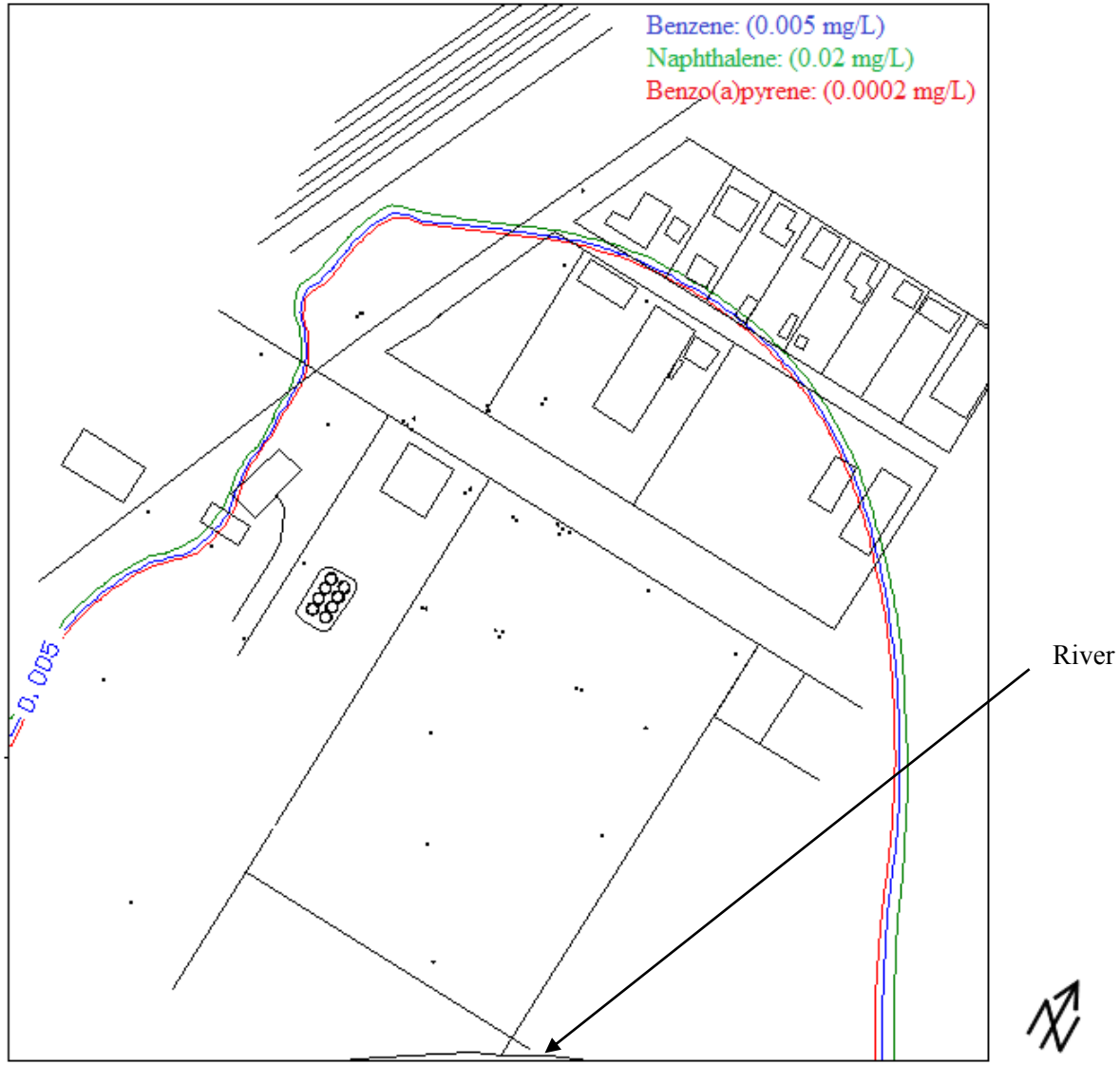

Figure 5.13: Plume at 75 years with advection and dispersion transport processes, parameters used for Run # 5 (see Table 5.1)

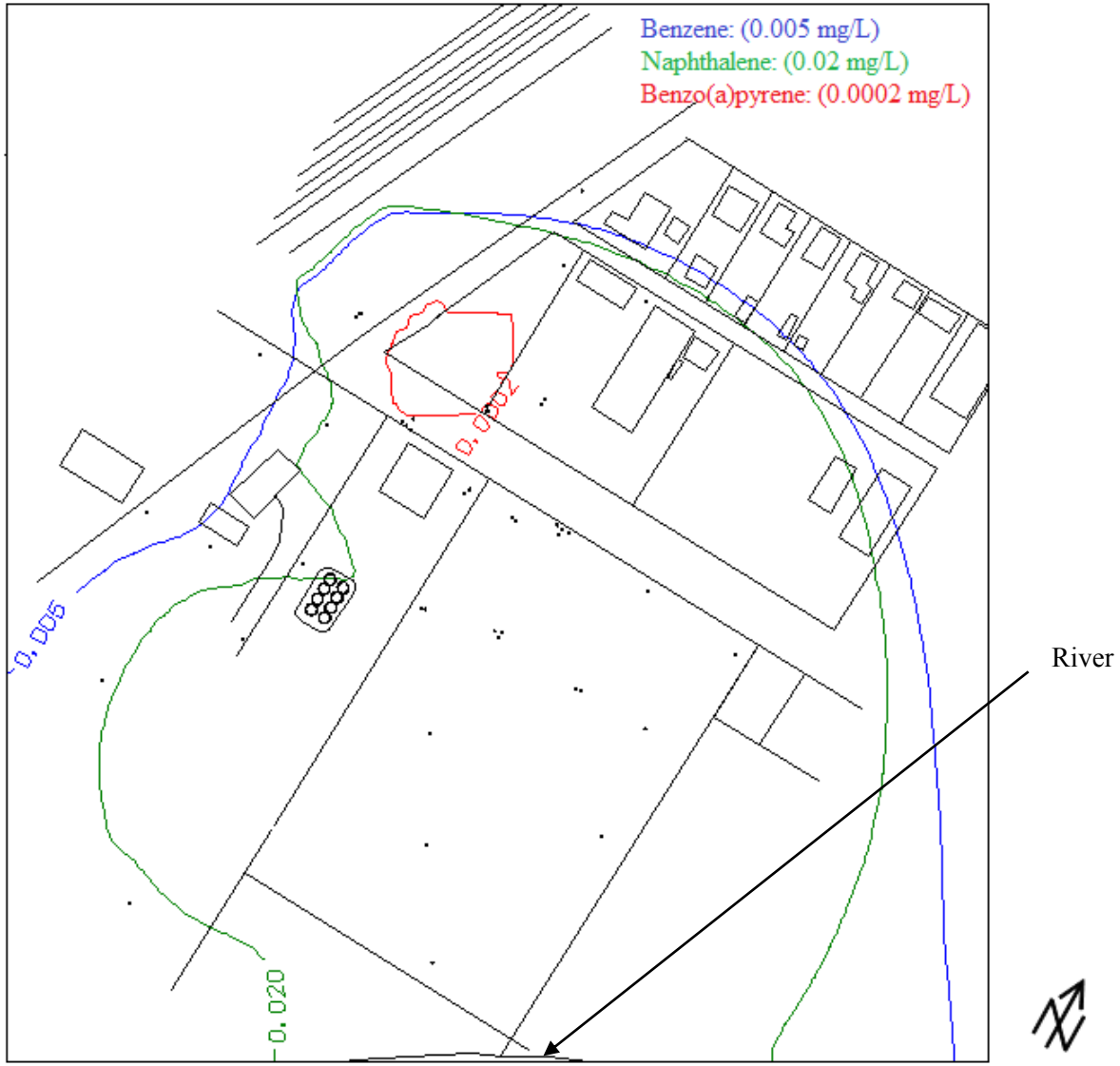

Figure 5.14: Plume at 75 years with advection, dispersion and sorption transport processes, parameters used for Run # 7 (see Table 5.1)

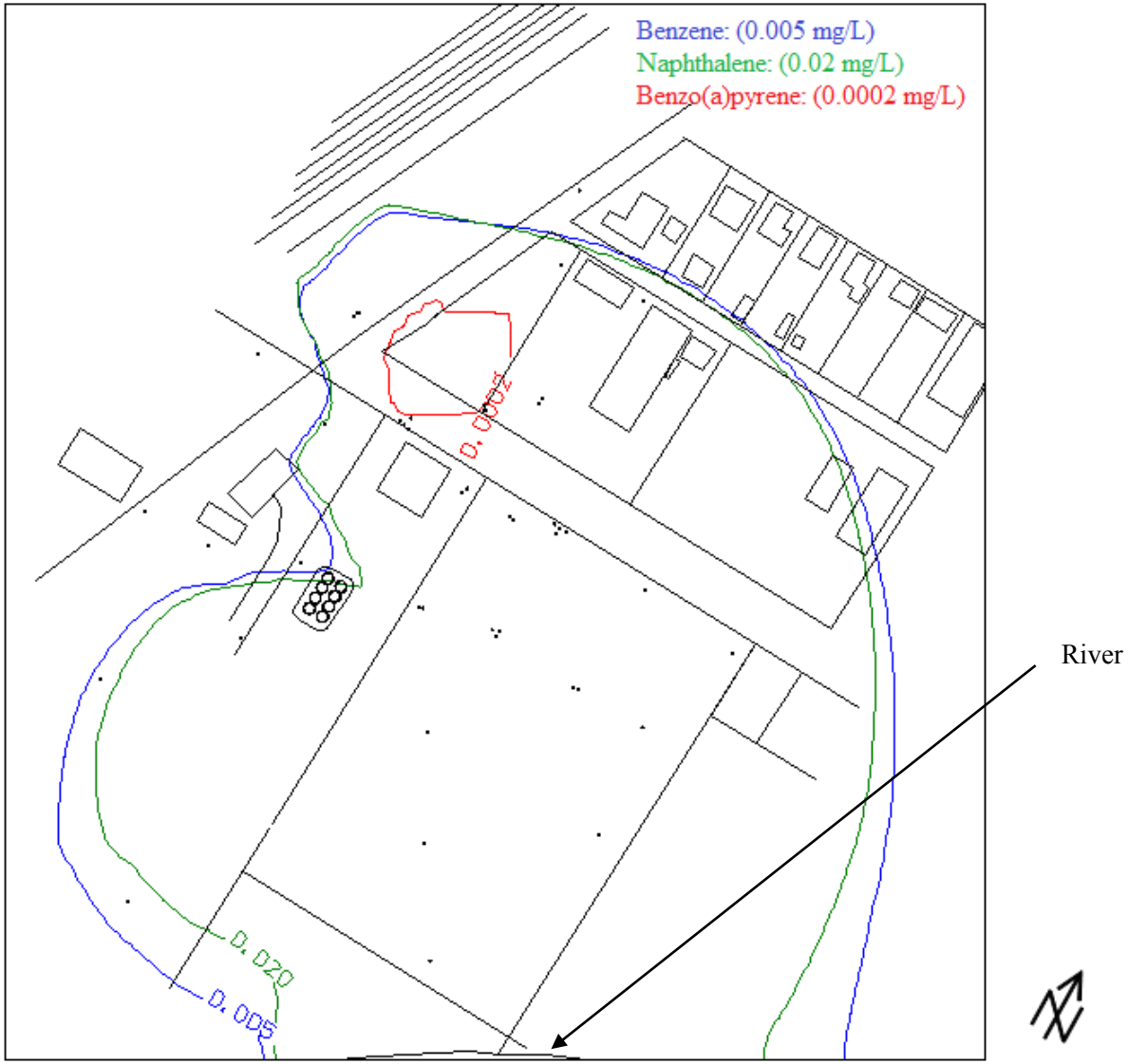

Figure 5.15: Plume at 75 years with advection, dispersion and sorption transport processes, parameters used for Run # 9 (see Table 5.1)

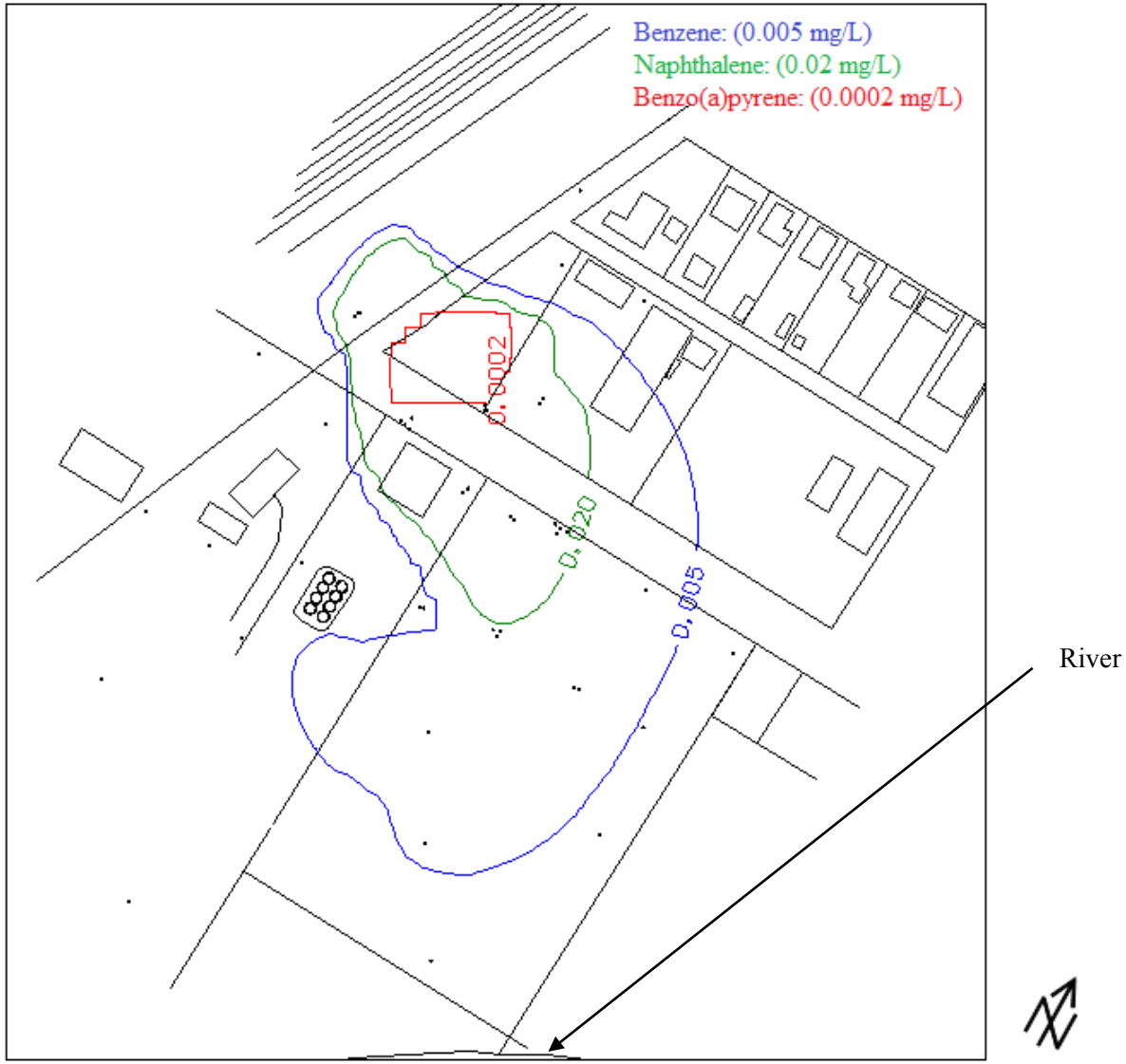

Figure 5.16: Plume at 75 years with advection, dispersion, sorption and biodegradation processes, parameters used for Run # 10 (see Table 5.1)

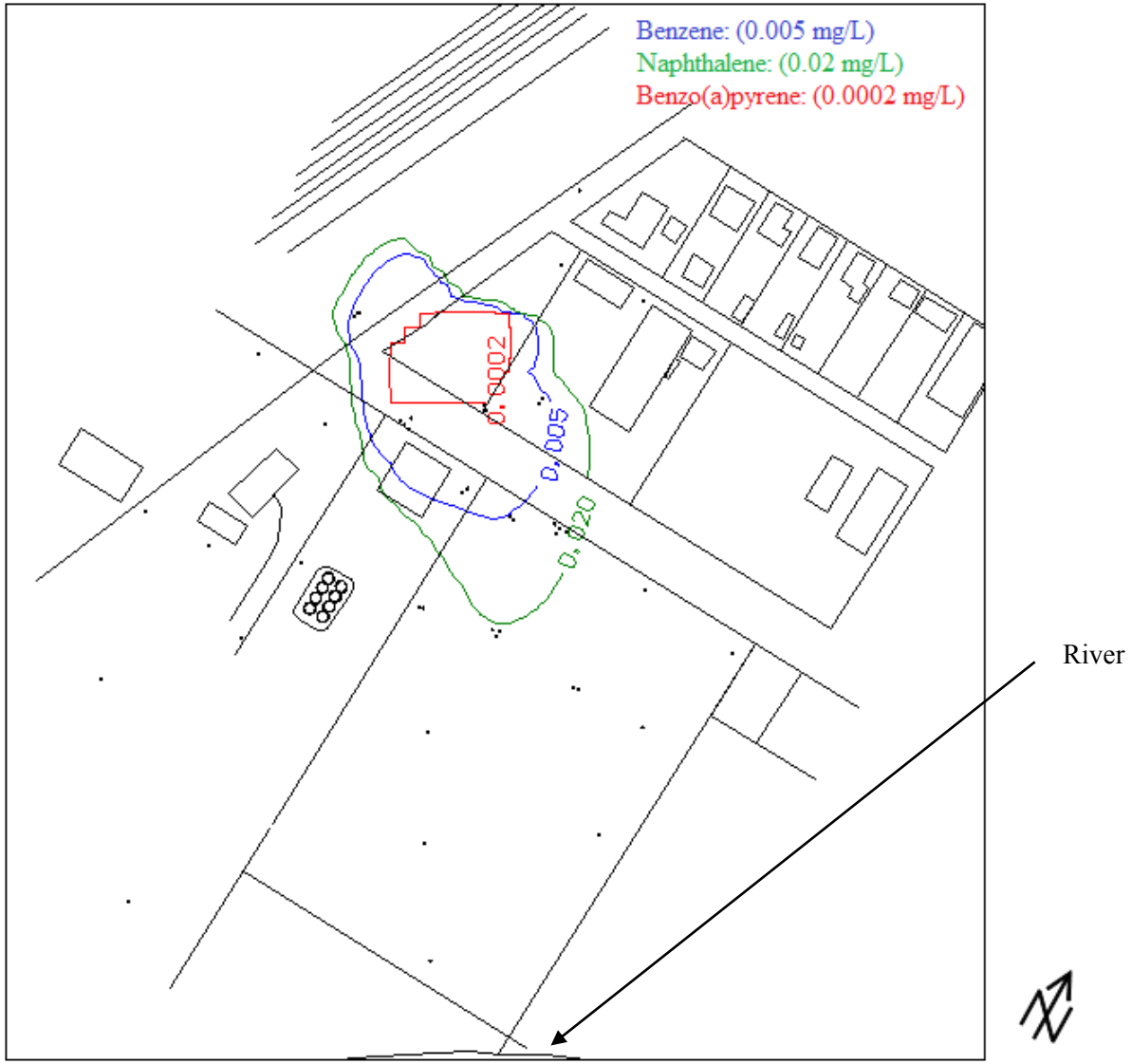

Figure 5.17: Plume at 75 years with advection, dispersion, sorption and biodegradation transport processes, parameters used for Run # 11 (see Table 5.1)

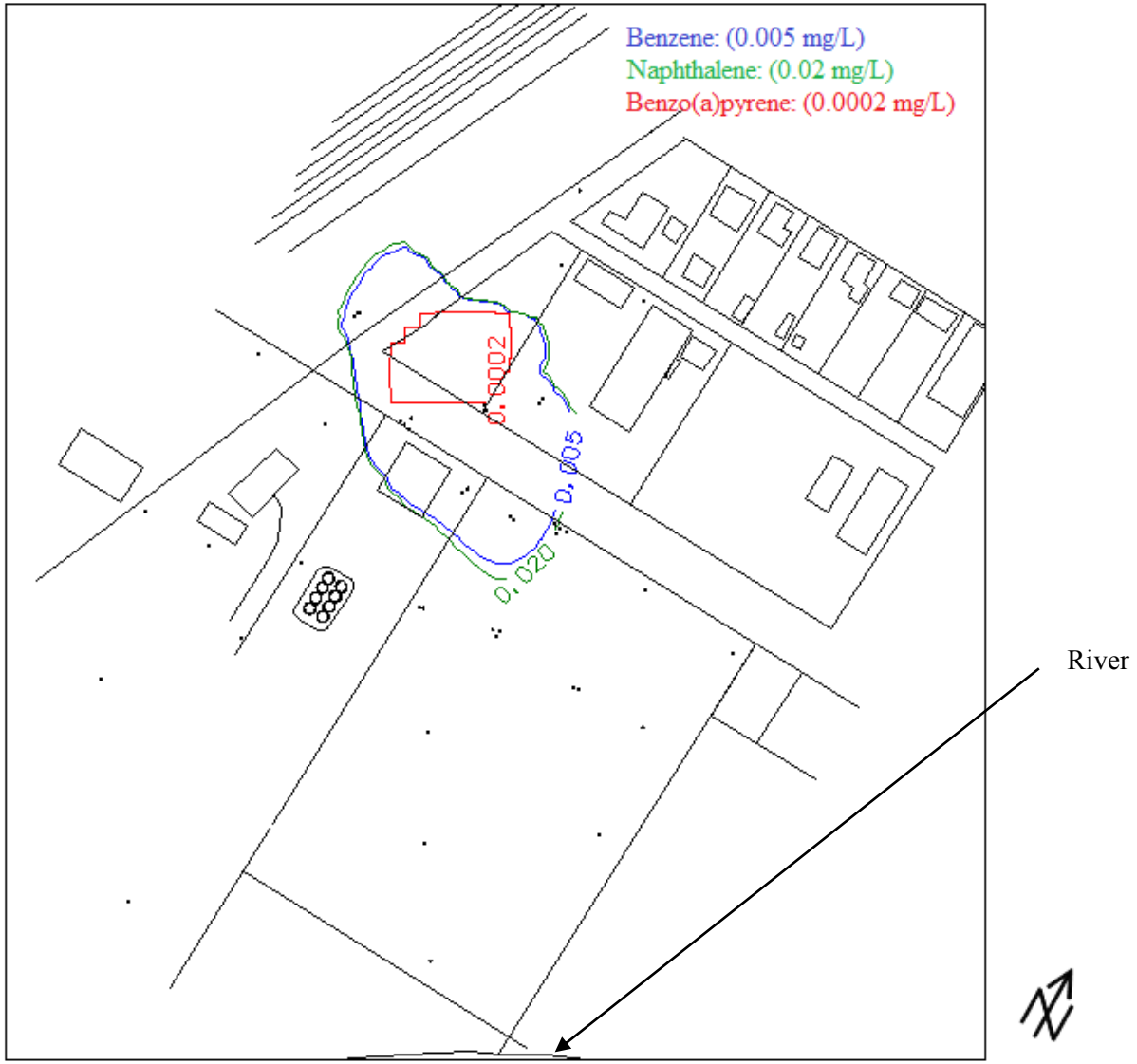

Figure 5.18: Plume at 75 years with advection, dispersion, sorption and biodegradation transport processes, parameters used for Run # 12 (see Table 5.1)

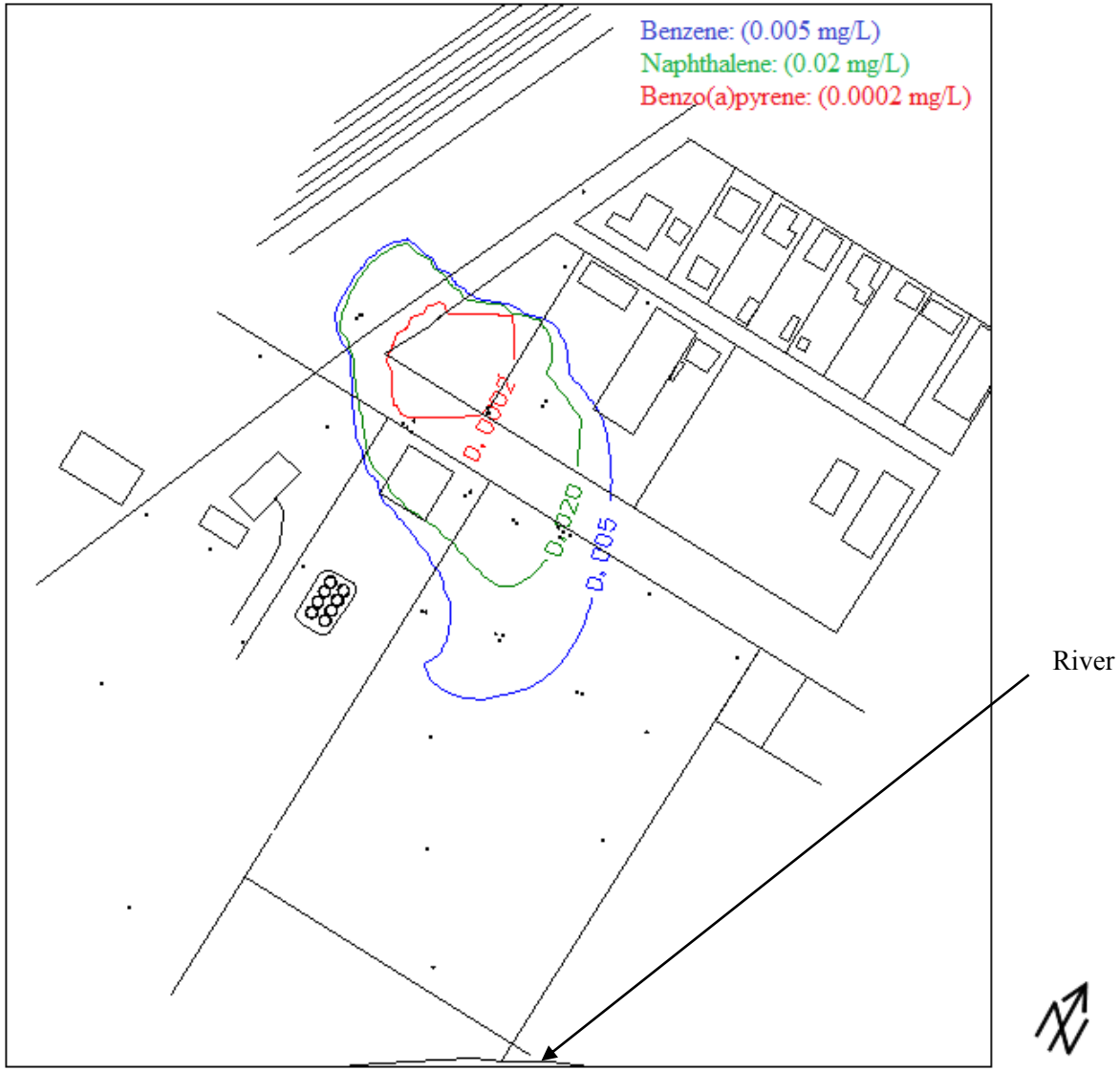

Figure 5.19: Plume at 75 years with advection, dispersion, sorption and biodegradation transport processes, parameters used for Run # 13 (see Table 5.1)

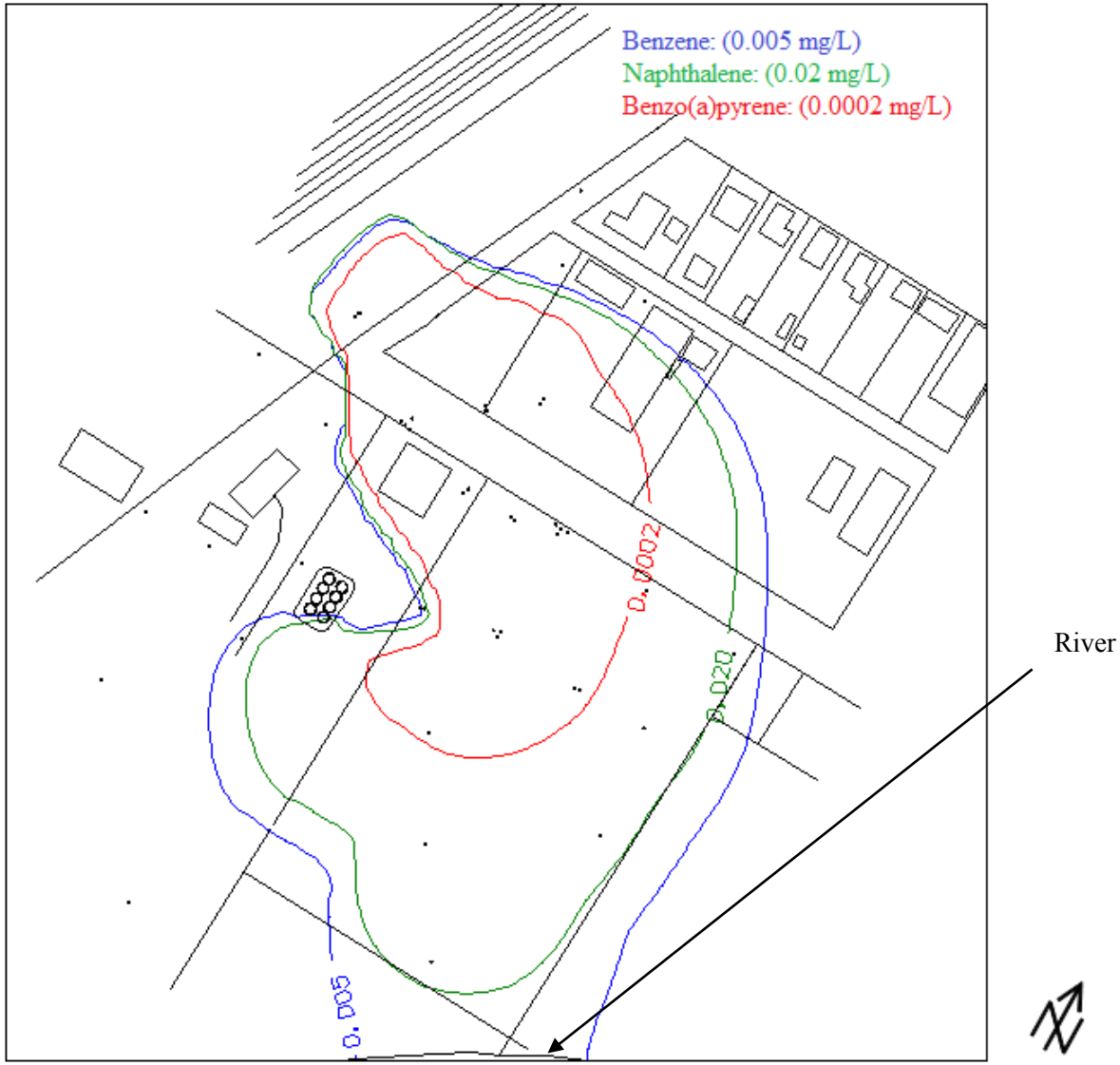

Figure 5.20: Plume at 75 years with decreasing sorption parameters from Run #13 by one order of magnitude

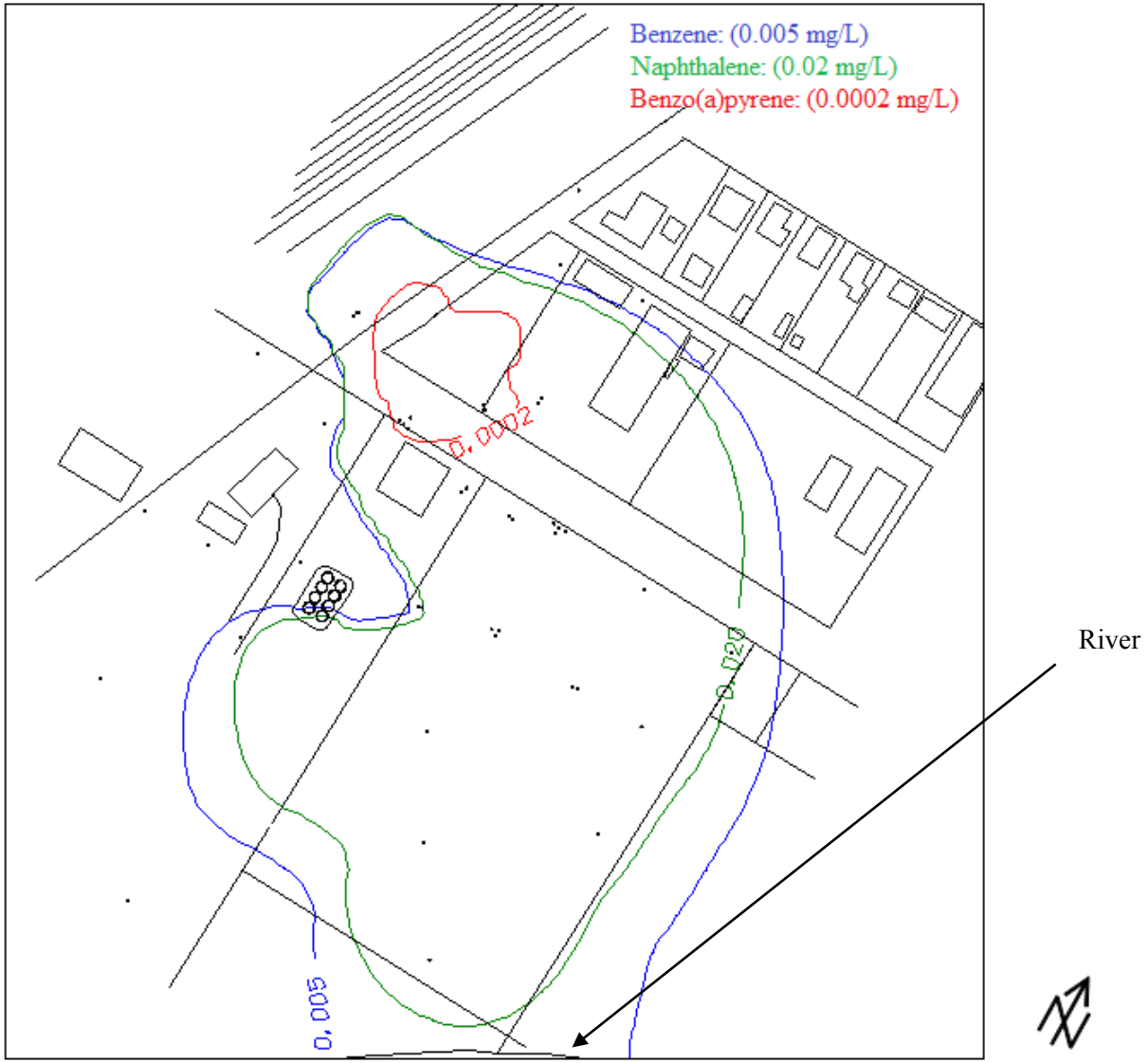

Figure 5.21: Plume at 75 years with decreasing biodegradation coefficients from Run #13 by one order of magnitude

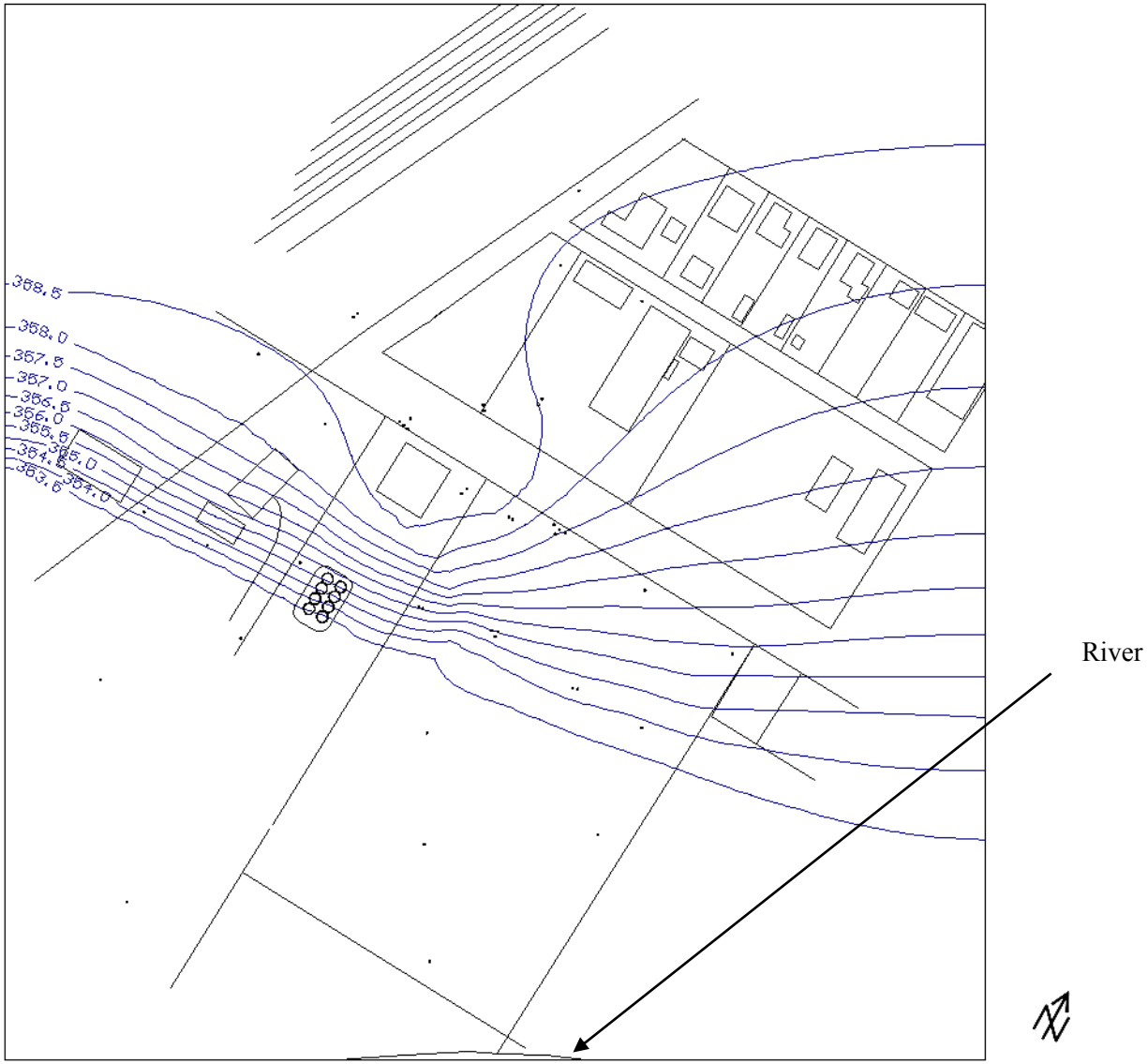

Figure 5.22: Potentiometric contours within the alluvium layer with increasing hydraulic conductivity of zone 8 by one order of magnitude, contour elevations are in meters

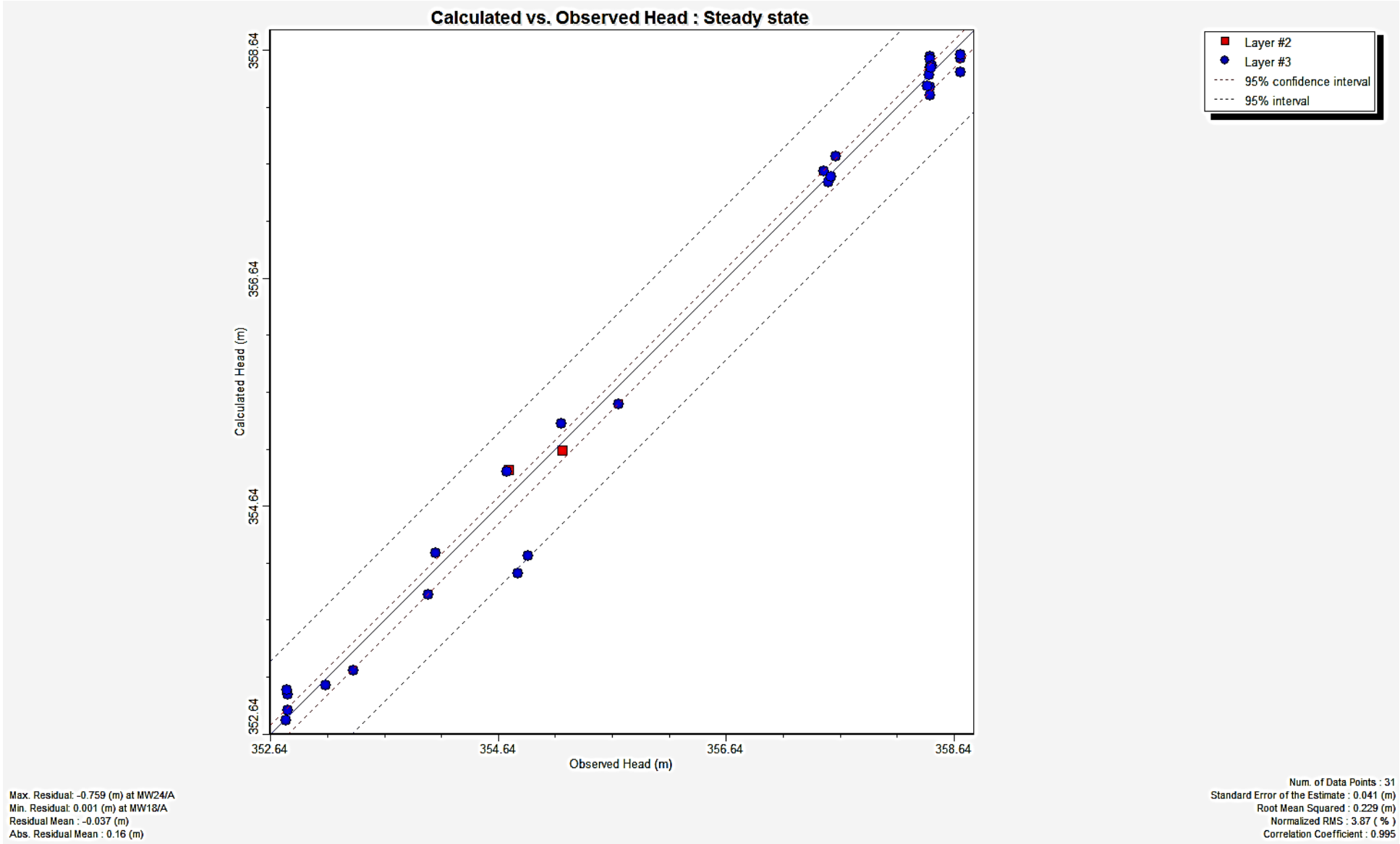

Figure 5.23: Calculated versus observed heads for the run with the alluvium zone 8 hydraulic conductivity increased by one order of magnitude

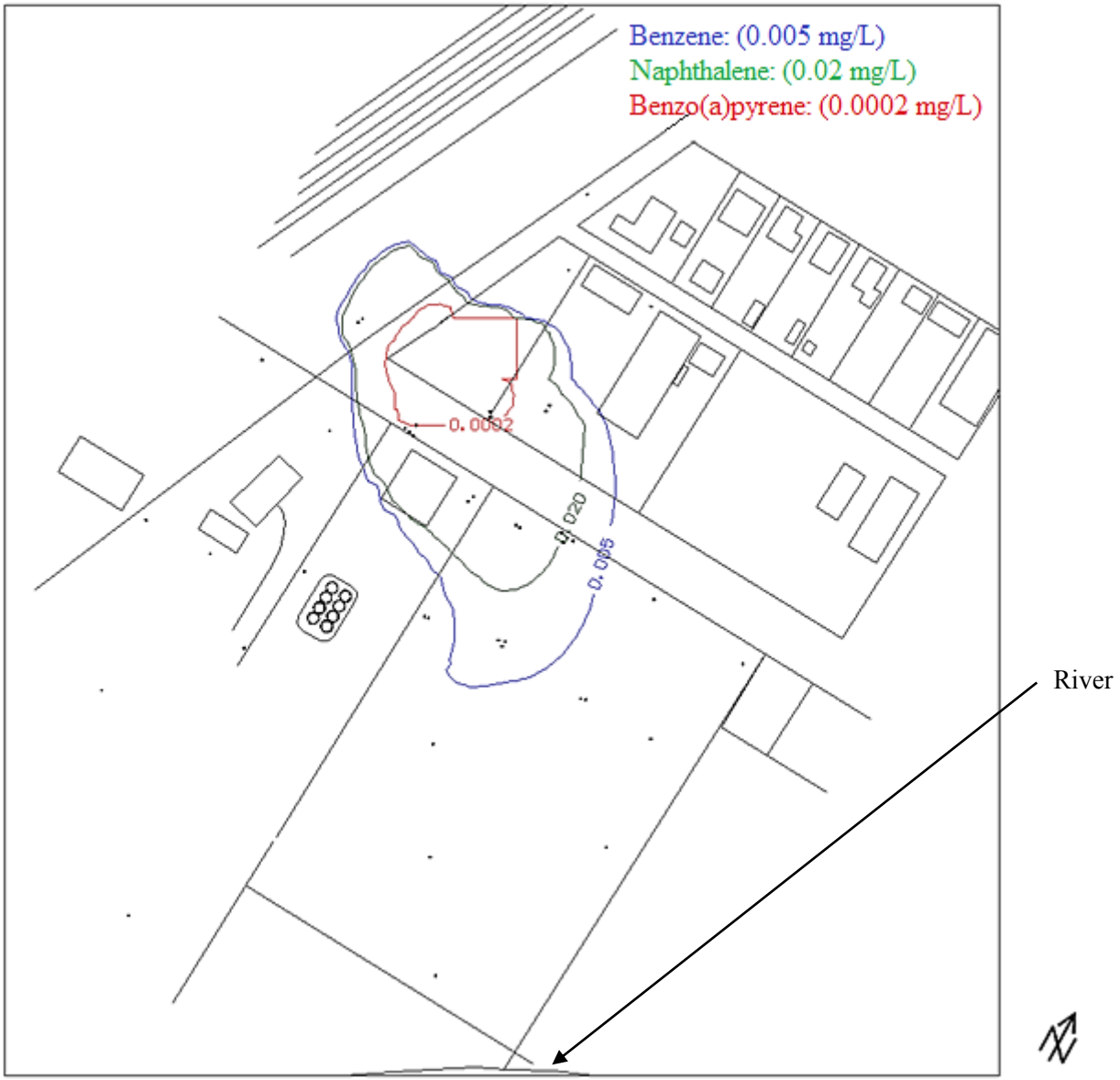

Figure 5.24: Plume at 75 years with increasing hydraulic conductivity of alluvium zone 8 by one order of magnitude

Chapter 6 Summary, Conclusions and Recommendations

6.1 Summary of the Research Work

The objectives of this study are described in Chapter 1. All of the objectives were achieved. Available site geology, hydrogeology, soil and groundwater contamination data compiled in Chapter 3 were used to produce geologic cross-sections, define the hydrogeologic properties and groundwater flow parameters, and produce groundwater potentiometric contours and groundwater flow patterns. The contaminant concentration data compiled from available literature were used to determine the extent of the dissolved contaminant plumes by plotting measured concentration contour plumes.

Three contaminant compounds were selected as the focus of this study: benzene, benzo(a)pyrene and naphthalene. These compounds represent MAH and PAH contaminant compounds with concentrations in the groundwater at the former MGP site found consistently above the USEPA drinking water regulatory standards. The mass flux and mass discharge for benzene and naphthalene were estimated across two selected monitoring well transects (see Figure 5.1) to understand the contaminant plumes behavior with time and to estimate the biodegradation rate constants for benzene and naphthalene.

A groundwater flow and contaminant transport model was developed for the former MGP site located in the Midwestern U.S. using the compiled site groundwater and contaminants data as described earlier. Visual MODFLOW was used to simulate the groundwater flow, and the model was calibrated using the WINPEST engine component of the Visual MODFLOW. The calibration process was based on varying the hydraulic conductivity and recharge rate values until a good match between measured and calculated head values was achieved and a

groundwater flow pattern closely matching the measured head contours was produced.

The calibrated groundwater flow model was utilized to run the contaminant transport simulations using the MT3DMS contaminant transport engine. Using the estimated transport parameters with some adjustments, simulated plumes that reasonably matched the observed plumes were produced. The effect of different attenuation processes on each of the three contaminants was examined during the sensitivity analysis. As part of the sensitivity analysis, the hydraulic conductivity in the west part of the pinch zone was increased by one order of magnitude to examine the effect on the benzene plume extent.

6.2 Conclusions

The following are key results and observations of this research.

1. The high level of hydraulic conductivity characterization and groundwater monitoring for the alluvium layer was very important and facilitated the ability to simulate the groundwater flow.
2. The pinch zone in the alluvium layer, a very important feature of the site geology, has a considerable effect on the site hydrogeology. The groundwater model simulations show that the lower hydraulic conductivity area in the western part of the pinch zone is not the preferred pathline for the contaminants to travel towards the southern model boundary.
3. Piecewise hydraulic conductivity zonation proved to be better than Kriging zonation of hydraulic conductivity for calibrating the groundwater flow model.
4. The WINPEST engine worked well in calibrating the groundwater flow model. The calibrated groundwater flow model had a correlation coefficient of 0.998 between simulated and observed head values, an absolute residual mean of 0.116 m, and a maximum head residual of 0.24 m at MW-27B. The calibrated hydraulic conductivity zone values were

within one order of magnitude variation from the measured values.

5. The mass flux calculations using two monitoring well transects downgradient of the coal tar source indicate that benzene and naphthalene mass discharges both decrease significantly between the two transects for a given time and generally decrease with time for a given transect between November 2002 and June 2007. This indicates that mass releases from the coal tar source are generally decreasing and/or natural attenuation process rates are increasing. Figures 5.4 and 5.5 show the decreasing flux trend since research studies conducted by Biyani (2003) as well as Stenback and Ong (2003).

6. The biodegradation rate constants estimated from the mass discharges of benzene and naphthalene were found to be within about one order of magnitude when compared to published biodegradation rates in research studies conducted at the same site (see Table 5.13).

7. Further characterization of the source area reported by Black and Veatch (2008) allowed for a well-defined source term area in the MT3DMS transport model.

8. The simulated benzene, naphthalene and benzo(a)pyrene plumes with advection and dispersion processes only extended well beyond the measured plumes, further indicating that attenuation processes are active at the site.

9. The benzene plume was mostly affected by varying the biodegradation rate constant while not being sensitive to the sorption mechanism. Contrary to this, benzo(a)pyrene was highly affected by varying the partition coefficient, indicating high sensitivity to the sorption process. The behavior of naphthalene, unlike benzene or benzo(a)pyrene, was showing a balance of sensitivity to biodegradation and sorption processes. Despite the different behaviors among the contaminants to varying the transport parameters, there is clear evidence that natural attenuation processes are limiting the contaminant plumes expansion. This can be taken into account when formulating a risk response plan and/or deciding on a remediation scheme.

10. This study emphasizes the importance of numerical modeling application in the former MGP contaminated site remediation program and illustrates how the application of Visual MODFLOW can lead to a representative groundwater flow and a contaminant transport model with simulated contaminant plumes reasonably representing the site observed plumes.

6.3 Recommendations for Future Work

Groundwater flow and contaminant transport models are highly dependent on input values and data obtained from the field to produce accurate simulations representing the recent conditions at a former MGP site. Further site characterization is recommended for a complete and up-to-date set of groundwater data (hydraulic heads at monitoring wells) as well as recent contaminant concentration data. This will help to further recognize any possible changes to the groundwater flow pattern and to detect any additional coal tar releases that may increase the contaminant concentrations and/or plume extents. Few additional monitoring wells can be added to the north-east of the source area to further delineate the possible lateral plume evolution. Although both the naphthalene and benzo(a)pyrene contaminant plumes do not extend relatively far away from the former MGP source area, additional samples should also be collected from existing monitoring wells to further monitor the contamination with recent field data. Additional soil and groundwater sampling and slug testing is also recommended specifically from the alluvium thinning zone to better describe the pinch zone hydraulic conductivity and to understand the variation of hydraulic conductivity across the zone running from east to west. The relatively high benzene concentrations measured at MW-13B should be subject to further investigations to understand the reasons behind such high concentrations and to recognize the spatial extent of the high concentration zone.

The simulated benzene plume somewhat deviated from the measured plume in the area near

the petroleum tanks as shown by comparing Figure 5.19 to Figure 3.20. This area of the pinch zone can be subject to further research and study to understand the possible seams or small layers of variable hydraulic conductivity within this region of the pinch zone that can affect the contaminant transport and was not captured by the model.

To better estimate the biodegradation rate constants, additional transect locations can be proposed to estimate additional contaminant fluxes and biodegradation rate constants. This may decrease the uncertainty associated with the averages of the biodegradation rate constants used for modeling. Further modeling activities are also recommended to understand the effect of varying the source area conditions. Reducing source area contaminant concentrations, and/or source area extents to simulate remedial actions can help in understanding the effect of source variations on the contaminant plume extent. In addition, the potential for modeling the actual estimated mass of the source and release of contaminants into the groundwater could be investigated. This would assist assessment and simulation of source removal options. Source removal simulations can also be coupled with other possible remediation alternatives such as pump and treat. Pump and treat remedial option can be evaluated by adding a single pumping well or assigning a group of pumping wells in the model to capture the groundwater plume following source removal, preventing further downgradient migration and simulating removal of the contaminated groundwater for treatment. By adjusting the pumping rate and screen intervals, the operational effectiveness and the efficiency of the remediation system can be maximized.

A permeable reactive barrier remediation option can be investigated by simulating the effect the barrier has on the contaminant plume extents. The model can be further used to predict the diversion of the groundwater around the barrier to the nearby sites or to detect possible groundwater mounding that can occur upgradient of the barrier system.

Further modeling simulations are recommended to understand the uncertainty involved in long term estimates and complexity of natural attenuation as a time dependent remediation option and to estimate the time scales necessary for natural attenuation to achieve acceptable levels of contaminant concentrations. This can also be coupled with source reduction or a complete source removal remediation option. More specifically, in situ bioremediation can be further examined by modeling the biodegradation process represented in the transport model by adding the biodegradation rate coefficient as a transport parameter to simulate existing microbial activity. Moreover, the effects of source reduction by in situ chemical oxidation on contaminant plume evolution and persistence could be modeled.

References

Agency for Toxic Substances and Disease Registry. 2011. Information About Contaminants Found at Hazardous Waste Sites. ATSDR Toxic Substances Portal. Available at atsdr.cdc.gov/toxprofiles/index.asp [accessed 20 June 2011].

Alvarez, P., and W. A. Illman. 2006. Bioremediation and Natural Attenuation: Process Fundamentals and Mathematical Models, John Wiley & Sons, pp. 609.

American Petroleum Institute. 2003. Groundwater Remediation Strategies Tool. Regulatory and Scientific Affairs Department, Washington, DC.

Annable, M.D., Teodorescu, M., Hlavinek, P., and Diels, L. 2008. Mass Flux as a Remedial Performance Metric at NAPL Contaminated Sites. In Methods and Techniques Published by Springer, Dordrecht, Netherlands. pp. 177-186.

Arlen, W. H., Edward, R. B., Mary, C. H., and Michael G. M. 2000. Modflow-2000, The U.S. Geological Survey Modular Groundwater Model: User Guide to Modularization Concepts and the Groundwater Flow Process. US Geological Survey, Reston, Virginia.

ASCE. 2003. Long-Term Groundwater Monitoring-The State of the Art. American Society of Civil Engineers. Reston, VA.

Baker, R.S., Brogan, D., and Lotti, M. 2006. In Situ Heating for MGP Remediation. Paper L-74. In Remediation of Chlorinated and Recalcitrant Compounds - 2006: Proceedings of the Fifth International Conference. Battelle, Columbus, OH.

Bedient, P.B., Rifai, H.S., and Newell, C.J. 1999. Ground Water Contamination, Transport and Remediation Prentice-Hall, Inc., Upple Saddle River, NJ.

Birak, P.S., and Miller, C.T. 2009. Dense non-aqueous phase liquids at former manufactured gas plants: Challenges to modelling and remediation. Journal of Contaminant Hydrology, **105**: 81–98.

Biyani, R. 2003. Modeling groundwater flow and transport of contaminants at the Cherokee Former Manufactured Gas Plant site. M.Sc. thesis, Department of Civil Engineering, Iowa State University, Ames, Iowa.

Black and Veatch. 1994. Remedial Investigation/Feasibility Study Report Cherokee, Iowa. Accessed from Iowa Department of Natural Resources Contaminated Sites website.

Black and Veatch. 1998. Cherokee, Iowa Former Manufactured Gas Plant Site. Interim Remedial Action Report for Soil and Source Material Removal. Prepared for IES Utilities Inc., Iowa. Accessed from Iowa Department of Natural Resources Contaminated Sites website.

Black and Veatch. 2004. Cherokee, Iowa Former Manufactured Gas Plant Site. Groundwater Monitoring Report. Prepared for Alliant Energy, Iowa. Accessed from Iowa Department of Natural Resources Contaminated Sites website.

Black and Veatch. 2008. Cherokee, Iowa Former Manufactured Gas Plant Site. DNAPL Recovery and Groundwater Monitoring Report. Prepared for Interstate Power and Light Company, Iowa. Accessed from Iowa Department of Natural Resources Contaminated Sites website.

Bockelmann, A., Ptak, T., and Teutsch G. 2001. An analytical quantification of mass fluxes and natural attenuation rate constants at a former gasworks site. Journal of Contaminant Hydrology, **53**(2001): 429–453.

Bockelmann, A., Zamfirescu, D., Ptak T., Grathwohl P., and Teutsch, G. 2003. Quantification of mass fluxes and natural attenuation rates at an industrial site with a limited monitoring network: a case study. Journal of Contaminant Hydrology, **60**(1-2): 97–121.

Borden, R.C., Daniel, R.A., LeBrun, L.E., and Davis, C.W. 1997. Intrinsic bioremediation of MTBE and BTEX in a gasoline-contaminated aquifer. Water Resources Research, **33**(5): 1105-1115.

Brown, D.G, Gupta L., Moo-Young, H.K., and Coleman A .J. 2005. Raoult's Law–Based Method for Determination of Coal Tar Average Molecular Weight. Environmental Toxicology and Chemistry, **24**(8): 1886–1892.

Brown, D.G. 2006. Comparative assessment of coal tars obtained from 10 former manufactured gas plant sites in the Eastern United States. Chemosphere, **65**(9): 1562–1569.

Buscheck, T.E., and C.M. Alcantar. 1995. Regression techniques and analytical solutions to demonstrate intrinsic bioremediation. In Intrinsic Bioremediation, R.E. Hinchee, J.T. Wilson, and D.C. Downey, 109-116. Battelle Press., Columbus, Ohio.

D'Affonseca, F.M., Blum, P., Finkel, M., Melzer, R., and Grathwohl, P. 2008. Field scale characterization and modeling of contaminant release from a coal tar source zone. Journal of Contaminant Hydrology, **102**(1-2): 120–139.

Doherty, J. 2005. PEST User Manual: Model-Independent Parameter Estimation. Watermark Numerical Computing, Brisbane, Australia.

Downs, T., and Webster, B. 2007. Modeling groundwater flow and transport of contaminants at the Former Manufactured Gas Plant in Vinton, Iowa. B.Sc. thesis, Department of Civil Engineering, Lakehead University, Ontario.

EPRI. 2003. Proven and Emerging Remediation Technologies for Residual Contamination in Soil and Groundwater at Former Manufactured Gas Plant Sites. Electric Power Research Institute, Palo Alto, California.

EPRI. 2007. Handbook of Remedial Alternatives for MGP Sites with Contaminated Sediments. Electric Power Research Institute, Palo Alto, California.

Falta, R.W., Suresh, R.P., and Basu, N. 2005. Assessing the impacts of partial mass depletion in DNAPL source zones: Analytical modeling of source strength functions and plume response. Journal of Contaminant Hydrology, **78**(4): 259–280.

Feenstra, S., and Guiguer, N., 1996. Dissolution of dense non-aqueous phase liquids in the subsurface, In_Dense Chlorinated Solvents and Other DNAPLs in Groundwater. Waterloo Press, ON, pp. 203-229.

Fraser, M., Barker, J.F., Butler, B., Blaine, F., Joseph, S., Cooke, C. 2008. Natural Attenuation of a Plume from an Emplaced Coal Tar Creosote Source Over 14 Years. Journal of Contaminant Hydrology, **100**(3-4): 101–115.

Gelhar, L. W., Welty C., and Rehfeldt K. R. 1992. A critical review of data on field-scale dispersion in aquifers, Water Resources Res., **28**(7): 1955–1974.

Golchin, J., Stenback, G.A., Ong, S.K., and Hargens, D. 2004. Plume Modeling at a FMGP Site Using a 2-D Analytical Contaminant Transport Equation. Prepared for Iowa Department of Natural Resources, Iowa.

Golchin, J., Kjartanson, B.H., Ong, S.K., Stenback, G.A., and Nelson, G.L. (Sam), 1998, "Monitored Enhanced Natural Attenuation (MENA)", Proceedings of the Eleventh International IGT Symposium on Environmental Biotechnologies and Site Remediation Technologies, Orlando, FL, Dec. 7-9.

Goltz, M.N., Kim, S., Yoon, H., and Park, J. 2007. Review of Groundwater Contaminant Mass Flux Measurement. Environmental Engineering research, Korean Society of Environmental Engineers, **12**(4): 176-193.

Hatheway, A .W. 1997. Former Manufactured Gas Plants: Yesterday's Pride, Today's Liability. American Society of Civil Engineering, 38-41.

Hatheway, A .W. 2012. History of Manufactured Gas and Coal-Tar Activities. In Remediation of Former Manufactured Gas Plants and Other Coal-Tar Sites. CRC Press, Taylor and Francis Group, NY.

Heritage Research Center. 2007. Manufactured Gas - The Genie's Legacy. Available from heritageresearch.com/ourlibrary/histories/manufactured_gas.html [accessed 14 June 2011].

Herold, M., Greskowiak, J., Ptak, T., and Prommer, H. 2011. Modeling of an enhanced PAH attenuation experiment and associated biogeochemical changes at a former gasworks site in Southern Germany. Journal of Contaminant Hydrology, **119**(1-4): 99–112.

Huling, S.G., and Pivetz, B.E. 2006. In Situ Chemical Oxidation. Environmental Protection Agency, Office of Research and Development, U.S.

Ingebritsen, S. E., and Sanford, W. E. 1999. Groundwater in geologic processes. New York, Cambridge University Press, U.K. 341 p.

ITRC. 2000. Dense Non-Aqueous Phase Liquids (DNAPLs): Review of Emerging Characterization and Remediation Technologies. Interstate Technology and Regulatory Cooperation Work Group, U.S.

ITRC. 2008. In Situ Bioremediation of Chlorinated Ethene DNAPL Source Zones: A Resource Guide. Bioremediation of DNAPLs Team, Washington D.C.

ITRC. 2010. Use and Measurement of Mass Flux and Mass Discharge. Integrated DNAPL Site Strategy Team, Washington D.C.

Kjartanson, B. H.; Stenback, G. A.; Ong, S. K.; Rogers S. W., and Biyani, R. 2002. Optimized Ground Water Monitoring for MENA and Site Closure, Interim Report, Work Performed for Year 1 at the Cherokee FMGP Site. Prepared by Iowa State University for Alliant Energy, Ames, Iowa.

Kumar, C.P. 2006. Groundwater Flow Models. National Institute of Hydrology, Roorkee, India, pp. 1-27.

Kumari, A. A. K. 2007. Development of Steady State Groundwater Flow Model in Lower Walawa Basin – Sri Lanka. MSc Thesis, International Institute for Geo-information Science and Earth Observation, Netherlands.

Kurniawan, B., and Jinno, K. 2006. Numerical Transport Model of Chlorinated Organic Compounds in Saturated Porous Media. Department of Urban and Environmental Engineering, Kyushu University, Japan.

Landmeyer, J.E., Chapelle, F.H., Petkewich, M.D., and Bradley, P.M. 1998. Assessment of natural attenuation of aromatic hydrocarbons in ground water near a former manufactured gas plant, South Carolina, USA: Environmental Geology, **34**(4): 279–292.

Lee, P. H., Braida, W., and Ong, S.K. 1998. Review of Physical-Chemical Properties of Coal Tar at Former Manufactured Gas Plant (MGP) Sites, Iowa State University.

Lingle, J.W., and Brehm, K.L. 2003. Application of source removal and natural attenuation remediation strategies at mgp sites in wisconsin. Remediation Journal, **13**(4): 29–39.

Liu, H.F., and Liptak, B.G. 2000. Groundwater and Surface Water Pollution. Lewis Publishers, CRC Press LLC, Washington D.C.

Martin, C., F. Blaine, J. Barker, C. Lamarche, N. R. Thomson, F. Lauzon, P. Lamarche, and J. Kerr. 2002. Natural attenuation, in situ source oxidation and enhanced natural attenuation of coal tar creosote chemicals – A controlled source field experiment in the Borden aquifer, In Proceedings from the 2002 Petroleum Hydrocarbons and Organic Chemicals in Ground Water Conference, Atlanta, GA, Nov 6-8.

Mayer, A., and Endres, K. 2007. Simultaneous optimization of dense non-aqueous phase liquid (DNAPL) source and contaminant plume remediation. Journal of Contaminant Hydrology, **91**(3-4): 288–311.

Miller, R.N. 2000. Assessment of Natural Attenuation at Two Manufactured Gas Plant Sites in Iowa. Master's Thesis, Iowa States University, Ames, IA.

Moretti, L. 2005. In Situ Bioremediation of DNAPL Source Zones. Environmental Protection Agency, Office of Solid Waste and Emergency Response, Washington D.C.

National Research Council. 2005. Contaminants in the subsurface: Source zone assessment and remediation . The National Academy of Sciences, Washington D.C.

Neuhauser, E. F., Ripp, J. A., Azzolina, N. A., Madsen, E. L., Mauro D M, and Taylor, T. 2009. Monitored natural attenuation of manufactured gas plant tar mono- and polycyclic aromatic hydrocarbons in ground water: A 14-year field study. Ground Water Monitoring and Remediation, **29**(3): 66–76.

Newell, C.J., Rifai, H.S., Wilson, J.T., Connor, J.A., Aziz, J.A., and Monica, P.S. 2002. Calculation and Use of First-Order Rate Constants for Monitored Natural Attenuation Studies. Environmental Protection Agency, Oklahoma.

Nielsen, D.M. 2006. Practical Handbook of Environmental Site Characterization and Ground-Water Monitoring. Taylor & Francis, Boca Raton, FL.

Pankow, J.F., and Cherry, J.A. 1996. Dense chlorinated solvents and other DNAPL's in groundwater: history, behavior, and remediation: Portland, Oreg., Waterloo Press.

Parker, J.C., and Park, E. 2004. Modeling field-scale dense nonaqueous phase liquid dissolution kinetics in heterogeneous aquifers. Oak Ridge National Laboratory, Oak Ridge, Tennessee, U.S.

Phelan, P., and Rhodes, E., 1966. Road tars and tar paving. In: Hoiberg, A. (Ed.), Bituminous Materials: Asphalts, Tars, and Pitches. Vol. 3 of Coal Tars and Pitches. Interscience Publishers, New York, pp. 411–531.

Pretorius, J.A., Usher, B.H., and Gebrekristos, R.A. 2008. Groundwater Monitoring Guidelines for DNAPLS in South African Aquifers. Water Research Commission Institute for Groundwater Studies, University of the Free State, South Africa.

Rao, S. 2008. Flux-Based DNAPL Site Assessment and Remediation: Overview of Concepts. In Triad Conference Proceedings, Ada, Oklahoma, 10 June 2008. National Risk Management Research Laboratory, Ground Water and Ecosystems Restoration Division.

Rogers, S. W., Ong, S. K., Kjartanson, B. H., Golchin, J., and Stenback, G. A. 2002. Natural Attenuation of PAH-Contaminated Sites: Review. American Society of Civil Engineers. Practice Periodical Hazard. Toxic Radioactive Waste Manage. pp. 1–15.

Rogers, S.W., Ong, S.K., and Moorman, T.B. 2007b. Mineralization of PAHs in coal-tar impacted aquifer sediments and associated microbial community structure investigated with FISH. Chemosphere Journal, **69**(10): 1563–1573.

Rogers, S.W., Ong, S.K., Stenback, G.A., Glochin, J., and Kjartanson, B.H. 2007a. Assessment of Intrinsic Bioremediation of a Coal-Tar-Affected Aquifer Using Two-Dimensional Reactive Transport and Biogeochemical Mass Balance Approaches. Water Environment Federation, **79**(1): 13–28.

Sara, M. N. 2003. Site Assessment and Remediation . In M. R. Sara, Site Assessment and Remediation, Second Edition, pp. 764 to 768. CRC Press.

Schlumberger Water Services. 2010. User's Manual: Visual Modflow, Dynamic Groundwater Flow and Contaminant Transport Modeling Software. Schlumberger Water Services, Waterloo, Ontario, Canada.

Schwartz, F.W., and H. Zhang, 2003. Fundamentals of Groundwater. John Wiley and Sons Inc., New York, pp: 577.

Schwarzenbach, R.P., and Westall, J., 1981. Transport of nonpolar organic compounds from surface water to groundwater. Laboratory sorption studies. Environmental Science and Technology **15**(11): 1360–1367.

Shackelford, C.D.1993. Contaminant Transport. In Geotechnical Practice for Waste Disposal. Civil Engineering, University of Texas, Austin, U.S.

Smith, J., and Lerner, D. 2011. A framework for assessing the contaminant sorption and retardation potential of aquifers. Geophysical Research Abstracts, EGU General Assembly, Sheffield, U.K.

Stenback, G.A., and Ong, S.K. 2003. MENA Research and Demonstration FMGP Site, Cherokee, Iowa. Progress Report for Iowa Department of Natural Resources, Iowa.

Stenback, G.A., Ong, S.K., Rogers, S.W. and Kjartanson, B.H., 2004. Impact of transverse and longitudinal dispersion on first-order degradation rate constant estimation. Journal of Contaminant Hydrology, **73**(1-4): 3–14.

Sudicky, E.A., and Illman, W.A. 2011. Lessons Learned from a Suite of CFB Borden Experiments. Department of Earth and Environmental Sciences, University of Waterloo

Thomson, N.R., Fraser, M.J., Lamarche, C., Barker, J.F., Forsey, S.P. 2008. Rebound of a Coal Tar Creosote Plume Following Partial Source Zone Treatment with Permanganate. Journal of Contaminant Hydrology, **102**(1-2): 154–171.

USEPA. 1991. Transport and fate of contaminants in the subsurface. In Handbook ground water; volume II. Office of research and development, Environmental Protection Agency, Washington D.C.

USEPA. 2004. DNAPL Remediation: Selected Projects Approaching Regulatory Closure. Environmental Protection Agency, U.S.

USEPA. 2004. DNAPL Remediation: Selected Projects Approaching Regulatory Closure. US Environmental Protection Agency, Washington, DC.

USEPA. 2005. Groundwater Sampling and Monitoring with Direct Push Technologies. Office of Solid Waste and Emergency Response, Environmental Protection Agency, U.S.

USEPA. 2006. Characterization of Site Hydrogeology. In Technical Guidance Manual for Groundwater investigations. Division of Drinking and Ground Waters, Ohio Environmental Protection, Columbus, Ohio.

USEPA. 2008. Design and Installation of Monitoring Wells. Science and Ecosystem Support Division, US Environmental Protection Agency, Athens, Georgia.

USEPA. 2007. Ground Water Flow and Fate and Transport Modeling. In Technical Guidance Manual for Ground Water Investigations. Division of Drinking and Ground Waters, Ohio Environmental Protection, Columbus, Ohio.

Wood, L. 2008. Flux-Based Site Management. In Triad Conference Proceedings, Ada, Oklahoma, 10 June 2008. National Risk Management Research Laboratory, Ground Water and Ecosystems Restoration Division.

Xu, Z., and Wu, Y. 2011. Dissolution Processes Modeling of Nonaqueous Phase Perchloroethylene in Saturated Soil Column. School of Environmental Science and Engineering, Shanghai Jiao Tong University, Shanghai, China.

Yoon, H. 2008. Validation of Methods to Measure Mass Flux of a Ground Contaminant. M.Sc. thesis, Department of Systems and Engineering Management, Graduate School of Engineering and Management, Air Force Institute of Technology, Wright-Patterson Air Force Base, Ohio.

Zamfirescu, D., and Grathwohl, P. 2001. Occurrence and attenuation of specific organic compounds in the groundwater plume at a former gasworks site. Journal of Contaminant Hydrology, **53**(3-4): 407–427.

Zhang, Y.K., and Heathcote, R.C. 2003. An Improved Method for Estimating of Biodegradation Rate with Field Data. Groundwater Monitoring and Remediation, **23**(3): 112–116.

Zheng, C., and Wang, P. 1999. MT3DMS: A Modular Three-Dimensional Multispecies Transport Model. U.S. Army Corps of Engineers, Washington, D.C.

Appendix A: Stratigraphic Data

Location	X	Y	Ground Surface Top	Loess Top	Alluvium Top	Glacial Till Top
EC10	382.50	262.94	358.34	357.27	349.80	348.19
EC11	402.88	271.04	358.24	357.17	349.92	349.40
EC12	340.59	394.28	362.99	362.60	361.83	351.71
EC13	394.26	347.80	360.52	360.13	358.76	353.03
EC14	368.09	348.01	361.11	360.81	358.52	351.82
EC15	351.63	348.33	361.58	361.43	358.53	350.30
EC16	328.77	353.14	362.23	362.08	360.56	350.96
EC17	314.67	331.84	361.93	361.77	358.88	353.09
EC18	331.99	315.06	361.01	360.25	358.27	352.17
EC19	351.86	290.61	359.02	358.41	356.46	352.32
EC2	364.56	284.11	358.64	357.88	355.38	353.31
EC20A	304.38	302.94	360.30	359.94	359.23	354.36
EC21	343.21	300.74	359.44	359.20	357.07	351.64
EC22	366.66	299.49	359.13	357.91	356.60	352.67
EC23	383.62	300.69	358.72	358.41	356.28	353.78
EC24	283.74	213.54	358.13	357.13	350.21	347.25
EC25A	318.99	187.86	357.34	357.19	351.86	346.67
EC26	319.17	285.17	359.56	358.03	356.94	353.00
EC27	354.98	244.00	358.10	357.19	349.69	348.53
EC28	339.25	227.79	357.68	356.61	350.49	347.16
EC29	349.57	246.87	358.26	357.35	352.17	349.27
EC3	423.48	281.18	358.09	356.87	349.86	347.82
EC30	395.70	250.00	358.03	356.35	349.55	348.40
EC31	404.08	268.38	358.28	356.91	349.78	349.32
EC32	397.15	282.64	358.28	357.52	353.13	350.66
EC33	349.58	267.92	358.42	357.81	354.70	352.78
EC34	322.41	260.70	358.84	358.69	356.01	353.05
EC35	314.95	241.05	358.33	356.95	354.36	351.13
EC36	300.47	273.99	359.88	358.66	355.74	354.18
EC37	290.84	303.68	360.69	360.69	359.47	355.60
EC38	302.25	324.02	361.47	361.47	359.64	356.23
EC39	327.34	321.37	361.51	361.51	358.76	353.13
EC40	317.40	310.68	361.26	361.11	360.56	353.19
EC41	334.45	301.50	359.78	359.17	357.64	351.88
EC42	341.21	279.32	358.77	358.25	356.15	352.13
EC43	325.54	139.13	357.06	356.91	351.33	344.35
EC44	417.09	272.98	358.23	358.07	350.54	348.32
EC45	416.27	282.66	358.09	357.03	350.17	347.21
EC46	366.90	250.17	358.04	356.52	349.60	349.02
EC47	285.34	185.25	357.70	356.78	350.75	349.01
EC48	291.91	232.56	359.40	357.15	351.42	350.54

Location	X	Y	Ground Surface Top	Loess Top	Alluvium Top	Glacial Till Top
EC49	270.86	229.94	358.62	357.40	351.67	350.91
EC4B	307.51	258.97	359.40	358.34	355.44	353.80
EC5	317.25	262.15	359.42	359.17	355.45	352.89
EC50	274.99	280.77	359.84	359.54	357.83	356.19
EC51	357.46	279.83	358.53	357.98	355.30	352.89
EC52	415.44	250.63	358.07	356.24	350.45	348.86
EC53	319.33	351.88	362.40	362.40	361.79	354.47
EC6	340.89	274.34	358.68	358.22	355.99	352.28
EC7	383.16	289.77	358.57	357.96	355.83	353.24
EC8	316.35	238.56	358.09	357.48	352.45	351.01
EC9	342.29	246.94	358.20	357.50	352.87	350.34
MW1	331.15	343.45	362.11	360.33	360.33	351.46
MW10	381.91	194.09	357.37	355.85	350.06	345.19
MW11	399.59	168.50	357.54	357.53	352.04	344.88
MW12	419.63	220.63	357.55	356.70	350.35	346.33
MW13A	368.71	252.34	358.14	356.20	349.33	348.60
MW13B	368.71	250.82	358.12	356.34	349.38	348.69
MW13C	367.04	251.61	358.10	356.31	349.47	348.82
MW14	348.44	246.87	358.16	357.34	352.27	349.42
MW14A	347.35	246.66	358.27	357.35	352.34	349.54
MW15A	340.99	278.16	358.64	358.25	356.12	352.17
MW15B	341.49	280.00	358.67	358.28	356.17	352.14
MW16A	334.56	300.02	359.51	359.10	357.48	351.93
MW16B	333.47	301.15	359.63	359.11	357.55	351.98
MW17	314.47	239.97	358.25	357.09	353.74	351.04
MW18	300.57	274.65	359.76	358.66	355.80	354.18
MW19A	291.87	302.72	360.47	360.46	359.32	355.47
MW19B	292.34	304.17	360.60	360.59	359.47	355.51
MW2	354.56	346.80	361.55	360.09	360.09	350.58
MW20	394.63	250.55	357.94	356.04	349.65	348.15
MW20A	393.36	250.08	358.10	355.95	349.69	348.01
MW21	395.91	282.22	358.16	357.54	353.14	350.75
MW22	323.23	139.32	357.00	356.91	351.36	344.44
MW23	285.95	185.65	357.68	356.79	350.75	348.92
MW24	291.17	230.84	359.46	357.16	351.29	350.21
MW25	272.21	229.46	358.72	357.36	351.59	350.74
MW26	275.67	281.03	359.83	359.39	357.72	356.09
MW27A	354.97	279.57	358.55	358.05	355.43	352.81
MW27B	356.13	279.50	358.55	358.01	355.34	352.84
MW28	414.49	250.87	358.10	356.26	350.40	348.84
MW3	318.97	287.92	359.60	358.84	356.40	352.59

Location	X	Y	Ground Surface Top	Loess Top	Alluvium Top	Glacial Till Top
MW3A	318.39	285.44	359.48	358.20	356.83	352.98
MW3B	316.97	285.70	359.53	358.38	356.73	353.01
MW3C	319.79	285.15	359.41	358.11	356.86	352.93
MW4	324.84	362.75	362.46	361.74	359.36	353.35
MW5A	345.72	309.09	359.88	358.62	357.61	351.03
MW5B	345.85	310.80	359.97	358.51	357.74	350.89
MW6	368.06	283.86	358.65	357.90	355.70	352.38
MW6A	366.20	284.25	358.66	357.89	355.56	352.89
MW6B	369.78	283.96	358.62	357.89	355.57	352.36
MW6C	367.81	282.25	358.60	357.84	355.33	352.40
MW7	311.72	214.60	357.76	356.46	350.06	346.41
MW8	424.51	280.15	358.01	356.19	349.64	348.26
MW9	366.94	219.57	357.64	356.71	350.15	348.63
SB1	313.94	304.80	360.46	358.84	357.96	353.59
SB11	330.71	314.55	360.73	359.12	357.38	352.31
SB12	326.14	331.93	361.52	360.00	360.00	352.47
SB13	332.38	316.53	360.85	358.26	358.26	352.17
SB17	316.99	319.13	361.49	360.46	359.05	353.58
SB18	323.39	313.03	361.04	359.97	357.99	352.96
SB19	339.24	313.64	360.18	359.42	357.80	351.50
SB2	322.17	304.19	360.18	358.66	357.29	353.23
SB20	319.37	246.74	358.44	356.31	353.11	352.35
SB21	319.13	206.96	357.65	355.98	351.86	346.66
SB6	325.22	326.14	361.58	360.52	359.60	352.88
SB7	327.66	316.08	360.85	359.33	358.26	352.71
GWPA1	301.14	253.59	357.68	355.15	353.42	352.20
GWPA2	340.16	253.59	357.68	355.76	353.42	350.98
GWPA3	367.28	253.59	357.84	356.01	349.30	348.54
GWPA4	393.80	253.29	357.68	355.24	349.91	347.62
GWPA5	422.45	253.29	357.68	356.16	349.61	348.69
GWPA6	270.05	252.07	357.68	356.16	354.48	352.93
GWPB1	336.19	223.42	357.68	357.07	349.45	348.54
GWPB2	366.98	223.42	357.68	356.77	349.64	345.95
GWPB3	397.15	223.42	357.68	356.16	351.28	346.41
GWPB4	427.33	223.42	357.68	357.07	349.91	346.25
GWPB5	466.65	218.24	357.53	357.53	350.92	346.13
GWPBG	335.28	403.25	362.41	359.97	358.44	352.07
GWPC2	366.98	192.94	357.38	356.77	350.98	346.19
GWPC3	396.54	192.94	357.41	355.27	350.70	345.92
GWPC4	427.33	192.94	357.38	356.46	351.28	345.53
GWPD1	284.99	282.85	358.81	357.29	356.07	354.85

Location	X	Y	Ground Surface Top	Loess Top	Alluvium Top	Glacial Till Top
GWPD2	402.34	282.55	358.05	355.61	351.95	348.14
GWPE1	411.48	166.12	358.14	357.84	352.35	345.03
GWPE2	442.26	166.12	358.14	357.84	352.35	345.19
P1	423.67	140.21	357.07	356.62	352.35	345.03
P2	480.06	175.26	357.23	356.62	352.35	345.03
P3	420.62	377.95	361.49	360.00	359.97	352.35
P4	271.27	339.85	361.49	361.22	361.19	356.31
P5	274.32	131.06	356.92	356.62	351.74	345.03
P6	457.20	254.51	357.67	356.84	350.00	347.55
P7	449.58	281.94	357.86	356.54	350.14	348.10
P8	438.91	320.04	359.38	357.94	354.18	349.94
P9	272.80	195.07	357.93	356.99	350.70	348.54

All data are in meter units

EC : Electric Conductivity points

MW : Monitoring Wells

SB : Soil Boring (B&V)

GWP : Groundwater Geoprobes (B&V)

P1 to P9 : Fabricated points extending geologic surfaces beyond the range of available data